INSTITUTE OF SOUND AND VIBRATION RESEARCH

FACULTY OF ENGINEERING AND APPLIED SCIENCE

UNIVERSITY OF SOUTHAMPTON

ACTIVE CONTROL OF FLEXURAL WAVES IN *IN-VACUO* PIPES

by

Weerachai Variyart

A Thesis submitted for the degree of

Doctor of Philosophy

November 2001

UNIVERSITY OF SOUTHAMPTON

ACKNOWLEDGEMENTS

I would like to express my full gratitude to my Supervisor, Dr. Michael John Brennan for his knowledgeable and skilful guidance throughout this project. His encouragement and supervision greatly contributed to the steady progress of the project.

Many suggestions from Professor Stephen Elliott and Dr. Neil Ferguson to improve my work are gratefully acknowledged.

I would also like to thank to Miss Sally Abrams for her help, especially in the seminar and the conference.

Finally, I could not start and finish this work unless the Thai Government supported my financial need.

ABSTRACT

INSTITUTE OF SOUND AND VIBRATION RESEARCH

FACULTY OF ENGINEERING AND APPLIED SCIENCE

Doctor of Philosophy

ACTIVE CONTROL OF FLEXURAL WAVES IN *IN-VACUO* PIPES

by

Weerachai Variyart

In pipe vibration, the n = 2 (ovalling mode) flexural wave causes a large increase of strain in the pipe wall at the cut-on frequency of the wave when it starts to propagate. Hence from the fatigue perspective, this wave is a major concern. In this thesis, an active control system is designed to suppress this wave. Before the control strategy can be considered, however, the dynamic behaviour of the pipe must first be understood. For this reason, the wavenumbers of the pipe and the mobilities of an infinite and semi-infinite pipe based on Flugge's shell theory are derived. Once the dynamic behaviour is known, the active control system can be modelled in a straightforward manner. An n = 2 PVDF (polyvinylidene fluoride) modal sensor and PZT (lead zirconate titanate) modal actuator are designed to selectively sense and control this wave. Other types of control systems, passive and adaptive-passive control, have also been investigated for comparison with the active control system.

For the infinite pipe, the mobility is derived using the method of residues and an analytical method with eight boundary conditions. Both methods are shown to give the same result. Analytical and wave methods are used to derive the mobility of the semi-infinite pipe. Like the infinite pipe, numerical evaluation shows that both methods are

identical. In addition, the mobilities of infinite and semi-infinite pipes are simplified for low frequencies, which facilitates physical insight, and allows explicit expressions for the circumferential wave amplitudes to be derived.

For the modal sensor, PVDF elements are shaped in the form of sine and cosine functions similar to the n = 2 mode shape of the pipe. Since the orientation of the n = 2 mode shape at some arbitrary point on the pipe is unknown, both of these elements are required to sense the wave. The relationship between the charge generated on the sensor to the combination of the axial and circumferential bending strains is established for the case of in-extensional deformation. It is found that a practical modal sensor is sensitive to higher order modes as well as the n = 2 mode, and this cross-sensitivity is dependent upon the width of the modal sensor. However, provided that the width is small enough to keep the axial strain constant over its surface, the sensor will only be dominantly sensitive to the circumferential bending strain of the pipe and hence to the n = 2 mode. For this to occur, the width of the modal sensor has to be less than one third of the wavelength of the flexural wave at the ring frequency.

A piezoelectric modal actuator for the n = 2 mode is also investigated. It is constructed from a set of piezoelectric elements bonded to the pipe. By arranging them in the form of the n = 2 mode, only the motion of that particular mode is generated, the amplitude of which is proportional to the applied voltage. With two PZT modal actuators, which are in the form of sine and cosine functions, the orientation of the wave can, in principle, be modified to any angle.

In the active control system, the modal sensor is used as an error sensor and modal actuator is used for suppressing the disturbance. With both n = 2 modal sensor and modal actuator, the disturbance of the n = 2 can in principle be completely suppressed. Fully active control is then much effective than passive and adaptive-passive control.

The theoretical models developed in this work are validated by some experimental work.

CONTENTS OF THESIS

NOMENCLATURE

a	Radius of the pipe
a, **b**, and **c**	Wave vector
b_s	Ratio of a half of width of the sensor to the radius of the pipe
b_{31} and b_{32}	Piezoelectric stress constants
d_{31} and d_{32}	Piezoelectric strain constants
e_s	Axial strain
e_θ	Circumferential strain
$e_{s\theta}$	Shear strain
f_r	Ring frequency of the pipe
g's	Polynomial coefficients of axial wavenumbers, $\hat{k}_{nb}$, obtained from the simplified characteristic equation.
g_s^{or}	Polynomial coefficients of axial wavenumbers, $\hat{k}_{nb}$, obtained from the Flugge's shell theory.
h	Thickness of the pipe
h_d	Thickness of the damping material
h_{pv}	Thickness of the PVDF sheet
h_z	Thickness of the PZT element
$\hat{k}_{nb}$	Non-dimensional branch axial wavenumber (the axial wavenumber is multiplied by the radius of the pipe)
$\hat{k}_{nb}^c$	Non-dimensional branch axial wavenumber of the composite pipe
$\hat{k}_l$	Non-dimensional longitudinal wavenumber (the wavenumber is multiplied by the radius of the pipe)
$\hat{k}_s$	Non-dimensional torsional wavenumber (the wavenumber is multiplied

	by the radius of the pipe)
$\hat{k}_b$	Non-dimensional flexural wavenumber of a beam (the wavenumber is multiplied by the radius of the pipe)
k_{31}	Electro-mechanical coupling coefficient of the PZT element
m_0	Moment induced on the pipe by the PZT element
n	Mode number
p_e	Circumferential position of the PZT elements used as the modal actuator
p_{mq}	Ratio of the moment to the force induced on the pipe by the PZT element
q	Charge generated from the PVDF sheet
q_0	Force induced on the pipe by the PZT element
s	Non-dimensional axial length
s_c	Non-dimensional axial location of centre of the modal sensor to the radius of the pipe
u	Axial component of the displacement
u^i	Axial displacement of the infinite pipe excited by the point force
u^{iz}	Axial displacement of the infinite pipe excited by the PZT element
u^c	Axial displacement of the composite pipe
v	Tangential component of the displacement
v^i	Tangential displacement of the infinite pipe excited by the point force
v^i	Tangential displacement of the infinite pipe excited by the PZT element
v^c	Tangential displacement of the composite pipe
w	Radial component of the displacement
w^i	Radial displacement of the infinite pipe excited by the point force
w^i	Radial displacement of the infinite pipe excited by the PZT element
w^c	Radial displacement of the composite pipe

z_o	Distance from the mid-plane of the pipe to that of the PVDF
A_z	Surface area of the PZT element
C_z	Capacitance of the PZT element
D	Bending stiffness of the pipe
D_c	Bending stiffness of the composite pipe section
D_d	Bending stiffness of the damping material
D_3	Electric displacement across the electrodes of the piezoelectric material
E	Young's modulus of the pipe
E_d	Young's modulus of the damping material
E_{pv}	Young's modulus of the PVDF sheet
E_z	Young's modulus of the PZT element
E_{zn}	Young's modulus of the shunted PZT element
E_3	Electric field across the electrodes of the piezoelectric material
F	Point force intensity
F_0	Amplitude of the point force
F_s	Static gain of the generated force
H( )	Unit step function
$H_{p\theta}$	Measured frequency response of the pipe
J( )	Bessel's function
K	Membrane stiffness of the pipe
K_c	Membrane stiffness of the composite pipe
K_d	Membrane stiffness of the damping material
L_a	A half of length of the PZT element normalised to the radius of the pipe
L_z	Inductance
M_s and M_θ	Bending moment in axial and circumferential

$M_{s\theta}$ and $M_{\theta s}$	Twisting moment
N_s and N_θ	Normal in-plane force in axial and circumferential
$N_{s\theta}$ and $N_{\theta s}$	In-plane shear force
N	Number of accelerometers for the modal decomposition
N_e	Number of PZT elements for the modal actuator
Q_s and Q_θ	Transverse shear force in axial and circumferential
Q^s	Generated charge of the modal sensor shaped in the sine function
Q^c	Generated charge of the modal sensor shaped in the cosine function
Q^t	Total generated charge of the modal sensor
$\mathbf{R_1}$	Reflection matrixes of waves in the pipe at the discontinuity
$\mathbf{R_2}$	Reflection matrixes of waves in the composite pipe section at the discontinuity
$\mathbf{R_f}$	Reflection matrix of waves
Res_{nb}	Residue term for the infinite pipe excited by the point force
Res^z_{nb}	Residue term for the infinite pipe excited by the PZT element
$\mathbf{T_1}$	Transmission matrixes of waves in the pipe to the composite section
$\mathbf{T_2}$	Transmission matrixes of waves in the composite section to the pipe
$\mathbf{T_f}$	Transfer matrix of waves
$T_{s\theta}$	Effective in-plane shear force
T_q^c and T_q^s	Transfer functions of the n = 2 cosine and sine modal sensors
T_q^t	Net transfer functions of the n = 2 modal sensor
T_z^c and T_z^s	Transfer functions (velocity / supplied voltage) of the cosine, and the sine modal actuators
T_z^{tot}	Net transfer functions (velocity / supplied voltage) of the modal actuators

$\overline{\overline{U}}_{nb}$	Axial amplitude for the b^{th} wave of the n^{th} mode of the pipe
$\overline{\overline{U}}^{c}_{nb}$	Axial amplitude for the b^{th} wave of the n^{th} mode of the composite pipe
$\overline{U}_n$	Axial amplitude of the n^{th} mode of the pipe in the wavenumber domain
U^i_n	Axial displacement of the n^{th} mode of the infinite pipe in the frequency domain
V	Voltage supplied to the PZT element
V^c	Voltage supplied to the cosine modal actuator
V^c_r	Voltage required for each PZT element to form the cosine modal actuator
V^s	Voltage supplied to the sine modal actuator
V^s_r	Voltage required for each PZT element to form the sine modal actuator
V^{tot}	Total voltage supplied to the modal actuator
V_s	Effective transverse shear force
V_z	Equivalent voltage generated by the PZT element
$\overline{\overline{V}}_{nb}$	Circumferential amplitude for the b^{th} wave of the n^{th} mode of the pipe
$\overline{\overline{V}}^{c}_{nb}$	Circumferential amplitude for the b^{th} wave of the n^{th} mode of the composite pipe
$\overline{V}_n$	Circumferential amplitude of the n^{th} mode of the pipe in the wavenumber domain
V^i_n	Circumferential displacement of the n^{th} mode of the infinite pipe in the frequency domain
$\overline{\overline{W}}_{nb}$	Radial amplitude for the b^{th} wave of the n^{th} mode of the pipe
$\overline{\overline{W}}^{c}_{nb}$	Radial amplitude for the b^{th} wave of the n^{th} mode of the composite pipe
$\overline{\overline{W}}^{i}_{nb}$	Radial amplitude for the b^{th} wave of the n^{th} mode of the infinite pipe
$\overline{\overline{W}}^{s}_{nb}$	Radial amplitude for the b^{th} wave of the n^{th} mode of the semi-infinite

	pipe
$\overline{W}_n$	Radial amplitude of the n^{th} mode of the pipe in the wavenumber domain
$\overline{W}_n^{iz}$	Radial amplitude of the n^{th} mode of the infinite pipe in the wavenumber domain, which is excited by the PZT element.
W_n^i	Radial displacement of the n^{th} mode of the infinite pipe in the frequency domain
W_n^s	Radial displacement of the n^{th} mode of the semi-infinite pipe in the frequency domain
W_n^{iz}	Radial displacement of the n^{th} mode of the infinite pipe in the frequency domain, which is excited by the PZT element
W^c	Radial displacement of the pipe excited by the cosine modal actuator
W^s	Radial displacement of the pipe excited by the sine modal actuator
W^{tot}	Radial displacement of the pipe simultaneously excited by the sine and cosine modal actuators
W_{cont}^c	Radial displacement resulting from using the cosine modal actuator in active vibration control system
W_{cont}^s	Radial displacement resulting from using the sine modal actuator in active vibration control system
W_{cont}	Radial displacement resulting from using the modal actuator in active vibration control system
Y_n^i	Radial mobility of the n^{th} mode of the infinite pipe in the frequency domain
Y_n^{iP}	Radial point mobility of the n^{th} mode of the infinite pipe in the frequency domain
Y_n^{iT}	Radial transfer mobility of the n^{th} mode of the infinite pipe in the frequency domain
Y_n^s	Radial mobility of the n^{th} mode of the semi-infinite pipe in the frequency domain

Y_n^{sP}	Radial point mobility of the n^{th} mode of the semi-infinite pipe in the frequency domain
Y_n^{sT}	Radial transfer mobility of the n^{th} mode of the semi-infinite pipe in the frequency domain
$Z_{N,nb}$	Coefficients of normal in-plane force, N_s
$Z_{T,nb}$	Coefficients of effective in-plane shear force, $T_{s\theta}$
$Z_{V,nb}$	Coefficients of effective transverse shear force, V_s
$Z_{M,nb}$	Coefficients of bending moment, M_s
Z_e	Net impedance of the PZT element shunted
$\hat{Z}_e$	Net impedance of the shunted PZT element normalised to its open-circuit electrical impedance
Z_o	Open-circuit electrical impedance of the PZT element
Z_s	External electrical circuit of impedance

Greek Letters

β	Wall thickness ratio of the pipe
β_c	Wall thickness ratio of the composite pipe
ν	Poisson's ratio of the pipe
ν_d	Poisson's ratio of the damping material
ν_{pv}	Poisson's ratio of the PVDF sheet
ν_z	Poisson's ratio of the PZT material
ν_{zn}	Poisson's ratio of the shunted PZT element
ρ	Density of the pipe
ρ_c	Density of the composite pipe
ρ_d	Density of the damping material

ω	Angular frequency
ω_r	Angular ring frequency of the pipe
ω_{rc}	Angular ring frequency of the composite pipe
ω_e	Electrical resonant frequency
Ω	Normalised frequency to the ring frequency of the pipe
Ω_c	Normalised frequency to the ring frequency of the composite pipe
Ω_{co}	Cut-on frequency normalised to the ring frequency of the pipe
θ	Azimuthal angle of the pipe
ϕ	Azimuthal orientation angle of the pipe with respect to the excitation force
ϕ_c	Orientation angle related to the cosine modal actuator
ϕ_p	Angle interval between the positions of the PZT elements
φ	Arc angle of the PZT element
λ_1	$\cos(n\theta)\cos(n\phi)$
λ_2	$\sin(n\theta)\sin(n\phi)$
ε_{33}	Permittivity at constant stress of the piezoelectric material
ε_n	1 for n = 0 mode
	2 for $n \geq 1$ modes
ε	Stretching strain of the middle surface of the pipe
ε_s and ε_θ	Stretching strain of the middle surface of the pipe in the axial and circumferential direction, respectively
$\varepsilon_{s\theta}$	Shear strain of the middle surface of the pipe
κ	Change of curvature of the middle surface of the pipe
κ_s and κ_θ	Change of curvature of the middle surface of the pipe in the axial and circumferential direction, respectively
$\kappa_{s\theta}$	Twist of the middle surface of the pipe

σ^p	Stress in the pipe
σ_s^p and σ_s^p	Stresses in the pipe in the axial and circumferential direction
$\sigma_{s\theta}^p$ and $\sigma_{\theta s}^p$	Shear stresses in the pipe
$\gamma_{s\theta}$	Shear strain in the pipe
α_{nb}	Branch axial coefficient of the n^{th} mode
ψ_{nb}	Branch circumferential coefficient of the n^{th} mode
η	Loss factor of the pipe
η_d	Loss factor of the damping material
η_z	Loss factor of the PZT material
$\delta(\ )$	Delta function
Λ	Free piezoelectric strain

LIST OF FIGURES

LIST OF TABLES

CHAPTER 1

INTRODUCTION

1.1 Introduction

In many processing and chemical industries, and in ships and aircraft, pipework is important for transporting fluids, for example gas, cooling water and hydraulic fluid. A piping system can be excited by many sources connected to the structure such as compressors, pumps, or valves. The resulting vibration, which is transmitted along the pipe in form of a propagating wave, can also excite other equipment attached to the structure. Excessive vibration may lead to fatigue and cause damage to the system. Hence, it is desirable to control the vibration of the pipe.

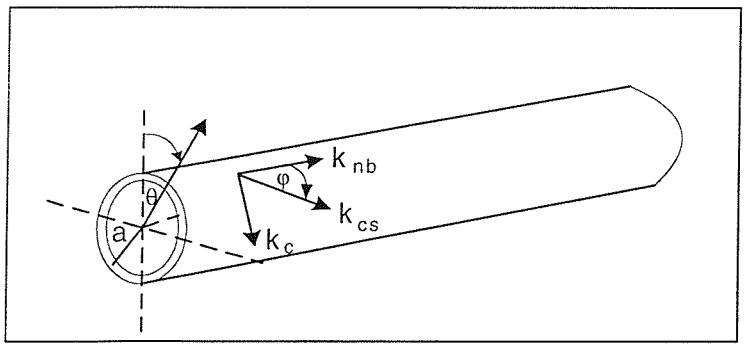

Figure 1.1: Diagram showing axial, circumferential and helical wavenumbers of an *in-vacuo* pipe

It is well-known that the motion of a pipe is complicated since its structure is three dimensional. For a thin-walled pipe, structural waves propagate in a helical pattern,

and can be represented by the wavenumber, k_{cs}, as shown in the figure 1.1 (Fahy [1]). The wavenumber of the helical wave, k_{cs}, is the vector combination of the wave components in the axial and circumferential directions, and is given by

$$k_{cs}^2 = k_{nb}^2 + k_c^2$$

where k_{nb} is the axial wavenumber and

k_c is the circumferential wavenumber.

The axial wavenumber is thus given by

$$k_{nb} = \sqrt{k_{cs}^2 - k_c^2}$$

It can be seen that k_{nb} is only real and hence propagating when $k_{cs}^2 \geq k_c^2$. Otherwise, the wave is evanescent.

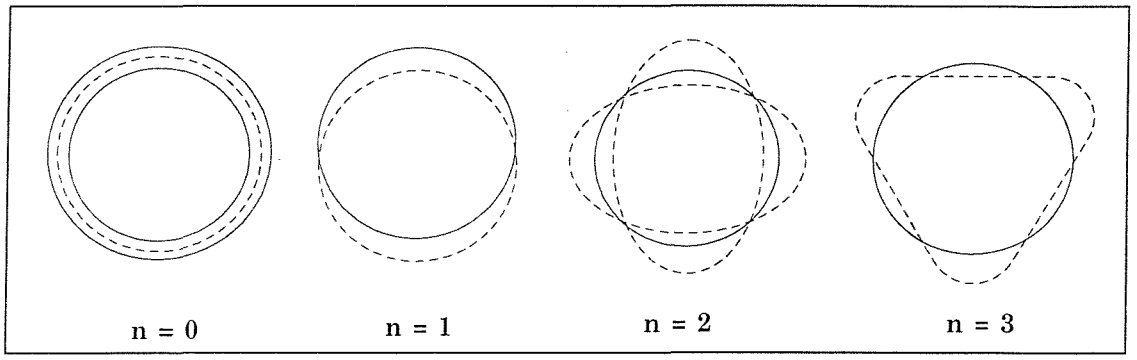

Figure 1.2: Mode shapes of a pipe.

Due to the closure of the pipe in the circumferential direction, the wave propagation must be continuous in this direction and hence, the circumferential characteristic takes the form of sine or cosine functions of $k_c a\theta$, where $k_c = n/a$; n is the mode number, a is the radius of a pipe and θ is the angle between the wavevectors. With the form of such a function in the circumferential direction, for the n = 0 mode (also known as the breathing mode) there is only stretching or contracting of the pipe wall. For the n = 1 mode called the bending mode, the pipe cross section is undeformed, and at n = 2 or

higher mode the pipe changes in shapes as shown in figure 1.2. Once the mode shapes are formed around the pipe, they are conveyed along the pipe by the axial waveguide.

With an *in-vacuo* pipe, there are eight axial waves that can potentially propagate along the pipe at any frequency for each circumferential mode as shown in figure 1.3. Four waves propagate in an upstream direction and another four waves propagate in a downstream direction. For the n = 2 mode, below the ring frequency (when the wavelength of a longitudinal wave is equal to the pipe circumference) in the downstream direction, there is a flexural propagating wave (b = 1), a near field wave (b = 2), and a decaying standing wave, which is a combination of two waves (b = 3 & 4), which are equal in amplitude but different in phase. Since the near field and standing near field waves are evanescent, only the flexural wave travels along the pipe. Because of this behaviour, the active control system considered in this thesis is designed to suppress this wave.

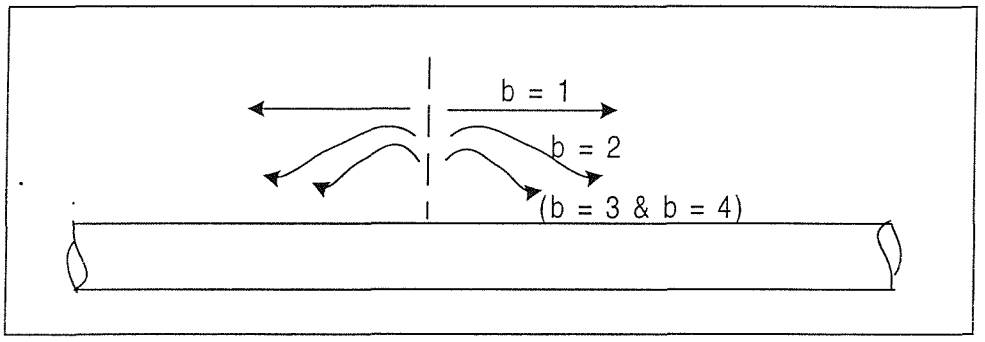

Figure 1.3: Propagating waves of an infinitely long pipe.

There are many shell theories based on the strain at a point to explain the motion of a pipe wall but none of these theories is universally accepted due to small differences between them. This arises from the different assumptions. Usually, most theories are based on the assumption of zero normal shear strain. Nowadays, the versions of shell theories generally used by researchers are Donnell-Mushtari, Love (Leissa [2]), Timoshenko [3], Kennard [4], and Flugge [5].

Most of the literature discusses pipes containing fluid, for example papers by Pavic [6], Pinnington and Briscoe [7] and Brennan *et al* [8]. The authors have concentrated on the

n = 0 mode (breathing mode) because of the coupling between the fluid and structure. Apart from the n = 0 mode, Fuller [9] has also considered higher order modes and showed that the fluid acts as a mass loading effect on these modes.

Unlike fluid-filled pipes, there has been relatively little work concentrating on the active control of vibrations in *in-vacuo* pipes, which is the objective of this thesis. Without the fluid, the pipe motion is generally dominated by the n = 1 and n = 2 modes at low frequencies (normally below 1 kHz). The low frequency dynamic behaviour of the n = 1 mode is similar to that of the beam, and hence the active control of this wave is similar to that of controlling beam vibration, and this has seen much development (Mace [10] and Brennan *et al* [11]). Hence, the work in this thesis concentrates on the development of a control strategy for the n = 2 mode.

In general, there are three established means used to suppress vibration. These are passive, semi-active (or adaptive-passive) and active control (Mead [12]). Passive control involves modification of the stiffness, mass and damping of the vibrating structure to make the structure less responsive to an excitation force. Semi-active control involves passively generating a secondary force, by actively changing the properties of the structure, such as the stiffness and damping. For a pipe, both approaches should be effective at the cut-on frequency of a wave where maximum vibration occurs, and the damping dominates (Hagood and von Flotow [13]). On the other hand, an active vibration control system requires an external energy source to supply or absorb energy from the structure as appropriate. This control approach is more effective in suppressing an unwanted disturbance because of its ability to control over a broadband frequency range, and this strategy is chosen in this thesis for cancelling the flexural wave of the n = 2 mode. However, this control strategy risks spillover due to unobserved modes excited by the control system (Fuller and Brevart [14]). To avoid this, a modal sensor and a modal actuator are used in the system to selectively sense and actuate a particular mode.

The development of an active control system to control the pipe motion may be divided into two parts. The first part involves the analysis of the physical system. This includes

the way in which the modal sensor and the modal actuator couple into the dynamics of the structure and the determination of the behaviour of the system when the control system is implemented. The second part involves the development of the electronic control system, which needs to be designed to implement the theory. This thesis is primarily concerned with the first part; the analysis of the dynamic behaviour of the system.

1.2 Literature Review

1.2.1 Modelling Pipe Vibration

There have been many researchers working on the equations of motion for a cylindrical shell. In contrast to the classical equation of motion for a beam or a plate having a single fourth order differential equation, a number of equations for the pipe have been derived because of slightly different simplifying assumptions. Most theories are based on the assumption of zero normal shear strain. The well-known shell theories were collected and extensively summarised by Leissa [2]. In order to make a comparison, he analysed various aspects such as a frequency parameter and the amplitude ratio of axial and circumferential displacements to radial displacement. He concluded that the theories are consistent to within a few percent. Similar to Leissa's work, Zhang *et al* [15] has recently compared a few shell theories using the frequency parameter. Nowadays, the versions of shell theories are generally referred to as Donnell-Mushtari (Leissa [2]), Love (Leissa [2]), Timoshenko [3], Kennard [4] and Flugge [5]. In this thesis, Flugge's shell theory is used in the analysis of the pipe behaviour.

Probably, the most convenient way to investigate the dynamic behaviour of the pipe is to examine a wave propagating axially in the pipe, described by an axial wavenumber or wave speed. In order to explain the dynamic behaviour of the pipe in a simple way, Lin and Morgan [16] used the concept of a rigid tube and an infinitely flexible tube to construct a curve of phase velocity in the axial direction. With this curve, they

concluded that all the modes except the first two modes have a minimum cut-on frequency and the first two modes exist at all frequencies. A more explicit explanation was provided by Cremer and Heckl [17], in which the curve of the phase velocity in the axial direction was calculated from Kennard's shell theory. By comparing this with the phase velocity of a simple structure, they explained the behaviour of the pipe in terms of a bar, a beam and a plate. However, both pieces of work were limited as they considered only real wave types. A complete set of dispersion curves was presented by Fuller and Fahy [18] based on Donnell-Mushtari shell theory. All of the wave types were considered and discussed in their paper. They demonstrated that there are also complex wave types, which combine to give a standing near field wave. Nevertheless, the wavenumbers given in their work are complicated and difficult to interpret. In order to provide a simple physical interpretation, Brennan *et al* [19] employed a complete set of dispersion curves along with Heckl's concept. They discussed the behaviour of individual waves propagating along the shell in terms of flexural beam-like, plate-like bending, longitudinal and shear waves. Recently, Finnveden [20] described the pipe as being equivalent to the model of Timoshenko beam on a Winkler foundation. With this analysis, the wavenumber for a propagating wave of the $n \geq 1$ modes of the pipe was established in a simple form and it was shown to depend on an equivalent mass and a spring constant for the Winkler foundation. It was clearly illustrated that before the wave cuts on the stiffness dominates the pipe behaviour resulting the wave type being a standing near field and after the wave cuts on the equivalent mass influences the resulting flexural wave. However, such a model is valid only at low frequencies and for a few circumferential modes.

There has been much discussion in the literature regarding the way of describing the motion of a pipe. In the case of an infinitely long pipe, most researchers have dealt with the problem in a similar way. They have used the Fourier series to describe the axial, circumferential and radial displacements in the wavenumber domain and the use of the Residue method for Fourier inversion into the spatial domain. Such work has been done by Franken [21], Heckl [22], Fuller [9] and Brevart and Fuller [23]. Unlike the infinite pipe, the derivation for a semi-infinite pipe can analysed in a straight-forward manner using four boundary conditions. Such work has been done by Flugge [5] and Vinson [24]. Young [25] and Pan and Hansen [26] extended the solution into a general form for any

excitation position by adding the condition of motion continuity at the point of excitation.

1.2.2 Vibration Control

1.2.2.1 Actuators for Active Control

In recent years, the application of piezoelectric actuators for active vibration control purposes has been increasing due to the attractive property of piezoelectric material in that it is able to convert electrical to mechanical energy. In addition, it is relatively lightweight, can be tailored into shapes (Morgan Martoc [27]), and can be readily integrated into a structure without changing the mechanical properties of the system.

Nowadays, two commercially produced types of piezoelectric materials are PZT (lead zirconate titanate) and PVDF (polyvinylidene fluoride). Because it is easily shaped, much effort has been concentrated on developing PVDF as an actuator. Such applications on beams and plates have been reported by Burke and Hubbard, Jr [28], Lee [29] and Lee and Moon[30], and on pipes by Tzou [31] and Sung *et al* [32]. However, this type of piezoelectric material is not very suitable for actuator applications as stated by Brennan *et al* [33]. This is because it has relatively low stiffness, which does not facilitate effective mechanical coupling to the structure, and small dielectric constant (d_{31}), which implies that it needs a high applied voltage as reported by Tani *et al* [34] and Qiu and Tani [35]. Having high stiffness and high dielectric constant, PZT is more appropriate for actuator applications. The analysis of the coupling between PZT and a beam was first developed by Crawley and de Luis [36], and later Crawley and Lazarus [37] extended it to the plate. In their analysis, the assumptions of linear strain across the thickness of the structure and uniform strain across the PZT carried by a shear stress in the bonding layer to induce the bending of the structure surface. Another two important pieces of work on PZT/plate coupling were conducted by Dimitriadis *et al* [38] and Kim and Jones [39]. Dimitriadis *et al* made the assumption of a perfect bonding

(zero bonding layer thickness), linear strain distribution through the thickness of the composite and constant stress slope. However, Kim and Jones argued that the last assumption causes an underestimation of the effective moment. They also contested that the uniform strain across the piezoelectric layer assumed by Crawley and de Luis and Crawley and Lazarus, overestimates the effective moment. Therefore, they used the assumption of the constant strain slope over the thickness of the composite in their analysis. Actuator applications on a finite pipe such as the work done by Lester and Lefebvre [40] and Lalande at al [41] used a pair of PZT elements bonded on the opposite sides of the pipe (inside and outside) to generate a pure moment and a pure in-plane force. However in reality, it is difficult to locate the PZT elements on both sides (inside and outside) of the pipe.

1.2.2.2 Sensors for Active Control

The modal sensor was first introduced by Lee and Moon [30], who applied it to a beam, and included an analysis of the modal sensor for a plate as well. It was extended in theory and practice for a plate by Gu *et al* [42]. The analysis of a PVDF sensor bonded to a shell was developed by Tzou [31]. The effects of many factors to the output of the segmented PVDF, i.e. thickness of the PVDF and shell, the curvature of the shell, were investigated by Tzou and Bao [43]. However, the sensors in both pieces of work were not discussed in the context of a modal sensor. Since the circumferential mode shapes of a pipe are in the form of sine and cosine functions, then from the work by Lee and Moon [30], the shapes of the modal sensors should take the form of sine and cosine functions as well. The modal sensor for an infinitely long pipe following such shapes were used in the work of Fuller and Brevart [14]. Since the shapes of the modal sensors need to be accurate, otherwise they cannot be used in an active control system to completely cancel undesired modes, Callahan and Baruh [44] preferred to use segmented PVDF elements (rectangular shape) with a sensor output cancellation technique. By using a number of sensors and decreasing the magnitude of the real part of the observer gain, then the sensor output converges to the desired mode. However, this method risks the ill-conditioning of the modal coordinate matrix and it takes some time to converge to the desired mode. Therefore, the modal sensor for the pipe in the work reported here still

uses PVDF in the form of sine and cosine functions. The main aim of this work is to investigate the use of a distributed sensor to discriminate against the n = 2 circumferential propagating mode in a pipe.

1.2.2.3 Active Vibration Control of Pipe Vibration

Nowadays, there is much research into active control. It uses a secondary source to suppress the unwanted disturbance. In active noise control, the secondary sources are generally loudspeakers, and in active vibration control, the actuator producing forces or moments is the secondary source. The active control of noise is possibly the earliest work in this field suggested by Leug nearly sixty years ago (Guicking [45]). However, its implementation was far in advance of the technology available at the time. Recently, fast microprocessors have been developed, and this has resulted in the dramatic growth of research in this field, which has been reported by Nelson and Elliott [46]. Even though active noise control has been well developed, active vibration control had been less so until Bailey and Hubbard [47] introduced the piezoelectric actuator to this field. They used actuators bonded to a cantilever beam in a feedback control system.

For a structure having infinite length, the dynamic behaviour of the system should be described by a wave model rather than a modal model. Normally, the control strategy is to suppress a wave propagating along the structure such as longitudinal, torsional and flexural. Much research has been conducted on the active control of waves on a beam such as Mace [10], Brennan *et al* [11], Scheuren ([48] and [49]). The strategy has been to use the secondary source to generate a force and moment to control the flexural wave. Apart from the flexural wave, Pan and Hansen [50] have also used an active system to control torsional and longitudinal waves travelling on a beam.

For the infinite pipe, there has been some work using active vibration control of propagating waves. With a fluid-filled pipe, there is also a propagating acoustic wave. In this application, the researchers have normally used the active system to control the

vibration of the n = 0 mode because of the coupling between the fluid and the pipe, which causes most of the energy to be carried in the acoustic wave (Fuller [9]). The researchers working on this application have been Fuller and Jones [51], Harper and Leung [52], and Brennan *et al* [8]. Later, Brevart and Fuller [23] extended their work to control the vibration of the fluid-filled pipe and *in-vacuo* pipe for the n = 0 and n = 1 modes. They numerically evaluated the effectiveness of control for individual modes in terms of the transmission loss. This work was extended again with more secondary sources, and more simultaneously controlled modes (n = 0 - 2 modes) by Fuller and Brevart [14]. Active control of the *in-vacuo* pipe has also been investigated by Hansen and Young [53], and Pan and Hansen [26].

1.2.2.4 Passive Vibration Control

Passive vibration control techniques have been known for decades for their ability to suppress vibration. Many researchers prefer this approach because the system is normally simple and is always stable. Generally, it involves the addition or removal of mass, damping and stiffness. Damping is used to dissipate vibration energy, and mass and stiffness are used to change natural frequencies. For a finite structure, a modal point of view is generally adopted, while the wave point of view is appropriate for an infinite structure. There are many control techniques for finite structures such as damping treatment, adding of stiffeners etc as described by Mead [12]. For the control of the waves, stiffness is employed to reflect waves, reducing power transmission along the structure. To do this, a discontinuous section, whose stiffness is different from the main structure, is normally inserted. Cremer and Heckl [17] have investigated this control strategy for longitudinal waves on a bar and flexural waves on a beam. They conducted analysis for various geometries. Mace [54] has also analysed the beam for a change in section. The tunable absorber has been used by Brennan [55] to change the dynamic stiffness at the discontinuity.

For passive control of an infinite pipe, Harari [56] has investigated the reflection and transmission of waves using stiffeners for the discontinuity. Fuller [57] has also

analysed the attenuation of waves by using a step discontinuity in wall thickness. These results have been used in later work done by Fuller and Brevart [14]. Munjal and Thawani [58] have used a flexible hose as the discontinuous section and investigated the transmission loss with the different changes of the properties of this section.

1.2.2.5 Semi-active Control Using a PZT Shunt

Recently, semi-active control of vibration has been growing in interest. This is because it combines the advantage of passive and active control, which are a stable system and the ability to change its properties in real-time.

Typical research using semi-active control has involved a hydraulic vibration absorber as described by Patter *et al* [59], and electrorheological fluids as described by Choi *et al* [60]. The use of a PZT element in a semi-active system has been considered after Hagood and von Flotow [13] provided the first analysis of a PZT element shunted with passive networks. They showed that the dynamic properties of a PZT element with a shunt such as the Young's modulus and the damping can be changed. Using a resistance, R, connected in series with an inductance, L (a series L-R circuit), and connected in parallel with a piezoelectric capacitance as a resonant circuit, they pointed out that the system is analogous to a tuned mass damper. In order to make an on-line change of the PZT properties, Hagood and Crawley [61] used a synthetic inductor in which the inductance can be adjusted by using a feedback system. The use of a series L-R circuit rather than parallel L-R circuit for a shunt was argued by Wu [62], and Wu and Bicos [63] becuase the inherent resistance of the inductor should be taken account. Hence, they used a parallel L-R circuit in their work. Like Hagood and von Flotow, they analysed the optimum shunt resistance and tuning inductance based on the tuned mass damper. Other research based on this analogy is the work done by Hollkamp and Starchville [64], and Davis and Lesieutre [65]. Most of the research on shunted PZT elements has been reviewed and discussed by Tang *et al* [66], and Lesieutre [67].

1.3 Contribution of this Thesis

The main objective of this thesis is to suppress the vibration of the n = 2 mode of an *in vacuo* pipe by means of an active control system using a modal sensor and modal actuator. The sensor and actuator are designed to selectively sense and actuate this mode. This application of using the n = 2 modal sensor and the n = 2 modal actuator for the active control of the pipe is new. Although the n = 2 modal sensor was used in the work done by Fuller and Brevart [14], its analysis is original. The design of the modal actuator for a pipe using discrete PZT elements is also a new concept.

The work in this thesis on passive and semi-active control of an infinite pipe has been conducted so that their performance can be compared with that of active control. For passive control of an infinite pipe, the attenuation of a propagating wave can be achieved by reflection at a discontinuous section. Some prior work by Fuller [57], Munjal and Thawani [58] for example, have considered this section as a homogeneous section but in this thesis a composite section is used.

The main contributions in this thesis are as follows:

- Derivation of a simplified characteristic equation of the pipe leading to the cut-on frequency and wavenumber
- Derivation of mobility expressions for an infinite pipe using an Analytical approach, while that analysed by the Residue method is extended from Fuller's work [9].
- Derivation of mobility expressions for a semi-infinite pipe using the Wave method.
- Simplified mobility expressions for an infinite pipe
- Simplified mobility expressions for a semi-infinite pipe
- Analysis of a modal sensor for the circumferential mode of the pipe
- The predicted response of an infinite pipe excited by the PZT actuator
- Design and analysis of a PZT modal actuator.

- Analysis of the wave motion of an infinite pipe having a composite section.

1.4 Thesis Outline

The thesis is organised as follows. In chapter 2, the dispersion equation based on Flugge's shell theory is simplified. This is done with the assumption that the wall thickness is thin, the frequency range of interest is below the ring frequency and the axial wave with a very long wavelength is neglected. Further analysis shows that the wavenumber of the pipe for the n = 0 and n = 1 mode can be represented by that of the simple structure such as a bar, a shaft and a beam.

The mobility of an infinite pipe is developed in chapter 3. It is derived using two methods, the Residue and Analytical methods, which act as a check on each other. Simplification of the mobility expression at low frequencies is also conducted.

Like the infinite pipe, the mobility of a semi-infinite pipe is also derived by using the two methods and is presented in chapter 4. These are the Analytical and Wave methods. The mobility expression is also simplified at low frequencies.

In chapter 5, the modal sensor is introduced. It is shaped from PVDF sheet so that its area has the form of sine and cosine functions, which are the shapes of the desired mode of the pipe to sense. With these shapes, a general expression of a circumferential mode sensor is derived.

The modal actuator, which consists of a set of PZT elements, is described in chapter 6. In this chapter, forces and moments generated from a single PZT element bonded on the pipe are derived, and are based on the assumptions made by Kim and Jones [39] with perfect bonding. The frequency response function of an infinite pipe excited by a single

PZT actuator is formulated and finally four PZT elements are applied to form a modal actuator for the n = 2 circumferential mode of the pipe.

With the combination of the modal sensor and the modal actuator, the active control system is established and is discussed in chapter 7. In this system, the n = 2 modal sensor is used as an error sensor and the n = 2 flexural wave is controlled by the n = 2 modal actuator.

Chapter 8 discusses passive and semi-active vibration control. For passive control, an infinite pipe with a composite pipe section formed by an unconstrained-layer damping is investigated. Its motion is predicted using the Analytical and Wave methods. For semi-active control, a PZT element shunted with a parallel L-R circuit (L is inductance and R is resistance) is used to control the pipe motion. The aim of investigating these control strategies is only for comparison with the active control system developed.

The three control strategies are summarised in chapter 9, and a comparison of passive, semi-active control and active control is presented. Some recommendations for further work are also suggested.

CHAPTER 2

DISPERSION CHARACTERISTICS OF *IN-VACUO* PIPES

2.1 Introduction

It was mentioned in chapter 1 that the objective of the thesis is to control vibration of an *in-vacuo* pipe using an active control system. However, before the control system can be employed, a thorough understanding of the behaviour of the pipe is needed since it is critical in an investigation of active vibration control applied to the pipe.

It is well-known that the dynamic behaviour of a pipe is complicated since its structure is three-dimensional. An investigation of its wavenumbers is a way to understand pipe behaviour, and has been conducted by Lin and Morgan [16], Cremer and Heckl [17], Fuller and Fahy [9], Brennan *et al* [19], and Finnveden [20].

In this chapter, a study of the dispersion characteristics of an *in-vacuo* pipe is conducted. To enable greater understanding, the wavenumbers are derived in terms of simple structural waves such as longitudinal, torsional, and flexural waves. However, before the wavenumber analysis can be done, the shell theory has to be simplified. A simplified theory is developed using Flugge's shell theory as a basis with some additional assumptions.

2.2 Simplified Version of Flugge Shell Theory *in vacuo*

Due to the complicated form of shell theories, it is difficult to apply them to the vibration problem of an infinitely long pipe, i.e. it is difficult to derive simple expressions for the dispersion relationships and for the point/transfer mobilities of a pipe. Thus, in this section the intention is to derive a simple form of the dispersion equation based on Flugge's shell theory. Once the simplified equation has been established, the relatively simple formula for the mobility of a pipe can be determined. In the derivation, it is assumed that the wall thickness is thin compared to the radius of the pipe, the frequency range of interest is below the ring frequency (when the wavelength of a longitudinal wave is equal to the pipe circumference) and the increasing non-dimensional axial flexural wavenumber after the wave cuts on is much greater than the non-dimensional frequency, which is the frequency normalised to the ring frequency.

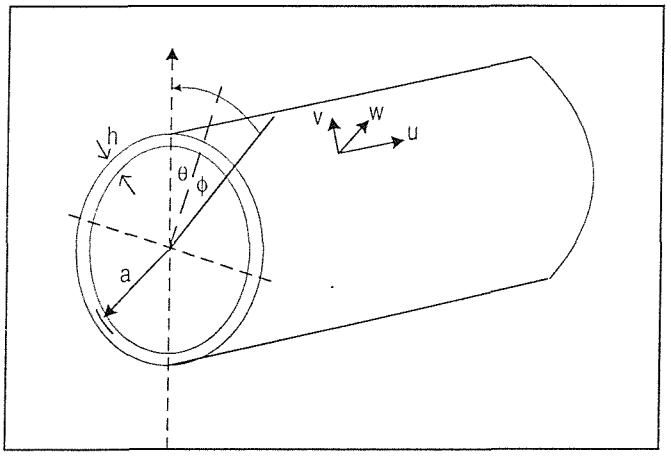

Figure 2.1: Cylindrical coordinate system for a pipe.

A schematic of the cylindrical coordinate system for the pipe of mid-surface radius a and wall thickness h is shown in figure 2.1. Since the circumferential reference position on a pipe is unknown, the orientation angle, ϕ, is defined. The equation of motion of free vibration of the pipe is given by (Flugge [5])

$$\begin{bmatrix} A_{11} & A_{12} & A_{13} \\ A_{21} & A_{22} & A_{23} \\ A_{31} & A_{32} & A_{33} \end{bmatrix} \begin{bmatrix} u \\ v \\ w \end{bmatrix} = \mathbf{0} \qquad \ldots(2.1)$$

where u is the axial component of the displacement,

v is the tangential component of the displacement,

w is the radial component of the displacement,

$$A_{11} = \left(\frac{\partial^2}{\partial s^2} + \frac{(1-\nu)}{2}\left(1+\beta^2\right)\frac{\partial^2}{\partial \theta^2} - \frac{\rho(1-\nu^2)a^2}{E}\frac{\partial^2}{\partial t^2} \right),$$

$$A_{12} = \left(\frac{(1+\nu)}{2}\frac{\partial^2}{\partial s \partial \theta} \right),$$

$$A_{13} = \left(\nu\frac{\partial}{\partial s} - \beta^2\frac{\partial^3}{\partial s^3} + \beta^2\frac{(1-\nu)}{2}\frac{\partial^3}{\partial s \partial \theta^2} \right),$$

$A_{21} = A_{12}$,

$$A_{22} = \left(\frac{(1-\nu)}{2}(1+3\beta^2)\frac{\partial^2}{\partial s^2} + \frac{\partial^2}{\partial \theta^2} - \frac{\rho(1-\nu^2)a^2}{E}\frac{\partial^2}{\partial t^2} \right),$$

$$A_{23} = \left(\frac{\partial}{\partial \theta} - \beta^2\frac{(3-\nu)}{2}\frac{\partial^3}{\partial s^2 \partial \theta} \right),$$

$A_{31} = A_{13}$,

$A_{32} = A_{23}$,

$$A_{33} = \left(1+\beta^2\nabla^4 + \beta^2 + 2\beta^2\frac{\partial^2}{\partial \theta^2} + \frac{\rho(1-\nu^2)a^2}{E}\frac{\partial^2}{\partial t^2} \right),$$

$$\nabla^4 = \frac{\partial^4}{\partial s^4} + \frac{\partial^4}{\partial \theta^4} + \frac{\partial^4}{\partial s^2 \partial \theta^2},$$

$s = x/a$ is the non-dimensional axial distance along the pipe,

$\beta = \dfrac{h}{a\sqrt{12}}$ is the wall thickness ratio of the pipe,

a is the radius of the pipe,

h is the thickness of the pipe,

E is the Young's modulus of the pipe,

ν is the Poisson's ratio of the pipe, and

ρ is the density of the pipe.

The solution of the equation of motion of an *in-vacuo* pipe may be written as (Variyart and Brennan [68])

$$
\begin{aligned}
u(s,\theta,t) &= \sum_{n=0}^{\infty}\sum_{b=1}^{8} \overline{\overline{U}}_{nb} \cos[n(\theta-\phi)]\, e^{j(\hat{k}_{nb}s-\pi/2-\omega t)} \\
v(s,\theta,t) &= \sum_{n=0}^{\infty}\sum_{b=1}^{8} \overline{\overline{V}}_{nb} \sin[n(\theta-\phi)]\, e^{j(\hat{k}_{nb}s-\omega t)} \\
w(s,\theta,t) &= \sum_{n=0}^{\infty}\sum_{b=1}^{8} \overline{\overline{W}}_{nb} \cos[n(\theta-\phi)]\, e^{j(\hat{k}_{nb}s-\omega t)}
\end{aligned}
\qquad \ldots(2.2)
$$

where n is the mode number,

b is the index for the waves,

$\hat{k}_{nb}$ is the non-dimensional branch axial wavenumber (the axial wavenumber multiplied by the radius of the pipe),

ω is the angular frequency,

$\overline{\overline{U}}_{nb}$ is the axial amplitude for the b^{th} wave of the n^{th} mode of the pipe,

$\overline{\overline{V}}_{nb}$ is the circumferential amplitude for the b^{th} wave of the n^{th} mode of the pipe,

$\overline{\overline{W}}_{nb}$ is the radial amplitude for the b^{th} wave of the n^{th} mode of the pipe,

ϕ is the azimuthal orientation angle and

θ is the azimuthal angle.

Equation (2.2) is a general form of the displacements in a pipe wall, consisting of an infinite number of circumferential modes. Since a pipe has eight propagating waves (b) for each mode (n), hence, the vibration of an individual mode is a combination of their

motion. In this equation, the orientation angle, ϕ, is used as the reference angle of a pipe.

Substitution of the displacements of equation (2.2) into the equation (2.1) yields

$$\begin{bmatrix} L_{11} & L_{12} & L_{13} \\ L_{21} & L_{22} & L_{23} \\ L_{31} & L_{32} & L_{33} \end{bmatrix} \begin{bmatrix} \overline{\overline{U}}_{nb} \\ \overline{\overline{V}}_{nb} \\ \overline{\overline{W}}_{nb} \end{bmatrix} = \mathbf{0} \qquad \ldots(2.3)$$

where $L_{11} = \hat{k}_{nb}^2 + \frac{(1-\nu)}{2}(1+\beta^2)n^2 - \Omega^2$

$L_{12} = \frac{(1+\nu)}{2} n\hat{k}_{nb}$

$L_{13} = \nu\hat{k}_{nb} + \beta^2\hat{k}_{nb}^3 - \frac{(1-\nu)}{2}\beta^2 n^2 \hat{k}_{nb}$

$L_{21} = L_{12}$

$L_{22} = \frac{(1-\nu)}{2}(1+3\beta^2)\hat{k}_{nb}^2 + n^2 - \Omega^2$

$L_{23} = n + \frac{(3-\nu)}{2}\beta^2 n\hat{k}_{nb}^2$

$L_{31} = L_{13}$

$L_{32} = L_{23}$

$L_{33} = 1 + \beta^2 + \beta^2(\hat{k}_{nb}^2 + n^2)^2 - 2\beta^2 n^2 - \Omega^2$

$\Omega = \omega/\omega_r$ is the frequency normalised to the ring frequency, where

$\omega_r = \frac{1}{a}\sqrt{\frac{E}{\rho(1-\nu^2)}}$ is the ring frequency.

The non-dimensional wavenumber, $\hat{k}_{nb}$, of the thin-walled *in-vacuo* pipe can be determined from

$$|\mathbf{L}|_{nb} = 0 \qquad \ldots(2.4)$$

The determinant of matrix $[\mathbf{L}]_{nb}$ is arranged with terms involving β grouped together, and since for a thin pipe $\beta^2 << 1$, then the higher order terms of β (i.e. β^4 and β^6) can be neglected. Thus, the determinant of the matrix $[\mathbf{L}]_{nb}$ becomes

$$\frac{1}{8}\beta^2\Big[\Big\{4(1-\nu)(\hat{k}_{nb}^2+n^2)^2(\hat{k}_{nb}^2+n^2-1)^2+8(1-\nu)^2\left(\hat{k}_{nb}^4-n^2\left(n^2-1\right)\right)\hat{k}_{nb}^2+12(1-\nu)^2(1+\nu)\hat{k}_{nb}^4\Big\}$$
$$-\Omega^2\Big\{4(3-\nu)(\hat{k}_{nb}^2+n^2)(\hat{k}_{nb}^2+n^2-1)^2+4(1-\nu)(\hat{k}_{nb}^2+n^2)(\hat{k}_{nb}^2+n^2+1)+8(1-\nu)(4\hat{k}_{nb}^2+1)\hat{k}_{nb}^2\Big\}\Big]$$
$$-\frac{1}{2}\Omega^2\Big[(1-\nu)(\hat{k}_{nb}^2+n^2)(\hat{k}_{nb}^2+n^2+1)+2(1-\nu^2)\hat{k}_{nb}^2\Big]+\frac{1}{2}(1-\nu)^2(1+\nu)\hat{k}_{nb}^4+\frac{1}{2}(3-\nu)(\hat{k}_{nb}^2+n^2)\Omega^4$$
$$+\Omega^4-\Omega^6 \;=\; 0 \qquad \ldots(2.5)$$

Apart from the assumption of $\beta^2 << 1$, another assumption that can be made is that $1/\hat{k}_{nb}^2 >> \beta^2$. This is reasonable for a thin walled pipe since $\beta^2 \approx 2.1\text{x}10^{-4}$ for h/a = 0.05 while $\hat{k}_{nb}$ increases from zero to about 6 in the non-dimensional frequency range of zero to one (provided by the dispersion curve presented in the next section). Since $\hat{k}_{nb} = 2\pi a/\lambda_{nb}$, where λ_{nb} is a branch axial wavelength, and $\beta = h/\sqrt{12}\,a$, the assumption can be expressed as, $\lambda_{nb} >> \pi h/\sqrt{3} \approx 2h$. Physically, this implies that waves with an axial wavelength smaller than about two times of the wall thickness are neglected. Since at higher frequencies the waves have smaller axial wavelengths, the above assumption also means that the very high frequency range is neglected.

By applying this assumption in the frequency range below the ring frequency, the terms containing the product of $\beta^2\,\Omega^2$ can be neglected in comparison with the terms that does not contain β^2. Hence equation (2.5) becomes

$$\frac{1}{2}\beta^2\Big[(1-\nu)(\hat{k}_{nb}^2+n^2)^2(\hat{k}_{nb}^2+n^2-1)^2+2(1-\nu)^2\left(\hat{k}_{nb}^4-n^2\left(n^2-1\right)\right)\hat{k}_{nb}^2\Big]$$
$$-\frac{1}{2}\Omega^2\Big[(1-\nu)(\hat{k}_{nb}^2+n^2)(\hat{k}_{nb}^2+n^2+1)+2(1-\nu^2)\hat{k}_{nb}^2\Big]+\frac{1}{2}(1-\nu)^2(1+\nu)\hat{k}_{nb}^4 \qquad \ldots(2.6)$$
$$+\frac{1}{2}(3-\nu)(\hat{k}_{nb}^2+n^2)\Omega^4+\Omega^4-\Omega^6 \;=\; 0$$

Below the ring frequency, the above equation can be used to determine the frequency characteristics of the pipe for any circumferential mode. However, it is still complicated even though it has been simplified.

Applying the assumption of $\hat{k}_{nb}^2 >> \Omega^2$ as used by Heckl [22], equation (2.6) can be greatly simplified. This assumption physically means that the motion with very long axial wavelengths does not contribute greatly to the overall motion of the pipe. In reality, this assumption is not true around the cut-on frequencies since $\hat{k}_{nb}$ is zero, when Ω has a value between zero and one. The assumption requires the condition of $\frac{\partial \hat{k}_{nb}}{\partial \Omega} > 1$ just after the wave has cut-on. Thus, it affects the longitudinal and torsional waves ($\hat{k}_{nb}$ is proportional to Ω for n = 0). So, this assumption can only be applied for the $n \geq 2$ modes below the ring frequency. It was pointed out by Cremer (Heckl [22]) that this assumption does not result in large errors. With no knowledge of the axial wavenumbers around the cut-on frequency, the last three terms containing Ω^4 and Ω^6 in equation (2.6) including the term of $(1-\nu^2)\hat{k}_{nb}^2\Omega^2$ can be neglected in comparison with the term of $\frac{1}{2}(1-\nu)^2(1+\nu)\hat{k}_{nb}^4$. The term of $(1-\nu)^2\beta^2\left[\hat{k}_{nb}^4 - n^2\left(n^2-1\right)\right]\hat{k}_{nb}^2$ can also be neglected using the previous assumption of $1/\hat{k}_{nb}^2 >> \beta^2$. Therefore, at the frequencies below the ring frequency ($\Omega < 1$), for $n \geq 2$ equation (2.6) becomes

$$\frac{1}{2}\beta^2(1-\nu)(\hat{k}_{nb}^2+n^2)^2(\hat{k}_{nb}^2+n^2-1)^2 - \frac{1}{2}\Omega^2(1-\nu)(\hat{k}_{nb}^2+n^2)(\hat{k}_{nb}^2+n^2+1) + \frac{1}{2}(1-\nu)^2(1+\nu)\hat{k}_{nb}^4 = 0 \qquad \ldots(2.7)$$

This can be rearranged to give the relationship between the non-dimensional frequency and the axial wavenumber.

$$\Omega^2 = \frac{\beta^2(\hat{k}_{nb}^2+n^2)^2(\hat{k}_{nb}^2+n^2-1)^2 + (1-\nu^2)\hat{k}_{nb}^4}{(\hat{k}_{nb}^2+n^2)(\hat{k}_{nb}^2+n^2+1)} \quad ; n \geq 2 \qquad \ldots(2.8)$$

The first term on the right hand side of equation (2.8) is related to membrane strain energy and the second term is related to strain energy of the pipe-wall flexure (Fahy [1]).

The cut-on frequencies of a circumferential mode of an infinitely long pipe, Ω_{co}, can be determined from the equation (2.8) by setting $\hat{k}_{nb} = 0$, which corresponds to an infinitely long axial wavelength. Therefore,

$$\Omega_{co}^2 = \frac{\beta^2 n^2 (n^2 - 1)^2}{n^2 + 1} \qquad \ldots(2.9)$$

The cut-on frequencies given in the above equation is similar to that reported by Pavic [6] and Finveden [20], and is compared with other formulae for cut-on frequencies found in the literature in section 2.4.

2.3 Wavenumber Solutions of a Pipe *in vacuo*

Many researchers such as Cremer and Heckl [17], Fuller and Fahy [9], and Brennan *et al* [19] have described the dynamic behaviour of a pipe at low frequencies to be similar to a membrane for the n = 0 mode and to be similar to a beam for the n = 1 mode. Such a statement comes from comparing the plot of the phase velocity or the wavenumber of the pipe with that of a bar, a shaft, and a beam. In this section, the axial wavenumbers for the n = 0 and n = 1 modes are derived in terms of the wavenumbers of those simple structures to explicitly support the above statement.

As described in the previous section, the characteristic equation of the n = 0 and n = 1 modes of a pipe is given by equation (2.6) and the characteristic equation of the n ≥ 2 modes is given by equation (2.7). In order to obtain the wavenumbers, the roots of the characteristic polynomial of both equations are found using a similar approach to that

taken by Young [25]. Even though the characteristic equation of the pipe has been simplified, the wavenumber solutions for each mode remain rather complicated. To obtain them in a similar form with more physical meaning, further simplification is carried out using some additional assumptions; i.e. (a) β^2 can be neglected compared to unity because it is much less than one, (b) higher order wavenumbers can be neglected when considering the small wavenumbers such as the longitudinal and torsional wavenumbers for the n = 0 mode and vice versa (Flugge [5]).

The characteristic equation of the pipe *in vacuo*, which is equation (2.6) for the n = 0 and n = 1 modes, and equation (2.7) for the n ≥ 2 modes, can be expressed as a polynomial of axial wavenumbers, $\hat{k}_{nb}$, as given by

$$g_8\hat{k}_{nb}^8 + g_6\hat{k}_{nb}^6 + g_4\hat{k}_{nb}^4 + g_2\hat{k}_{nb}^2 + g_0 = 0 \qquad \ldots(2.10)$$

where the g's are coefficients.

Solution of this equation leads to the eight-wavenumbers. However at low frequencies these can be divided into two groups. One group contains the four small wavenumbers known as the longitudinal and torsional wavenumbers for the n = 0 mode, flexural and near field wavenumbers for the n = 1 mode and the flexural plate-like propagate and near field for the n ≥ 2 modes. The other group contains the four large wavenumbers known as standing near field wavenumbers. Since they are obviously distinctive, Flugge [5] suggested that the small wavenumbers could readily be determined by neglecting higher orders and the above equation becomes the quadratic equation:

$$g_4\hat{k}_{nb}^4 + g_2\hat{k}_{nb}^2 + g_0 = 0 \qquad \ldots(2.11)$$

which gives the following wavenumbers

$$\hat{k}_{n1}^2,\ \hat{k}_{n2}^2 = \frac{1}{2g_4}\left[-g_2 \pm \sqrt{g_2^2 - 4g_0g_4}\right] \qquad \ldots(2.12)$$

By ignoring the lower orders of equation (2.10), the large wavenumbers can also be determined from the resulting quadratic equation:

$$g_8 \hat{k}_{nb}^4 + g_6 \hat{k}_{nb}^2 + g_4 = 0 \qquad \ldots(2.13)$$

which gives the wavenumbers

$$\hat{k}_{n3}^2,\ \hat{k}_{n4}^2 = \frac{1}{2g_8}\left[-g_6 \pm \sqrt{g_6^2 - 4g_4 g_8}\right] \qquad \ldots(2.14)$$

Since the above method depends on the distinction between the small and large wavenumbers, this method is useful for the first few circumferential modes of the pipe. However, for the higher modes, such a method can still be applied but is valid only just after the waves cut on where the flexural wavenumber is small.

The polynomial coefficients of axial wavenumbers, $\hat{k}_{nb}$, for the n = 0 and 1 modes can be obtained by expanding equation (2.6) into a polynomial with the form of equation (2.10) in which the terms containing $(n^2-1)n^2$ are set to be equal to zero. These are given as follows.

$$g_8 = \frac{(1-\nu)}{2}\beta^2$$

$$g_6 = (1-\nu)\left(2n^2 - \nu\right)\beta^2$$

$$g_4 = \frac{(1-\nu)}{2}\left(1 + \beta^2 - \nu^2 - \Omega^2\right) \qquad \ldots(2.15)$$

$$g_2 = -\frac{(1-\nu)}{2}\left[\left(2n^2+1\right) + 2(1+\nu)\right]\Omega^2 + \frac{3-\nu}{2}\Omega^4$$

$$g_0 = \frac{1}{2}\left[(3-\nu)n^2 - \left(n^2+1\right)n^2\Omega^2 + 2\left(1-\Omega^2\right)\right]\Omega^4$$

Axial wavenumbers of the n = 0 mode of *in-vacuo* pipes

For the n = 0 mode, the pipe behaves like a membrane, which supports longitudinal and torsional waves. To provide evidence for this argument, the axial wavenumber for this mode is derived in terms of these waves. The longitudinal (k_l) and torsional wavenumbers (k_s) are respectively given by (Fahy [1])

$$k_l^2 = \frac{\rho\omega^2}{E} \quad \text{and} \quad k_s^2 = \frac{\rho\omega^2}{G} \qquad \ldots(2.16\text{ a, b})$$

where $G = \frac{E}{2(1+\nu)}$ is the shear modulus.

To non-dimensionalise equation (2.16), the wavenumbers are normalised by the radius of the pipe, and are given by

$$\hat{k}_l^2 = \frac{\Omega^2}{1-\nu^2} \quad \text{and} \quad \hat{k}_s^2 = \frac{2\Omega^2}{1-\nu} \qquad \ldots(2.17\text{ a, b})$$

By neglecting β^2 in comparison with unity, the coefficients for the n = 0 mode given in equation (2.15) can be written in terms of the longitudinal and torsional wavenumbers as:

$$g_8 = \frac{(1-\nu)}{2}\beta^2$$

$$g_6 = -(1-\nu)\nu\beta^2$$

$$g_4 = \frac{(1-\nu)(1-\nu^2)}{2}\left(1-\hat{k}_l^2\right) \qquad \ldots(2.18)$$

$$g_2 = -\frac{(1-\nu)(1-\nu^2)}{2}\left[\left(1-\hat{k}_l^2\right)\left(\hat{k}_l^2+\hat{k}_s^2\right)+\nu^2\hat{k}_l^4\right]$$

$$g_0 = \frac{(1-\nu)(1-\nu^2)}{2}\left[1-\left(1-\nu^2\right)\hat{k}_l^2\right]\hat{k}_l^2\hat{k}_s^2$$

Solving for small wavenumbers using the quadratic equation (2.12) gives

$$\hat{k}_{01}^2 = \hat{k}_l^2 + \frac{\nu^2\hat{k}_l^4}{1-\hat{k}_l^2} \qquad \text{...(2.19 a, b)}$$
$$\hat{k}_{02}^2 = \hat{k}_s^2$$

Because at low frequencies, $\Omega^2 << 1$, the longitudinal wavenumber is small. Hence, the second term in equation (2.19 a) containing a power of 4 can be neglected in comparison with the first term, which gives

$$\hat{k}_{01}^2 = \hat{k}_l^2 \qquad \text{...(2.20 a, b)}$$
$$\hat{k}_{02}^2 = \hat{k}_s^2$$

as expected.

The wavenumbers of standing near field waves, which are large, can be found from the polynomial coefficients of g_8, g_6 and g_4 by solving the quadratic equation given in equation (2.14) and they are

$$\hat{k}_{03}^2, \hat{k}_{04}^2 = \nu \pm \sqrt{\nu^2 - \left(1-\nu^2\right)\left(1-\hat{k}_l^2\right)/\beta^2} \qquad \text{...(2.21 a, b)}$$

At low frequencies, the second term in the square root containing β^2 is much larger than the first term and hence, equation (2.21 a, b) becomes

$$\hat{k}_{03}^2, \hat{k}_{04}^2 = \pm j\sqrt{\left(1-\nu^2\right)\left(1-\hat{k}_l^2\right)/\beta^2} \qquad \text{...(2.22 a, b)}$$

Axial wavenumbers of the n = 1 mode of *in-vacuo* pipes

Using a similar approach to that used for the axial wavenumbers of the n = 0 mode, the wavenumbers of the n = 1 mode can be found. In this mode, the flexural wavenumber of the beam will be used to present the behaviour of the pipe, and is (Fahy [1])

$$k_b^4 = \frac{\rho A}{EI}\omega^2 \qquad \ldots(2.23)$$

where $A = 2\pi ah$ is the cross-sectional area of the pipe, and

$I = \pi ah\,(a^2 + \frac{h^2}{4})$ is the second moment of area of the pipe.

Normalised to the radius of the pipe, the non-dimensional flexural wavenumber of the beam is

$$\hat{k}_b^4 = \frac{2\Omega^2}{(1+3\beta^2)(1-\nu^2)} \cong 2\hat{k}_l^2 \qquad \ldots(2.24)$$

By substituting $\hat{k}_l$, $\hat{k}_s$ and $\hat{k}_b$ into equation (2.15) and neglecting β^2 in comparison with unity, the polynomial coefficients for the n = 1 mode can be written as

$$g_8 = \frac{(1-\nu)}{2}\beta^2$$

$$g_6 = (1-\nu)(2-\nu)\beta^2$$

$$g_4 = \frac{(1-\nu)(1-\nu^2)}{2}\left(1-\hat{k}_l^2\right) \qquad \ldots(2.25)$$

$$g_2 = -\frac{(1-\nu)(1-\nu^2)}{2}\left[\left(1-\hat{k}_l^2\right)\left(\hat{k}_l^2+\hat{k}_s^2\right)+\nu^2\hat{k}_l^4+\hat{k}_b^4\right]$$

$$g_0 = \frac{(1-\nu)(1-\nu^2)}{2}\left[\left\{1-\left(1-\nu^2\right)\hat{k}_l^2\right\}\hat{k}_l^2\hat{k}_s^2 + \left\{\hat{k}_s^2 + (1-\nu^2)\hat{k}_l^2\right\}\hat{k}_l^2 - \hat{k}_b^4\right]$$

Small wavenumber solutions of the n = 1 mode are obtained by solving the quadratic equation (2.12), which gives

$$\hat{k}_{l1}^2, \hat{k}_{l2}^2 = \frac{\left[(1-\hat{k}_l^2)(\hat{k}_l^2+\hat{k}_s^2)+\nu^2\hat{k}_l^4+\hat{k}_b^4\right] \pm \sqrt{\left[(1-\hat{k}_l^2)(\hat{k}_l^2-\hat{k}_s^2)+\nu^2\hat{k}_l^4\right]^2 + 4\hat{k}_b^4 - (1-\nu^2)\hat{k}_b^8}}{2(1-\hat{k}_l^2)}$$

...(2.26 a, b)

Since at low frequencies $\hat{k}_l^2$, $\hat{k}_s^2$ and $\hat{k}_b^4$ are less than unity, their higher order terms can be ignored and hence the wavenumbers may be approximated to

$$\hat{k}_{l1}^2, \hat{k}_{l2}^2 = \frac{1}{2(1-\hat{k}_l^2)}\left[(1-\hat{k}_l^2)(\hat{k}_l^2+\hat{k}_s^2)+\hat{k}_b^4 \pm 2\hat{k}_b^2\right] \qquad ...(2.27 \text{ a, b})$$

It can be seen that the wavenumbers, $\hat{k}_{l1}^2, \hat{k}_{l2}^2$, of the n = 1 mode of the pipe from the above equation is close to those of a Timoshenko beam (Brennan *et al* [19]).

When $\Omega^2 << 1$, equation (2.27) becomes

$$\hat{k}_{l1}^2, \hat{k}_{l2}^2 = \pm\hat{k}_b^2 \qquad ...(2.28 \text{ a, b})$$

Thus, at very low frequencies, the pipe behaves like a beam. The large wavenumbers of the n = 1 mode can also be determined by the quadratic equation (2.13) and are given by:

$$\hat{k}_{13}^2, \hat{k}_{14}^2 = -(2-\nu) \pm \sqrt{(2-\nu)^2 - \left(1-\nu^2\right)\left(1-\hat{k}_1^2\right)/\beta^2} \qquad \ldots(2.29\ a, b)$$

Again, at low frequencies the second term in the square root containing β^2 is much larger than the first term and therefore, equation (2.29) becomes

$$\hat{k}_{13}^2, \hat{k}_{14}^2 = \pm j\sqrt{\left(1-\nu^2\right)\left(1-\hat{k}_1^2\right)/\beta^2} \qquad \ldots(2.30\ a, b)$$

which are the same as the wavenumbers obtained for the n = 0 mode.

Axial wavenumbers of the n ≥ 2 mode of *in-vacuo* pipes

For the n = 2 mode, the polynomial coefficients can be obtained from equation (2.7), and are expressed as:

$$\begin{aligned}
g_8 &= \beta^2 \\
g_6 &= 2\beta^2\left(2n^2-\nu\right) \\
g_4 &= 6\left(n^2-1\right)n^2 + \left(1+\beta^2-\nu^2-\Omega^2\right) \qquad \ldots(2.31) \\
g_2 &= 2\left(2n^2-1\right)\left(n^2-1\right)n^2 - \left[\left(2n^2+1\right)+2(1+\nu)\right]\Omega^2 \\
g_0 &= \beta^2\left(n^2-1\right)^2 n^4 - \left(n^2+1\right)n^2\Omega^2
\end{aligned}$$

After the waves cut on, the flexural wavenumber increases rapidly with increasing frequency. Thus the flexural wavenumbers obtained by the method discussed above are limited to very low frequencies where they are small. Even though the near-field wavenumbers can still be obtained using the method, they are difficult to simplify unlike the n = 0 and n = 1 modes.

Hence, the wavenumber solutions for the $n \geq 2$ modes are better taken from equation (2.7) using the roots of the polynomial as discussed by Young [25].

2.4 Numerical Analysis to Evaluate the Simplified Version

To verify the simplified version of the characteristic equation of the *in-vacuo* pipe, it is compared in terms of cut-on frequencies from equation (2.9) with those obtained from Heckl [20], Kennard's shell theory (Leissa [21]), and Flugge's shell theory (Leissa [9]). The simplified model of the dispersion curve described in the previous section is also compared with that from Kennard's shell theory used by Brevart and Fuller [21], and from the original model based on Flugge's shell theory. The properties of the pipe used in the comparison are given in table 2.1. This is from the pipe used in the experimental work in this thesis which will be described later.

Table 2.1: PVC Pipe data

E (N/m^2)	ρ (kg/m^3)	ν	a (mm)	h (mm)
$3.974*10^9$	1460	0.33	33.2	2.2

Comparison of cut-on frequencies of the circumferential modes

The various frequency equations of the circumferential modes for infinitely long pipes are given as follows.

The frequency equation developed by Heckl [20] is

$$\Omega_{co}^2 = \beta^2 n^4 \left[1 - \frac{1}{2}\left(\frac{1}{1-\nu} \right)\left(\frac{4-\nu}{n^2} - \frac{2+\nu}{n^4} \right) \right], \qquad \ldots(2.32\ a)$$

by Kennard (Leissa [9]) is

$$\Omega_{co}^2 = \frac{1}{2}\left\{ \left[1 + \frac{2+\nu}{2(1-\nu)}\beta^2 + n^2 - \frac{4-\nu}{2(1-\nu)}\beta^2 n^2 + \beta^2 n^4 \right] \right.$$
$$\left. \mp \sqrt{1 + \frac{2+\nu}{1-\nu}\beta^2 + 2\left(1 - 3\beta^2\right)n^2 + n^4 + \frac{3(2-3\nu)}{1-\nu}\beta^2 n^4 - 2\beta^2 n^6} \right\}, \qquad \ldots(2.32\ b)$$

by Flugge's theory given by Leissa [9] is

$$\Omega_{co}^2 = \frac{1}{2}\left\{ 1 + n^2 + \beta^2\left(n^2 - 1\right)^2 \mp \sqrt{\left[1 + n^2 + \beta^2\left(n^2 - 1\right)^2 \right]^2 - 4\beta^2 n^2 (n^2 - 1)^2} \right\} \qquad \ldots(2.32\ c)$$

and in this thesis is given in the equation (2.9) as:

$$\Omega_{co}^2 = \frac{\beta^2 n^2 (n^2 - 1)^2}{n^2 + 1}$$

Taking the data of the pipe from table 2.1, the ring frequency of the pipe is

$$f_r = \frac{1}{2\pi a}\sqrt{\frac{E}{\rho(1-\nu)^2}}$$
$$= 8378 \text{ Hz.}$$

and the maximum number of circumferential modes below the ring frequency can approximately be determined by (Fahy [67])

$$n_r \cong \beta^{-1/2}$$

$$= 7$$

The cut-on frequencies of the modes below the ring frequency, which are calculated from the above frequency equations, are shown in table 2.2.

Table 2.2: Cut-on frequency of the circumferential modes according to various versions of the frequency equations.

Mode Number	Heckl	Kennard	Flugge	Equation (2.9)
2	417.43	430.08	430.02	430.05
3	1221.52	1216.67	1216.21	1216.36
4	2344.09	2333.57	2331.92	2332.26
5	3786.79	3775.41	3771.17	3771.76
6	5549.90	5541.24	5532.18	5533.10
7	7633.48	7631.43	7614.30	7615.60

Note: the cut-on frequencies for n = 0 and 1 modes are zero and Heckl's frequency equation is valid for $n \geq 2$.

Since Heckl's expression is developed from Kennard's shell theory (Heckl [20]), it is reasonable to compare his expressions with those of Kennard rather than the others. From the numerical results in table 2.2, the cut-on frequency obtained from Heckl's expression is close to that obtained from Kennard's shell theory at the higher modes but there is some difference at the lower modes. It is also shown in the table that the simplified expression derived in this thesis (equation 2.7) is in good agreement with the original model, Flugge's shell theory. The different cut-on frequencies obtained from Kennard's and Flugge's theories are because of the different assumptions used to derive the shell theory; for example Flugge [13] ignored transverse normal and transverse shear stresses in the shell analysis but Kennard [12] included these stresses in his

analysis. However, below the ring frequency, the maximum difference of the cut-on frequency (n = 7) between both theories is only 0.22%.

Comparison of dispersion curves

In this section, a set of dispersion curves from the simplified model developed in the previous sections is compared with those obtained from some other versions of shell theory, namely from Kennard and Flugge. To verify the model, the comparisons are carried out for each mode number. This simplified model is calculated from equations (2.19) and (2.21) for the n = 0 mode, equations (2.27) and (2.29) for the n = 1 mode, and equation (2.7) for the n ≥ 2 modes. The results from the simulations are shown in figure 2.2.

The simulations in figure 2.2 show clearly that Kennard's and Flugge's shell theories give a similar result. There are slight differences at the cut-on frequency for the higher modes due to the different assumption of both theories.

The discussion for the simplified model of the wavenumber is separated into three groups, breathing, bending, and circumferential modes. For the n = 0 mode (breathing mode), the model is consistent with Kennard's and Flugge's shell theory up to about Ω = 0.9 before the longitudinal wavenumber ($\hat{k}_1$) reaches unity leading the singularity of the term $\nu^2\hat{k}_1^4/(1-\hat{k}_1^2)$ (equation 2.29) resulting in $\hat{k}_{01}$ becoming infinite. When $\hat{k}_1^2 < 1$, this term is small so that the wavenumber $\hat{k}_{01}$ can be approximated by $\hat{k}_1$. The other wavenumbers, $\hat{k}_{02}$ represented by the torsional wave $\hat{k}_s$, and $\hat{k}_{03}$, $\hat{k}_{04}$ represented by the standing near field wave, are in good agreement with both referenced theories up to the ring frequency.

The simplified model of the flexural and near field wavenumber of the n = 1 mode (equation 2.30) are valid up to about Ω = 0.7 and Ω = 0.5, respectively. For the pipe used for this thesis, these correspond to about 4 and 6 kHz. These frequencies are high

enough so that the model can be used for the n = 1 mode of the pipe. Moreover, the response of the pipe is no longer dominated by this mode after the higher modes cut on (430 Hz for the n = 2 mode). The departure occurs for the n = 1 mode due to the assumption that $\hat{k}_l^2, \hat{k}_s^2$, and $\hat{k}_b^4$ are less than unity. Apart from this, the quadratic method relies on the fact that there is a large difference between the standing near field wavenumbers ($\hat{k}_{03}$, $\hat{k}_{04}$) and the flexural and near field wavenumbers, $\hat{k}_{01}$ and $\hat{k}_{02}$, respectively.

For the circumferential modes (n ≥ 2), the simplified version of the wavenumbers (equation 2.7) are consistent with the referenced theories, except for the near field wavenumber. With the higher circumferential modes, however, the departure of this wavenumber is smaller.

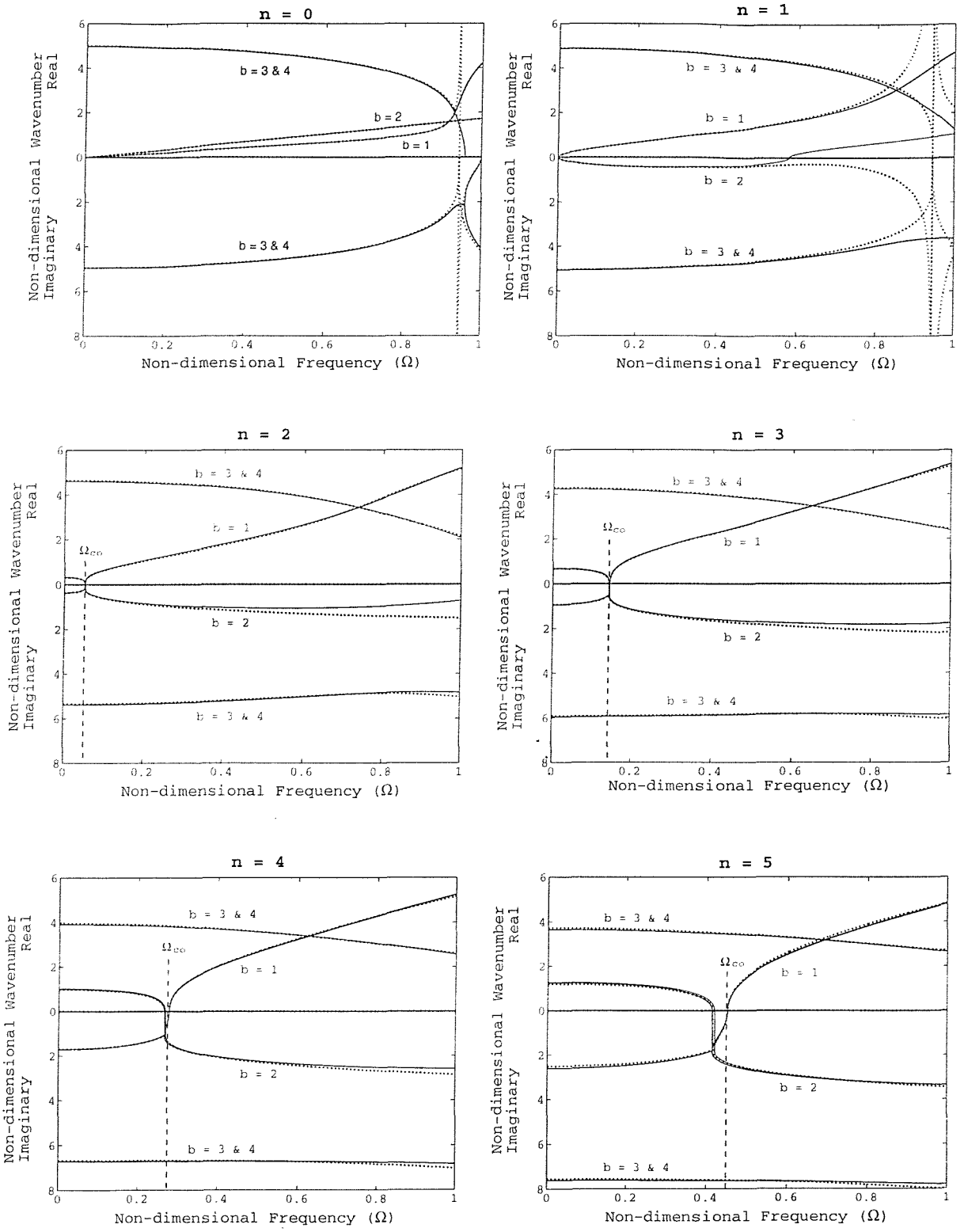

Figure 2.2. Dispersion curves for the mode number n = 0 to n = 5; ... Simplified model, _ _ Flugge theory, – Kennard theory.

2.5 Conclusions

In the derivations in this chapter, the characteristic equation of a pipe has been established using Flugge's shell theory as a basis together with some simplifying assumptions. The assumptions of a thin wall thickness, and the frequency of interest being below the ring frequency of a pipe are used for the n = 0 and n = 1 mode. In addition, the very long axial wavelength is neglected for the higher modes. The last assumption cannot be used for the n = 0 and n = 1 mode, which contains longitudinal and torsional waves because it requires $\frac{\partial \hat{k}_{nb}}{\partial \Omega} > 1$. With the simplified characteristic equation, the expression of the cut-on frequency can be found and it has been numerically validated.

Even though the characteristic equation can give the wavenumber solutions by finding the roots of the polynomial, a further derivation obtained by reducing the characteristic equation to a quadratic (the quadratic method), provides them in a simpler form. However, this method is based on their being a large difference between the large and small wavenumber groups so that it can only be applied to the n = 0 and n = 1 modes because the longitudinal, torsional, flexural and near field wavenumbers are comparatively smaller than the standing near field waves. In reality, this method can also be used for the higher modes but it is valid just after the wave cuts on, where the flexural wavenumber is still small. Using the quadratic method, the wavenumber of the n = 0 mode at low frequencies ($\Omega < 0.9$) can be presented in terms of the longitudinal and torsional wavenumbers, and of the n = 1 mode at low frequencies ($\Omega < 0.7$) can be represented in terms of the flexural and near field waves of a Timoshenko beam.

CHAPTER 3

POINT AND TRANSFER MOBILITY OF INFINITE PIPES

3.1 Introduction

As mentioned in the previous chapter, for each circumferential mode eight waves can potentially propagate in the pipe wall. Generally, all these waves are generated by an excitation force. For an infinite pipe, four waves propagate in the positive direction, and the other four waves propagate in the negative direction. Even though there are four positive-going waves for each mode, only the longitudinal and torsional waves for the n = 0 mode, and the flexural propagating wave for the higher order modes can propagate along the pipe because the near field and standing near field waves are evanescent. At the excitation point, however, all waves contribute to the motion of the pipe. Apart from the characteristic equation discussed in the previous chapter, the pipe motion due to an excitation force can be used to describe the dynamic behaviour of the infinite pipe, and is presented in terms of the mobility frequency response function in this chapter.

The analysis of the mobility (radial velocity/applied force) of an infinite pipe requires eight boundary conditions at the excitation point. To avoid the boundary condition problem, most researchers have adopted the Residue method to develop the mobility of the infinite pipe. This method does not require boundary conditions as the analysis uses wavenumber solutions of the pipe. Such work using this method has been done by Franken [21], Heckl [22], Fuller [9], and Brevart and Fuller [23].

In this chapter, the mobility of the infinite pipe is derived by using two methods, which are called the Residue and Analytical methods. The Residue method employs the Fourier transform to convert vibration in the spatial domain to the wavenumber domain, and uses the residue theory to analyse the pipe motion. Conversely, the Analytical method involves a vibration analysis in the spatial domain. This requires eight boundary conditions at the excitation position. The reason for doing this is to cross-check the results of each method. Once the mobility expression is established, it is simplified for low frequency behaviour to compare the dynamics of a pipe with that of a simple structure like a membrane and a beam. Finally, the mobility expressions are validated by some experiment work.

3.2 Residue Method

The dynamic response of an infinite pipe due to a point force normal to the surface of the pipe is of interest in this section. One useful method to derive the response of a pipe is to analyse the force mobility (the mobility due to a point force) in the wavenumber domain by using the spatial Fourier transform. Using residue theory and the simplified shell theory, the point force mobility of the pipe can be established in a simple form.

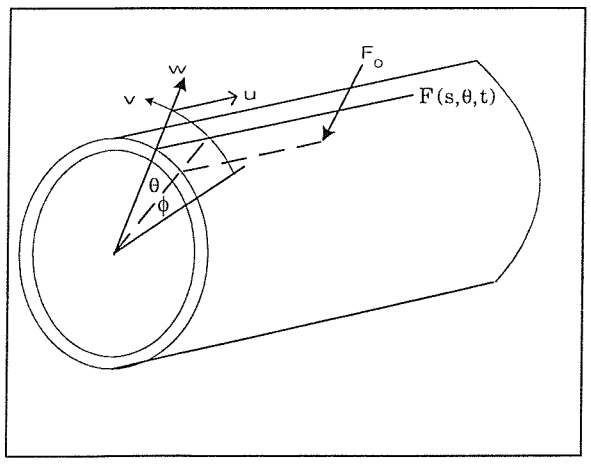

Figure 3.1: The cylindrical co-ordinate system for an *in-vacuo* pipe excited by a point force.

The cylindrical coordinate system of a pipe with an excitation point force, F_0, is schematically shown in figure 3.1. As discussed in the previous chapter, an orientation angle, ϕ, is used to define the circumferential reference position on the pipe. The point force, F_0, in Newtons can be expressed as a distributed force intensity, $F(s,\theta,t)$, in Newtons per square metre, (Soedel [69])

$$F(s,\theta,t)=\frac{1}{a^2}F_0\delta(s)\delta(\theta-\phi)e^{-j\omega t} \qquad ...(3.1)$$

where F_0 is the amplitude of the point force.

The equation of motion of the pipe when excited by a point force in the radial direction may be written as the same form as equation (2.1), but with an external force loading as (Leissa [2]):

$$\begin{bmatrix} A_{11} & A_{12} & A_{13} \\ A_{21} & A_{22} & A_{23} \\ A_{31} & A_{32} & A_{33} \end{bmatrix} \begin{bmatrix} u^i \\ v^i \\ w^i \end{bmatrix} = \begin{bmatrix} 0 \\ 0 \\ -\dfrac{a^2(1-\nu^2)}{Eh}F(s,\theta,t) \end{bmatrix} \qquad ...(3.2)$$

The superscript i of the displacements used in equation (3.2) denotes an infinite pipe. The Fourier transform is used to analyse the vibration response of a pipe due to a point force and the pipe displacements may be written as (Fuller [9])

$$\begin{aligned} u^i(s,\theta,t) &= \frac{1}{2\pi}\int_{-\infty}^{\infty}\sum_{n=0}^{\infty}\varepsilon_n\,\overline{U_n(\hat{k}_n)}\cos(n\theta)\,e^{j(\hat{k}_n s-\pi/2-\omega t)}d\hat{k}_n \\ v^i(s,\theta,t) &= \frac{1}{2\pi}\int_{-\infty}^{\infty}\sum_{n=0}^{\infty}\varepsilon_n\,\overline{V_n(\hat{k}_n)}\sin(n\theta)\,e^{j(\hat{k}_n s-\omega t)}d\hat{k}_n \\ w^i(s,\theta,t) &= \frac{1}{2\pi}\int_{-\infty}^{\infty}\sum_{n=0}^{\infty}\varepsilon_n\,\overline{W_n(\hat{k}_n)}\cos(n\theta)\,e^{j(\hat{k}_n s-\omega t)}d\hat{k}_n \end{aligned} \qquad ...(3.3)$$

where $\overline{U_n(\hat{k}_n)}$ is the axial amplitude of the n^{th} mode in the wavenumber domain,

$\overline{V_n(\hat{k}_n)}$ is the circumferential amplitude of the n^{th} mode in the wavenumber domain

$\overline{W_n(\hat{k}_n)}$ is the radial amplitude of the n^{th} mode in the wavenumber domain

$\varepsilon_n = 1$ for $n = 0$ and

$\varepsilon_n = 2$ for $n \geq 1$.

Because axial wavenumbers are continuous and the mode number is discrete, the delta functions of $\delta(s)$ and $\delta(\theta - \phi)$ in equation (3.1) may be expressed as

$$\delta(s) = \frac{1}{2\pi}\int_{-\infty}^{\infty} e^{j\hat{k}_n s} d\hat{k}_n$$
$$\delta(\theta-\phi) = \frac{1}{2\pi}\sum_{n=-\infty}^{\infty} e^{jn(\theta-\phi)} \qquad \ldots(3.4)$$

So, the force intensity in equation (3.1) can be written in the wavenumber domain as

$$F(s,\theta,t) = \frac{1}{4\pi^2 a^2}\int_{-\infty}^{\infty}\sum_{n=0}^{\infty}\varepsilon_n F_o \cos[n(\theta-\phi)] e^{j(\hat{k}_n s-\omega t)} d\hat{k}_n \qquad \ldots(3.5)$$

By substituting for the displacements and force given in equations (3.3) and (3.5) respectively into equation (3.2), the spectral response of the pipe to the applied force is given by

$$\begin{bmatrix} L_{11} & L_{12} & L_{13} \\ L_{21} & L_{22} & L_{23} \\ L_{31} & L_{32} & L_{33} \end{bmatrix} \begin{bmatrix} \overline{U_n(\hat{k}_n)} \\ \overline{V_n(\hat{k}_n)} \\ \overline{W_n(\hat{k}_n)} \end{bmatrix} = \begin{bmatrix} 0 \\ 0 \\ -\dfrac{F_o}{2\pi\rho h a^2 \omega_r^2}\dfrac{\cos[n(\theta-\phi)]}{\cos(n\theta)} \end{bmatrix} \qquad \ldots(3.6)$$

where the matrix $\mathbf{L}_n$ is given by equation (2.3) where $\hat{k}_{nb}$ is set to $\hat{k}_n$.

By inversion of the matrix $\mathbf{L}_n$, the amplitudes of the displacements in the wavenumber domain for each circumferential mode n can be written as

$$\begin{bmatrix} \overline{U_n(\hat{k}_n)} \\ \overline{V_n(\hat{k}_n)} \\ \overline{W_n(\hat{k}_n)} \end{bmatrix} = \begin{bmatrix} I_{11} & I_{12} & I_{13} \\ I_{21} & I_{22} & I_{23} \\ I_{31} & I_{32} & I_{33} \end{bmatrix} \begin{bmatrix} 0 \\ 0 \\ -\dfrac{F_o}{2\pi\rho h a^2 \omega_r^2} \dfrac{\cos(n(\theta-\phi))}{\cos(n\theta)} \end{bmatrix} \qquad \ldots(3.7)$$

The radial displacement for the n^{th} mode in the wavenumber domain is thus given by

$$\overline{W_n(\hat{k}_n)} = -\frac{F_o}{2\pi\rho h a^2 \omega_r^2} \frac{\cos[n(\theta-\phi)]}{\cos(n\theta)} I_{33}(\hat{k}_n) \qquad \ldots(3.8)$$

where $I_{33}(\hat{k}_n) = \dfrac{(L_{11}L_{22} - L_{12}L_{21})_n}{|\mathbf{L}|_n}$ $\qquad \ldots(3.9)$

The radial displacement for a particular mode in the frequency domain is obtained by substituting equation (3.8) into equation (3.3) where terms $e^{-j\omega t}$ are omitted for simplification to give

$$W_n^i(s,\theta) = -\frac{\varepsilon_n F_o \cos[n(\theta-\phi)]}{4\pi^2 \rho h a^2 \omega_r^2} \int_{-\infty}^{\infty} I_{33}(\hat{k}_n) e^{j\hat{k}_n s} d\hat{k}_n \qquad \ldots(3.10)$$

As shown in figure 2.2 in chapter 2, the wavenumbers of the pipe are frequency dependent. So, for each frequency, $|\mathbf{L}|_n$ in equation (3.9) gives eight poles to the integral in equation (3.10) at $\hat{k}_n$ equal to the wavenumber solution, $\hat{k}_{nb}$, of the pipe. The integral can be evaluated using residue theory, which is the method of contour integration as shown in figure 3.2. With this method, only the upper half plane of the complex plane needs to be analysed, so that only four poles are evaluated. Physically, this means that only the waves in the positive direction are taken into account. However, because of the symmetry of an infinite pipe in the positive and negative

directions, the solutions for the waves in the negative direction are the same. The solution to equation (3.10) can be expressed as (Arfken [70])

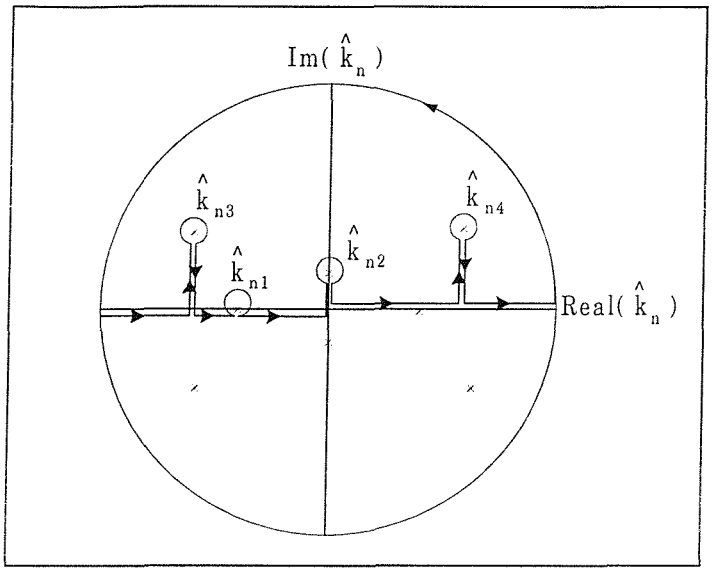

Figure 3.2: Contour integral for the residue method where $\hat{k}_{n1}, \hat{k}_{n2}, \hat{k}_{n3}$ and $\hat{k}_{n4}$ are the wavenumber solutions of the pipe for the n^{th} circumferential mode.

$$W_n^i(s,\theta) = -\frac{j\varepsilon_n F_o \cos[n(\theta-\phi)]}{2\pi\rho h a^2 \omega_r^2} \sum_{b=1}^{4} Res_{nb} e^{j\hat{k}_{nb}s} \qquad ...(3.11)$$

where $$Res_{nb} = \frac{(L_{11}L_{22} - L_{12}L_{21})_{nb}}{|L|'_{nb}} \qquad ...(3.12)$$

$$|L|'_{nb} = \frac{\partial |L|_{nb}}{\partial \hat{k}_{nb}}$$

The mobility of the forced response for the n^{th} mode is given by

$$Y_n^i(s,\theta) = -j\omega\frac{W_n^i(s,\theta)}{F_o} = -\frac{\varepsilon_n \omega \cos[n(\theta-\phi)]}{2\pi\rho h a^2 \omega_r^2} \sum_{b=1}^{4} Res_{nb} e^{j\hat{k}_{nb}s} \qquad ...(3.13)$$

Equation (3.13) is a general form of the mobility of an infinite pipe. It cannot be obtained in a simple form unless a simplified shell theory is used. This has been done by Fuller [9], who used Donnell-Mustari's theory, and by Brevart and Fuller [23], who used Kennard's theory. With an approximated shell theory, Franken [21] using the membrane equation, and Heckl [22], using the simplified shell theory of Cremer and Kennard [17], gave the mobility of an infinite pipe in a relatively simple form.

In chapter 2, the characteristic equation was simplified, and it is employed here in the derivation of an approximate mobility expression. However, the analysis is separated into two parts because of the different assumptions being used. The first part is the analysis for the n = 0 and n = 1 modes, for which the assumption of $\hat{k}_{nb}^2 >> \Omega^2$, which requires the condition of $\frac{\partial \hat{k}_{nb}}{\partial \Omega} > 1$ does not hold. It cannot be applied to the longitudinal and torsional waves, whose characteristic equation is presented in equation (2.6). The other part is for the n ≥ 2 modes, for which the assumption can be used because the wavenumber of the flexural wave dramatically increases after the wave cuts on, and whose characteristic equation is given in equation (2.7).

Simplified mobility for the n = 0 and n = 1 modes

The derivative of $|\mathbf{L}|_{nb}$ with respect to $\hat{k}_{nb}$ given in equation (3.12), which is the characteristic equation obtained from equation (2.6), is given by

$$\frac{\partial |\mathbf{L}|_{nb}}{\partial \hat{k}_{nb}} = 2(1-\nu)\hat{k}_{nb}\left\{\beta^2\left[2(\hat{k}_{nb}^2+n^2)(\hat{k}_{nb}^2+n^2-1)(\hat{k}_{nb}^2+n^2-\frac{1}{2})\right]+(1-\nu^2)\hat{k}_{nb}^2\right.$$
$$\left.-\Omega^2(\hat{k}_{nb}^2+n^2+\nu+\frac{3}{2})+\frac{1}{2}\left(\frac{3-\nu}{1-\nu}\right)\Omega^4\right\} \qquad \ldots(3.14)$$

With the assumption of $\beta^2 << 1$, the term $(L_{11}L_{22} - L_{12}L_{21})_{nb}$ is given by

$$(L_{11}L_{22}-L_{12}L_{21})_{nb}=\frac{1}{2}(1-\nu)(\hat{k}_{nb}^{2}+n^{2})^{2}-\frac{1}{2}(3-\nu)(\hat{k}_{nb}^{2}+n^{2})\Omega^{2}+\Omega^{4} \qquad ...(3.15)$$

By substituting for the derivative of $|\mathbf{L}|_{nb}$ from equation (3.14) and for $(L_{11}L_{22}-L_{12}L_{21})_{nb}$ given in equation (3.15) into equations (3.12) and (3.13), the mobility of the n = 0 and n = 1 modes can be predicted.

At this point, it should be noted that, with the given residue term and the wavenumbers described in chapter 2, the mobility of each axial wave for the n = 0 mode is not zero. However, this is not correct for the radial motion of a torsional wave. It is zero in reality because torsional motion is not excited by a radial force due to symmetry (Vinson [24]). For this to occur in the model, the correct torsional wavenumber has to be determined which can be found from the $|\mathbf{L}|_{0b} = 0$. Without simplification, the term of $|\mathbf{L}|_{0b}$ for the n = 0 mode is given by

$$|L|_{0b}=\begin{vmatrix} L_{11} & 0 & L_{13} \\ 0 & L_{22} & 0 \\ L_{31} & 0 & L_{33} \end{vmatrix}=\left[L_{22}(L_{11}L_{33}-L_{13}L_{31})\right]_{0b}=0 \qquad ...(3.16)$$

The above equation yields $(L_{22})_{0b} = 0$, which leads to the torsional wavenumber given by

$$\hat{k}_{0b}^{2}=\frac{\hat{k}_{s}^{2}}{(1+3\beta^{2})} \qquad ...(3.17)$$

It can be seen that the difference between the exact torsional wavenumber of the pipe obtained from equation (3.17) and the simplifed torsional wavenumber described in chapter 2 (equation 2.20 b) is only in the term $3\beta^2$, which is very small.

Because L_{12} and L_{21} are zero for the n = 0 mode and L_{22} is also zero when the correct torsional wavenumber of the pipe given in equation (3.17) is used, the numerator of the

residue term of this wavenumber (equation 3.12) becomes zero ($L_{11}L_{22} - L_{12}L_{21} = 0$) resulting in no radial motion for the torsional wave.

Simplified mobility for the n ≥ 2 modes

The derivative of $|\mathbf{L}|_{nb}$ with respect to $\hat{k}_{nb}$ (the characteristic equation) obtained from equation (2.7), is given by

$$\frac{\partial |\mathbf{L}|_{nb}}{\partial \hat{k}_{nb}} = 2(1-\nu)\hat{k}_{ab}\left[2\beta^2(\hat{k}_{nb}^2+n^2)(\hat{k}_{nb}^2+n^2-1)(\hat{k}_{nb}^2+n^2-\frac{1}{2})+(1-\nu^2)\hat{k}_{nb}^4-\Omega^2(\hat{k}_{nb}^2+n^2+\frac{1}{2})\right] \quad \ldots(3.18)$$

The term $(L_{11}L_{22} - L_{12}L_{21})_{nb}$ is given by

$$(L_{11}L_{22}-L_{12}L_{21})_{nb} = \frac{1}{2}(1-\nu)(\hat{k}_{nb}^2+n^2)^2-\frac{1}{2}(3-\nu)(\hat{k}_{nb}^2+n^2)\Omega^2+\frac{1}{4}\beta^2\left[(1-\nu)\hat{k}_{nb}^2(\hat{k}_{nb}^2+n^2)-\frac{5}{2}\hat{k}_{nb}^2n^2\right] \quad \ldots(3.19)$$

By assuming that $\beta^2 << 1$ and $\hat{k}_{nb}^2 >> \Omega^2$, then the second and the last term can be neglected and equation (3.19) becomes

$$(L_{11}L_{22}-L_{12}L_{21})_{nb} = \frac{1}{2}(1-\nu)(\hat{k}_{nb}^2+n^2)^2 \quad \ldots(3.20)$$

So, the residue term is

$$Res_{nb} = \frac{(\hat{k}_{nb}^2+n^2)^2}{4\hat{k}_{ab}\left[2\beta^2(\hat{k}_{nb}^2+n^2)(\hat{k}_{nb}^2+n^2-1)(\hat{k}_{nb}^2+n^2-\frac{1}{2})+(1-\nu^2)\hat{k}_{nb}^4-\Omega^2(\hat{k}_{nb}^2+n^2+\frac{1}{2})\right]} \quad (3.21)$$

Once the residue term is determined, the mobility of the infinite pipe can be obtained by substituting for this term into equation (3.13).

Residue method with Laurent expansion

In the above discussion, the mobility of the pipe is determined using the residue method with Maclaurin's expansion. Instead of using this, the mobility can be derived by using Laurent 's theory to expand the residue terms. To explicitly demonstrate this method, the radial displacement of the infinite pipe given in equation (3.10) is repeated here for convenience.

$$W_n^i(s,\theta) = -\frac{\varepsilon_n F_o \cos[n(\theta-\phi)]}{4\pi^2 \rho h a^2 \omega_r^2} \int_{-\infty}^{\infty} I_{33}(\hat{k}_n)\, e^{j\hat{k}_n s} d\hat{k}_n \qquad \ldots(3.22)$$

$$\text{where} \quad I_{33}(\hat{k}_n) = \frac{(L_{11}L_{22} - L_{12}L_{21})_n}{|\mathbf{L}|_n}. \qquad \ldots(3.23)$$

From the above equation, it can be seen that $I_{33}(\hat{k}_n)$ is a function of the wavenumbers. This is also the case for $|\mathbf{L}|_n$, which may be expressed in polynomial form (described in section 2.3) as:

$$|\mathbf{L}|_n = g_8 \hat{k}_n^8 + g_6 \hat{k}_n^6 + g_4 \hat{k}_n^4 + g_2 \hat{k}_n^2 + g_0 \qquad \ldots(3.24)$$

It can be seen from section 2.3 that the polynomial coefficients (g) depend on the shell theory used. When the simplified model described in chapter 2 is used, these coefficients are given by equation (2.15) for the n = 0 and n = 1 modes, and equation 2.31 for the n ≥ 2 modes.

The eight wavenumbers of the pipe are determined from the characteristic equation, $|\mathbf{L}|_n = 0$, and are given by $\pm\hat{k}_{n1}$, $\pm\hat{k}_{n2}$, $\pm\hat{k}_{n3}$ and $\pm\hat{k}_{n4}$. From these wavenumbers, the polynomial function in equation (3.24) can be rearranged to give

$$|\mathbf{L}|_n = g_8^{or}(\hat{k}_n^2 - \hat{k}_{n1}^2)(\hat{k}_n^2 - \hat{k}_{n2}^2)(\hat{k}_n^2 - \hat{k}_{n3}^2)(\hat{k}_n^2 - \hat{k}_{n4}^2) \qquad ...(3.25)$$

It was mentioned that the coefficient g_8 given in chapter 2 and equation (3.24) is obtained from the simplified version of the shell theory. However, to make a theoretical comparison between the mobility obtained by the Residue method and that obtained by the Analytical method (described in section 3.3), the coefficient g_8 should be determined from the original Flugge's shell theory. By arranging the characteristic equation ($|\mathbf{L}|_n = 0$ where $\mathbf{L}$ is given in equation (2.3)) of the original model into a polynomial of axial wavenumbers as expressed in equation (3.24), the coefficient g_8^{or} (superscript or is to denote the original Flugge's shell theory) is given by

$$g_8^{or} = \frac{1}{2}(1-\nu)(1+3\beta^2)(1-\beta^2)\beta^2 .$$

With $|\mathbf{L}|_n$ given by equation (3.25), the term $I_{33}(\hat{k}_n)$ from equation (3.23) can be written as

$$I_{33}(\hat{k}_n) = \sum_{b=1}^{8} \frac{Res_{nb}}{(\hat{k}_n - \hat{k}_{nb})} \qquad ...(3.26)$$

In equation (3.26), the unknown term Res_{nb} can be determined relatively easily. For example, by multiplying by $(\hat{k}_n - \hat{k}_{n1})$, the term Res_{n1}, can be determined when $\hat{k}_n$ approaches the value $\hat{k}_{n1}$, which makes the other residue terms relatively very small. Equation (3.26) then becomes

$$Res_{n1} = \lim_{\hat{k}_n \to \hat{k}_{n1}} (\hat{k}_n - \hat{k}_{n1}) I_{33}(\hat{k}_n) \qquad \ldots(3.27)$$

The other Residue terms can be obtained the same way as Res_{n1}. By substituting for $I_{33}(\hat{k}_n)$ from equation (3.23) into equation (3.27), the residue term in general form is written as

$$Res_{nb} = \lim_{\hat{k}_n \to \hat{k}_{nb}} (\hat{k}_n - \hat{k}_{nb}) \frac{(L_{11}L_{22} - L_{12}L_{21})_{nb}}{|\mathbf{L}|_{nb}} \qquad \ldots(3.28)$$

Even though the integral in equation (3.22) has eight poles, only the upper half plane of the complex plane shown in figure 3.2 is analysed so that the solution of equation (3.22) can be expressed as

$$W_n^i(s,\theta) = \sum_{b=1}^{4} \overline{\overline{W}}^{i}_{nb} \cos[n(\theta-\phi)] e^{j\hat{k}_{nb}s} \qquad \ldots(3.29)$$

where $\overline{\overline{W}}^{i}_{nb} = -\frac{j\varepsilon_n F_0}{2\pi\rho h a^2 \omega_r^2} Res_{nb}$ is the b^{th} wave amplitude of the n^{th} mode...(3.30)

Substituting the residue term, Res_{nb}, from equation (3.28) into equation (3.29) gives the radial wave amplitudes for the n^{th} mode as

$$\overline{\overline{W}}^{i}_{n1} = \frac{-j\varepsilon_n F_0 (L_{11}L_{22} - L_{12}L_{21})_{n1}}{2\pi\rho h a^2 \beta^2 \omega_r^2 (1-\nu)(1+3\beta^2)(1-\beta^2)(\hat{k}_{n1}^2 - \hat{k}_{n2}^2)(\hat{k}_{n1}^2 - \hat{k}_{n3}^2)(\hat{k}_{n1}^2 - \hat{k}_{n4}^2)\hat{k}_{n1}}$$

$$\overline{\overline{W}}^{i}_{n2} = \frac{-j\varepsilon_n F_0 (L_{11}L_{22} - L_{12}L_{21})_{n2}}{2\pi\rho h a^2 \beta^2 \omega_r^2 (1-\nu)(1+3\beta^2)(1-\beta^2)(\hat{k}_{n2}^2 - \hat{k}_{n1}^2)(\hat{k}_{n2}^2 - \hat{k}_{n3}^2)(\hat{k}_{n2}^2 - \hat{k}_{n4}^2)\hat{k}_{n2}} \qquad \ldots(3.31)$$

$$\overline{\overline{W}}^{i}_{n3} = \frac{-j\varepsilon_n F_0 (L_{11}L_{22} - L_{12}L_{21})_{n3}}{2\pi\rho h a^2 \beta^2 \omega_r^2 (1-\nu)(1+3\beta^2)(1-\beta^2)(\hat{k}_{n3}^2 - \hat{k}_{n1}^2)(\hat{k}_{n3}^2 - \hat{k}_{n2}^2)(\hat{k}_{n3}^2 - \hat{k}_{n4}^2)\hat{k}_{n3}}$$

$$\overline{\overline{W}}^{i}_{n4} = \frac{-j\varepsilon_n F_0 (L_{11}L_{22} - L_{12}L_{21})_{n4}}{2\pi\rho h a^2 \beta^2 \omega_r^2 (1-\nu)(1+3\beta^2)(1-\beta^2)(\hat{k}_{n4}^2 - \hat{k}_{n1}^2)(\hat{k}_{n4}^2 - \hat{k}_{n2}^2)(\hat{k}_{n4}^2 - \hat{k}_{n3}^2)\hat{k}_{n4}}$$

Like the case of the polynomial coefficients (g), the terms of $(L_{11}L_{22} - L_{12}L_{21})_{nb}$, where b is 1, 2, 3, and 4, in equation (3.31) depend on the shell theory used. For the simplified model, these terms are given in equation 3.15 for the n = 0 and n = 1 modes, and equation 3.21 for the n ≥ 2 modes. Without simplification, they are determined from equation (3.19).

By comparing the radial wave amplitudes given in equation (3.31) with those obtained from equation (3.11), it can be seen that different theories used for expanding the residue term give the different forms of the solutions. With the Macluarin's expansion, the radial wave amplitude of each wave depends on its wavenumber, while it depends on all wavenumbers when Laurent's theory used.

The mobility of the infinite pipe obtained using the residue theory with the Laurent expansion is given by

$$Y_n^i(s,\theta) = -j\omega\frac{W_n^i(s,\theta)}{F_0} = -j\omega\frac{1}{F_0}\sum_{b=1}^{4}\overline{\overline{W}}^{i}_{nb}\cos[n(\theta-\phi)]e^{j\hat{k}_{nb}s} \qquad \ldots(3.32)$$

3.3 Analytical Method

As shown in the previous section, the residue method can be used to determine the mobility of an infinite pipe. However, it does not give detailed information of what happens to the pipe when subjected to a point harmonic load. Unlike the residue method, the analytical method, which can also be used to derive the dynamic response of an infinite pipe, can give this information, and is of interest of this section.

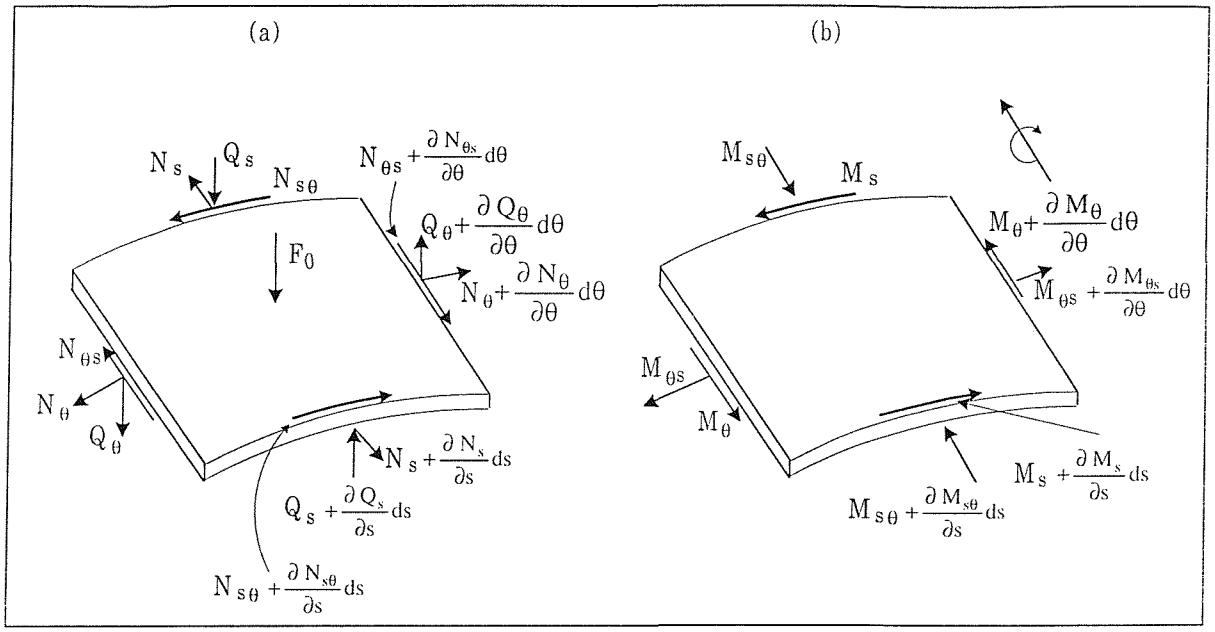

Figure 3.3: Notation and co-ordinate system for an element of a pipe.

Figure 3.3 shows an element of an infinite pipe together with the co-ordinate system. By summing radial forces (expressed in units of force per unit mid-surface length of the pipe), the following equation results: (Soedel [69])

$$-N_\theta+\frac{\partial Q_s}{\partial s}+\frac{\partial Q_\theta}{\partial \theta}-\rho a h\frac{\partial^2 w}{\partial t^2}=\frac{F_o}{a}\delta(s)\delta(\theta-\phi)e^{-j\omega t} \qquad \ldots(3.33)$$

where N_θ is the in-plane circumferential force per unit length (Newton/metre)

$Q_s=\frac{1}{a}\left(\frac{\partial M_s}{\partial s}+\frac{\partial M_{\theta s}}{\partial \theta}\right)$ is the transverse shear force in the axial direction per unit length (Newton/metre),

$Q_\theta=\frac{1}{a}\left(\frac{\partial M_\theta}{\partial \theta}+\frac{\partial M_{s\theta}}{\partial s}\right)$ is the transverse shear force in the circumferential direction per unit length (Newton/metre).

Integrating equation (3.33) in the axial direction from $-\epsilon$ to ϵ, where ϵ tends to zero gives

$$V_s\Big|_{s=0} = \frac{1}{a} F_0 \delta(\theta - \phi) \qquad \ldots(3.34)$$

where $V_s = \left(Q_s + \frac{1}{a} \frac{\partial M_{s\theta}}{\partial \theta} \right)$ is called the effective transverse shear force per unit length.

Since $\delta(\theta - \phi) = \frac{1}{2\pi} \sum_{n=0}^{\infty} \varepsilon_n \cos[n(\theta - \phi)]$ (given in equation 3.4), the applied force term on the right-hand side of equation (3.34) corresponds to the generalised force at any particular angle, θ.

If the pipe is split at s = 0 (excitation position), the resultant forces and moments react at the edges of the split pipe as shown schematically in figure 3.4.

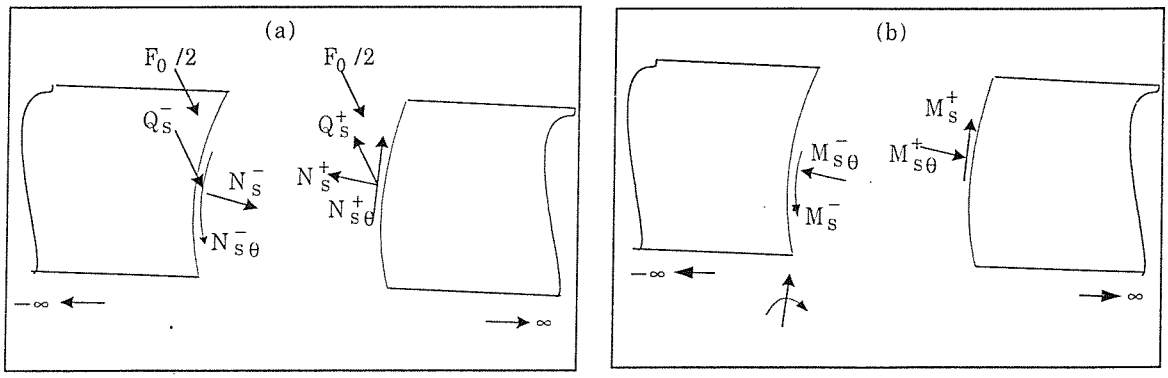

Figure 3.4: Notation and co-ordinate system for two connecting pipe elements;

a) Force, b) Moment

The work done at the boundaries of the split pipe from angle θ_1 to θ_2 must equal and may be expressed as (Liessa [2] and Soedel [69])

$$\int_{\theta_1}^{\theta_2} \left[\left(N_s^+ u^+ - N_s^- u^- \right) + \left(T_{s\theta}^+ v^+ - T_{s\theta}^- v^- \right) + \left((F_0 / 2a - V_s^+) w^+ - (F_0 / 2a + V_s^-) w^- \right) - \frac{1}{a} \left(M_s^+ \frac{\partial w^+}{\partial s} - M_s^- \frac{\partial w^-}{\partial s} \right) \right] d\theta$$

$$- \frac{1}{a} \left(M_{s\theta}^+ w^+ - M_{s\theta}^- w^- \right) \Big|_{\theta_1}^{\theta_2} = 0 \qquad \ldots(3.35)$$

Where $T_{s\theta}^{+} = N_{s\theta}^{+} + \frac{1}{a} M_{s\theta}^{+}$ is called the effective in-plane shear force.

Equation (3.35) is satisfied if the integral and the second term are both zero. Hence, it leads to the boundary conditions on the edges which are joined. For equilibrium of forces and moments, they are

$$N_s^{+} = N_s^{-}, \quad T_{s\theta}^{+} = T_{s\theta}^{-}, \quad V_s^{+} = -V_s^{-} \quad \text{and} \quad M_s^{+} = M_s^{-} \qquad \ldots(3.36)$$

and for continuity of motion, the boundary conditions are

$$u^{+} = u^{-}, \quad v^{+} = v^{-}, \quad w^{+} = w^{-} \quad \text{and} \quad \frac{\partial w^{+}}{\partial s} = \frac{\partial w^{-}}{\partial s} \qquad \ldots(3.37)$$

Based on Flugge's shell theory, the resultant forces and moments in equation (3.36) may be written in the term of displacements as

$$N_s^{+} = \frac{K}{a}\left[\frac{\partial u^{+}}{\partial s} + \nu\frac{\partial v^{+}}{\partial \theta} + \left(\nu - \beta^2\frac{\partial^2}{\partial s^2}\right)w^{+}\right]$$

$$T_{s\theta}^{+} = \frac{(1-\nu)K}{2a}\left[\frac{\partial u^{+}}{\partial \theta} + \left(1+3\beta^2\right)\frac{\partial v^{+}}{\partial s} - 3\beta^2\frac{\partial^2 w^{+}}{\partial s \partial \theta}\right] \qquad \ldots(3.38\ \text{a, b, c, d})$$

$$V_s^{+} = \frac{D}{a^3}\left[\left(\frac{\partial^2}{\partial s^2} - \frac{(1-\nu)}{2}\frac{\partial^2}{\partial \theta^2}\right)u^{+} + \frac{(3-\nu)}{2}\frac{\partial^2 v^{+}}{\partial s \partial \theta} - \left(\frac{\partial^3}{\partial s^3} + (2-\nu)\frac{\partial^3}{\partial s \partial \theta^2}\right)w^{+}\right]$$

$$M_s^{+} = \frac{D}{a^2}\left[\frac{\partial u^{+}}{\partial s} + \nu\frac{\partial v^{+}}{\partial \theta} - \left(\frac{\partial^2}{\partial s^2} + \nu\frac{\partial^2}{\partial \theta^2}\right)w^{+}\right]$$

where $K = \dfrac{Eh}{1-\nu^2}$ is the membrane stiffness,

$D = \dfrac{Eh^3}{12(1-\nu^2)}$ is the bending stiffness,

Since the boundary conditions at the edges of the split pipe involve displacements in all directions, axial, circumferential and radial, to determine their amplitudes the relationships among them should be established. The displacements of an infinite pipe in the positive direction are given by (equation 2.2)

$$\begin{aligned} u^+(s,\theta,t) &= \sum_{n=0}^{\infty}\sum_{b=i}^{4} \overline{\overline{U}}^{i}_{nb} \cos[n(\theta-\phi)]\, e^{j(\hat{k}_{nb}s-\pi/2-\omega t)} \\ v^+(s,\theta,t) &= \sum_{n=0}^{\infty}\sum_{b=1}^{4} \overline{\overline{V}}^{i}_{nb} \sin[n(\theta-\phi)]\, e^{j(\hat{k}_{nb}s-\omega t)} \\ w^+(s,\theta,t) &= \sum_{n=0}^{\infty}\sum_{b=1}^{4} \overline{\overline{W}}^{i}_{nb} \cos[n(\theta-\phi)]\, e^{j(\hat{k}_{nb}s-\omega t)} \end{aligned} \qquad \ldots(3.39)$$

The amplitudes of axial motion, $\overline{\overline{U}}^{i}_{nb}$, and circumferential motion, $\overline{\overline{V}}^{i}_{nb}$, can be found in terms of the radial motion, $\overline{\overline{W}}^{i}_{nb}$, as (Flugge [5] and Young [25])

$$\left(\begin{bmatrix} L_{11} & L_{12} \\ L_{21} & L_{22} \end{bmatrix}\right)_{nb} \begin{bmatrix} \overline{\overline{U}}^{i}_{nb} \\ \overline{\overline{V}}^{i}_{nb} \end{bmatrix} = -\left(\begin{bmatrix} L_{13} \\ L_{23} \end{bmatrix}\right)_{nb} \overline{\overline{W}}^{i}_{nb} \qquad \ldots (3.40)$$

Inverting the 2x2 matrix gives

$$\overline{\overline{U}}^{i}_{nb} = \alpha_{nb}\, \overline{\overline{W}}^{i}_{nb} \quad \text{and} \qquad \ldots(3.41\ a, b)$$

$$\overline{\overline{V}}^{i}_{nb} = \psi_{nb}\, \overline{\overline{W}}^{i}_{nb}$$

Where $\alpha_{nb} = \left(\dfrac{L_{12}L_{23} - L_{22}L_{13}}{L_{11}L_{22} - L_{12}L_{21}}\right)_{nb}$ is the axial coefficient and $\qquad \ldots(3.41\ c)$

$$\psi_{nb} = \left(\frac{L_{21}L_{13} - L_{11}L_{23}}{L_{11}L_{22} - L_{12}L_{21}} \right)_{nb} \quad \text{is the circumferential coefficient.} \quad ...(3.41\ d)$$

In the infinite pipe, there are four positive-going waves, which are represented by the wavenumbers $\hat{k}_{n1}, \hat{k}_{n2}, \hat{k}_{n3}$ and $\hat{k}_{n4}$, and another four negative-going waves, which are represented by the wavenumbers $\hat{k}_{n5}, \hat{k}_{n6}, \hat{k}_{n7}$ and $\hat{k}_{n8}$. Because the wavenumbers in both directions are associated each other (details are described in chapter 2), the axial and circumferential displacement factors in both directions are also related and can be determined by substituting $\hat{k}_{nb} = -\hat{k}_{n(b+4)}$ where b = 1,2,3 and 4, into equation (3.41 c, d) giving

$$\alpha_{nb} = -\alpha_{n(b+4)} \text{ and } \psi_{nb} = \psi_{n(b+4)} \text{ where b = 1,2,3 and 4} \qquad ...(3.42\ a, b)$$

Omitting the term $e^{-j\omega t}$ for simplification, a set of the boundary conditions at the edges of the split pipe (s = 0) can be rewritten as a function of the radial motion by substituting the displacements of the pipe obtained from equation (3.39) and the relationship of their amplitudes obtained from equation (3.41 a, b) into equation (3.38) for the resultant forces and moments, and into equation (3.37) for continuity of motion, which for a particular mode n gives

$$(N_s^+)_n = \frac{K}{a} \sum_{b=1}^{4} Z_{N,nb} \overline{\overline{W}}^{i}_{nb} \cos[n(\theta - \phi)]$$

$$(T_{s\theta}^+)_n = j\frac{(1-\nu)K}{2a} \sum_{b=1}^{4} Z_{T,nb} \overline{\overline{W}}^{i}_{nb} \sin[n(\theta - \phi)]$$

$$(V_s^+)_n = j\frac{D}{a^3} \sum_{b=1}^{4} Z_{V,nb} \overline{\overline{W}}^{i}_{nb} \cos[n(\theta - \phi)]$$

$$(M_s^+)_n = \frac{D}{a^2} \sum_{b=1}^{4} Z_{M,nb} \overline{\overline{W}}^{i}_{nb} \cos[n(\theta - \phi)] \qquad ...(3.43)$$

$$U_n^{i+}(s = 0, \theta) = -j \sum_{b=1}^{4} \alpha_{nb} \overline{\overline{W}}^{i}_{nb} \cos[n(\theta - \phi)]$$

$$V_n^{i+}(s=0,\theta)=\sum_{b=1}^{4}\psi_{nb}\,\overline{\overline{W}}_{nb}^{i}\sin[n(\theta-\phi)]$$

$$W_n^{i+}(s=0,\theta)=\sum_{b=1}^{4}\overline{\overline{W}}_{nb}^{i}\cos[n(\theta-\phi)]$$

$$\frac{\partial W_n^{i+}(s=0,\theta)}{\partial s}=j\sum_{b=1}^{4}\hat{k}_{nb}\,\overline{\overline{W}}_{nb}^{i}\cos[n(\theta-\phi)]$$

where $\overline{\overline{W}}_{nb}^{i}$ is the radial amplitude of the bth wave of the nth circumferential mode, $U_n^{i+}, V_n^{i+}, W_n^{i+}$ are the axial, circumferential and radial displacements of the nth circumferential mode, respectively, and the Z's are given by:

$$Z_{N,nb}=\left[\hat{k}_{nb}\alpha_{nb}+\nu n\psi_{nb}+\beta^2\hat{k}_{nb}^2+\nu\right]$$

$$Z_{T,nb}=\left[n\alpha_{nb}+\left(1+3\beta^2\right)\hat{k}_{nb}\psi_{nb}+3\beta^2 n\hat{k}_{nb}\right]$$

$$Z_{M,nb}=\left[\hat{k}_{nb}\alpha_{nb}+\nu n\psi_{nb}+\hat{k}_{nb}^2+\nu n^2\right] \qquad \ldots(3.44\ a, b, c, d)$$

$$Z_{V,nb}=\left[\left(\hat{k}_{nb}^2-\left(\frac{1-\nu}{2}\right)n^2\right)\alpha_{nb}+\left(\frac{3-\nu}{2}\right)n\hat{k}_{nb}\psi_{nb}+\hat{k}_{nb}\left(\hat{k}_{nb}^2+(2-\nu)n^2\right)\right]$$

The relationships between the radial displacement amplitudes in the positive and negative directions are determined by applying the boundary conditions at the edges of the split pipe such as $N_s^+=N_s^-$, $M_s^+=M_s^-$, $V_n^{i+}/n=V_n^{i-}/n$ and $W_n^{i+}=W_n^{i-}$. In vector form, they are given by

$$\begin{bmatrix}\overline{\overline{W}}_{n1}^{i}\\ \overline{\overline{W}}_{n2}^{i}\\ \overline{\overline{W}}_{n3}^{i}\\ \overline{\overline{W}}_{n4}^{i}\end{bmatrix}=\begin{bmatrix}\overline{\overline{W}}_{n5}^{i}\\ \overline{\overline{W}}_{n6}^{i}\\ \overline{\overline{W}}_{n7}^{i}\\ \overline{\overline{W}}_{n8}^{i}\end{bmatrix} \qquad \ldots(3.45)$$

It should be noted that $V_n^{i+}/n = V_n^{i-}/n$ is used instead of $V_n^{i+} = V_n^{i-}$. This is because ψ_{nb} in equation (3.41 d) can be written as $\psi_{nb} = n\psi_{nb}^0$ (where ψ_{nb}^0 is not equal to zero for any mode number), which gives $V_n^{i+} = V_n^{i-} = 0$ for the n = 0 mode. However, the boundary condition should hold for any mode.

As expected the result obtained from the above equation shows the continuous motion of the pipe in the radial direction. In order to investigate the rest of the boundary conditions, the same relationships, which are $\hat{k}_{nb} = -\hat{k}_{n(b+4)}$, $\alpha_{nb} = -\alpha_{n(b+4)}$, $\psi_{nb} = \psi_{n(b+4)}$, where b = 1,2,3 and 4, are again applied to equation (3.43), which results in

$$(T_{s\theta}^+)_n = -(T_{s\theta}^-)_n,\ (V_s^+)_n = -(V_s^-)_n,\ U_n^{i+} = -U_n^{i-} \text{ and } \frac{\partial W_n^{i+}}{\partial s} = -\frac{\partial W_n^{i-}}{\partial s} \qquad ...(3.46)$$

By comparing the boundary conditions obtained from equation (3.46) with those in equations (3.36) and (3.37), it clearly shows the conflict except that of $(V_s^+)_n = -(V_s^-)_n$. This means that in order to satisfy both equations the axial displacement, U_n^{i+}, the axial rotation, $\frac{\partial W_n^{i+}}{\partial s}$, and the effective in-plane shear force, $(T_{s\theta}^+)_n$, must be equal to zero at the excitation point. Thus the boundary conditions at the edges of the split pipe are given by:

$$\begin{aligned} &(N_s^+)_n = (N_s^-)_n,\quad (V_s^+)_n = -(V_s^-)_n,\quad (M_s^+)_n = (M_s^-)_n \text{ and } (T_{s\theta}^+)_n = (T_{s\theta}^+)_n = 0 \\ &V_n^i = V_n^{i+} = V_n^{i-},\quad W_n^i = W_n^{i+} = W_n^{i-},\quad U_n^i = U_n^{i+} = U_n^{i-} = 0 \quad \text{and} \qquad ...(3.47) \\ &\frac{\partial W_n^i}{\partial s} = \frac{\partial W_n^{i+}}{\partial s} = \frac{\partial W_n^{i-}}{\partial s} = 0 \end{aligned}$$

Since $(T_{s\theta}^+)_n = 0$, with zero slope and no axial displacement it implies that at the excitation there is no twist.

$$\frac{\partial V_n^i}{\partial s} = \frac{\partial V_n^{i+}}{\partial s} = \frac{\partial V_n^{i-}}{\partial s} 0 \qquad \ldots(3.48)$$

From the conditions, $U_n^i = 0$, $\frac{\partial W_n^i}{\partial s} = 0$, $\frac{\partial V_n^i}{\partial s} = 0$, the effective transverse shear force, V_s, given in equation (3.38.c) becomes

$$V_s^+ = \frac{D}{a^3}\left(\frac{\partial^2 U_n^i}{\partial s^2} - \frac{\partial^3 W_n^i}{\partial s^3}\right) = j\frac{D}{a^3}\sum_{n=0}^{\infty}\sum_{b=1}^{4}\left(\hat{k}_{nb}^2\alpha_{nb} + \hat{k}_{nb}^3\right)\overline{\overline{W}}_{nb}^i \cos[n(\theta-\phi)] \qquad \ldots(3.49)$$

So, the wave amplitudes can easily be determined by using equation (3.34), in which half of the excitation force is applied as follows.

$$V_s^+\Big|_{s=0} = \frac{1}{2a}F_0\delta(\theta-\phi) \qquad \ldots(3.50)$$

Substituting for V_s^+ from equation (3.49) and $\delta(\theta-\phi) = \frac{1}{2\pi}\sum_{n=0}^{\infty}\varepsilon_n \cos[n(\theta-\phi)]$ obtained from equation (3.3) into equation (3.50) yields the relationship between the radial amplitude and excitation force for a particular mode as given by

$$\sum_{b=1}^{4}\left(\hat{k}_{nb}^2\alpha_{nb} + \hat{k}_{nb}^3\right)\overline{\overline{W}}_{nb}^i = -j\frac{a^2}{4\pi D}F_0\varepsilon_n \qquad \ldots(3.51)$$

where $\varepsilon_n = 1$ for $n = 0$ and

$\varepsilon_n = 2$ for $n \geq 1$.

Once the boundary conditions at the position of the force are established, the wave amplitudes can be determined by applying the conditions, $U_n^i = 0$, $\frac{\partial W_n^i}{\partial s} = 0$, $\frac{1}{n}\frac{\partial V_n^i}{\partial s} = 0$,

and by using force equilibrium, $V_s^+\Big|_{s=0} = \frac{1}{2a} F_0 \delta(\theta - \phi)$. Expressing the conditions and the force equilibrium in terms of the radial displacement, which are given in equation (3.43) and (3.51), respectively, and constructing them in matrix form yields

$$\begin{bmatrix} \alpha_{n1} & \alpha_{n2} & \alpha_{n3} & \alpha_{n4} \\ \hat{k}_{n1} & \hat{k}_{n2} & \hat{k}_{n3} & \hat{k}_{n4} \\ \frac{\hat{k}_{n1}\psi_{n1}}{n} & \frac{\hat{k}_{n2}\psi_{n2}}{n} & \frac{\hat{k}_{n3}\psi_{n3}}{n} & \frac{\hat{k}_{n4}\psi_{n4}}{n} \\ \hat{k}_{n1}^2\alpha_{n1} + \hat{k}_{n1}^3 & \hat{k}_{n2}^2\alpha_{n2} + \hat{k}_{n2}^3 & \hat{k}_{n3}^2\alpha_{n3} + \hat{k}_{n3}^3 & \hat{k}_{n4}^2\alpha_{n4} + \hat{k}_{n4}^3 \end{bmatrix} \begin{bmatrix} \overline{\overline{W}}_{n1}^{i} \\ \overline{\overline{W}}_{n2}^{i} \\ \overline{\overline{W}}_{n3}^{i} \\ \overline{\overline{W}}_{n4}^{i} \end{bmatrix} = \begin{bmatrix} 0 \\ 0 \\ 0 \\ -j\frac{\varepsilon_n a^2 F_0}{4\pi D} \end{bmatrix} \quad \ldots(3.52)$$

where α_{nb} and ψ_{nb} are given in equation 3.41 c, d respectively.

For the same reason as previously mentioned, $\frac{1}{n}\frac{\partial V_n^i}{\partial s} = 0$, is used instead of $\frac{\partial V_n^i}{\partial s} = 0$.

For the convenience of determining the radial wave amplitudes, the terms of α_{nb} and ψ_{nb} given in equations (3.41.c) and (3.41.d) are rearranged in the following form:

$$\alpha_{nb} = \frac{\hat{k}_{nb}(a_{n4}\hat{k}_{nb}^4 + a_{n2}\hat{k}_{nb}^2 + a_{n0})}{(d_{n4}\hat{k}_{nb}^4 + d_{n2}\hat{k}_{nb}^2 + d_{n0})} \quad \ldots(3.53\ a, b)$$

$$\frac{1}{n}\psi_{nb} = \frac{p_{n4}\hat{k}_{nb}^4 + p_{n2}\hat{k}_{nb}^2 + p_{n0}}{(d_{n4}\hat{k}_{nb}^4 + d_{n2}\hat{k}_{nb}^2 + d_{n0})}$$

where $a_{n4} = -\frac{1}{2}(1-\nu)(1+3\beta^2)\beta^2$

$$a_{n2} = \frac{3}{4}(1-\nu)^2\beta^4 n^2 - \frac{1}{2}(1-\nu)\nu(1+3\beta^2) + \beta^2\Omega^2$$

$$a_{n0} = \frac{1}{2}(1-\nu)\beta^2 n^4 + \frac{1}{2}(1-\nu)(1-\beta^2\Omega^2)n^2 + \nu\Omega^2$$

$$p_{n4} = -(1-\nu)\beta^2$$

$$p_{n2} = -\frac{1}{4}\left[2(2-(1+\nu)\nu)+\beta^2\left\{(1-\nu)(4+(3-\nu)\beta^2)n^2-2(3-\nu)\Omega^2\right\}\right]$$

$$p_{n0} = -\frac{1}{2}\left[(1-\nu)(1+\beta^2)n^2-2\Omega^2\right]$$

$$d_{n4} = \frac{1}{2}(1-\nu)(1+3\beta^2)$$

$$d_{n2} = \frac{1}{4}\left[(1-\nu)\left\{4+(1-\nu)(4+3\beta^2)\beta^2\right\}n^2-2\left\{2+(1-\nu)(1+3\beta^2)\right\}\Omega^2\right]$$

$$d_{n0} = \frac{1}{2}(n^2-\Omega^2)\left[(1-\nu)(1+\beta^2)n^2-2\Omega^2\right]$$

Replacing α_{nb} and ψ_{nb} in equation (3.52) yields the wave amplitudes for a particular mode in simple form as

$$\overline{\overline{W}}^{i}_{n1} = \frac{-j\varepsilon_n a^2 F_0 (d_{n4}\hat{k}_{n1}^4 + d_{n2}\hat{k}_{n1}^2 + d_{n0})}{2\pi D(1-\nu)(1+3\beta^2)(1-\beta^2)(\hat{k}_{n1}^2-\hat{k}_{n2}^2)(\hat{k}_{n1}^2-\hat{k}_{n3}^2)(\hat{k}_{n1}^2-\hat{k}_{n4}^2)\hat{k}_{n1}}$$

$$\overline{\overline{W}}^{i}_{n2} = \frac{-j\varepsilon_n a^2 F_0 (d_{n4}\hat{k}_{n2}^4 + d_{n2}\hat{k}_{n2}^2 + d_{n0})}{2\pi D(1-\nu)(1+3\beta^2)(1-\beta^2)(\hat{k}_{n2}^2-\hat{k}_{n1}^2)(\hat{k}_{n2}^2-\hat{k}_{n3}^2)(\hat{k}_{n2}^2-\hat{k}_{n4}^2)\hat{k}_{n2}} \quad \ldots(3.54\text{ a, b, c, d})$$

$$\overline{\overline{W}}^{i}_{n3} = \frac{-j\varepsilon_n a^2 F_0 (d_{n4}\hat{k}_{n3}^4 + d_{n2}\hat{k}_{n3}^2 + d_{n0})}{2\pi D(1-\nu)(1+3\beta^2)(1-\beta^2)(\hat{k}_{n3}^2-\hat{k}_{n1}^2)(\hat{k}_{n3}^2-\hat{k}_{n2}^2)(\hat{k}_{n3}^2-\hat{k}_{n4}^2)\hat{k}_{n3}}$$

$$\overline{\overline{W}}^{i}_{n4} = \frac{-j\varepsilon_n a^2 F_0 (d_{n4}\hat{k}_{n4}^4 + d_{n2}\hat{k}_{n4}^2 + d_{n0})}{2\pi D(1-\nu)(1+3\beta^2)(1-\beta^2)(\hat{k}_{n4}^2-\hat{k}_{n1}^2)(\hat{k}_{n4}^2-\hat{k}_{n2}^2)(\hat{k}_{n4}^2-\hat{k}_{n3}^2)\hat{k}_{n4}}$$

Since $\frac{a^2}{D} = \frac{1}{\rho h a^2 \beta^2 \omega_r^2}$, the wave amplitudes given in the above equation are similar to those obtained from the residue method expressed in equation (3.31).

For the n = 0 mode, $\overline{\overline{W}}^{i}_{02} = 0$ because the wavenumber of this branch is torsional as discussed in the previous section.

The positive-going mobility by this method is given by

$$Y^{i}_{n}(s,\theta) = -j\omega\frac{W^{i}_{n}(s,\theta)}{F_0} = -j\omega\frac{1}{F_0}\sum_{b=1}^{4}\overline{\overline{W}}^{i}_{nb}\cos\left[n(\theta-\phi)\right]e^{j\hat{k}_{nb}s} \qquad \ldots(3.55)$$

3.4 Evaluation of Mobility obtained from the Analytical Method

Numerical evaluation of the residue method described in the section (3.2) together with the simplifications made by the assumptions in that section is conducted and compared with the analytical method. Taking the pipe data from table 2.1 (page 30), the numerical results of the simplified point mobility for circumferential modes n = 0, 1, 2, and 3 obtained using the residue method (equation 3.13), in which the residue term for the n = 0 and n = 1 modes are determined from equations (3.14) and (3.15), and for the n ≥ 2 modes is given in equation (3.21), are presented in figure 3.5. The mobilities are plotted against non-dimensional frequencies from 0.0012 to 0.8, which corresponds to 10 Hz to 6.7 kHz for the pipe used in this thesis. The predictions calculated using the analytical method using equation (3.55) are also shown in this figure.

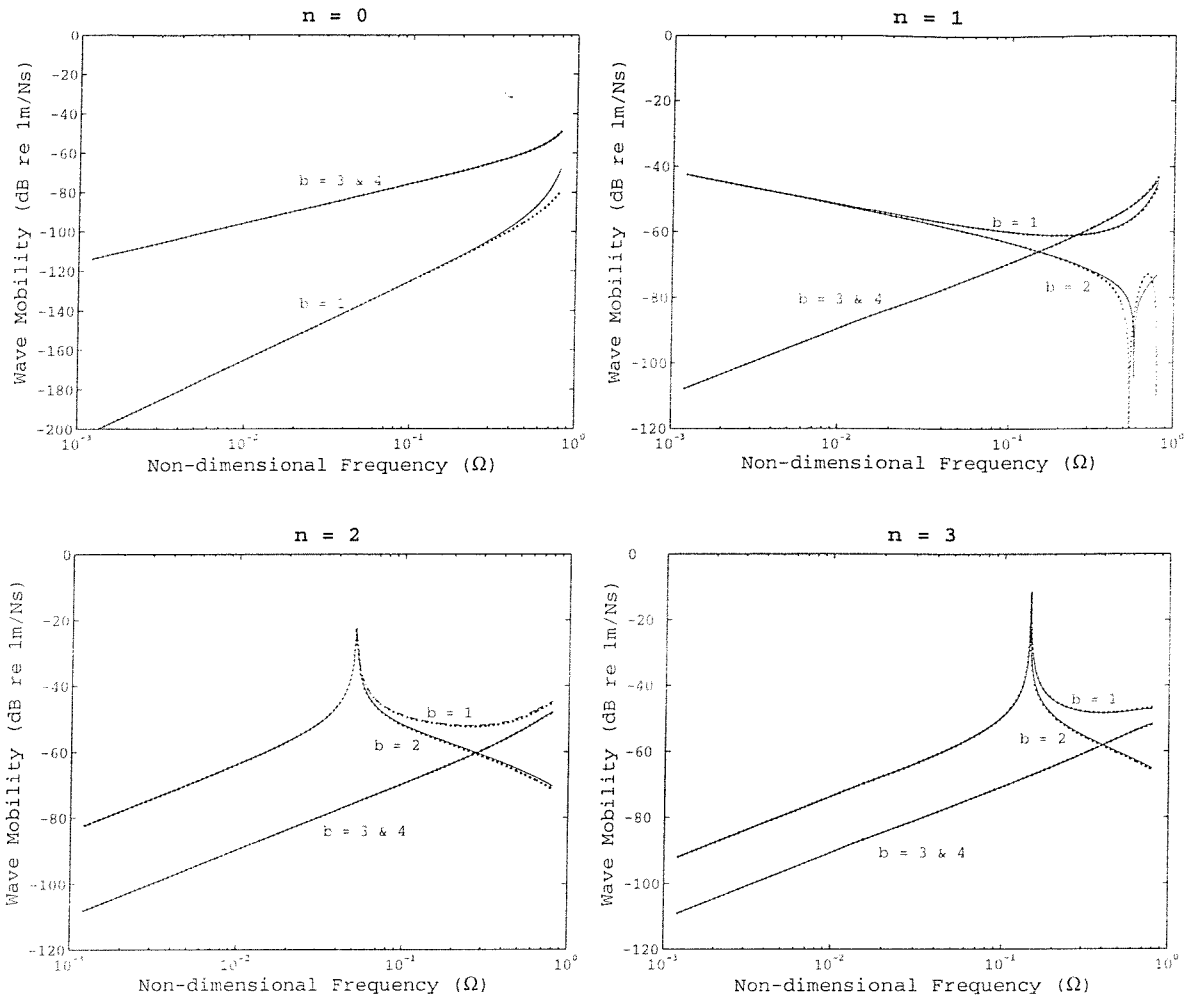

Figure 3.5: Wave mobility of the modes n = 0 to n = 3 of the infinite pipe; __ Analytical method, ... Simplification obtained from equations (3.14), (3.15), and (3.21) for the n = 0, 1 and ≥ 2 modes, respectively.

The simplified formulae show good agreement with the original formulae. It can be seen for the n = 0 mode that the standing near field waves, b = 3 and 4, dominate the motion of the pipe. However, these waves rapidly decay away from the excitation point. So, in the far field, where there are no effects of evanescent waves generated by the point force, only the longitudinal wave, b = 1, propagates along the infinite pipe. Due to the small amplitude of the longitudinal wave, it should be noted that the scale used in the figure for this mode is different from that for the other modes. For the n = 1 mode, the flexural (b = 1) and the near field (b = 2) waves dominate the response of the infinite pipe, especially at low frequencies. The effect of the standing near field waves, b = 3 and

4, increases with increasing frequency. For the n = 2 mode, before the waves cut on, all waves are standing near field waves. These waves can be separated into two groups, which have small (b = 1 and 2) and large (b = 3 and 4) wavenumbers as shown in the dispersion curve (figure 2.3). Those with small wavenumbers have a larger wavelength resulting in larger motion. After the waves cut on, the standing near field waves with small wavenumbers disappear and the flexural (b = 1) and near field (b = 2) waves start to propagate. Both waves dominate the pipe motion. Like the n = 1 mode, the standing near field waves influence the response of the n = 2 mode at high frequencies. The dynamic behaviour of the n = 3 mode is similar to that of the n = 2 mode except it has a higher cut-on frequency.

3.5 Approximate Mobility of Infinite Pipes at Low Frequencies

In this section, the expressions for the wave amplitudes derived in the previous section are simplified by making low frequency approximations. The n = 0 and higher modes are considered separately because of their distinguishable behaviour, and the simplified expressions are compared with the original form using point and transfer mobilities. It should be noted that the term called transfer mobility here is the mobility in the far field, where there are negligible effects of evanescent waves generated by the point force.

At very low frequencies ($\Omega^2 << 1$), $\hat{k}_{n1}$ and $\hat{k}_{n2}$ are much smaller than $\hat{k}_{n3}$ and $\hat{k}_{n4}$, which are the standing near field wavenumbers, and can be ignored. Also neglecting β^2 in comparison with unity, the wave amplitudes obtained from equation (3.54) become

$$\overline{\overline{W}}^{i}_{n1} = \frac{-j\varepsilon_n a^2 F_0 (d_{n4}\hat{k}_{n1}^4 + d_{n2}\hat{k}_{n1}^2 + d_{n0})}{2\pi D (1-\nu)\hat{k}_{n1}\hat{k}_{n3}^2\hat{k}_{n4}^2(\hat{k}_{n1}^2 - k_{n2}^2)}$$

$$\overline{\overline{W}}^{i}_{n2} = \frac{-j\varepsilon_n a^2 F_0 \,(d_{n4}\hat{k}_{n2}^4 + d_{n2}\hat{k}_{n2}^2 + d_{n0})}{2\pi D\,(1-\nu)\,\hat{k}_{n2}\hat{k}_{n3}^2\hat{k}_{n4}^2(\hat{k}_{n2}^2 - \hat{k}_{n1}^2)} \qquad \ldots(3.56\text{ a, b, c, d})$$

$$\overline{\overline{W}}^{i}_{n3} = \frac{-j\varepsilon_n a^2 F_0 \,(d_{n4}\hat{k}_{n3}^4 + d_{n2}\hat{k}_{n3}^2 + d_{n0})}{2\pi D\,(1-\nu)\,\hat{k}_{n3}^5(\hat{k}_{n3}^2 - \hat{k}_{n4}^2)}$$

$$\overline{\overline{W}}^{i}_{n4} = \frac{-j\varepsilon_n a^2 F_0 \,(d_{n4}\hat{k}_{n4}^4 + d_{n2}\hat{k}_{n4}^2 + d_{n0})}{2\pi D\,(1-\nu)\,\hat{k}_{n4}^5(\hat{k}_{n4}^2 - \hat{k}_{n3}^2)}$$

Mobility of the n = 0 mode of an infinite pipe

From the previous discussion in section 3.4, the standing near field waves dominate the response of the pipe at the excitation point and only the longitudinal propagating wave dominates the response in the far field. Hence, the point mobility of the n = 0 mode of an infinite pipe is the combination of both standing near field waves and the transfer mobility consists only of the longitudinal propagating wave.

For convenience, the wavenumbers of the n = 0 mode obtained in chapter 2 are written down here with the negative sign denoting a real wave type and the positive sign of the imaginary part of complex wave types denoting wave motion in the positive direction. They are

$$\hat{k}_{01} = -\hat{k}_l, \qquad \hat{k}_{02} = -\hat{k}_s \qquad \text{and} \quad \hat{k}_{03}, \hat{k}_{04} = \left[\frac{\left(1-\nu^2\right)\left(1-\hat{k}_f^2\right)}{4\beta^2}\right]^{1/4}(\pm 1 + j) \qquad \ldots(3.57\text{ a, b, c, d})$$

The term $(d_{n4}\hat{k}_{0b}^4 + d_{n2}\hat{k}_{0b}^2 + d_{n0})$ of the n = 0 mode is given by

$$(d_{n4}\hat{k}_{0b}^4 + d_{n2}\hat{k}_{0b}^2 + d_{n0}) = (\hat{k}_{0b}^2 - \Omega^2)\left[\frac{1}{2}(1-\nu)\,(1+3\beta^2)\,\hat{k}_{0b}^2 - \Omega^2\right] \qquad \ldots(3.58)$$

The analysis is for low frequencies, in which $\hat{k}_l^2$ is very small, and so can be neglected in comparison with unity. Substituting for the bending stiffness, $D = \frac{Eh^3}{12(1-\nu^2)}$, and the wavenumbers into equation (3.56.a) gives the amplitude of the $\overline{\overline{W}}_{01}^{i}$ radial wave as

$$\overline{\overline{W}}_{01}^{i} = \frac{j\nu^2\hat{k}_l F_0}{4\pi K(1-\nu^2)} \qquad \ldots(3.59\ a)$$

In addition to the assumption of a very small longitudinal wave amplitude at low frequencies, for the standing near field waves, $\hat{k}_{03}^2, \hat{k}_{04}^2 >> \Omega^2$ can also be assumed. Hence, the standing near field radial wave amplitudes becomes

$$\overline{\overline{W}}_{03}^{i} = \frac{-jF_0}{8\pi\beta^2 K\hat{k}_{03}^3}$$

$$\overline{\overline{W}}_{04}^{i} = \frac{-jF_0}{8\pi\beta^2 K\hat{k}_{04}^3} \qquad \ldots(3.59\ b, c)$$

The relationship of both wave amplitudes is readily established by substituting their wavenumbers and is

$$\overline{\overline{W}}_{04}^{i} = \frac{\hat{k}_{03}^3}{\hat{k}_{04}^3}\overline{\overline{W}}_{03}^{i} = j\overline{\overline{W}}_{03}^{i} \qquad \ldots(3.60)$$

It should be noted here that the radial wave amplitude of the torsional wave, $\overline{\overline{W}}_{02}^{i}$, is not simplified because it is equal to zero as described in section 3.2.

As previously discussed, the standing near field waves dominate the motion of the infinite pipe at the excitation point. Hence, the approximate point mobility is given by

$$Y_0^{iP} = -j\omega \frac{(\overline{\overline{W}}_{03}^{i} + \overline{\overline{W}}_{04}^{i})}{F_0} = -\frac{(1+j)\omega}{8\pi\beta^2 K \hat{k}_{03}^3} \qquad \ldots(3.61)$$

The approximate transfer mobility is dominated by the longitudinal propagating wave and is thus given by

$$Y_0^{iT}(s,\theta) = -j\omega \frac{\overline{\overline{W}}_{01}^{i}}{F_0} = \frac{\omega\nu^2 \hat{k}_1}{4\pi K(1-\nu^2)} e^{-j\hat{k}_1 s} \qquad \ldots(3.62)$$

Mobility of the n ≥ 1 mode of an infinite pipe

Unlike the n = 0 mode, for the n ≥ 1 modes the radial wave amplitude due to the standing near field waves is much smaller than that caused by the flexural and near field waves at low frequencies as discussed in the previous section. Therefore the response of the pipe at the excitation is dominated by the flexural and near field waves. However, in the far field only the flexural propagating wave dominates the motion of the infinite pipe.

In order to simplify the mobility of the n ≥ 1 mode at low frequencies, the same assumptions are employed as in the analysis for the n = 0 mode. That is $\beta^2 << 1$, $\hat{k}_1^2 << 1$ and $\hat{k}_{nb}^2 >> \Omega^2$. The last assumption is because the flexural wavenumber rapidly

increases after the wave cuts on. By applying these assumptions, the term $(d_{n4}\hat{k}_{nb}^4 + d_{n2}\hat{k}_{nb}^2 + d_{n0})$ may be approximated to:

$$(d_{n4}\hat{k}_{nb}^4 + d_{n2}\hat{k}_{nb}^2 + d_{n0}) \equiv \frac{1}{2}(1-\nu)(n^2 + \hat{k}_{nb}^2)^2 \qquad \ldots(3.63)$$

Substituting this into equation (3.56 a, b) gives

$$\overline{\overline{W}}_{n1}^{i} = \frac{-ja^2 F_0 (n^2 + \hat{k}_{n1}^2)^2}{2\pi D\, \hat{k}_{n1}\hat{k}_{n3}^2\hat{k}_{n4}^2(\hat{k}_{n1}^2 - \hat{k}_{n2}^2)}$$

$$\overline{\overline{W}}_{n2}^{i} = \frac{-ja^2 F_0 (n^2 + \hat{k}_{n2}^2)^2}{2\pi D\, \hat{k}_{n2}\hat{k}_{n3}^2\hat{k}_{n4}^2(\hat{k}_{n2}^2 - \hat{k}_{n1}^2)} \qquad \ldots(3.64\text{ a, b})$$

So, the point mobility can be formulated as

$$Y_n^{iP} = -j\omega\frac{(\overline{\overline{W}}_{n1}^{i} + \overline{\overline{W}}_{n2}^{i})}{F_0}$$

$$= -\frac{a^2}{2\pi D\, \hat{k}_{n3}^2\hat{k}_{n4}^2(\hat{k}_{n1}^2 - \hat{k}_{n2}^2)}\left[\frac{(n^2 + \hat{k}_{n1}^2)^2}{\hat{k}_{n1}} - \frac{(n^2 + \hat{k}_{n2}^2)^2}{\hat{k}_{n2}}\right] \qquad \ldots(3.65)$$

and the transfer mobility is given by:

$$Y_n^{iT}(s,\theta) = -j\omega\frac{\overline{\overline{W}}_{n1}^{i}}{F_0} = -\frac{a^2(n^2 + \hat{k}_{n1}^2)^2}{2\pi D\, \hat{k}_{n1}\hat{k}_{n3}^2\hat{k}_{n4}^2(\hat{k}_{n1}^2 - \hat{k}_{n2}^2)}\cos[n(\theta-\phi)]e^{j\hat{k}_{nb}s} \qquad \ldots(3.66)$$

For the n = 1 mode, the axial wavenumbers of the n = 1 mode are given in section 2.3 and are repeated here for convenience.

$$\hat{k}_{11}^2, \hat{k}_{12}^2 = \frac{(\hat{k}_f^2 + \hat{k}_s^2) + \hat{k}_b^4}{2} \pm \frac{\hat{k}_b^2}{1-\hat{k}_f^2}$$

$$\hat{k}_{13}, \hat{k}_{14} = \left[\frac{\left(1-\nu^2\right)\left(1-\hat{k}_f^2\right)}{4\beta^2}\right]^{1/4}(\pm 1 + j) \qquad \ldots(3.67\ a, b, c, d)$$

where $\hat{k}_b^4 \equiv \frac{2\Omega^2}{1-\nu^2}$.

When $\Omega^2 << 1$, $\hat{k}_b^2 >> \hat{k}_b^4, \hat{k}_f^2, \hat{k}_s^2$, so the flexural and near field wavenumbers can be approximated as $\hat{k}_{11} = -\hat{k}_b$ and $\hat{k}_{12} = j\hat{k}_b$. Using these assumptions and setting $\hat{k}_b^2 << 1$, the radial wave amplitudes of the flexural and near field waves are given by

$$\overline{\overline{W}}_{11}^{i} = \frac{j(1+2\hat{k}_b^2)F_0}{4\pi h E \hat{k}_b^3}$$

$$\overline{\overline{W}}_{12}^{i} = \frac{(1-2\hat{k}_b^2)F_0}{4\pi h E \hat{k}_b^3} \qquad \ldots(3.68\ a, b)$$

Thus, the point mobility for the n = 1 mode is given by

$$Y_1^{iP} = \frac{\omega\left[(1-j)+2\hat{k}_b^2(1+j)\right]}{4\pi h E \hat{k}_b^3} \qquad \ldots(3.69)$$

and the transfer mobility for this mode is given by

$$Y_1^{iT}(s,\theta) = \frac{\omega(1+2\hat{k}_b^2)}{4\pi h E \hat{k}_b^3}\cos\left[n(\theta-\phi)\right]e^{j\hat{k}_b s} \qquad \ldots(3.70)$$

When $\Omega^2 << 1$, the flexural wavenumber tends to zero and thus the term containing $\hat{k}_b^2$ in the numerator of equations (3.69) and (3.70) can be neglected in comparison with unity and therefore the mobility of the n = 1 mode of the infinite pipe becomes that of an Euler-Bernoulli beam.

3.6 Evaluation of the Simplified Mobility of Infinite Pipes at Low Frequencies

In this section, the low frequency point and transfer mobilities discussed in the previous section, are validated by comparing them with the mobilities calculated using the original model. The point mobilities of the first four circumferential modes are shown in figure 3.6. So that the evanescent wave is sufficiently small in the far field, the transfer mobility is calculated at the non-dimensional distance s = 100 and is shown in figure 3.7.

It should be noted that the scale for the n = 0 mode in figure 3.7 is different to that for the other modes. From figures 3.6 and 3.7, the simplification of the mobility expressions clearly depends on there being a negligible contribution to the motion from other waves. For example, the radial wave amplitude for the n = 0 mode, which is dominated by the standing near field wave, is much higher than the longitudinal wave up to high frequencies resulting in a simplified mobility, which is valid at high frequencies as well. Unlike the n = 0 mode, the mobility of the n = 1 mode is only valid at relatively low frequencies where the flexural and near field waves dominate. For the same reason as for the n = 0 mode, the simplified mobility of the $n \geq 2$ mode is also valid at high frequencies. The table 3.1 gives a summary of the approximate mobility formulae derived in this section.

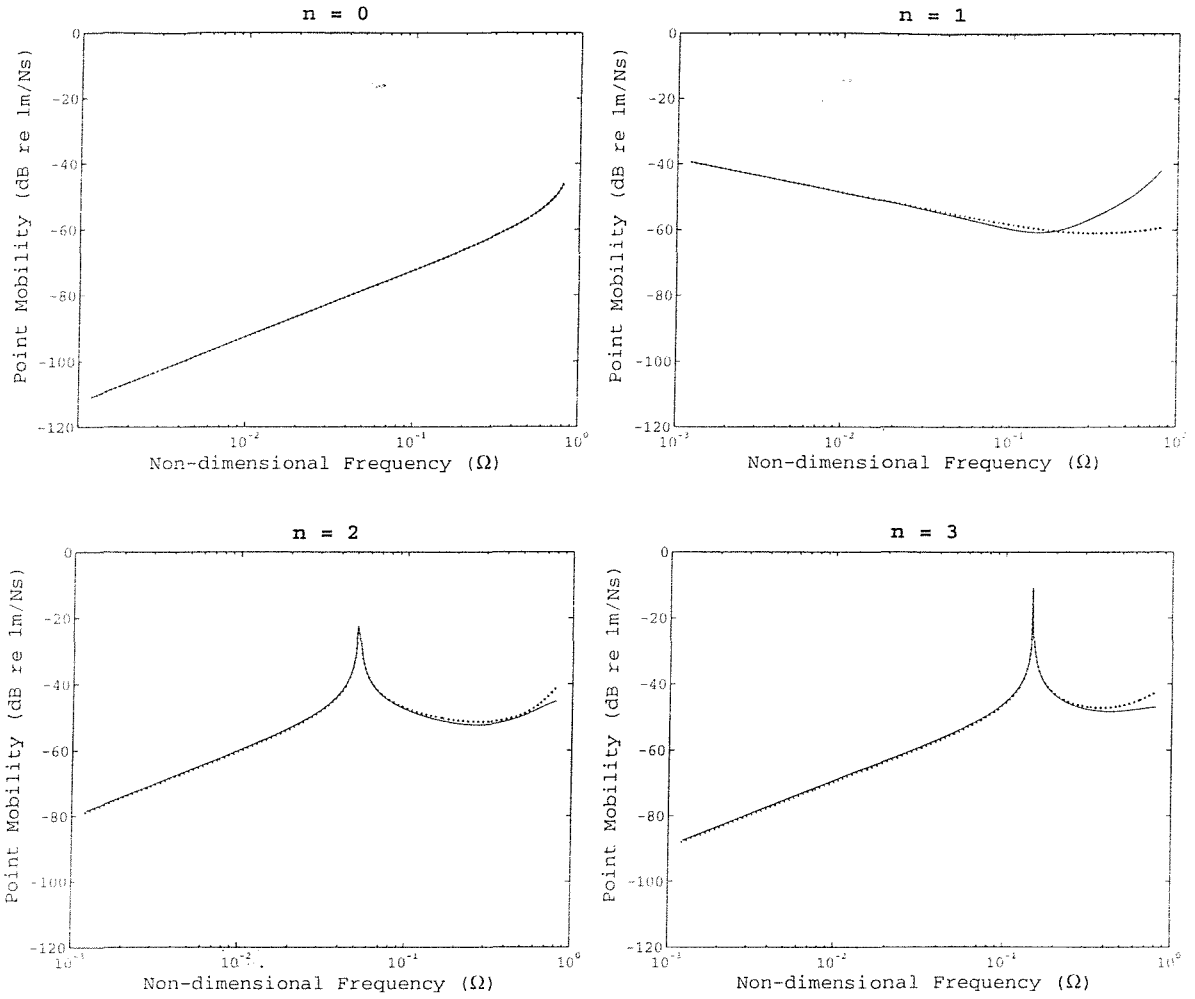

Figure 3.6: Point mobility of the n = 0 to n = 3 modes of an infinite pipe; __ Analytical method (equation 3.55), ... Simplification at low frequencies (equation 3.61, 3.69, and 3.65 for the n = 0, 1, ≥ 2 modes, respectively).

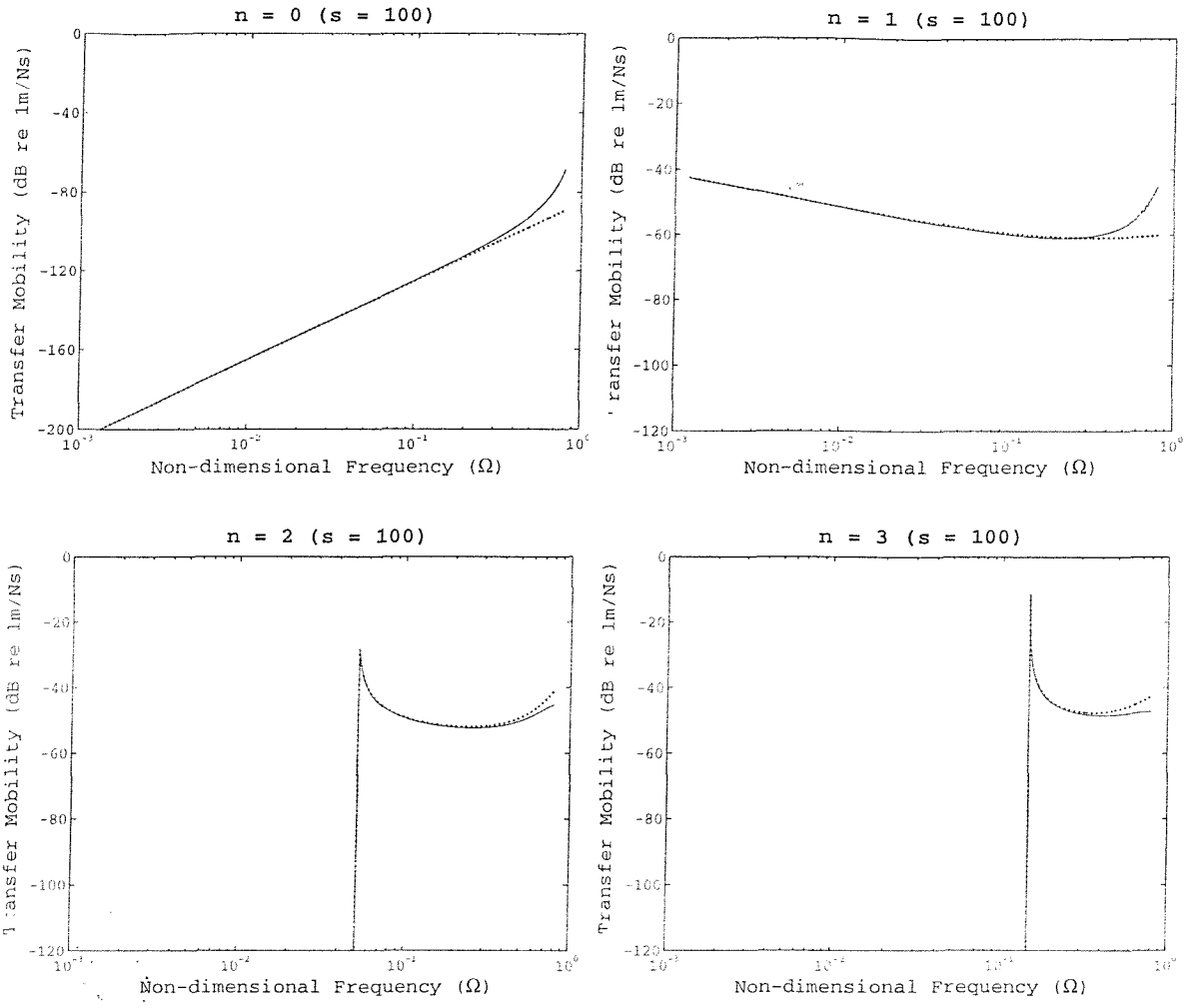

Figure 3.7: Transfer mobility of the n = 0 to n = 3 modes of an infinite pipe, which is calculated at the distance of s = 100; __ Analytical method (equation 3.55), ... Simplification at low frequencies (equation 3.62, 3.70, and 3.66 for the n = 0, 1, and ≥ 2 modes, respectively).

Table 3.1: Summary of the approximate mobility of an infinite pipe ($K = Eh/(1-\nu^2)$ is the membrane stiffness, $D = Eh^3/12(1-\nu^2)$ is the bending stiffness, equations 3.61, 3.69, 3.65 give the point mobility of the n = 0, 1, 2, and equations 3.62, 3.70, 3.66 give the transfer mobility of the n = 0, 1, 2, respectively).

Mode	Mobility	
	Point	Transfer
0	$-\dfrac{(1+j)\omega}{8\pi\beta^2 K\hat{k}_{03}^3}$	$\dfrac{\omega\nu^2\hat{k}_1}{4\pi K(1-\nu^2)}$
1	$\dfrac{\omega\left[(1-j)+2\hat{k}_b^2(1+j)\right]}{4\pi hE\hat{k}_b^3}$	$\dfrac{\omega(1+2\hat{k}_b^2)}{4\pi hE\hat{k}_b^3}$
≥ 2	$-\dfrac{a^2}{2\pi D\hat{k}_{n3}^2\hat{k}_{n4}^2(\hat{k}_{n1}^2-\hat{k}_{n2}^2)}\left[\dfrac{(n^2+\hat{k}_{n1}^2)^2}{\hat{k}_{n1}}-\dfrac{(n^2+\hat{k}_{n2}^2)^2}{\hat{k}_{n2}}\right]$	$-\dfrac{a^2(n^2+\hat{k}_{n1}^2)^2}{2\pi D\hat{k}_{n1}\hat{k}_{n3}^2\hat{k}_{n4}^2(\hat{k}_{n1}^2-\hat{k}_{n2}^2)}$

3.7 Experimental Validation

3.7.1 Introduction

In the previous sections, expressions for the mobility of infinite pipes were derived using two methods. Even though the theory obtained from both methods is consistent, it is worthwhile verifying them by conducting some experiments. In this section, the experiment, which is set up to validate the theoretical model, is described.

3.7.2 Experimental Setup

Before the experiments were carried out, the sensitivity of the PZT element, which was used as a force gauge, and the properties of the pipe, had to be determined. The PZT sensitivity in terms of charge per Newton was calibrated with a known mass of 4.357 kg and was found to be 341.7 pC/N.

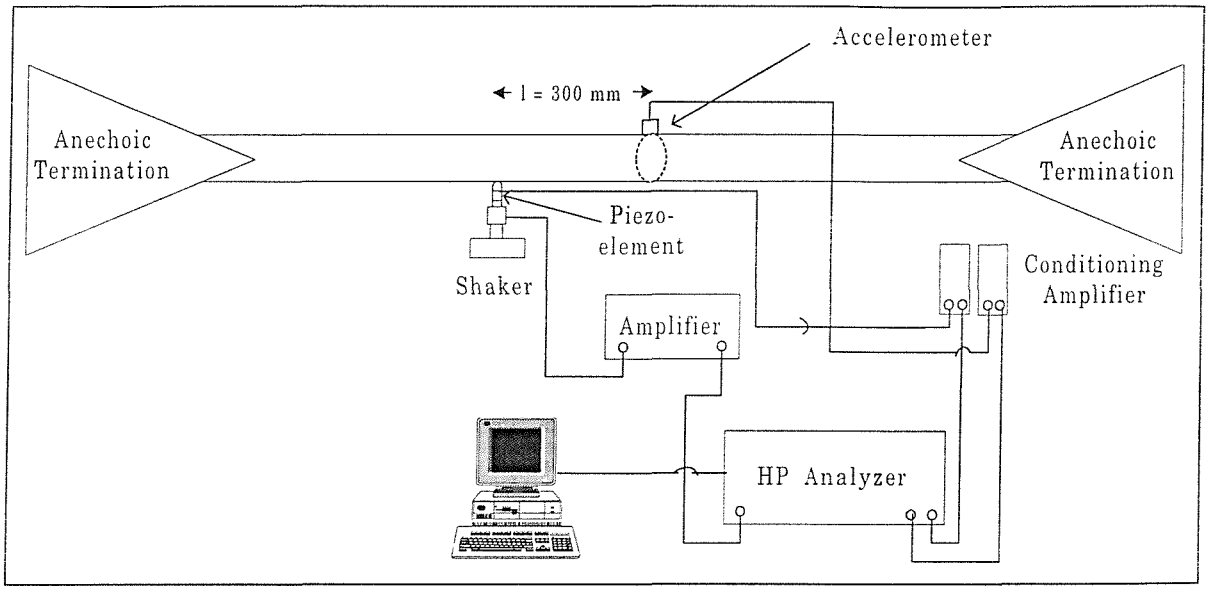

Figure 3.8: Experimental setup for the infinite pipe

Schematically, the diagram of the experimental setup for an infinite pipe is shown in figure 3.8. The 4.6 m PVC pipe, whose properties are given in table D.1 (appendix D), was suspended by cords and was fitted with anechoic terminations at both free ends in order to make the finite pipe behave as if it had infinite length. These terminations were wooden boxes containing sand. However, they do not perfectly absorb vibration so that some reflection from them still remains and interferes with the incident waves. To ensure that they had a reasonable performance so that the reflected waves could be ignored in comparison with the incident waves, a method of wave decomposition as described in appendix B was applied. A random signal from an HP 3566A Signal Analyzer was supplied to the shaker exciting the pipe at the mid-point between the anechoic terminations and the measurements were taken at a distance of 300 mm from the shaker by using two Bruel & Kjaer accelerometers type 4374, which were located at

a 180^0 circumferential angle to each other on the pipe. Once these two measurements were taken, both accelerometers were moved to the next circumferential angles (the interval angle is $\pi/32$) until a set of thirty-two measurements around the pipe was completed. This set of frequency response functions was used to verify the theory. In order to separate the incident and reflected waves by means of the wave decomposition, another two sets of thirty-two measurements were carried out at the distances of 975 and 1025 mm from the shaker. Since two accelerometers were used for this method, phase matching and cross sensitivity between them had to be determined prior to applying such a technique to avoid ill-conditioning. To do this both were fixed on the shaker and their measured responses were compared.

3.7.3 Experimental Results

In this section, the experimental results for the infinite pipe are presented and compared with predictions obtained from the theoretical models described in the previous sections. Comparisons between practice and theory are carried out with regard to two aspects, which are for each mode and for the total response for various angles of measurements. To make the comparison with the experimental results the complex elastic modulus of the pipe, $E' = E(1+j\eta)$ where η is the loss factor, was used in the predictions because of structural damping in the pipe. Wave decomposition of the motion of the infinite pipe is also presented.

Accelerometers used in the experiments detect the responses of all pipe modes. Thus to make a comparison for a particular mode between experimental results and predictions, the modal decomposition technique, described in appendix A, has to be applied to extract the modes from the total response. Before comparisons can be made, the orientation angle of the pipe has also to be determined, and the way in which this is obtained is also described in appendix A. For convenience, the formulae of the radial amplitude, A_m, and the orientation angle, ϕ, to be extracted from the experimental results, are repeated here

$$A_m = \frac{1}{N}\sqrt{\left[\sum_{p_\theta=0}^{N-1} H_{p_\theta} \cos\left(\frac{2\pi p_\theta}{N} m\right)\right]^2 + \left[\sum_{p_\theta=0}^{N-1} H_{p_\theta} \sin\left(\frac{2\pi p_\theta}{N} m\right)\right]^2}$$

$$\phi = \frac{1}{m}\tan^{-1}\left(\frac{\sum_{p_\theta=0}^{N-1} H_{p_\theta} \sin\left(\frac{2\pi p_\theta}{N} m\right)}{\sum_{p_\theta=0}^{N-1} H_{p_\theta} \cos\left(\frac{2\pi p_\theta}{N} m\right)}\right)$$

where m is the desired mode to be decomposed,

p_θ is the position of the measurement and

N is the number of measurements around the pipe.

H_{p_θ} is the frequency response at the position p_θ (Mobility).

Because in the experiment a finite pipe was used with anechoic terminations attached at both free ends, an incident wave generated by a point force was reflected at these terminations. To investigate the performance of the anechoic terminations on absorbing the reflected waves, all waves, which were incident and reflected, are decomposed. The method of decomposing waves is described in appendix B and shown in figure 3.9.

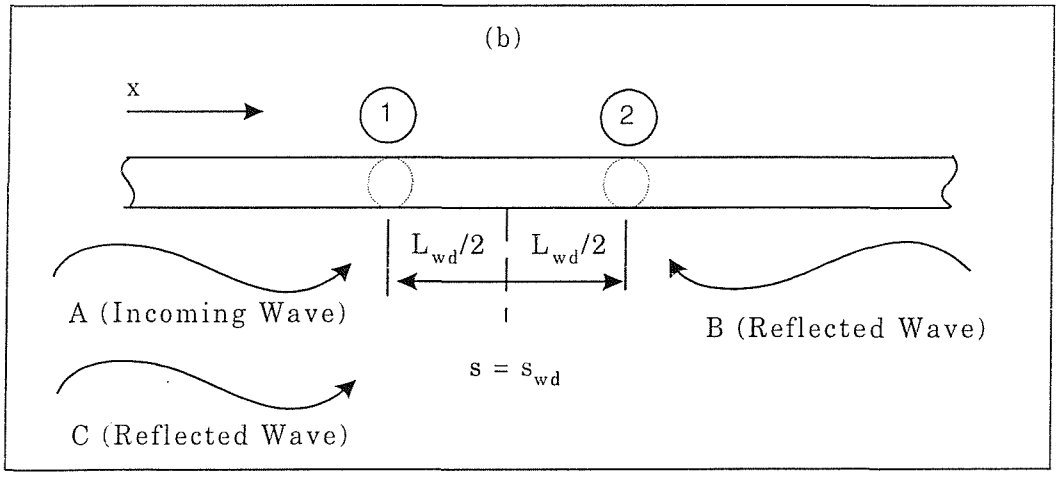

Figure 3.9: Wave decomposition of an infinite pipe, in which measurements around the pipe are taken at the point 1 and 2.

The waves (B) and (C) arise from the reflection of the incident waves at the anechoic terminations where both reflected waves are assumed to have the same radial amplitude. The expressions for Incoming wave (A) and both reflected waves (B) and (C) at the position $s = s_{wd}$ are given in appendix B.

It was shown in previous sections that the radial velocity of the pipe increases with increasing frequency. This implies that the sensor used in the experiment should be massless; otherwise it is difficult to move at high frequencies resulting in lower motion detected by the sensor. Unfortunately, the smallest accelerometer available for the experiment had a mass of 0.65 gram. Apart from the mass of the sensor, another factor, which affects the experimental results, is the tip mass of the PZT force sensor. It has the effect of reducing the excitation force. To reduce this effect, it was designed to have a very small mass of 0.08 gram. Both effects are described in appendix C.

The experimental results presented are as follows.

Frequency responses of each mode of the infinite pipe measured at a distance of 300 mm from the excitation position.

Figure 3.10 Amplitude of mobility of the n = 0 mode of the infinite pipe

Figure 3.11 Amplitude of mobility of the n = 1 mode of the infinite pipe

Figure 3.12 Amplitude of mobility of the n = 2 mode of the infinite pipe

Figure 3.13 Amplitude of mobility of the n = 3 mode of the infinite pipe

Orientation angle, ϕ, of the infinite pipe with respect to the force position extracted from the frequency response of each mode.

Figure 3.14 Orientation angle extracted from frequency response of the n = 1 mode

Frequency responses of the infinite pipe for various angles, θ, of measurements taken at distance 300 mm from the excitation position.

Wave decomposition for each mode of the infinite pipe measured at distance 975 mm and 1025 mm from the excitation position.

In figures 3.21, 3.22 and 3.23, the predicted mobility of the incident waves is calculated from equation (3.55) at the axial distance of 1000 mm, while that of the reflected waves is obtained by multiplying equation (3.55) with some values that give the approximate curve fitting to experimental results.

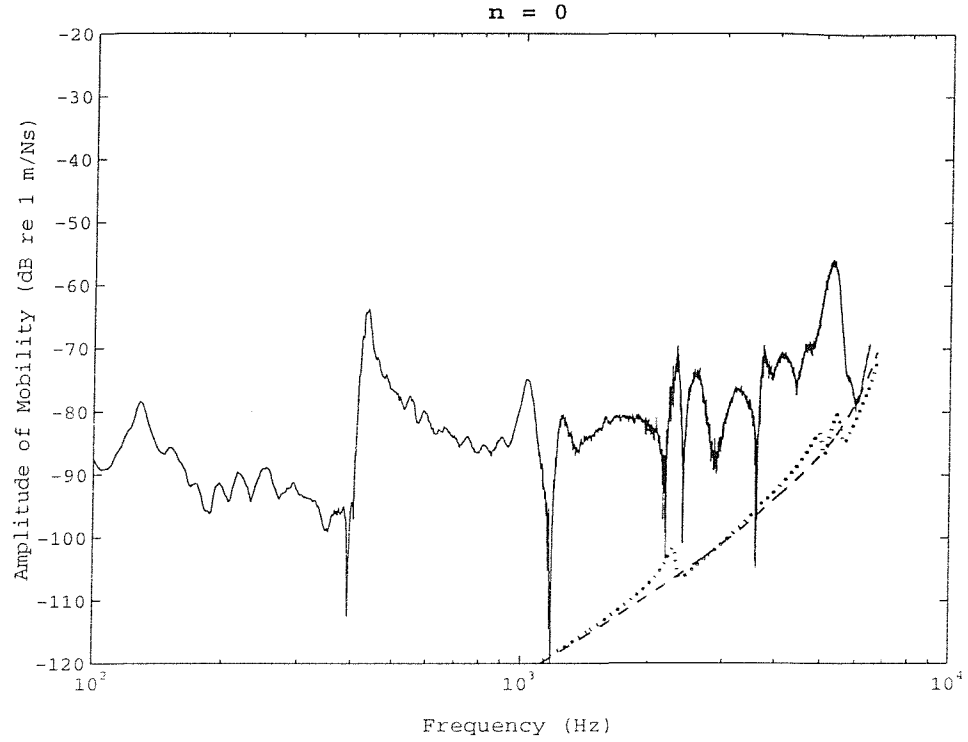

Figure 3.10: Amplitude of mobility of the n = 0 mode of the infinite pipe: __ Measured result; _ _ Prediction; ... Prediction with mass effect accounted for.

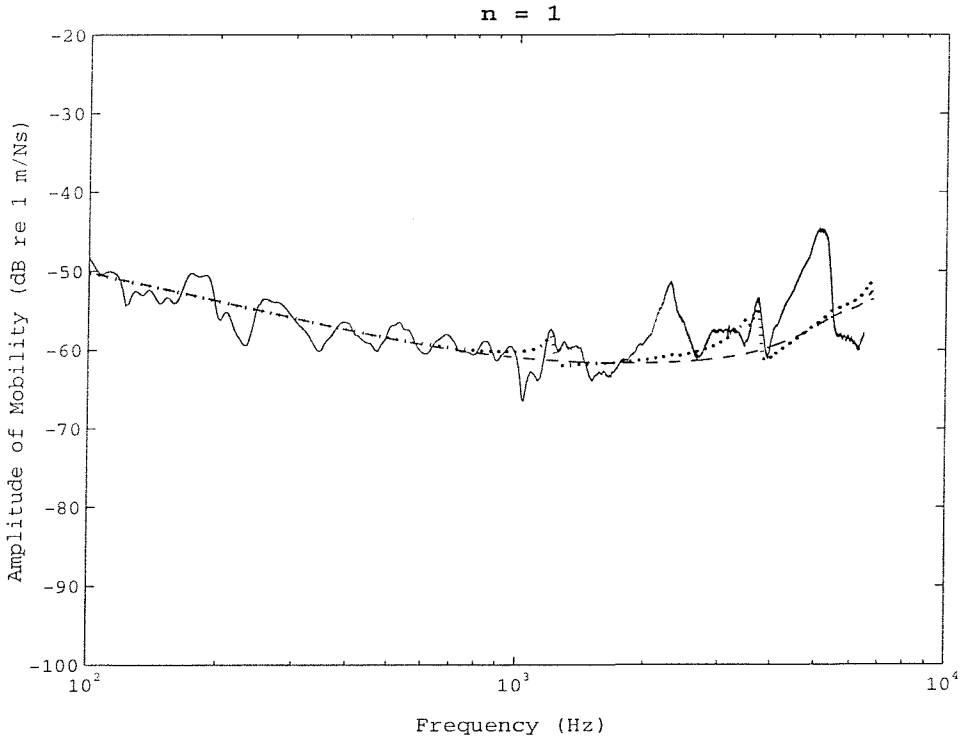

Figure 3.11: Amplitude of mobility of the n = 1 mode of the infinite pipe: __ Measured result; _ _ Prediction; ... Prediction with mass effect accounted for.

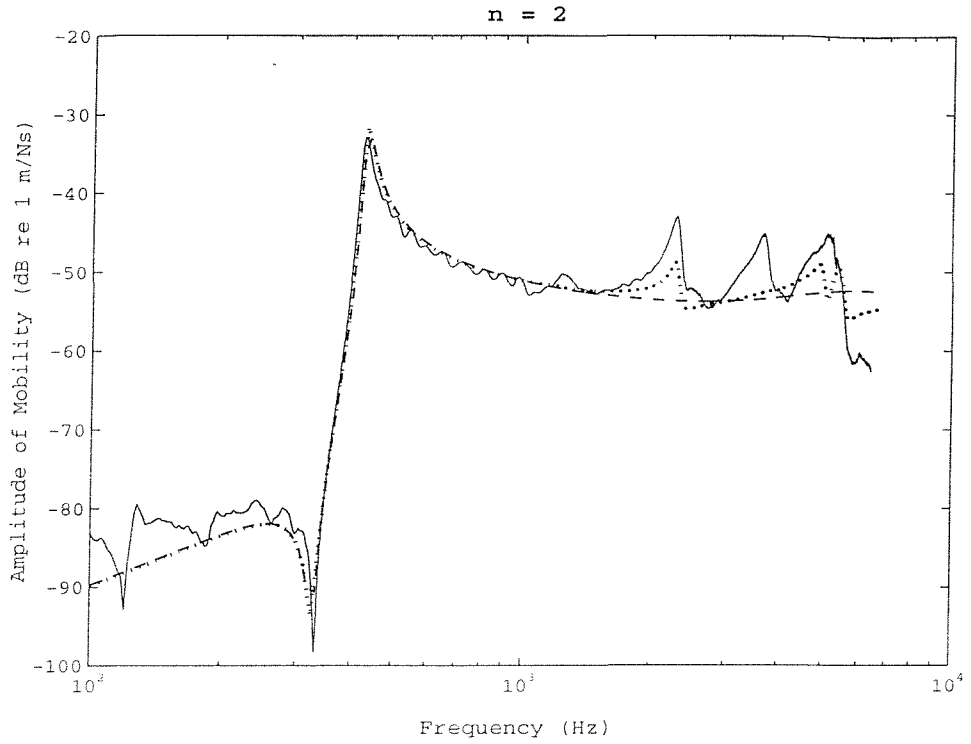

Figure 3.12: Amplitude of mobility of the n = 2 mode of the infinite pipe: __ Measured result; _ _ Prediction; ... Prediction with mass effect accounted for.

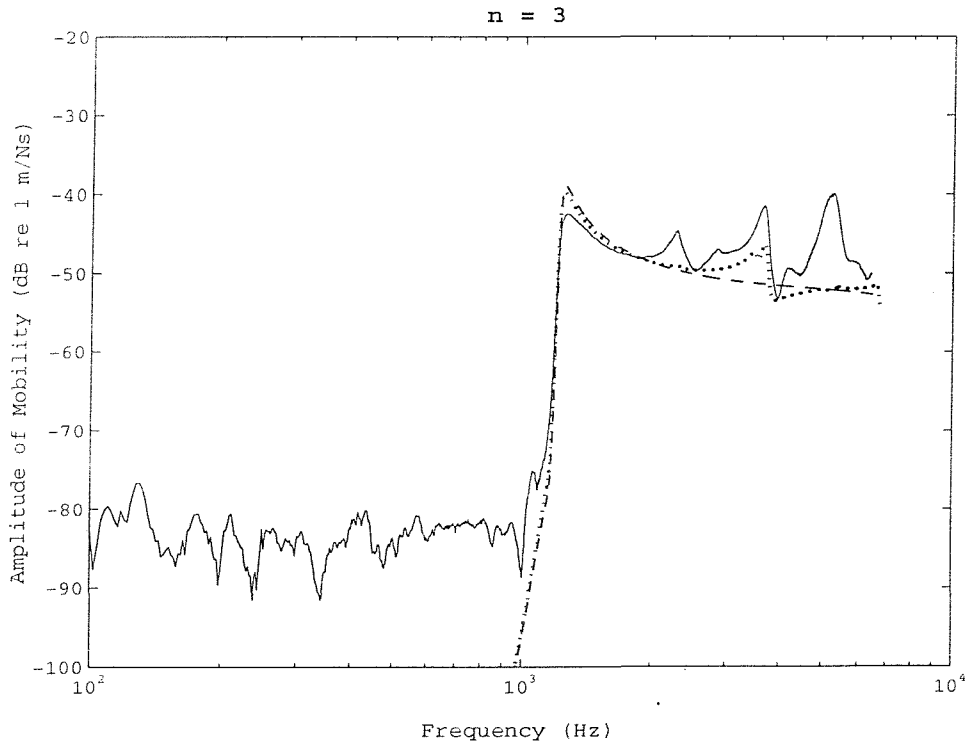

Figure 3.13: Amplitude of mobility of the n = 3 mode of the infinite pipe: __ Measured result; _ _ Prediction; ... Prediction with mass effect accounted for.

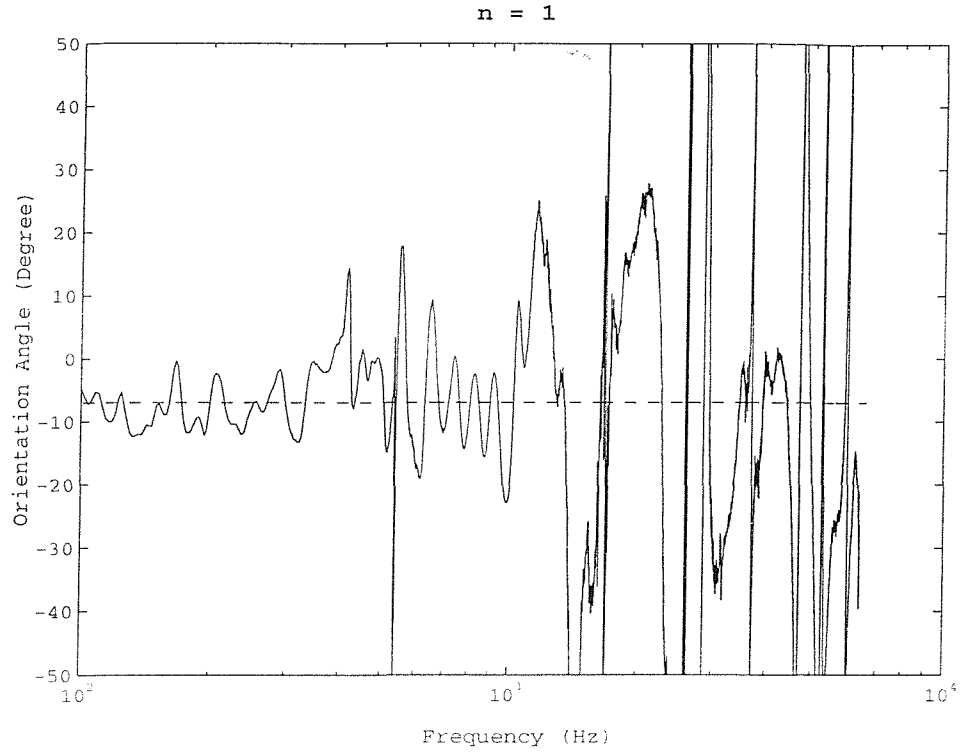

Figure 3.14: Orientation angle extracted from frequency response of the n = 1 mode.

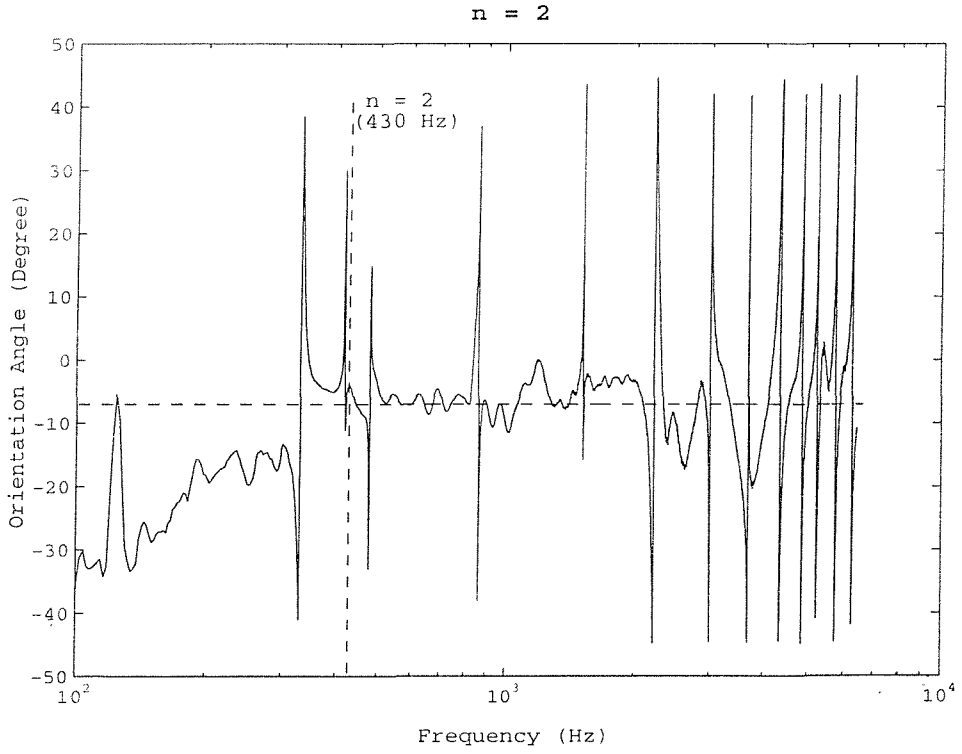

Figure 3.15: Orientation angle extracted from frequency response of the n = 2 mode.

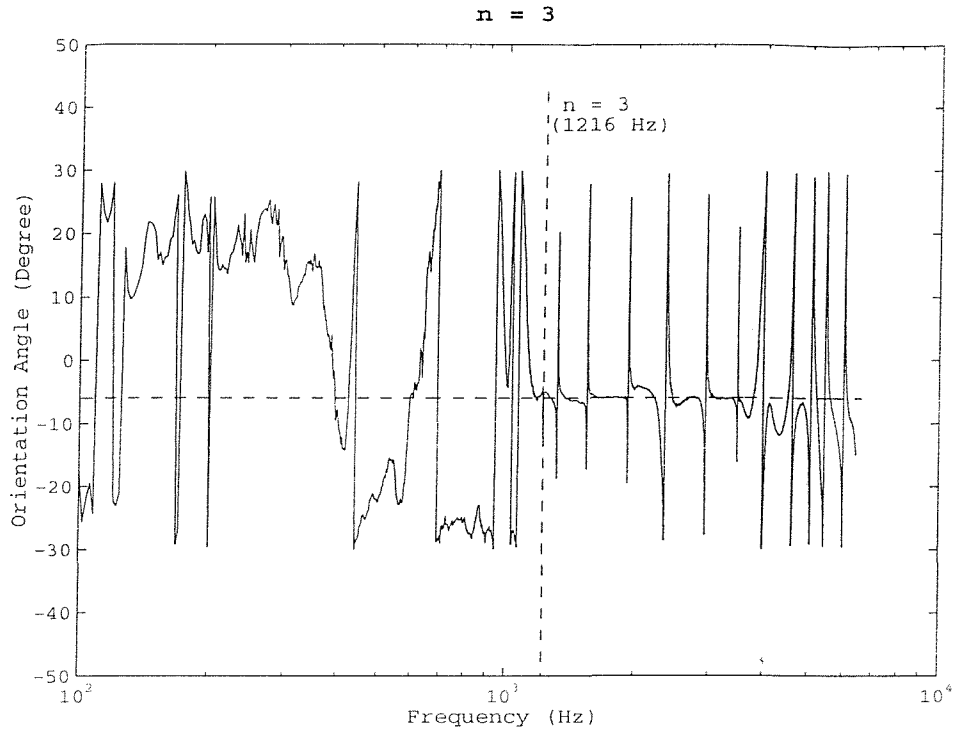

Figure 3.16: Orientation angle extracted from frequency response of the n = 3 mode.

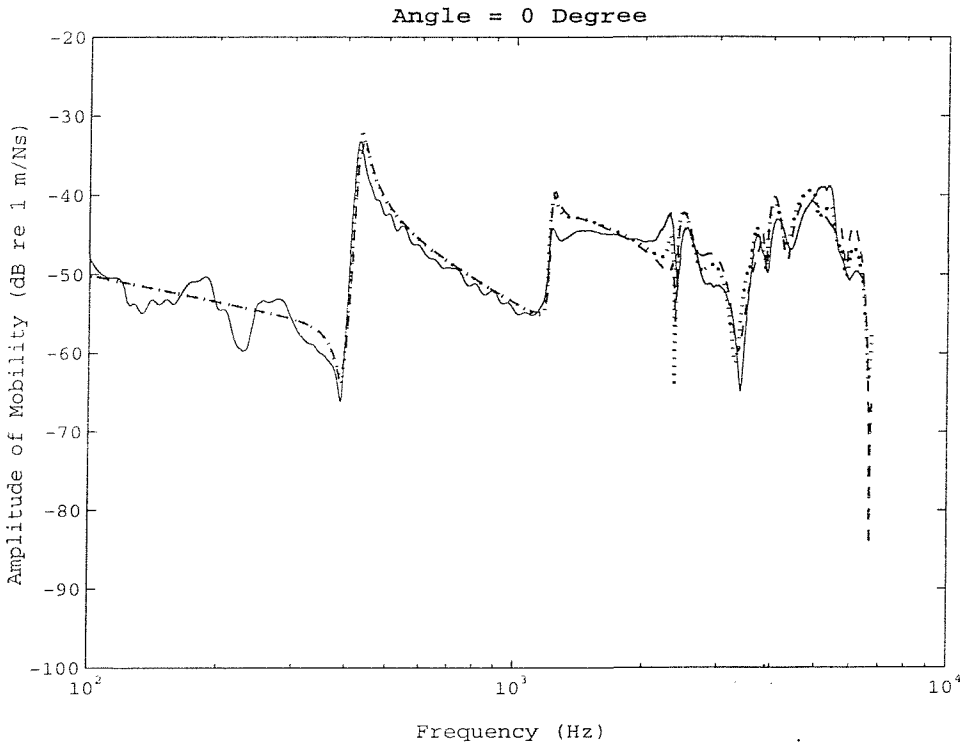

Figure 3.17: Amplitude of mobility of the pipe at θ = 0 and ϕ= -5: ___ Measured result; _ _ Prediction; ... Prediction with mass effect accounted for.

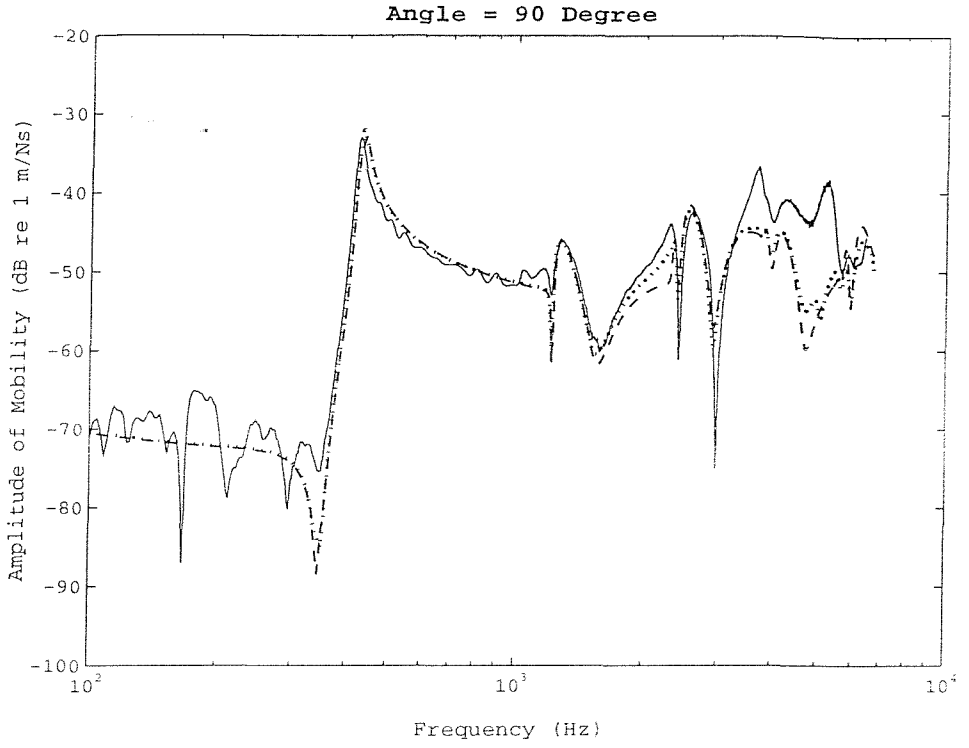

Figure 3.18: Amplitude of mobility of the pipe at θ = 90 and ϕ= -5: ___ Measured result; _ _ Prediction; ... Prediction with mass effect accounted for.

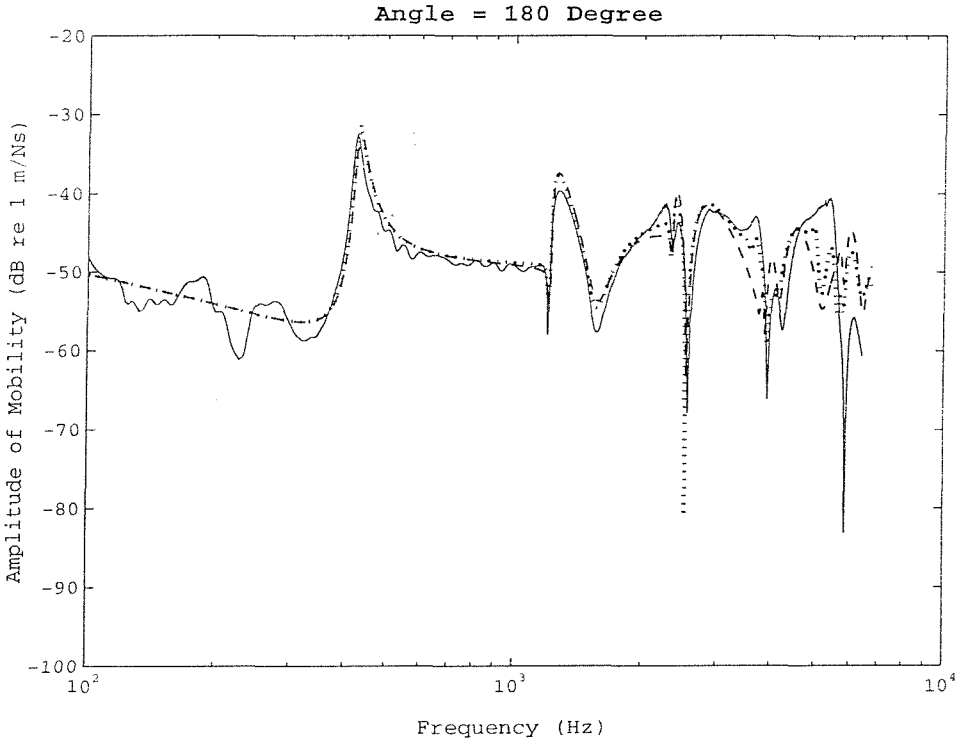

Figure 3.19: Amplitude of mobility of the pipe at θ = 180 and ϕ= -5: ___ Measured result; _ _ Prediction; ... Prediction with mass effect accounted for.

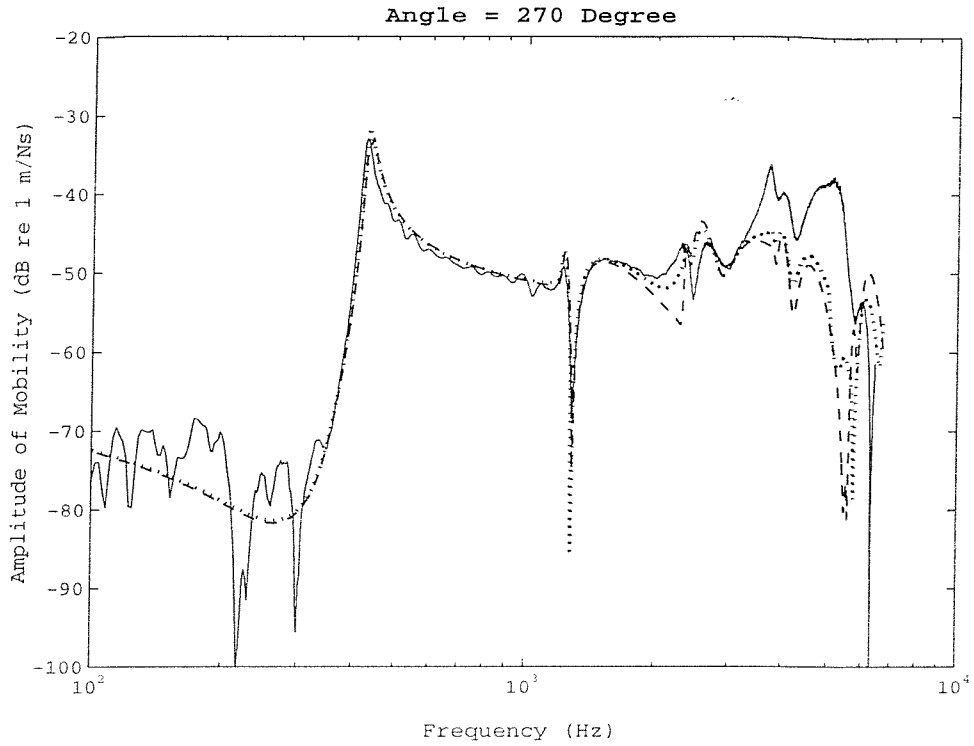

Figure 3.20: Amplitude of mobility of the pipe at θ = 270 and ϕ= -5: ___ Measured result; _ _ Prediction; ... Prediction with mass effect accounted for.

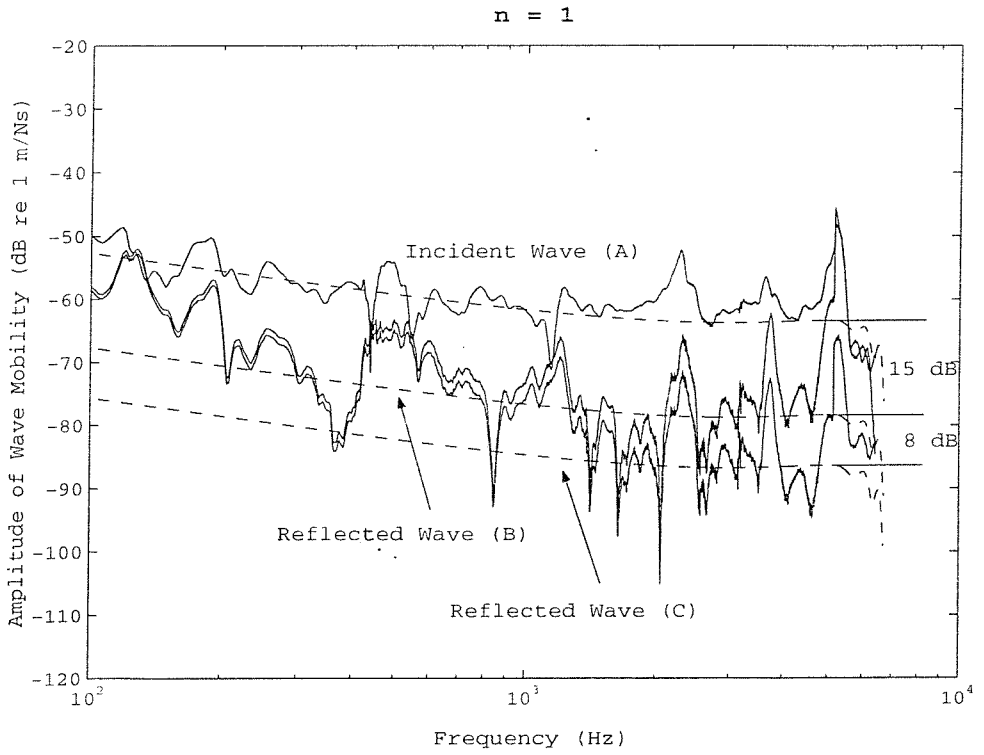

Figure 3.21: Wave decomposition for the n = 1 mode of the infinite pipe; _ _ Prediction.

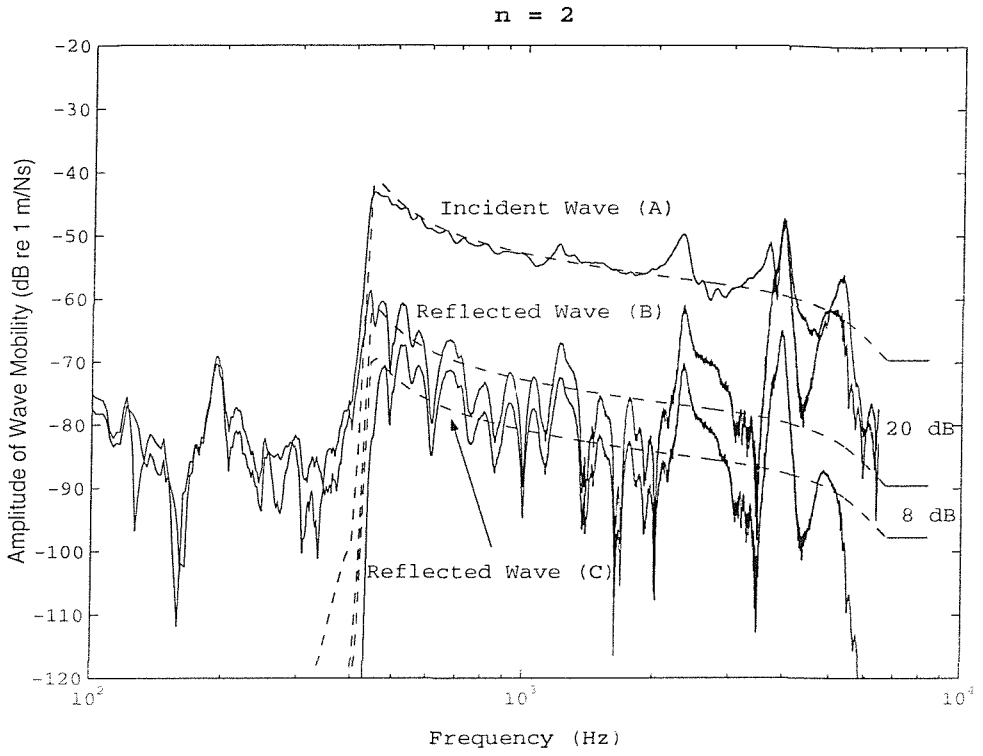

Figure 3.22: Wave decomposition for the n = 2 mode of the infinite pipe; _ _ Prediction.

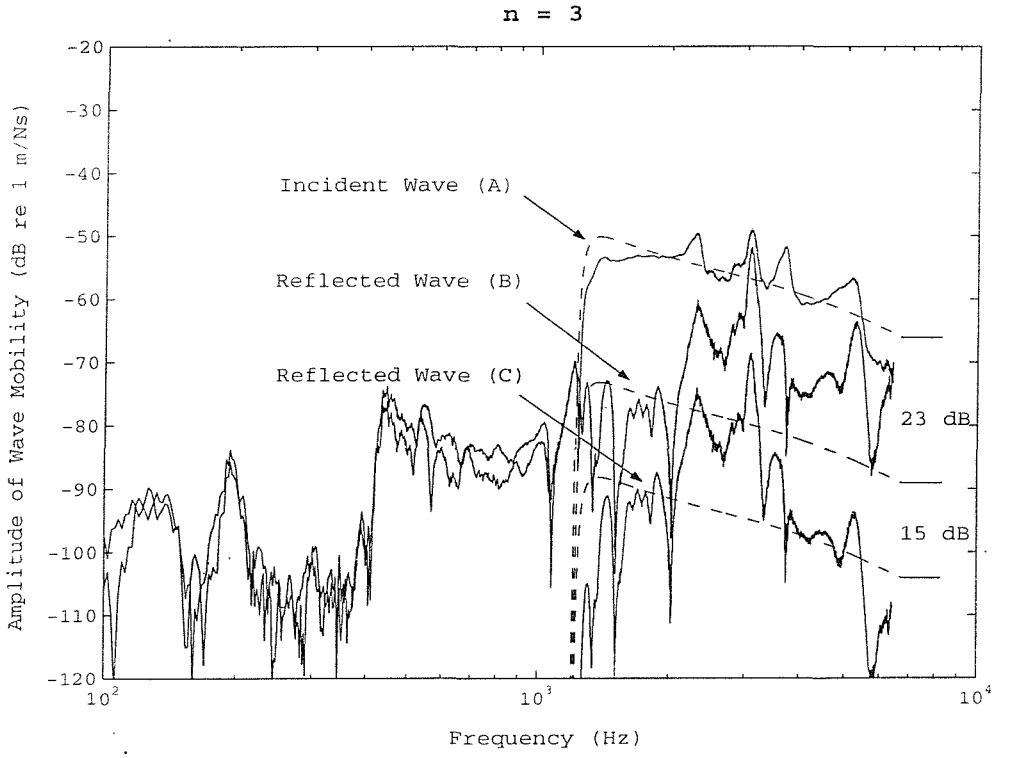

Figure 3.23: Wave decomposition for the n = 3 mode of the infinite pipe; _ _ Prediction.

3.7.4 Discussion

Because a PVC pipe is a light structure, it tends to be affected by the mass loading of accelerometers and from the reduction of the excitation force due to the tip mass of the PZT force gauge as described in appendix C. In order to reduce such effects, those masses were set to be small in the experimental design stage, and were 0.65 grams for the accelerometer and 0.08 grams for the tip of the PZT. Even though small masses were used, however, their effect, especially at high frequencies, was still present in the experimental results as shown in figures 3.10-3.13 and 3.17-3.20. For the n = 0 mode, the mobility is very small, especially at low frequencies. So, it is difficult to detect this using accelerometers leading to a poor signal to noise ratio and an inaccurate result as shown in figure 3.10. Another way to detect this mode is to use PVDF wire, which senses strain proportional to the radial displacement of the pipe (Pinnington and Briscoe [7] and Brennan *et al* [8]). Unlike the n = 0 mode, the experimental results of the modes, n = 1, 2 and 3, were consistent with the predictions except at the cut-on frequencies of $n \geq 4$ modes as shown in figure 3.11-3.13. This might be because of the inaccurate positioning of the accelerometers around the pipe or the high wave reflections from the anechoic terminations of the higher modes at their cut-on frequencies as shown in figures 3.21-3.23. In order to reduce such high wave reflections, Fuller and Brevart [9] used damping material wrapped around a pipe but the effect of reflected higher order modes still remained in their experiment results. This implies that it is difficult to suppress the reflected waves of the higher order modes unless the pipe is long enough or has a high loss factor. The orientation angle, ϕ, of the pipe with respect to the force position was illustrated in figures 3.14-3.16. This angle is constant for all modes and should be taken into account after the wave of the considered mode cuts on and before the higher modes cut on. Since, before the mode of interest cuts on, the pipe motion of this mode is very small, it is difficult to detect using the accelerometers. After the higher modes cut on there is some interference due to the reflected waves from the anechoic terminations and inaccurate positions of the acccelerometers. Once the orientation angle of the pipe had been determined, the total mobility obtained from the experiment results could be compared with the predictions. They are in good agreement up to high frequencies where the strong reflected waves occurred as shown in figures 3.17-3.20 for various measurement angles of the

accelerometers. In order to be sure that the pipe behaves like an infinite pipe the reflected waves, which arise from both anechoic terminations, were investigated by means of wave decomposition and are shown in figures 3.21-3.23 for the modes n = 1, 2 and 3. The n = 0 mode was not considered because of the small mobility of this mode as previously discussed. Moreover, the anechoic terminations used in this work have little effect on the longitudinal wave, which dominates the response of the n = 0 mode. A suitable method of reducing the longitudinal wave is to use a plate attached at the end of the pipe as described by Brennan *et al* [72]. From the figures of wave decomposition, it is clearly demonstrated that the anechoic terminations are good enough to ignore the effect of the reflected waves except at the cut-on frequencies of higher order modes, $n \geq 4$. The figures also show the reduction of the response due to the damping of the pipe itself, which is the difference between the reflected waves from both anechoic terminations.

3.8 Conclusions

Expressions for the mobility of infinite pipes have been derived using two methods, the Residue and the Analytical methods. Even though the Residue method has a certain mathematical elegance, the Analytical method gives additional physical information, such as there is no slope, no twist and no axial displacement at the excitation position. Theoretical evaluation illustrates that the mobility obtained from both methods is exactly the same.

In addition, the simplification of the expressions at low frequencies, $\Omega^2 << 1$, for the point and transfer mobilities is also developed. Good agreement with the original expressions is achieved. By numerical evaluation, it is clearly shown that the simplified mobility for the n = 0 mode is valid up to high frequencies. Excluding the n = 1 mode, the simplification of the higher modes are also valid up to high frequencies.

Experimental validation for the theoretical models of infinite pipes has been achieved. Even though an accelerometer with a small mass was selected, the effect of its mass was still apparent, especially at high frequencies. This is because the pipe is highly mobile at high frequencies, which is in contrast with the accelerometer. To compare the theoretical predictions and the experimental results the mass loading of the accelerometers and the force gauge had to be accounted for.

CHAPTER 4

MOBILITY OF SEMI-INFINITE PIPES

4.1 Introduction

In the previous chapter, the dynamic behaviour of an infinite pipe in terms of the mobility has been investigated. A further study of the mobility is carried out in this chapter, but the application is on a semi-infinite pipe. Unlike the infinite pipe, the derivation for a semi-infinite pipe can be analysed in a straight forward manner using four boundary conditions. Such work using the Analytical method has been done by Flugge [5], Vinson [24], Young [25], and Pan and Hansen [26].

Apart from the Analytical method, the Wave method, in which the analysis is based on a wave point of view rather than a mode point of view, is also employed to analyse the mobility of a semi-infinite pipe in this chapter. This method has been used for a beam before as described by Mace [54], Mead [12], Brennan [73]. However to the author's knowledge, it has never been applied to a semi-infinite pipe.

With the mobility obtained from the Wave method, simplification at low frequencies can be carried out. Like the infinite pipe, the analysis of the approximate mobility is conducted so that the behaviour of a semi-infinite pipe can be compared with that of a simple structure. At the end of the chapter, the theoretical model is verified by experiment work.

4.2 Analytical Method for Semi-infinite Pipes

The analytical method is used to analyse the mobility of a semi-infinite pipe. Four boundary conditions are needed to give four wave amplitudes. Considering that zero work is done by the reaction forces at the free-end boundary as schematically shown in figure 4.1, the condition at the boundary can be established.

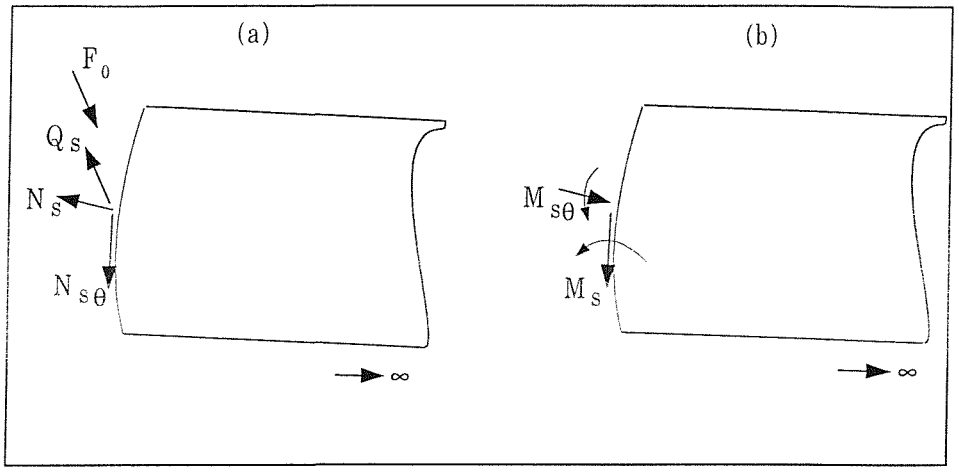

Figure 4.1: Notation and co-ordinate system of a semi-infinite pipe with a free end; a) Force, b) Moment

For a free edge, a set of the boundary conditions is given by (Leissa [2] and Soedel [69])

$$N_s = 0$$

$$T_{s\theta} = N_{s\theta} + \frac{M_{s\theta}}{a} = 0$$

$$M_s = 0 \qquad \ldots(4.1\ a, b, c)$$

This means there is no reaction force and moment at the edge of the pipe. For the radial direction, equilibrium due to the point force is obtained from equation (3.34), which is

$$V_s\Big|_{s=0} = \frac{1}{a} F_0 \delta(\theta - \phi) \qquad \ldots(4.2)$$

All forces and moments are given by equation (3.43) and are repeated here for convenience.

$$N_s\Big|_{s=0} = \frac{K}{a}\sum_{b=1}^{4} Z_{N,nb}\,\overline{\overline{W}}^{s}_{nb}\cos[n(\theta-\phi)]$$

$$T_{s\theta}\Big|_{s=0} = j\frac{(1-\nu)K}{2a}\sum_{b=1}^{4} Z_{T,nb}\,\overline{\overline{W}}^{s}_{nb}\sin[n(\theta-\phi)] \qquad \ldots(4.3\text{ a, b, c, d})$$

$$V_s\Big|_{s=0} = j\frac{D}{a^3}\sum_{b=1}^{4} Z_{V,nb}\,\overline{\overline{W}}^{s}_{nb}\cos[n(\theta-\phi)]$$

$$M_s\Big|_{s=0} = \frac{D}{a^2}\sum_{b=1}^{4} Z_{M,nb}\,\overline{\overline{W}}^{s}_{nb}\cos[n(\theta-\phi)]$$

where $\overline{\overline{W}}^{s}_{nb}$ is the radial amplitude for the b^{th} wave of the n^{th} mode of a semi-infinite pipe (the superscript s denotes semi-infinite in a similar way to i denoting infinite),

$$Z_{N,nb} = \left[\hat{k}_{nb}\alpha_{nb} + \nu n\psi_{nb} + \beta^2\hat{k}_{nb}^2 + \nu\right]$$

$$Z_{T,nb} = \left[n\alpha_{nb} + \left(1+3\beta^2\right)\hat{k}_{nb}\psi_{nb} + 3\beta^2 n\hat{k}_{nb}\right] \qquad \ldots(4.4\text{ a, b, c, d})$$

$$Z_{M,nb} = \left[\hat{k}_{nb}\alpha_{nb} + \nu n\psi_{nb} + \hat{k}_{nb}^2 + \nu n^2\right]$$

$$Z_{V,nb} = \left[\left(\hat{k}_{nb}^2 - \left(\frac{1-\nu}{2}\right)n^2\right)\alpha_{nb} + \left(\frac{3-\nu}{2}\right)n\hat{k}_{nb}\psi_{nb} + \hat{k}_{nb}\left(\hat{k}_{nb}^2 + (2-\nu)n^2\right)\right]$$

The wave amplitudes can be determined by substituting for V_s from equation (4.3 c) and $\delta(\theta-\phi)$ from equation (3.4) into equation (4.2), which gives

$$\sum_{b=1}^{4} Z_{V,nb}\,\overline{\overline{W}}^{s}_{nb} = -j\frac{\varepsilon_n a^2}{2\pi D}F_o \qquad \ldots(4.5)$$

Because of the orthogonal property of the pipe modes, the boundary conditions should also hold for any modes. So, the equation of motion for a particular mode of a semi-infinite pipe can easily be established in matrix form as

$$\begin{bmatrix} Z_{N,n1} & Z_{N,n2} & Z_{N,n3} & Z_{N,n4} \\ Z_{T,n1} & Z_{T,n2} & Z_{T,n3} & Z_{T,n4} \\ Z_{M,n1} & Z_{M,n2} & Z_{M,n3} & Z_{M,n4} \\ Z_{V,n1} & Z_{V,n2} & Z_{V,n3} & Z_{V,n4} \end{bmatrix} \begin{bmatrix} \overline{\overline{W}}^{s}_{n1} \\ \overline{\overline{W}}^{s}_{n2} \\ \overline{\overline{W}}^{s}_{n3} \\ \overline{\overline{W}}^{s}_{n4} \end{bmatrix} = \begin{bmatrix} 0 \\ 0 \\ 0 \\ -j\dfrac{\varepsilon_n a^2 F_0}{2\pi D} \end{bmatrix} \qquad \ldots(4.6)$$

Inverting the 4x4 matrix [**Z**], the wave amplitudes are given by

$$\begin{bmatrix} \overline{\overline{W}}^{s}_{n1} \\ \overline{\overline{W}}^{s}_{n2} \\ \overline{\overline{W}}^{s}_{n3} \\ \overline{\overline{W}}^{s}_{n4} \end{bmatrix} = \begin{bmatrix} Z_{N,n1} & Z_{N,n2} & Z_{N,n3} & Z_{N,n4} \\ Z_{T,n1} & Z_{T,n2} & Z_{T,n3} & Z_{T,n4} \\ Z_{M,n1} & Z_{M,n2} & Z_{M,n3} & Z_{M,n4} \\ Z_{V,n1} & Z_{V,n2} & Z_{V,n3} & Z_{V,n4} \end{bmatrix}^{-1} \begin{bmatrix} 0 \\ 0 \\ 0 \\ -j\dfrac{\varepsilon_n a^2 F_0}{2\pi D} \end{bmatrix} \qquad \ldots(4.7)$$

The mobility by this method is given by

$$Y_n^s(s,\theta) = -j\omega \frac{W_n^s(s,\theta)}{F_0} = -j\frac{\omega}{F_0} \sum_{b=1}^{4} \overline{\overline{W}}^{s}_{nb} \cos\left[n(\theta-\phi)\right] e^{j\hat{k}_{nb}s} \qquad \ldots(4.8)$$

However, for the n = 0 mode, the radial wave amplitude due to the torsional wave should be zero due to the symmetric load. This specific case for the n = 0 mode of the semi-infinite pipe is similar to that of the infinite pipe, which is discussed in the section 3.2. To verify this some mathematical analysis is carried out. Arranging terms, the force and moment coefficients become

$$Z_{N,0b}=\frac{Z^*_{N,0b}}{\gamma_{0b}},\ Z_{T,0b}=\frac{Z^*_{T,0b}}{\gamma_{0b}},\ Z_{M,0b}=\frac{Z^*_{M,0b}}{\gamma_{0b}}\ \text{and}\ Z_{V,0b}=\frac{Z^*_{V,0b}}{\gamma_{0b}} \qquad \ldots(4.9\ \text{a, b, c, d})$$

where $Z^*_{N,0b}=\left[\hat{k}_{0b}\alpha^*_{0b}+(\beta^2\hat{k}^2_{0b}+\nu)\gamma_{0b}\right]$

$$Z^*_{T,0b}=\left[\alpha^*_{0b}+\left(1+3\beta^2\right)\hat{k}_{0b}\psi^*_{0b}+(3\beta^2\hat{k}_{0b})\gamma_{0b}\right]$$

$$Z^*_{M,0b}=\left[\hat{k}_{0b}\alpha^*_{0b}+\hat{k}^2_{0b}\gamma_{0b}\right]$$

$$Z^*_{V,0b}=\left[\hat{k}^2_{0b}\alpha^*_{0b}+\hat{k}^3_{0b}\gamma_{0b}\right]$$

$$\alpha^*_{0b}=(L_{12}L_{23}-L_{21}L_{13})_{0b}$$

$$\psi^*_{0b}=\frac{1}{2}\left[(1+\nu)(\nu+\beta^2\hat{k}^2_{0b})\hat{k}^2_{0b}-(1+\frac{3-\nu}{2}\beta^2\hat{k}^2_{0b})(\hat{k}^2_{0b}-\Omega^2)\right]$$

$$\gamma_{0b}=(L_{11}L_{22}-L_{12}L_{21})_{0b}$$

It should be noted here that for the same reason as V^i_n/n rather than V^i_n was used in the section on the infinite pipe, the condition of $T_{s\theta}/n = 0$ is applied instead of $T_{s\theta} = 0$.

Substituting the coefficients obtained from equation (4.9) into equation (4.7) gives

$$\begin{bmatrix}\overline{\overline{W}}^s_{01}\\ \overline{\overline{W}}^s_{02}\\ \overline{\overline{W}}^s_{03}\\ \overline{\overline{W}}^s_{04}\end{bmatrix}=\begin{bmatrix}\gamma_{01}&0&0&0\\0&\gamma_{02}&0&0\\0&0&\gamma_{03}&0\\0&0&0&\gamma_{04}\end{bmatrix}\begin{bmatrix}Z^*_{N,01}&Z^*_{N,02}&Z^*_{N,03}&Z^*_{N,04}\\Z^*_{T,01}&Z^*_{T,02}&Z^*_{T,03}&Z^*_{T,04}\\Z^*_{M,01}&Z^*_{M,02}&Z^*_{M,03}&Z^*_{M,04}\\Z^*_{V,01}&Z^*_{V,02}&Z^*_{V,03}&Z^*_{V,04}\end{bmatrix}^{-1}\begin{bmatrix}0\\0\\0\\-j\dfrac{\varepsilon_0 a^2 F_0}{2\pi D}\end{bmatrix} \qquad \ldots(4.10)$$

As mentioned in section 3.2, $\gamma_{02} = 0$ for the torsional wave. Hence, there is no radial motion associated with the torsional wave. So, the formula for determining the radial wave amplitudes for the n = 0 mode is given by

$$\begin{bmatrix} \overline{W}^{s}_{01} \\ \overline{W}^{s}_{03} \\ \overline{W}^{s}_{04} \end{bmatrix} = \begin{bmatrix} Z_{N,01} & Z_{N,03} & Z_{N,04} \\ Z_{M,01} & Z_{M,03} & Z_{M,04} \\ Z_{V,01} & Z_{V,03} & Z_{V,04} \end{bmatrix}^{-1} \begin{bmatrix} 0 \\ 0 \\ -j\dfrac{\varepsilon_0 a^2 F_0}{2\pi D} \end{bmatrix} \qquad \ldots(4.11)$$

4.3 Wave Method for Semi-infinite Pipes

In this section, the point mobility of a semi-infinite pipe is derived by the wave approach similar to that used for an infinite beam by Mace [54] and for a finite beam by Brennan [73]. This method applied on the beam was also described in a textbook written by Mead [12].

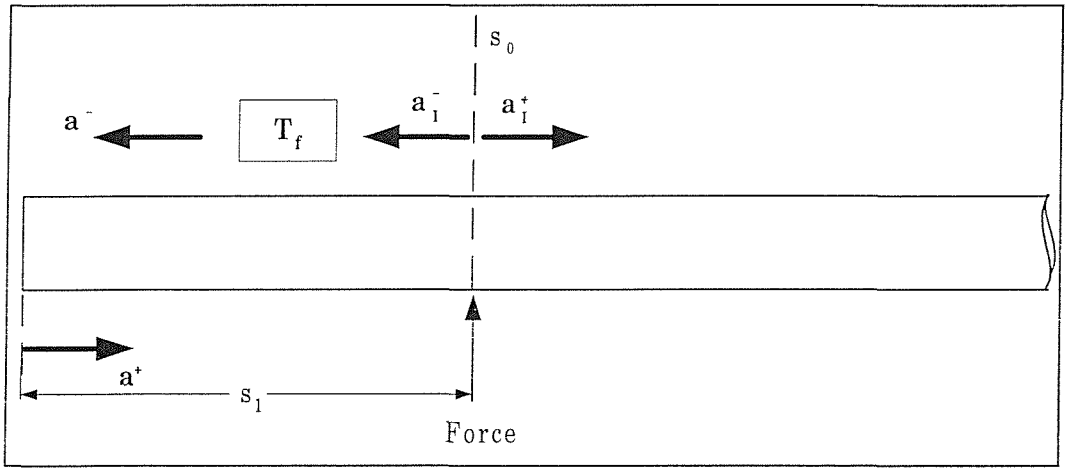

Figure 4.2: Diagram of wave propagating and reflected in a pipe.

Schematically, propagating and reflected waves in a semi-infinite pipe due to a point force excitation are shown in figure 4.2. From the wave point of view, the excitation generates the wave vectors, $\mathbf{a}_I^+$ and $\mathbf{a}_I^-$, whose amplitudes are equal to those of the positive-going and negative-going waves of the infinite pipe respectively and they are given for a particular circumferential mode as

$$\mathbf{a}_I^+ = \begin{bmatrix} \overline{=}i W_{n1} \\ \overline{=}i W_{n2} \\ \overline{=}i W_{n3} \\ \overline{=}i W_{n4} \end{bmatrix} \quad ; \quad \mathbf{a}_I^- = \begin{bmatrix} \overline{=}i W_{n5} \\ \overline{=}i W_{n6} \\ \overline{=}i W_{n7} \\ \overline{=}i W_{n8} \end{bmatrix} \qquad \ldots(4.12\ a, b)$$

The incident waves propagate along the pipe until the negative-going waves, $\mathbf{a}_I^-$, strike the boundary resulting in wave reflection. For the pipe application, every single wave produces four reflected waves. Having four negative-going propagating waves, the incident and reflected waves are related to the 4x4 matrix reflection matrix as given below (Mace [54])

$$\mathbf{a}^+ = \mathbf{R}_f \mathbf{a}^- \qquad \ldots(4.13)$$

where $\mathbf{R_f}$ is the reflection matrix at the end of the pipe, $\mathbf{a}^- = \mathbf{a}_I^-(s_0 - s_1) = \mathbf{T_f}\mathbf{a}_I^-(s_0)$ is the incident negative-going wave at the edge, and $\mathbf{T_f}$ is the transfer matrix of the vector $\mathbf{a}_I^-$ from the position s_0 to s_1 and is given by

$$\mathbf{T_f} = \begin{bmatrix} e^{j\hat{k}_{n1}s_1} & 0 & 0 & 0 \\ 0 & e^{j\hat{k}_{n2}s_1} & 0 & 0 \\ 0 & 0 & e^{j\hat{k}_{n3}s_1} & 0 \\ 0 & 0 & 0 & e^{j\hat{k}_{n4}s_1} \end{bmatrix},$$

where $s_1 = \frac{x_1}{a}$ is the non-dimensional distance between the force and the end of the pipe.

The reflection matrix can be obtained by considering the boundary conditions at the edge of the pipe, at which all forces and moments are zero because in the case considered in this thesis the end is free. From the discussion in the previous section, these boundary conditions can be given as

$$\begin{Bmatrix} N_s(s=-s_1) \\ T_{s\theta}(s=-s_1) \\ M_s(s=-s_1) \\ V_s(s=-s_1) \end{Bmatrix} = \mathbf{Z}_+\mathbf{a}^+ + \mathbf{Z}_-\mathbf{a}^- = \mathbf{0} \qquad \ldots(4.14)$$

where

$$\mathbf{Z}_+ = \begin{bmatrix} Z_{N,n1} & Z_{N,n2} & Z_{N,n3} & Z_{N,n4} \\ Z_{T,n1} & Z_{T,n2} & Z_{T,n3} & Z_{T,n4} \\ Z_{M,n1} & Z_{M,n2} & Z_{M,n3} & Z_{M,n4} \\ Z_{V,n1} & Z_{V,n2} & Z_{V,n3} & Z_{V,n4} \end{bmatrix} \text{ and}$$

$$\mathbf{Z}_- = \begin{bmatrix} Z_{N,n5} & Z_{N,n6} & Z_{N,n7} & Z_{N,n8} \\ Z_{T,n5} & Z_{T,n6} & Z_{T,n7} & Z_{T,n8} \\ Z_{M,n5} & Z_{M,n6} & Z_{M,n7} & Z_{M,n8} \\ Z_{V,n5} & Z_{V,n6} & Z_{V,n7} & Z_{V,n8} \end{bmatrix}$$

As described in section 3.3, $\hat{k}_{nb} = -\hat{k}_{n(b+4)}$, $\alpha_{nb} = -\alpha_{n(b+4)}$ and $\psi_{nb} = \psi_{n(b+4)}$ where b = 1,2,3 and 4. The relationships between the positive-going and negative-going waves lead to

$Z_{N,nb} = Z_{N,n(b+4)}$,

$Z_{T,nb} = -Z_{T,n(b+4)}$,

$Z_{M,nb} = Z_{M,n(b+4)}$ and $\qquad \ldots(4.15\text{ a, b, c, d})$

$Z_{V,nb} = -Z_{V,n(b+4)}$

So, the matrix of $\mathbf{Z}_-$ can be rewritten in terms of the first four waves as

$$\mathbf{Z}_- = \begin{bmatrix} Z_{N,n1} & Z_{N,n2} & Z_{N,n3} & Z_{N,n4} \\ -Z_{T,n1} & -Z_{T,n2} & -Z_{T,n3} & -Z_{T,n4} \\ Z_{M,n1} & Z_{M,n2} & Z_{M,n3} & Z_{M,n4} \\ -Z_{V,n1} & -Z_{V,n2} & -Z_{V,n3} & -Z_{V,n4} \end{bmatrix} \qquad \ldots(4.16)$$

Substituting for the vector $\mathbf{a}^+$ from equation (4.13) into equation (4.14) and inverting the matrix $\mathbf{Z}_+$ give the reflection matrix

$$\mathbf{R}_f = -\mathbf{Z}_+^{-1}\mathbf{Z}_- \qquad \ldots(4.17)$$

The waves reflected at the boundary are proportional to the incident waves related by the reflection matrix as $\mathbf{a}^+ = \mathbf{R}_f\mathbf{a}^-$ (equation 4.13).

The vector of wave amplitudes at the excitation position in the positive direction is the combination of the vector of incident positive-going waves and the vector of reflected waves and is given by

$$\begin{aligned}\mathbf{a}_{s_0}^+ &= \mathbf{a}_I^+ + \mathbf{T}_f\mathbf{a}^+ \\ &= \mathbf{a}_I^+ + \mathbf{T}_f\mathbf{R}_f\mathbf{a}^- \\ &= \mathbf{a}_I^+ + \mathbf{T}_f\mathbf{R}_f\mathbf{T}_f\mathbf{a}_I^-\end{aligned} \qquad \ldots(4.18)$$

Since $\mathbf{a}_I^+ = \mathbf{a}_I^-$ as described in the previous chapter, the net wave amplitude at $s = s_0$ in the positive direction becomes

$$\mathbf{a}_{s_0}^+ = (\mathbf{I} + \mathbf{T}_f\mathbf{R}_f\mathbf{T}_f)\mathbf{a}_I^+ \qquad \ldots(4.19)$$

where $\mathbf{I}$ is the identity matrix.

Because the total vector of wave amplitudes is the combination of the vector of incident positive-going waves and the vector of reflected waves, the vector of reflected waves at $s = s_0$, $\mathbf{a}_{s_0}^{+r}$, can be determined by subtracting the vector of incident waves from the vector of all the waves, and is given by

$$\mathbf{a}_{s_0}^{+r} = \mathbf{a}_{s_0}^{+} - \mathbf{a}_{I}^{+} = (\mathbf{T}_f \mathbf{R}_f \mathbf{T}_f)\, \mathbf{a}_{I}^{+} \qquad \ldots(4.20)$$

In the case of a pipe excited at the end, the transfer matrix, $\mathbf{T}_f$, is equal to the identity matrix. Since $\mathbf{I} = \mathbf{Z}_+^{-1}\mathbf{Z}_+$, substituting the reflection matrix obtained from equation (4.17) into equation (4.19) gives:

$$\mathbf{a}_{s_0}^{+} = \begin{bmatrix} \overline{\overline{W}}_{n1}^{s} \\ \overline{\overline{W}}_{n2}^{s} \\ \overline{\overline{W}}_{n3}^{s} \\ \overline{\overline{W}}_{n4}^{s} \end{bmatrix} = 2\,\mathbf{Z}_+^{-1} \begin{bmatrix} 0 & 0 & 0 & 0 \\ Z_{T,n1} & Z_{T,n2} & Z_{T,n3} & Z_{T,n4} \\ 0 & 0 & 0 & 0 \\ Z_{V,n1} & Z_{V,n2} & Z_{V,n3} & Z_{V,n4} \end{bmatrix} \begin{bmatrix} \overline{\overline{W}}_{n1}^{i} \\ \overline{\overline{W}}_{n2}^{i} \\ \overline{\overline{W}}_{n3}^{i} \\ \overline{\overline{W}}_{n4}^{i} \end{bmatrix} \qquad \ldots(4.21\text{ a})$$

However, for the n = 0 mode, the radial motion does not couple to the torsional wave. Hence, the solution for this mode becomes

$$\begin{bmatrix} \overline{\overline{W}}_{01}^{s} \\ \overline{\overline{W}}_{03}^{s} \\ \overline{\overline{W}}_{04}^{s} \end{bmatrix} = 2\left(\mathbf{Z}_+^{-1}\right)_{n=0} \begin{bmatrix} 0 & 0 & 0 \\ 0 & 0 & 0 \\ Z_{V,01} & Z_{V,03} & Z_{V,04} \end{bmatrix} \begin{bmatrix} \overline{\overline{W}}_{01}^{i} \\ \overline{\overline{W}}_{03}^{i} \\ \overline{\overline{W}}_{04}^{i} \end{bmatrix} \qquad \ldots(4.21\text{ b})$$

where $(\mathbf{Z}_+)_{n=0} = \begin{bmatrix} Z_{N,01} & Z_{N,03} & Z_{N,04} \\ Z_{M,01} & Z_{M,03} & Z_{M,04} \\ Z_{V,01} & Z_{V,03} & Z_{V,04} \end{bmatrix}$

4.4 Numerical Analysis to Evaluate the Mobility of Semi-infinite Pipes

In the previous sections, the force mobility of a semi-infinite pipe was derived using two methods, analytical and wave methods. Because both methods are different, the theoretical results also appear to be different. Hence, it is worthwhile evaluating them. Due to the complexity of the expressions for the radial wave amplitudes, a numerical comparison between them is conducted in this section. The comparison is carried out for every single wave mobility of the circumferential modes n = 0 to 3, which is calculated by using the pipe data given in table 2.1 (page 30) and the results are shown in figure 4.3.

From the numerical results shown in figure 4.3, it can be seen that both methods are identical even though they are obtained using a different approach. By comparing the point mobility of the infinite pipe shown in figure 3.5, the semi-infinite pipe with the free end seems to give a similar point mobility to the infinite pipe except that it is higher for most wave types. However, for the n = 0 mode, the point mobility of the semi-infinite pipe for the longitudinal propagating wave is much smaller than that of the infinite pipe.

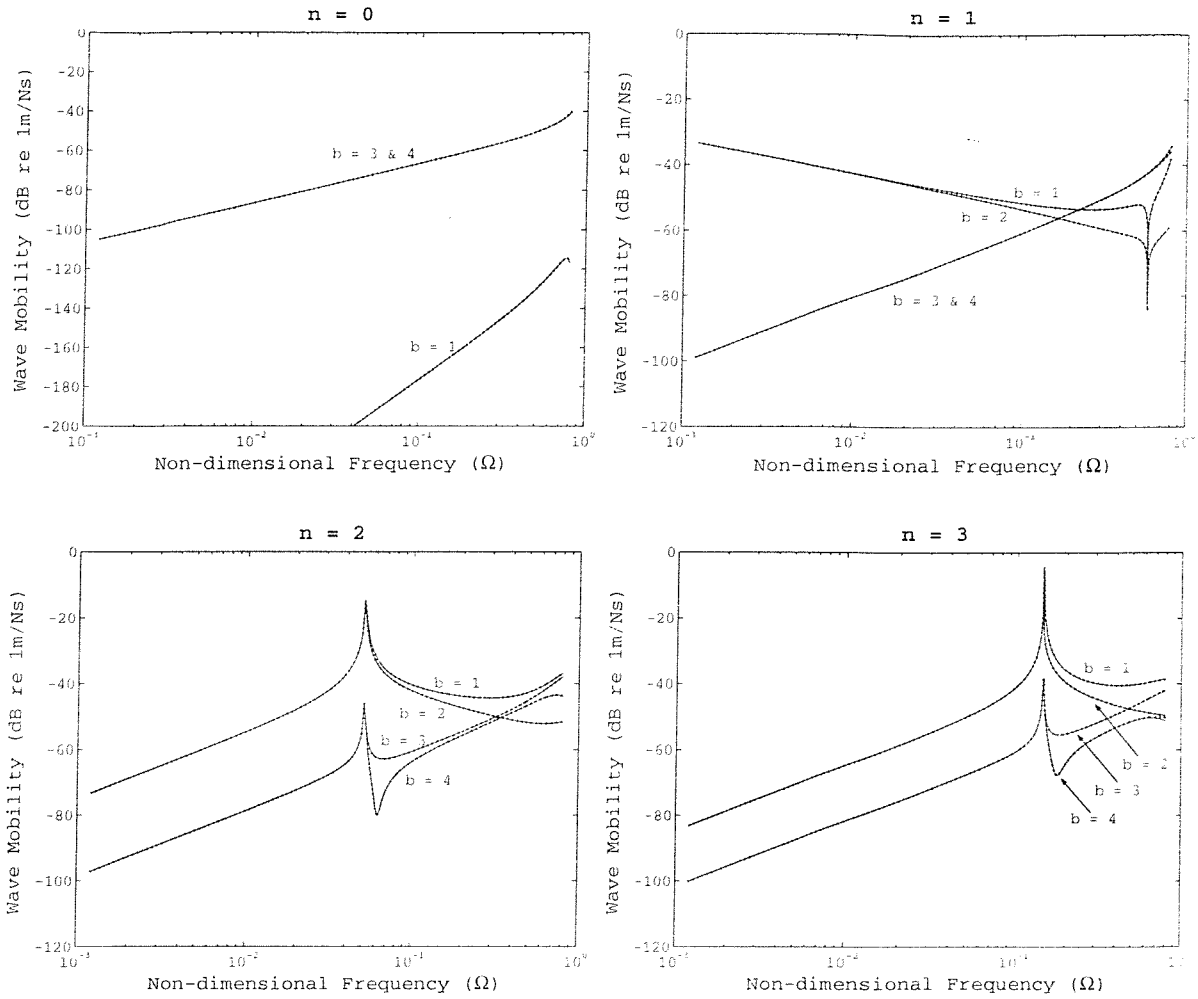

Figure 4.3: Wave mobility of the mode n = 0 to n = 3 of a semi-infinite pipe excited at the end; __ Analytical method, _ _ Wave method.

4.5 Approximate Mobility of Semi-infinite Pipes at Low Frequencies

In sections 4.2 and 4.3, the wave amplitudes of a semi-infinite pipe with a free end have been derived. Clearly, the results of the analysis are more complicated than those obtained from an infinite pipe due to the reflected waves at the boundary. It is thus difficult to get a simple form for the radial wave amplitudes. In order to achieve this, the motion of a semi-infinite pipe is analysed at low frequencies ($\Omega^2 << 1$). Because of

the distinguishable behaviour between the n = 0 and the higher modes, the analysis is carried out in the same way as for the infinite pipe at low frequencies.

At the free end, the forces and moments given in equations (4.1) and (4.2) are functions of the components of axial, circumferential and radial displacements, making their coefficients more complicated. Making some assumptions for low frequency behaviour such as $\beta^2 << 1$ and $\beta^2 \hat{k}_{nb}^2 << 1$, the analysis is conducted more easily and is carried out for each wave. Rearranging equations (4.21.a) and (4.21.b), the expression for the n = 0 mode becomes

$$\begin{bmatrix} Z_{N,01} & Z_{N,03} & Z_{N,04} \\ Z_{M,01} & Z_{M,03} & Z_{M,04} \\ Z_{V,01} & Z_{V,03} & Z_{V,04} \end{bmatrix} \begin{bmatrix} \overline{\overline{W}}^{s}_{01} \\ \overline{\overline{W}}^{s}_{03} \\ \overline{\overline{W}}^{s}_{04} \end{bmatrix} = 2 \begin{bmatrix} 0 & 0 & 0 \\ 0 & 0 & 0 \\ Z_{V,01} & Z_{V,03} & Z_{V,04} \end{bmatrix} \begin{bmatrix} \overline{\overline{W}}^{i}_{01} \\ \overline{\overline{W}}^{i}_{03} \\ \overline{\overline{W}}^{i}_{04} \end{bmatrix} \qquad \ldots(4.22)$$

and for the n ≥ 1 modes becomes

$$\begin{bmatrix} Z_{N,n1} & Z_{N,n2} & Z_{N,n3} & Z_{N,n4} \\ Z_{T,n1} & Z_{T,n2} & Z_{T,n3} & Z_{T,n4} \\ Z_{M,n1} & Z_{M,n2} & Z_{M,n3} & Z_{M,n4} \\ Z_{V,n1} & Z_{V,n2} & Z_{V,n3} & Z_{V,n4} \end{bmatrix} \begin{bmatrix} \overline{\overline{W}}^{s}_{n1} \\ \overline{\overline{W}}^{s}_{n2} \\ \overline{\overline{W}}^{s}_{n3} \\ \overline{\overline{W}}^{s}_{n4} \end{bmatrix} = 2 \begin{bmatrix} 0 & 0 & 0 & 0 \\ Z_{T,n1} & Z_{T,n2} & Z_{T,n3} & Z_{T,n4} \\ 0 & 0 & 0 & 0 \\ Z_{V,n1} & Z_{V,n2} & Z_{V,n3} & Z_{V,n4} \end{bmatrix} \begin{bmatrix} \overline{\overline{W}}^{i}_{n1} \\ \overline{\overline{W}}^{i}_{n2} \\ \overline{\overline{W}}^{i}_{n3} \\ \overline{\overline{W}}^{i}_{n4} \end{bmatrix}$$

$$\ldots(4.23)$$

Mobility of the n = 0 mode of a semi-infinite pipe

In this part, the mobility of the n = 0 mode of a semi-infinite pipe at low frequencies is simplified and is compared with the original formulation. To achieve this the coefficients of the forces and moments for each type of waves are first simplified.

The coefficients of the forces and moments for the n = 0 mode are given in equation (4.4). To reduce them to a simple form, it is assumed that $\beta^2 << 1$ and $\beta^2\hat{k}_{nb}^2 << 1$ at low frequencies. This results in the coefficient for axial displacement given in equation (3.41 c) as

$$\alpha_{0b} = -\frac{\hat{k}_{0b}(\beta^2\hat{k}_{0b}^2 + \nu)}{\hat{k}_{0b}^2 - \Omega^2} \qquad \ldots(4.24)$$

Substituting for α_{0b} from equation (4.24) and the wavenumbers of the n = 0 mode, which are given in chapter 2, into equation (4.4) yields the coefficients of the normal force, N_s, from equation (4.4 a), which are

$$Z_{N,01} = -(\beta^2\hat{k}_1^2 + \nu)\left(\frac{1-\nu^2}{\nu^2}\right)$$

$$Z_{N,03} = (\beta^2\hat{k}_{03}^2 + \nu)\left(1 - \frac{\hat{k}_{03}^2}{\hat{k}_{03}^2 - \Omega^2}\right) \qquad \ldots(4.25\text{ a, b, c})$$

$$Z_{N,04} = (\beta^2\hat{k}_{04}^2 + \nu)\left(1 - \frac{\hat{k}_{04}^2}{\hat{k}_{04}^2 - \Omega^2}\right)$$

When $\Omega^2 << 1$, $\hat{k}_1^2 << 1$, so the coefficient $Z_{N,01}$ is given by:

$$Z_{N,01} = -\left(\frac{1-\nu^2}{\nu}\right) \qquad \ldots(4.26)$$

With the same assumptions as above, the coefficients of axial moment, M_s, become

$$Z_{M,01} = \hat{k}_1^2 - \frac{1}{\nu}$$

$$Z_{M.03} = \hat{k}_{03}^2 - \nu \qquad \text{...(4.27 a, b, c)}$$

$$Z_{M.04} = \hat{k}_{04}^2 - \nu$$

As described in chapter 2, the standing near field wavenumbers at low frequencies are given by (equations 2.22 a, b)

$$\hat{k}_{03}^2, \hat{k}_{04}^2 = \pm j\sqrt{\left(1-\nu^2\right)\left(1-\hat{k}_1^2\right)/\beta^2}$$

With these assumptions, the axial moment coefficients are given by

$$Z_{M.01} = -\frac{1}{\nu} \text{ and } Z_{M.03} = -Z_{M.04} = j\sqrt{\left(1-\nu^2\right)\left(1-\hat{k}_1^2\right)/\beta^2} \qquad \text{...(4.28 a, b, c)}$$

Substitution of the wavenumbers for the n = 0 mode into equation (4.4 d) gives the coefficients of V_s, which are

$$Z_{V.01} = \frac{1}{\nu}\hat{k}_1$$

$$Z_{V.03} = 2\left[\frac{\left(1-\nu^2\right)\left(1-\hat{k}_1^2\right)}{4\beta^2}\right]^{3/4}(-1+j) \qquad \text{...(4.29 a, b, c)}$$

$$Z_{V.03} = 2\left[\frac{\left(1-\nu^2\right)\left(1-\hat{k}_1^2\right)}{4\beta^2}\right]^{3/4}(1+j)$$

From the analysis for the n = 0 mode, most of the normal force, N_s, is due to the longitudinal wave. Conversely, the standing near field waves are the dominant cause of the axial moment, M_s, and effective transverse shear force, V_s. Neglecting the small influence of the longitudinal wave for M_s and V_s, the wave amplitudes of the standing near field waves can be determined from equation (4.22) and are given by

$$\begin{bmatrix} Z_{M,03} & Z_{M,04} \\ Z_{V,03} & Z_{V,04} \end{bmatrix} \begin{bmatrix} \overline{\overline{W}}^{s}_{03} \\ \overline{\overline{W}}^{s}_{04} \end{bmatrix} = 2 \begin{bmatrix} 0 & 0 \\ Z_{V,03} & Z_{V,04} \end{bmatrix} \begin{bmatrix} \overline{\overline{W}}^{i}_{03} \\ \overline{\overline{W}}^{i}_{04} \end{bmatrix} \qquad \ldots(4.30)$$

By substituting for the coefficients of M_s and V_s (the Z's), in equation (4.30) and rearranging, the wave amplitudes of the standing near field waves can be expressed as

$$\begin{bmatrix} \overline{\overline{W}}^{s}_{03} \\ \overline{\overline{W}}^{s}_{04} \end{bmatrix} = (1+j)(\overline{\overline{W}}^{i}_{03} - j\overline{\overline{W}}^{i}_{04}) \begin{bmatrix} 1 \\ 1 \end{bmatrix} \qquad \ldots(4.31)$$

Substitution of $\overline{\overline{W}}^{i}_{03}$ and $\overline{\overline{W}}^{i}_{04}$ given in equation (2.43 b, c) yields

$$\overline{\overline{W}}^{s}_{03} = \overline{\overline{W}}^{s}_{04} = \frac{(1-j)F_0}{4\pi\beta^2 K \hat{k}^3_{03}} \qquad \ldots(4.32\ a, b)$$

From equation (4.22), the radial component of the longitudinal wave is easily determined from its simple relationship with the standing near field waves:

$$\begin{aligned} \overline{\overline{W}}^{s}_{01} &= -\frac{1}{Z_{N,01}} \left(Z_{N,03} \overline{\overline{W}}^{s}_{03} + Z_{N,04} \overline{\overline{W}}^{s}_{04} \right) \\ &= -\frac{1}{Z_{N,01}} (Z_{N,03} + Z_{N,04}) \overline{\overline{W}}^{s}_{03} \end{aligned} \qquad \ldots(4.33)$$

Substituting for the wavenumbers of the n = 0 mode gives

$$\overline{\overline{W}}^{s}_{01} = -\frac{2\nu\beta^2\Omega^2 \left[1-(1+\nu)\Omega^2 \right] \overline{\overline{W}}^{s}_{03}}{(1-\nu^2)\left[(1-\nu^2-\Omega^2) - (2\nu-\Omega^2)\beta^2\Omega^2 \right]} \qquad \ldots(4.34)$$

Because at low frequencies, $\Omega^2 << 1$, this becomes

$$\overline{\overline{W}}^{s}_{01} = -\frac{2\nu\beta^2\Omega^2\overline{\overline{W}}^{s}_{03}}{(1-\nu^2)^2} \qquad ...(4.35)$$

Substituting for the term $\overline{\overline{W}}^{s}_{03}$ from equation (4.32 a) and noting that $\hat{k}_l^2 = \frac{\Omega^2}{1-\nu^2}$ gives:

$$\overline{\overline{W}}^{s}_{01} = -\frac{(1-j)\nu\hat{k}_l^2 F_0}{2\pi(1-\nu^2)K\hat{k}_{03}^3} \qquad ...(4.36)$$

Once the radial wave amplitudes are known, the mobility of the n = 0 of the semi-infinite pipe is readily established. Like the infinite pipe, the point mobility of the semi-infinite pipe is dominated by the standing near field waves and is given by:

$$Y_0^{sP} = -j\omega\frac{(\overline{\overline{W}}^{s}_{03} + \overline{\overline{W}}^{s}_{04})}{F_0} = 4Y_0^{iP} \qquad ...(4.37)$$

Equation (4.37) shows clearly that the point mobility of the n = 0 mode of the semi-infinite pipe is in phase with and four times larger than that of the infinite pipe, Y_0^{iP}.

Dominated by the longitudinal propagating wave, the transfer mobility of the semi-infinite pipe is given by

$$Y_0^{sT}(s,\theta) = -j\omega\frac{\overline{\overline{W}}^{s}_{01}}{F_0} = \frac{(1+j)\nu\omega\hat{k}_l^2}{2\pi(1-\nu^2)K\hat{k}_{03}^3}e^{-j\hat{k}_l s}$$

$$= \frac{2(1+j)\hat{k}_1}{\nu\hat{k}_{03}^3}Y_0^{iT}(s,\theta) \qquad ...(4.38)$$

In contrast with the point mobility, the transfer mobility of the semi-infinite pipe is much smaller than that of the infinite pipe, Y_0^{iT} (equation 3.62).

Mobility of the n ≥ 1 modes of a semi-infinite pipe

The mobility of the n ≥ 1mode of a semi-infinite pipe is analysed in the same manner as that of the n = 0 mode. Before the wave amplitudes are obtained, the coefficients of forces and moments are first determined. Employing the assumptions used for the n = 0 mode including $\hat{k}_{nb}^2 >> \Omega^2$ (the flexural wavenumber rapidly increases with increasing frequencies), the coefficients can be written in a simple form.

For convenience, the coefficients for the forces and moments given in equation (4.4) are repeated here and are given by:

$$Z_{N,nb} = \left[\hat{k}_{nb}\alpha_{nb} + \nu n\psi_{nb} + \beta^2\hat{k}_{nb}^2 + \nu\right]$$

$$Z_{T,nb} = \left[n\alpha_{nb} + \left(1+3\beta^2\right)\hat{k}_{nb}\psi_{nb} + 3\beta^2 n\hat{k}_{nb}\right] \qquad \ldots(4.39\text{ a, b, c, d})$$

$$Z_{M,nb} = \left[\hat{k}_{nb}\alpha_{nb} + \nu n\psi_{nb} + \hat{k}_{nb}^2 + \nu n^2\right]$$

$$Z_{V,nb} = \left[\left(\hat{k}_{nb}^2 - \left(\frac{1-\nu}{2}\right)n^2\right)\alpha_{nb} + \left(\frac{3-\nu}{2}\right)n\hat{k}_{nb}\psi_{nb} + \hat{k}_{nb}\left(\hat{k}_{nb}^2 + (2-\nu)n^2\right)\right]$$

Applying the assumptions, the coefficients of the axial and circumferential displacements are given by

$$\alpha_{nb} \cong \hat{k}_{nb}\left[\frac{n^2 - \nu\hat{k}_{nb}^2}{(n^2+\hat{k}_{nb}^2)^2}\right]$$

$$\psi_{nb} \equiv -n\left[\frac{(2+\nu)\hat{k}_{nb}^2 + n^2}{(n^2+\hat{k}_{nb}^2)^2}\right] \qquad \ldots(4.40\text{ a, b})$$

Substituting for α_{nb} and ψ_{nb} into the force and moment coefficients given in equation (4.39) results in

$$\begin{aligned} Z_{N,nb} &= \frac{(1-\nu^2)n^2\hat{k}_{nb}^2}{(n^2+\hat{k}_{nb}^2)^2} + \beta^2\hat{k}_{nb}^2 \\ &\cong \frac{(1-\nu^2)n^2\hat{k}_{nb}^2}{(n^2+\hat{k}_{nb}^2)^2} \end{aligned}$$

$$\begin{aligned} Z_{T,nb} &= -\frac{\left[2(1+\nu)\hat{k}_{nb}^2 + 3\beta^2\left(n^2+(2+\nu)\hat{k}_{nb}^2\right)\right]n\hat{k}_{nb}}{(n^2+\hat{k}_{nb}^2)^2} + 3\beta^2 n\hat{k}_{nb} \\ &\cong -\frac{2(1+\nu)n\hat{k}_{nb}^3}{(n^2+\hat{k}_{nb}^2)^2} \end{aligned} \qquad \ldots(4.41\text{ a, b, c, d})$$

$$\begin{aligned} Z_{M,nb} &= Z_{N,nb} + (1-\beta^2)\hat{k}_{nb}^2 + \nu(n^2-1) \\ &\cong Z_{N,nb} + \hat{k}_{nb}^2 + \nu(n^2-1) \end{aligned}$$

$$Z_{V,nb} = \hat{k}_{nb}\left[(n^2+\hat{k}_{nb}^2) + (1-\nu)\left(1-\frac{2}{n^2+\hat{k}_{nb}^2}\right)n^2 - \nu\right]$$

Since at low frequencies the wavenumbers of the standing near field waves are much larger than those of the flexural and near field waves, the coefficients of the axial moment, $Z_{M,b3}$ and $Z_{M,b4}$, and the effective transverse shear force, $Z_{V,b3}$ and $Z_{V,b4}$, are dominated by the standing near field waves. This gives similar results to the n = 0 mode. To make the simplification, equation (4.23) is rewritten as

$$Z_{M,n1}\overline{\overline{W}}^{s}_{n1} + Z_{M,n2}\overline{\overline{W}}^{s}_{n2} + Z_{M,n3}\overline{\overline{W}}^{s}_{n3} + Z_{M,n4}\overline{\overline{W}}^{s}_{n4} = 0$$

$$Z_{V,n1}\overline{\overline{W}}^{s}_{n1} + Z_{V,n2}\overline{\overline{W}}^{s}_{n2} + Z_{V,n3}\overline{\overline{W}}^{s}_{n3} + Z_{V,n4}\overline{\overline{W}}^{s}_{n4} = 2\left(Z_{V,n1}\overline{\overline{W}}^{i}_{n1} + Z_{V,n2}\overline{\overline{W}}^{i}_{n2} + Z_{V,n3}\overline{\overline{W}}^{i}_{n3} + Z_{V,n4}\overline{\overline{W}}^{i}_{n4} \right)$$

...(4.42 a, b)

From the above discussion of equation (4.41), it can be seen that the standing near field waves dominate the axial moment, M_s and the effective transverse shear force V_s. Hence, the effect of the flexural and near field waves for M_s and V_s can be neglected. The wave amplitudes of the standing near field waves can be written as

$$\begin{bmatrix} Z_{M,n3} & Z_{M,n4} \\ Z_{V,n3} & Z_{V,n4} \end{bmatrix} \begin{bmatrix} \overline{\overline{W}}^{s}_{n3} \\ \overline{\overline{W}}^{s}_{n4} \end{bmatrix} = 2 \begin{bmatrix} 0 & 0 \\ Z_{V,n3} & Z_{V,n4} \end{bmatrix} \begin{bmatrix} \overline{\overline{W}}^{i}_{n3} \\ \overline{\overline{W}}^{i}_{n4} \end{bmatrix} \qquad ...(4.43)$$

The coefficients of the normal force, N_s, and of effective in-plane shear force, $T_{s\theta}$, are very small for all wave types. However, the amplitudes of flexural and near field waves of the semi-infinite and infinite pipes are much larger than those of standing near field waves as shown in figures 3.5 in section 3.4 and figures 4.3 in section 4.4. Hence, the effect of the standing near field waves on the normal force, N_s, and on the effective in-plane shear force, $T_{s\theta}$, may be ignored. With the same approach taken for the standing near field waves, the wave amplitudes of the flexural and near field waves are given by

$$\begin{bmatrix} Z_{N,n1} & Z_{N,n2} \\ Z_{T,n1} & Z_{T,n2} \end{bmatrix} \begin{bmatrix} \overline{\overline{W}}^{s}_{n1} \\ \overline{\overline{W}}^{s}_{n2} \end{bmatrix} = 2 \begin{bmatrix} 0 & 0 \\ Z_{T,n1} & Z_{T,n2} \end{bmatrix} \begin{bmatrix} \overline{\overline{W}}^{i}_{n1} \\ \overline{\overline{W}}^{i}_{n2} \end{bmatrix} \qquad ...(4.44)$$

Because the motion of the semi-infinite pipe due to the large wavenumbers of the standing near field waves is very small at low frequencies, they can be neglected when calculating the pipe mobility. Hence, analysis is conducted to find out the radial wave amplitudes of the small wavenumbers of the standing near field waves arising before the waves cut on and of the flexural and near field waves arising after the waves cut on.

Substituting for the coefficients of normal force, $Z_{N,nb}$, and effective in-plane shear force, $Z_{T,nb}$, where b = 1 and 2, into equation (4.44) gives the radial wave amplitudes as

$$\begin{bmatrix} \overline{\overline{W}}^{s}_{n1} \\ \overline{\overline{W}}^{s}_{n2} \end{bmatrix} = 2 \frac{\left\{ \overline{\overline{W}}^{i}_{n1} + \left(\frac{n^2 + \hat{k}_{n1}^2}{n^2 + \hat{k}_{n2}^2} \right)^2 \frac{\hat{k}_{n2}^3}{\hat{k}_{n1}^3} \overline{\overline{W}}^{i}_{n2} \right\}}{(1 - \frac{\hat{k}_{n2}}{\hat{k}_{n1}})} \begin{bmatrix} 1 \\ -\left(\frac{n^2 + \hat{k}_{n2}^2}{n^2 + \hat{k}_{n1}^2} \right)^2 \frac{\hat{k}_{n1}^2}{\hat{k}_{n2}^2} \end{bmatrix} \qquad \ldots(4.45)$$

In section 3.5, it was found that the wave amplitudes of flexural and near field waves of the infinite pipe are related by

$$\overline{\overline{W}}^{i}_{n2} = -\left(\frac{n^2 + \hat{k}_{n2}^2}{n^2 + \hat{k}_{n1}^2} \right)^2 \frac{\hat{k}_{n1}}{\hat{k}_{n2}} \overline{\overline{W}}^{i}_{n1} \qquad \ldots(4.46)$$

Substitution of this relationship into equation (4.45) yields

$$\begin{bmatrix} \overline{\overline{W}}^{s}_{n1} \\ \overline{\overline{W}}^{s}_{n2} \end{bmatrix} = 2 \left(1 + \frac{\hat{k}_{n2}}{\hat{k}_{n1}} \right) \overline{\overline{W}}^{i}_{n1} \begin{bmatrix} 1 \\ -\left(\frac{n^2 + \hat{k}_{n2}^2}{n^2 + \hat{k}_{n1}^2} \right)^2 \frac{\hat{k}_{n1}^2}{\hat{k}_{n2}^2} \end{bmatrix} \qquad \ldots(4.47)$$

For the n = 1 mode of the semi-infinite pipe, the flexural and near field wavenumbers at low frequencies may be presented by those of the beam as $-\hat{k}_b$ and $j\hat{k}_b$, respectively. Because $\hat{k}_b << 1$ at low frequencies, the wave amplitudes of the flexural and near field wave of the n = 1 mode of the semi-infinite pipe can be approximated as

$$\begin{bmatrix} \overline{\overline{W}}^{s}_{11} \\ \overline{\overline{W}}^{s}_{12} \end{bmatrix} = 2(1 - j) \overline{\overline{W}}^{i}_{11} \begin{bmatrix} 1 \\ \left(\frac{1 - 2\hat{k}_b^2}{1 + 2\hat{k}_b^2} \right) \end{bmatrix} \qquad \ldots(4.48)$$

Substituting $\overline{\overline{W}}_{11}^{i}$ obtained from equation (3.68 a) into the above equation yields

$$\begin{bmatrix} \overline{\overline{W}}_{11}^{s} \\ \overline{\overline{W}}_{12}^{s} \end{bmatrix} = \frac{(1+j)\,F_0}{2\pi h E \hat{k}_b^3} \begin{bmatrix} 1+2\hat{k}_b^2 \\ 1-2\hat{k}_b^2 \end{bmatrix} \qquad \ldots(4.49)$$

At very low frequencies ($\Omega^2 << 1$), where $\hat{k}_b^2 << 1$, these results of the semi-infinite pipe are the same as for a semi-infinite beam (Brennan [73]). The point mobility of the n = 1 mode of the semi-infinite pipe is dominated by the flexural and near field waves as discussed in the previous section and is given by

$$Y_1^{sP} = -j\omega \frac{(\overline{\overline{W}}_{11}^{s} + \overline{\overline{W}}_{12}^{s})}{F_0} = \frac{(1-j)\,\omega}{\pi h E \hat{k}_b^3} \qquad \ldots(4.50)$$

It was shown in section 3.5 that when $\Omega^2 << 1$, where $\hat{k}_b^2$ can be ignored in comparison with unity, the point mobility of the n = 1 mode of the infinite pipe can be presented as

$$Y_1^{iP} = \frac{(1-j)\,\omega}{4\pi h E \hat{k}_b^3} \qquad \ldots(4.51)$$

Therefore, at very low frequencies, the relationship between the semi-infinite and infinite pipe in terms of point mobility for the n = 1 mode is given by

$$Y_1^{sP} = 4Y_1^{iP} \qquad \ldots(4.52)$$

In the far field, only the flexural wave propagates along the pipe and hence the transfer mobility is given by

$$Y_1^{sT}(s,\theta) = -j\omega\frac{\overline{\overline{W}}_{11}^{s}}{F_0} = \frac{(1-j)(1+2\hat{k}_b^2)\omega}{2\pi hE\hat{k}_b^3}\cos\left[n(\theta-\phi)\right]e^{-j\hat{k}_n s} \qquad \ldots(4.53)$$

Comparing this with the infinite pipe, the transfer mobility for the n = 1 mode of the semi-infinite pipe can be written as

$$Y_1^{sT}(s,\theta) = 2(1-j)\,Y_1^{iT}(s,\theta) \qquad \ldots(4.54)$$

The relationship between the semi-infinite and infinite pipe for the point and transfer mobility given in equation (4.52) and (4.54) is similar to that of the Euler-Bernoulli beam.

Like the n = 1 mode, the point mobility of the n≥ 2, which is dominated by the flexural and near field waves, can be expressed as

$$Y_n^{sP} = -j\omega\frac{(\overline{\overline{W}}_{n1}^{s} + \overline{\overline{W}}_{n2}^{s})}{F_0} \qquad \ldots(4.55)$$

Substituting for $\overline{\overline{W}}_{n1}^{s}$ and $\overline{\overline{W}}_{n2}^{s}$ obtained from equation (4.47) and $\overline{\overline{W}}_{n1}^{i}$ obtained from equation (3.64) into equation (4.55) gives

$$Y_n^{sP} = -\frac{a^2\omega}{\pi D}\frac{(\hat{k}_{n1}+\hat{k}_{n2})(\hat{k}_{n1}^2\hat{k}_{n2}^2 - n^4)}{\hat{k}_{n1}^2\hat{k}_{n2}^2\hat{k}_{n3}^2\hat{k}_{n4}^2} \qquad \ldots(4.56)$$

In the far field, the transfer mobility is given by

$$Y_n^{sT}(s,\theta) = -j\omega\frac{\overline{\overline{W}}_{n1}^{s}}{F_0} = -\frac{a^2\omega}{\pi D}\frac{(n^2+\hat{k}_{n1}^2)^2}{\hat{k}_{n1}^2\hat{k}_{n3}^2\hat{k}_{n4}^2(\hat{k}_{n1}-\hat{k}_{n2})}\cos[n(\theta-\phi)]e^{j\hat{k}_{n1}s}$$

$$= 2\left(1+\frac{\hat{k}_{n2}}{\hat{k}_{n1}}\right)Y_n^{iT}(s,\theta) \qquad \ldots(4.57)$$

4.6 Evaluation of the Simplified Low Frequency Mobilities of Semi-infinite Pipes

In this section, the simplified point and transfer mobility of the semi-infinite pipe at low frequencies, which have been described in the previous section, are examined by comparing them with the predicted mobility calculated from the original expressions given in the section 4.3. Using the pipe data in table 2.1 (page 30) in the calculations, the point mobility for circumferential modes n = 0-3 are shown in figure 4.4. In order to reduce the effect of the evanescent wave in the far field, the transfer mobility is calculated at the non-dimensional distance s = 100 and is shown in figure 4.5.

Like the infinite pipe, the simplification of the mobilities for the semi-infinite pipe depends on their being a negligible contribution from other waves. That is for the n = 0 mode the simplified mobility is valid up to high frequencies because of the large difference in wavenumber between the standing near field waves and the longitudinal wave. At the excitation position, the standing near field waves dominate the response of this mode. However, in the far field region, the pipe is dominated by the longitudinal propagating wave. For the n = 1 mode it is valid at low frequencies where the flexural and near field waves dominate over the standing near field waves, and for the higher modes it is also valid to high frequencies except at the cut-on frequencies for the $n \geq 3$ modes. A summary of the approximate mobilities derived in the previous section is given in table 4.1.

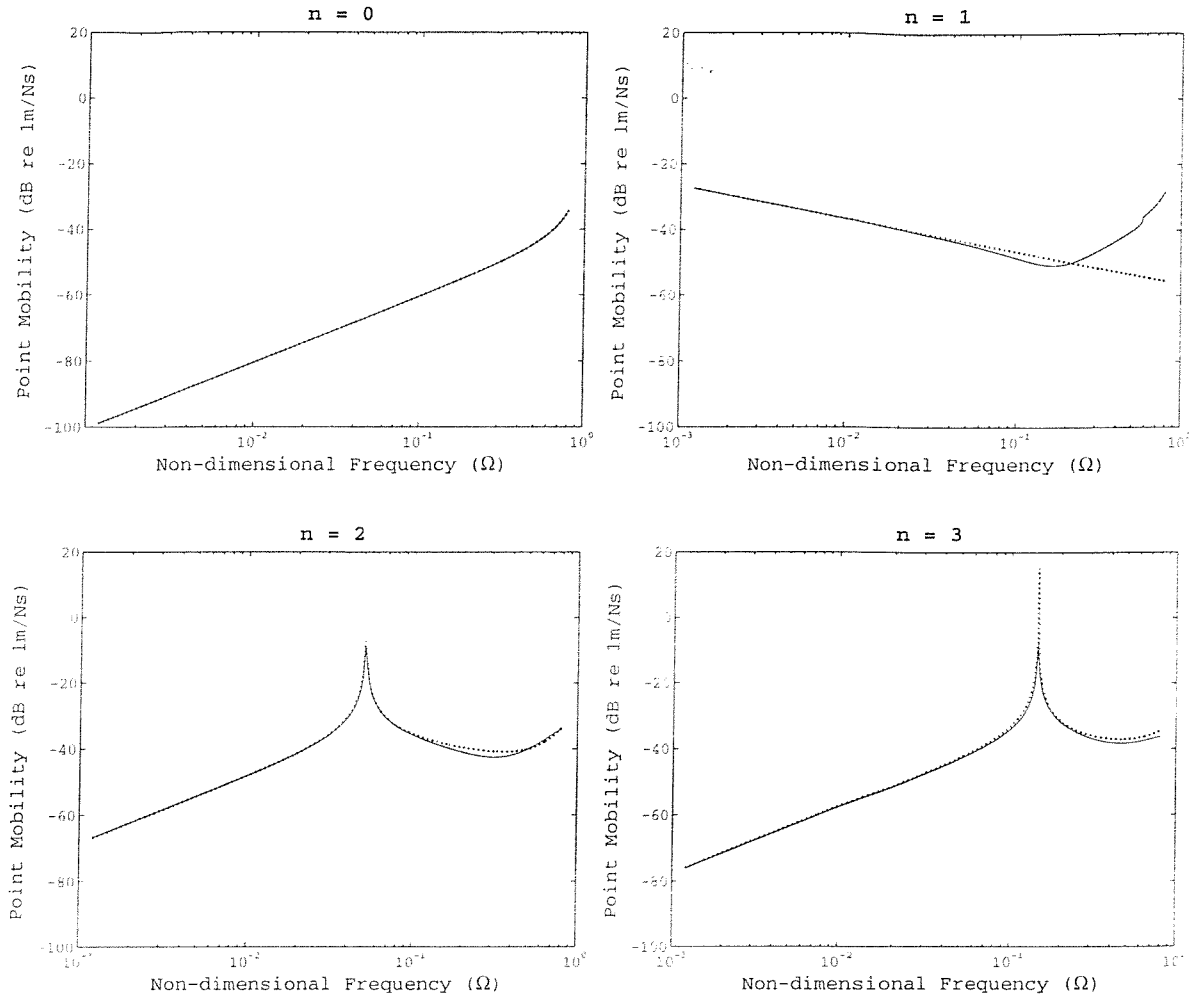

Figure 4.4: Point mobility of the n = 0 to n = 3 modes of a semi-infinite pipe; __ Analytical method, ... Simplification at low frequencies.

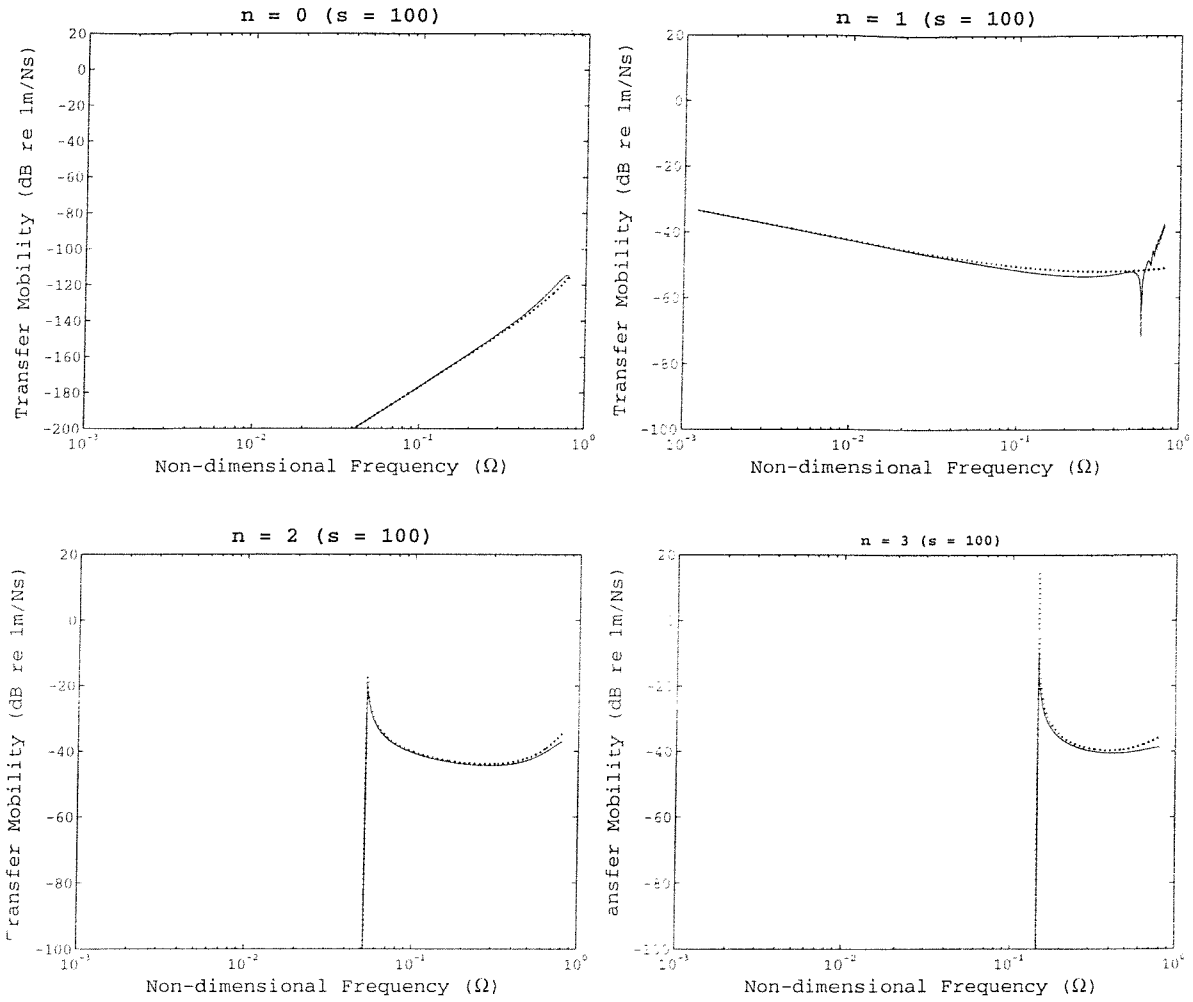

Figure 4.5: Transfer mobility of the n = 0 to n = 3 modes of a semi-infinite pipe, which is calculated at the distance of s = 100; __ Analytical method, ... Simplification at low frequencies (note that the scale of the n = 0 mode is different from that of the other modes).

Table 4.1: Summary of the approximate mobility of a semi-infinite pipe.

Mode	Mobility	
	Point	Transfer
0	$-\frac{(1+j)\omega}{2\pi\beta^2 K\hat{k}_{03}^3}$	$\frac{(1+j)\nu\omega\hat{k}_1^2}{2\pi(1-\nu^2)K\hat{k}_{03}^3}$
1	$\frac{(1-j)\omega}{\pi hE\hat{k}_b^3}$	$\frac{(1-j)(1+2\hat{k}_b^2)\omega}{2\pi hE\hat{k}_b^3}$
≥ 2	$-\frac{a^2\omega}{\pi D}\frac{(\hat{k}_{n1}+\hat{k}_{n2})(\hat{k}_{n1}^2\hat{k}_{n2}^2-n^4)}{\hat{k}_{n1}^2\hat{k}_{n2}^2\hat{k}_{n3}^2\hat{k}_{n4}^2}$	$-\frac{a^2\omega}{\pi D}\frac{(n^2+\hat{k}_{n1}^2)^2}{\hat{k}_{n1}^2\hat{k}_{n3}^2\hat{k}_{n4}^2(\hat{k}_{n1}-\hat{k}_{n2})}$

Note that $\overline{\overline{W}}_{n1}^{i}$ is the radial amplitude of the flexural wave for the n^{th} mode of the infinite pipe and is given in equation (3.64 a).

4.7 Experimental Validation

4.7.1 Introduction

In the previous sections, expressions for the mobility of semi-infinite pipes were derived using the Analytical and the Wave methods. Even though the numerical results obtained from both methods are consistent, it is worthwhile verifying them by

conducting some experiments. In this section, the experiments, which are set up to validate the theoretical model, are described.

4.7.2 Experimental Setup

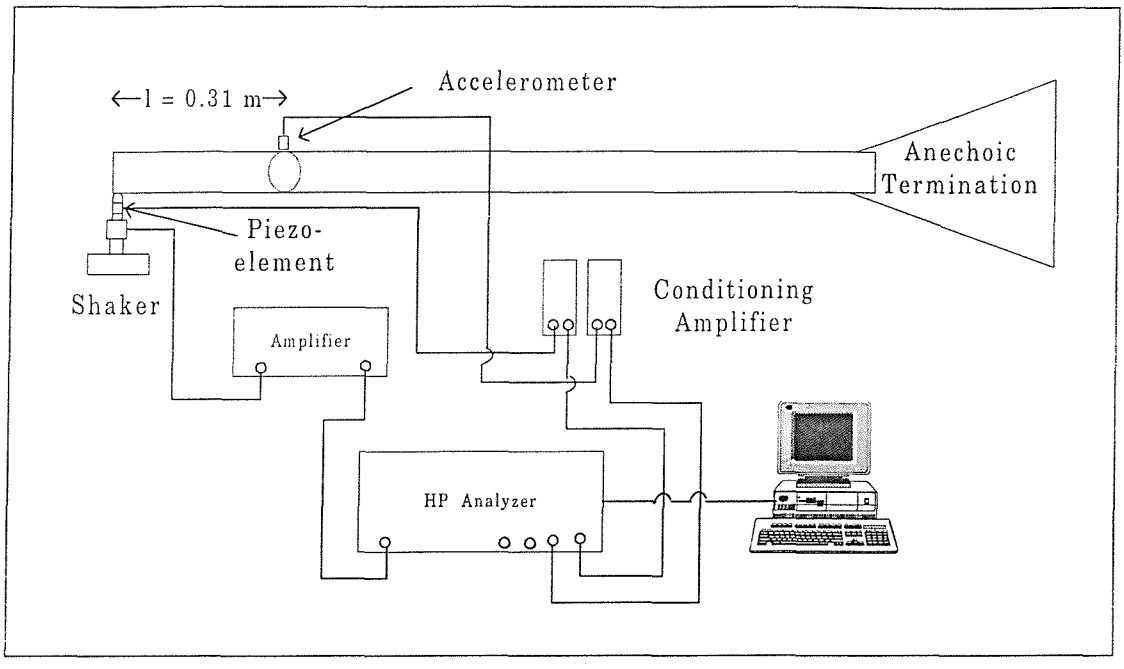

Figure 4.6: Experimental setup for the semi-infinite pipe

The properties of the pipe given in table D.1 (appendix D) and the sensitivity of 341.7 pC/N of the PZT force gauge were determined by the experiment in the previous chapter, and they are used in this section.

Since the pipe discussed in the previous section was assumed to be semi-infinite, which has no reflected waves from one end of the pipe, an anechoic termination was used for this purpose. However, this does not perfectly absorb vibration so that some reflection from the anechoic termination still remains which interferes with the incident waves. In the previous chapter, the experimental results of the wave decomposition (figures 3.17-3.20) showed clearly that the reflected waves were small in comparison with the incident waves, and can be ignored.

The configuration for a semi-infinite pipe shown in figure 4.6 was similar to that of the infinite pipe (described in the section 3.7) except only a single anechoic termination was attached to one end and the shaker excited the pipe at the other end. The 5 m PVC pipe was suspended by cords and was attached by a wooden box containing sand as an anechoic terminations at the one free end in order to make the finite pipe being a semi-infinite pipe. The pipe was excited at the free end by a shaker. A random signal from an HP 3566A Signal Analyzer was supplied to the shaker, and a set of thirty-two measurements around the pipe with equal angle was carried out at a distance of 310 mm from the shaker by using two Bruel & Kjaer accelerometers type 4374, which were located at a 180^0 circumferential angle to each other on the pipe.. This set of frequency responses was used to verify the theory.

4.7.3 Experimental Results

In this section, the experimental results for the semi-infinite pipe are presented and compared with predictions obtained from the theoretical models described in section 4.3 (Wave method). Comparisons between practice and theory are carried out with regard to two aspects, which are for each mode and for the total response for various angles of measurements.

Accelerometers used in the experiments detect the responses of all pipe modes. Thus to make a comparison for a particular mode between experimental results and predictions, the modal decomposition technique, described in appendix A, and used in the previous chapter, has to be applied to extract the modes from the total response. Before comparisons can be made, the orientation angle of the pipe has also to be determined, and the way in which this is obtained is also described in appendix A. For convenience, the formulae of the radial amplitude, A_m, and the orientation angle, ϕ, required to extract them from the experimental results, are repeated here

$$A_m = \frac{1}{N}\sqrt{\left[\sum_{p_\theta=0}^{N-1} H_{p_\theta} \cos\left(\frac{2\pi p_\theta}{N} m\right)\right]^2 + \left[\sum_{p_\theta=0}^{N-1} H_{p_\theta} \sin\left(\frac{2\pi p_\theta}{N} m\right)\right]^2}$$

$$\phi = \frac{1}{m}\tan^{-1}\left(\frac{\sum_{p_\theta=0}^{N-1} H_{p_\theta} \sin\left(\frac{2\pi p_\theta}{N} m\right)}{\sum_{p_\theta=0}^{N-1} H_{p_\theta} \cos\left(\frac{2\pi p_\theta}{N} m\right)}\right)$$

where m is the desired mode to be decomposed,

p_θ is the position of the measurement and

N is the number of measurements around the pipe.

H_{p_θ} is the frequency response at the position p_θ.

It was shown in the previous sections that the radial velocity of the pipe increases with increasing frequency. This implies that the sensor used in the experiment should be massless; otherwise it is difficult to move at high frequencies resulting lower motion detected by the sensor. Unfortunately, the smallest accelerometer available for the experiment has a mass of 0.65 gram. Apart from the mass of the sensor, another factor, which affects the experimental results, is the tip mass of the PZT element used as a force gauge. It has the effect of reducing the excitation force. To reduce this effect, it was designed to have a very small mass of 0.08 gram. Both effects are described in appendix C.

The experimental results presented are as follows.

Frequency responses of each mode of the semi-infinite pipe measured at a distance of 310 mm from the excitation position.

Figure 4.7 Amplitude of mobility of the n = 1 mode of the semi-infinite pipe

Figure 4.8 Amplitude of mobility of the n = 2 mode of the semi-infinite pipe

Figure 4.9 Amplitude of mobility of the n = 3 mode of the semi-infinite pipe

Orientation angle, ϕ, of the semi-infinite pipe with respect to the force position.

Figure 4.10 Orientation angle extracted from frequency response of the n = 2 mode of the semi-infinite pipe

Frequency responses of the semi-infinite pipe for various angles, θ, of measurements taken at distance 310 mm from the excitation position.

Figure 4.11 Amplitude of mobility of the semi-infinite pipe at $\theta = 0$

Figure 4.12 Amplitude of mobility of the semi-infinite pipe at $\theta = \pi/2$

Figure 4.13 Amplitude of mobility of the semi-infinite pipe at $\theta = \pi$

Figure 4.14 Amplitude of mobility of the semi-infinite pipe at $\theta = 3\pi/2$

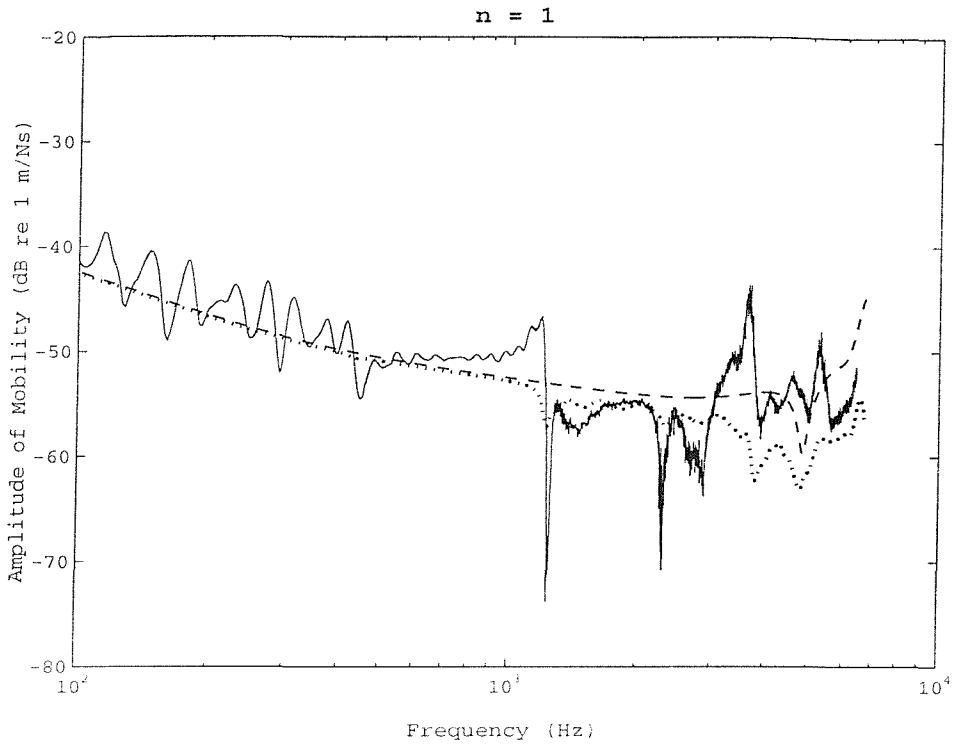

Figure 4.7: Amplitude of mobility of the n = 1 mode of the semi-infinite pipe: __ Measured result; _ _ Prediction; ... Prediction with mass effect accounted for.

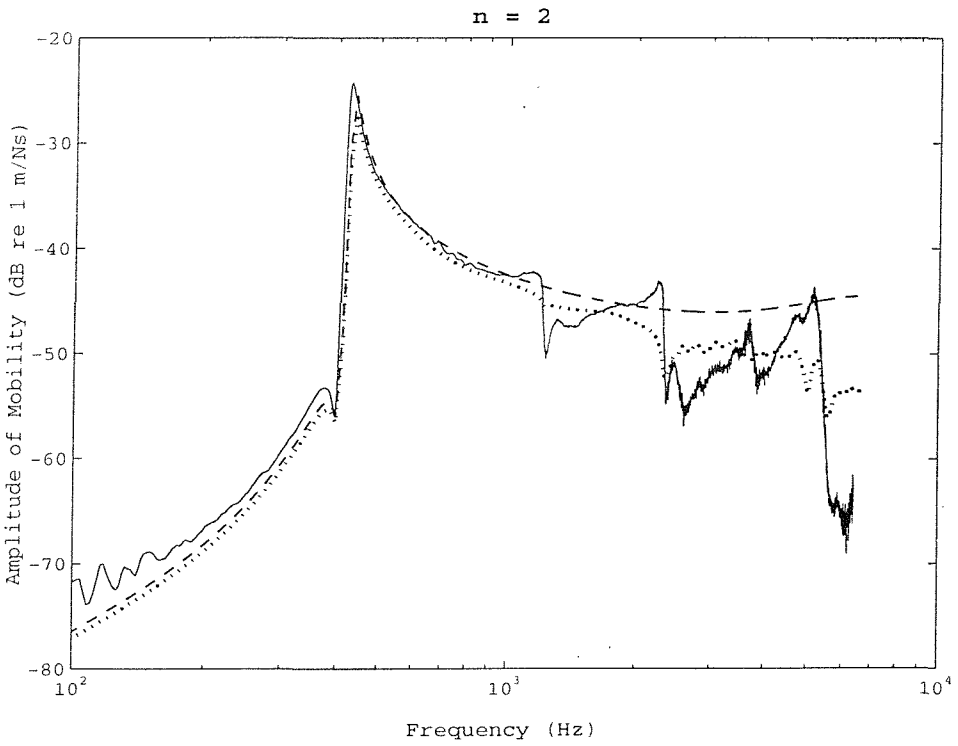

Figure 4.8: Amplitude of mobility of the n = 2 mode of the semi-infinite pipe: __ Measured result; _ _ Prediction; ... Prediction with mass effect accounted for.

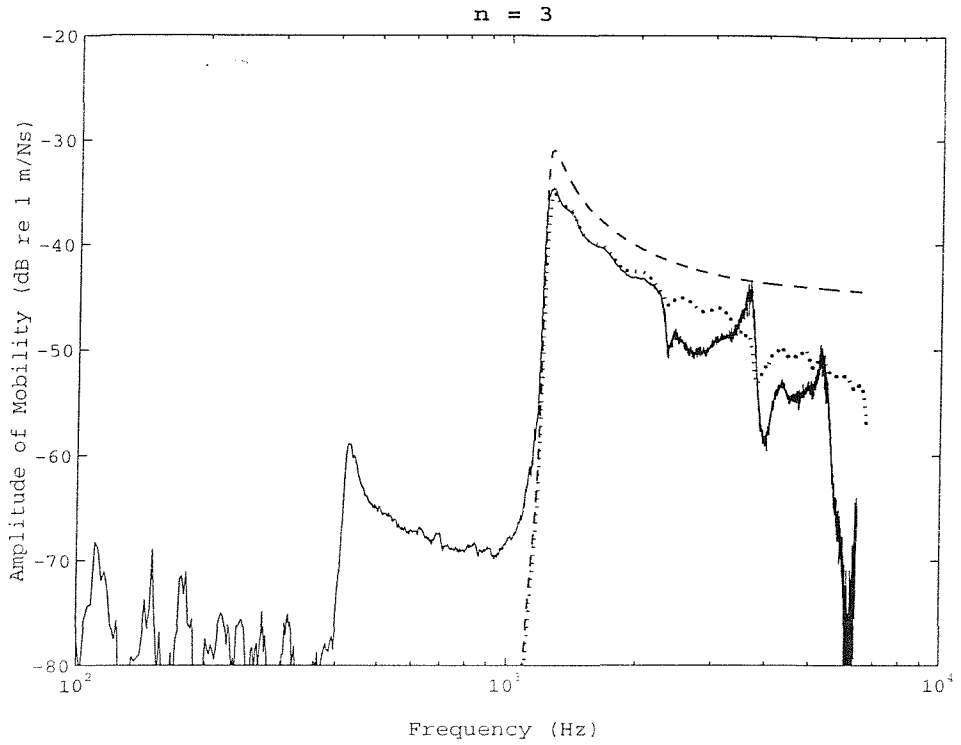

Figure 4.9: Amplitude of mobility of the n = 3 mode of the semi-infinite pipe: __ Measured result; _ _ Prediction; ... Prediction with mass effect accounted for.Figure

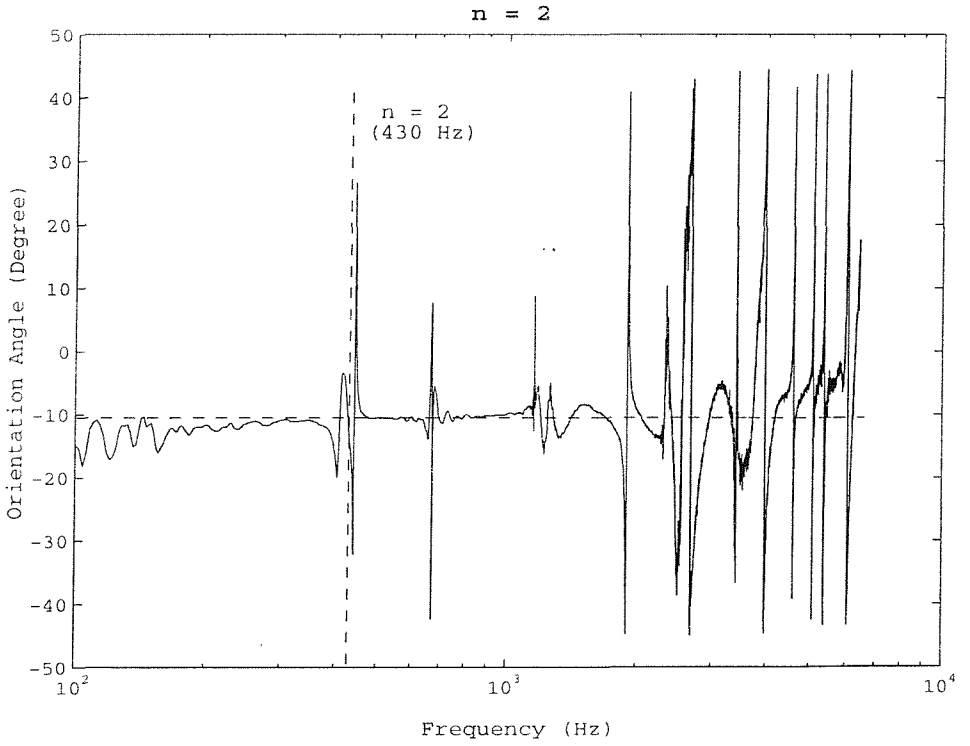

Figure 4.10: Orientation angle extracted from frequency response of the n = 2 mode of the semi-infinite pipe.

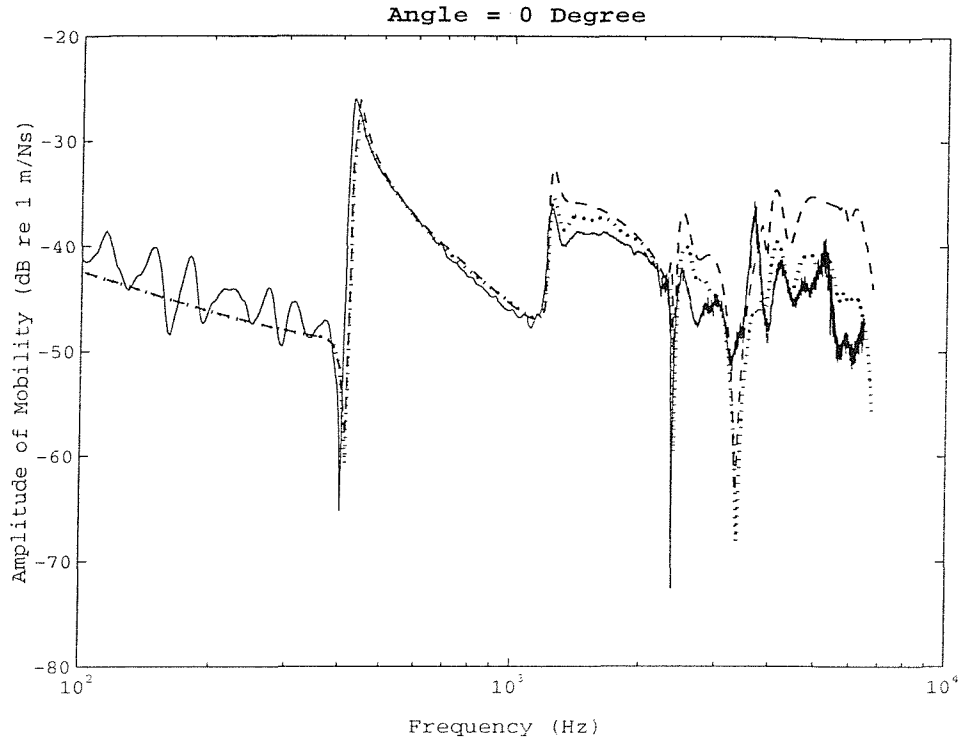

Figure 4.11: Amplitude of mobility of the pipe at θ = 0 and ϕ= -11: ___ Measured result; _ _ Prediction; ... Prediction with mass effect accounted for.

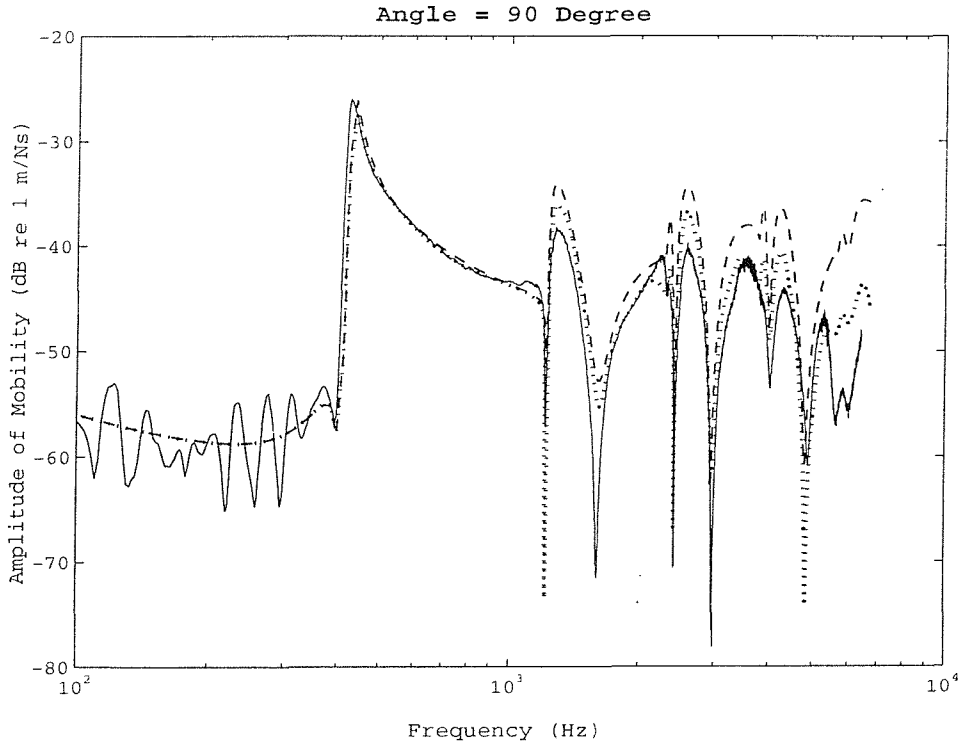

Figure 4.12: Amplitude of mobility of the pipe at θ = 90 and ϕ= -11: ___ Measured result; _ _ Prediction; ... Prediction with mass effect accounted for.

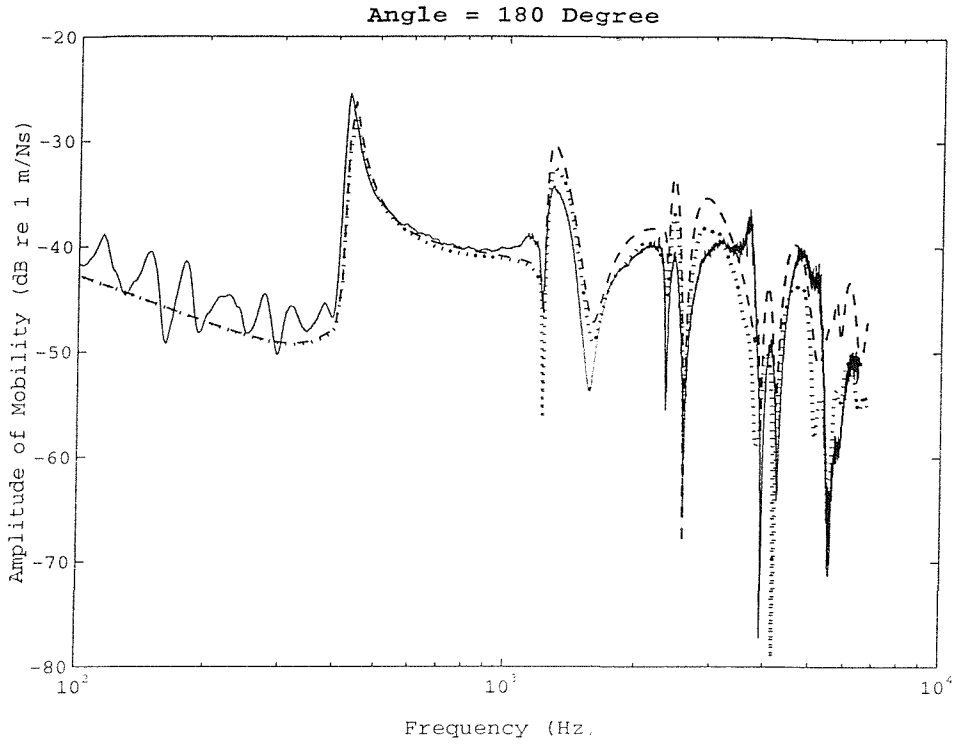

Figure 4.13: Amplitude of mobility of the pipe at θ = 180 and ϕ= -11: ___ Measured result; _ _ Prediction; ... Prediction with mass effect accounted for.

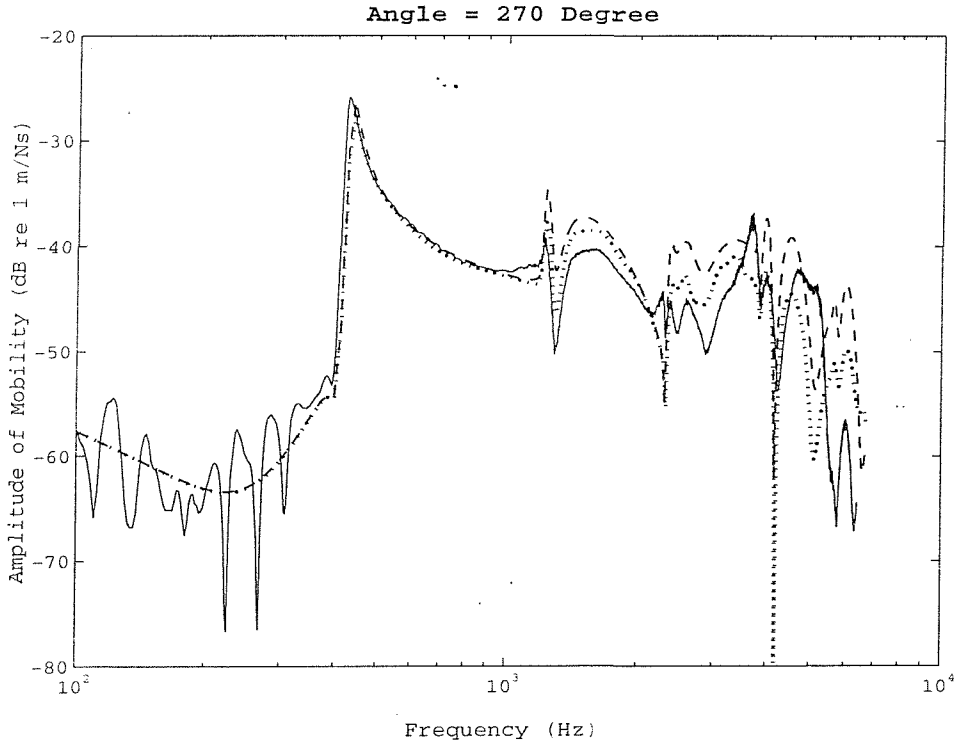

Figure 4.14: Amplitude of mobility of the pipe at θ = 270 and ϕ= -11: ___ Measured result; _ _ Prediction; ... Prediction with mass effect accounted for.

4.7.4 Discussion

Using a similar experimental setup as the infinite pipe, the anechoic termination should be as effective except at the higher modes. Such effects caused the experimental results to depart from the predictions at high frequencies as shown in figure 4.7-4.9 and 4.11-4.14. Unlike the infinite pipe, the semi-infinite pipe is more subject to the mass loading from the mass of the accelerometers and the reduction of the excitation force due to the tip mass of the PZT element used as the force gauge. Even though the masses are small, a large effect is still observed, especially at high frequencies whereas this effect is insignificant with the infinite pipe with similar masses. This is because the motion of a semi-infinite pipe are much larger than the infinite pipe. As discussed in the previous section the orientation angle of the pipe with respect to the force is constant, so it can be determined from any mode. This angle ϕ, which was extracted from the n = 2 mode, is shown in figure 4.10.

4.8 Conclusions

Expressions for the mobility of a semi-infinite pipe have been derived using analytical and wave methods. Unlike the infinite pipe, for the semi-infinite pipe with a free end, there are no theoretical comparisons for wave amplitudes due to the complexity of the pipe. However, the numerical simulations show that both methods give the same result.

In addition, the mobilities at low frequencies, $\Omega^2 << 1$ are simplified. Good agreement with the original expressions is achieved. By numerical evaluation, it clearly shows that the simplified mobility for the n = 0 mode is valid up to high frequencies. Excluding the n = 1 mode, the simplification of the higher modes are also valid up to high frequencies except at the cut-on frequencies.

Experimental validation for the theoretical models of semi-infinite pipes has been achieved. Even though an accelerometer with a small mass was selected, the effect of its mass was still apparent, especially at high frequencies. This is because the pipe is highly mobile at high frequencies but it is difficult for the accelerometer to move. To compare the theoretical predictions and the experimental results the mass loading of the accelerometers and the force gauge had to be accounted for.

CHAPTER 5

MODAL SENSORS

5.1 Introduction

Both the mass effect and the number of point measurements required for modal decomposition are disadvantages in using an accelerometer to sense the radial motion of a pipe. It was expected that a shaped polyvinylidene fluoride (PVDF) sensor would overcome some of these problems. Since PVDF is lightweight, it will not change the mechanical property of the pipe. Because it has a distributed surface for sensing the motion of the pipe and can be cut into the shapes of sine and cosine functions, it can measure the response of a particular circumferential mode without any processing of the measurements.

In this chapter, a theoretical model for a modal sensor for a circumferential mode of a pipe, especially the n = 2 mode, is developed. Some experiments are carried out to verify this theory. In addition, the performance of the modal sensor is compared with that of an accelerometer in sensing the n = 2 mode of the pipe.

5.2 Modal Sensor for Pipes

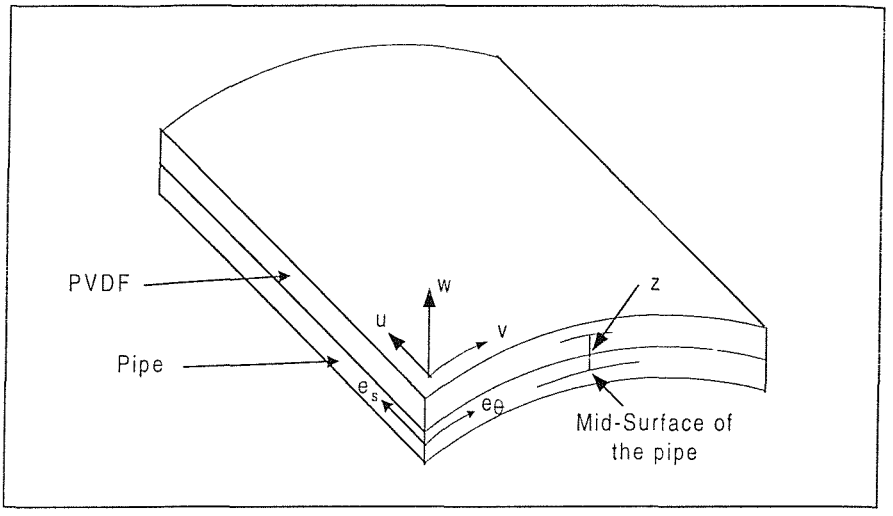

Figure 5.1: Schematic of composite section of a pipe

A schematic of a composite section of a pipe, which consists of an inner pipe layer and an outer sensor layer, is shown in figure 5.1. Generally, the mid-surface (neutral axis) of the composite pipe section is different to the mid-surface of the pipe section due to addition of the sensor layer but since the distributed PVDF sensor is very thin, it is assumed that the mid-surface of the pipe is unchanged. The assumption that the sensor is completely bonded on the pipe is also made so that the strain is continuously distributed through the composite pipe. It is well known that PVDF uses the direct piezoelectric effect, which converts mechanical strain to an electrical charge (Lee [29]). Without a skew angle, which is the angle between axes of the sensor and of the pipe, this phenomenon may be represented (Lee [29] and Lee and Moon [30]) as

$$D_3 = \varepsilon_{33}E_3 + b_{31}e_\theta + b_{32}e_s \qquad \ldots(5.1)$$

where

D_3 is the electric displacement (C/m^2),

e_s and e_θ are the axial and circumferential strains, respectively,

ε_{33} is the permittivity at constant stress (F/m),

E_3 is the electric field (V/m),

b_{31} and b_{32} are the piezoelectric stress constants (C/m^2).

The relationship between the piezoelectric stress and strain constants is given by (Lee [29])

$$\begin{bmatrix} b_{31} \\ b_{32} \end{bmatrix} = \begin{bmatrix} E_{pv}/(1-\nu_{pv}^2) & \nu_{pv}E_{pv}/(1-\nu_{pv}^2) \\ \nu_{pv}E_{pv}/(1-\nu_{pv}^2) & E_{pv}/(1-\nu_{pv}^2) \end{bmatrix} \begin{bmatrix} d_{31} \\ d_{32} \end{bmatrix} \qquad \ldots(5.2)$$

where E_{pv} is Young's modulus of PVDF (N/m^2),

ν_{pv} is Poisson's ratio of PVDF (no unit),

d_{31} and d_{32} are the piezoelectric strain constants (C/N).

Following Flugge's shell theory (Liessa [2], Flugge [5]), the axial (e_s) and circumferential (e_θ) strains at an arbitrary distance z from the mid-surface of a pipe may be expressed in terms of the pipe strain combination between stretching (extensional deformation) and bending (in-extensional deformation) strains as

$e_s = \varepsilon_s + z\kappa_s$ and

$$e_\theta = \frac{1}{1+z/a}(\varepsilon_\theta + z\kappa_\theta) \qquad \ldots(5.3\ a, b)$$

where $\varepsilon_s = \dfrac{\partial u}{a\partial s}$ is the stretching strain of the mid-surface of the pipe in the axial direction,

$z\kappa_s = -z\dfrac{\partial^2 w}{a^2\partial s^2}$ is the bending strain in the axial direction,

$\varepsilon_\theta = \dfrac{1}{a}\left(\dfrac{\partial v}{\partial\theta} + w\right)$ is the stretching strain of the mid-surface of the pipe in the circumferential direction, and

$z\kappa_\theta = -\frac{z}{a^2}\left(\frac{\partial^2 w}{\partial\theta^2} - \frac{\partial v}{\partial\theta}\right)$ is the bending strain in the circumferential direction,

κ_s is the circumferential change of curvature of the mid-surface of the pipe, and

κ_θ is the axial change of curvature of the mid-surface of the pipe.

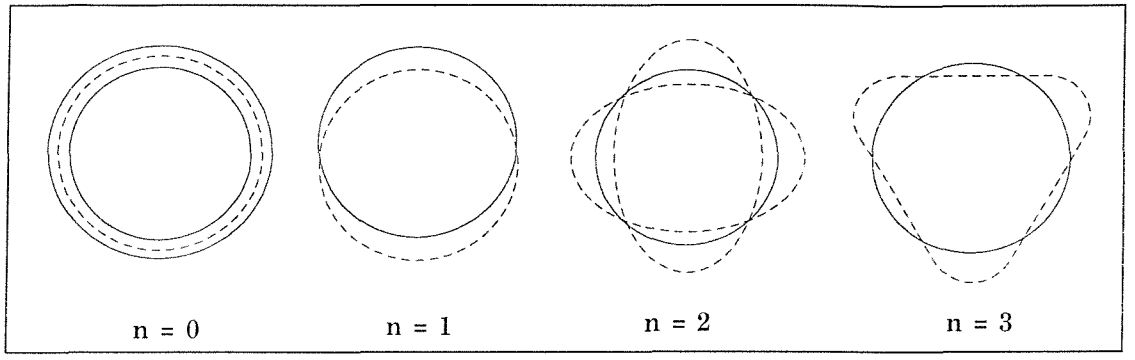

Figure 5.2: Forms of mode deformation of a pipe.

It is well known that the extensional deformation dominates the motion of the pipe for the n = 0 mode, while the deformation of n = 1 or higher modes is in-extensional as shown in figure 5.2 (Flugge [5] and Timoshenko [3]). Since the main aim of this work is to develop a modal sensor for the n = 2 mode of the pipe, in which the stretching strains (ε_s and ε_θ) equal to zero, only the bending strains ($z\kappa_s$ and $z\kappa_\theta$) represent the motion of the pipe. One of the conditions for in-extensional deformation (Timoshenko [3]) is $\frac{\partial v}{\partial\theta} = -w$, then $z\kappa_\theta = -\frac{z}{a^2}\left(\frac{\partial^2 w}{\partial\theta^2} + w\right)$. For simplification, the term z/a may also be neglected in comparison with unity so that equation (5.3) becomes

$$e_s = -\frac{z}{a^2}\frac{\partial^2 w}{\partial s^2} \quad \text{and}$$

$$e_\theta = -\frac{z}{a^2}\left(\frac{\partial^2 w}{\partial\theta^2} + w\right) \qquad \text{for } n \geq 1 \qquad \ldots(5.4\ a, b)$$

With the strains discussed above for the n ≥ 1 modes, the electric displacement given in equation (5.1) becomes

$$D_3 = \varepsilon_{33}E_3 - b_{31}\frac{z}{a^2}\left(w + \frac{\partial^2 w}{\partial\theta^2} + \frac{b_{32}}{b_{31}}\frac{\partial^2 w}{\partial s^2}\right) \qquad \ldots(5.5)$$

In order to measure the charge generated from the PVDF sensor, a closed-circuit arrangement (Lee [29] and Callahan and Baruh [44]), in which the surface electrodes of both sides of the sensor are short-circuited, is employed so that the electric field E_3 is zero. By such an arrangement, the generated charge, $q(t)$, is approximately the average of the electric displacement integrated over the area of both sides of the effective surface electrodes. So

$$q(t) = \frac{1}{2}\left(\iint_{A_p(z=z_o+h_{pv}/2)} D_3 a^2 ds d\theta + \iint_{A_p(z=z_o-h_{pv}/2)} D_3 a^2 ds d\theta\right) \qquad \ldots(5.6)$$

where A_p is the effective surface area of the PVDF,

h_{pv} is the thickness of the PVDF, and

$z_o = (h + h_{pv})/2$ is the distance from the mid-plane of the pipe to that of the PVDF.

By substituting the electric displacement from equation (5.5), equation (5.6) becomes

$$q(t) = -z_o b_{31}\iint_{A_p}\left(w + \frac{\partial^2 w}{\partial\theta^2} + \frac{b_{32}}{b_{31}}\frac{\partial^2 w}{\partial s^2}\right) ds d\theta \qquad \ldots(5.7)$$

The radial shell displacement for an infinite pipe has already been discussed in chapter 2 (equation 2.2) and is given here for clarity. By writing the term $\cos[n(\theta - \phi)]$ in equation (2.2) in terms of sine and cosine functions, the radial displacement with superscript i for denoting the infinite pipe can be rewritten as

$$w^i(s,\theta,t) = \sum_{n=1}^{\infty}\sum_{b=1}^{4}\overline{\overline{W}}^{i}_{nb}\left[\lambda_1\cos(n\theta) + \lambda_2\sin(n\theta)\right]e^{j(\hat{k}_{nb}s - \omega t)} \qquad \ldots(5.8)$$

where $\lambda_1 = \cos(n\phi)$,

$\lambda_2 = \sin(n\phi)$ and

ϕ is the orientation angle.

It can be seen from equation (5.8) that the radial displacement consists of sine and cosine components. It should also be noted that the displacement of the n = 0 mode is not included in the above expression since the extensional deformation is not taken into account in this work. Actually, for an *in-vacuo* pipe the motion of the n = 0 mode is very small compared with that of the $n \geq 1$ modes as presented in figures 3.6 and 3.7 so that it can be neglected.

Substituting equation (5.8) into equation (5.7) gives

$$q(t) = \sum_{n=1}^{\infty}\sum_{b=1}^{4} A_{nb}\,\overline{\overline{W}}^{i}_{nb} \iint_{A_p} \left[\lambda_1 \cos(n\theta) + \lambda_2 \sin(n\theta)\right] e^{j(\hat{k}_{nb}s-\omega t)}\,ds\,d\theta \qquad \ldots(5.9)$$

where $A_{nb} = z_o b_{31}\left(n^2 + \frac{b_{32}}{b_{31}}\hat{k}_{nb}^2 - 1\right)$.

Since the total charge generated, $q(t)$, is the sum of the response over the surface of the PVDF sensor, it may be expressed as (Gu *et al* [42])

$$q(t) = \sum_{n=1}^{\infty}\sum_{b=1}^{4} A_{nb}\,\overline{\overline{W}}^{i}_{nb} \int_0^{2\pi}\int_{s_c-b_s S_p(\theta)}^{s_c+b_s S_p(\theta)} \left[\lambda_1 \cos(n\theta) + \lambda_2 \sin(n\theta)\right] e^{j(\hat{k}_{nb}s-\omega t)}\,ds\,d\theta \qquad \ldots (5.10)$$

where s_c is the non-dimensional axial location of centre of the sensor to the radius of the pipe,

b_s is the ratio of a half of width of the sensor to the radius of the pipe,

$S_p(\theta)$ is the shape of the sensor.

By omitting the terms of $e^{-j\omega t}$ for simplification, evaluating the integral gives

$$Q = \sum_{n=1}^{\infty}\sum_{b=1}^{4}\frac{2e^{j\hat{k}_{nb}s_c}}{\hat{k}_{nb}}A_{nb}\overline{\overline{W}}^{i}_{nb}\int_0^{2\pi}[\lambda_1\cos(n\theta)+\lambda_2\sin(n\theta)]\sin\{\hat{k}_{nb}b_sS_p(\theta)\}d\theta \qquad \ldots (5.11)$$

In equation (5.11), Q is the generated charge in the frequency domain. If the sensor is shaped in the form of $S_p(\theta) = \cos(p_v\theta)$, where p_v is the desired mode number, equation (5.11) becomes

$$Q^c = \sum_{n=1}^{\infty}\sum_{b=1}^{4}\frac{2e^{j\hat{k}_{nb}s_c}}{\hat{k}_{nb}}A_{nb}\overline{\overline{W}}^{i}_{nb}\int_0^{2\pi}[\lambda_1\cos(n\theta)+\lambda_2\sin(n\theta)]\sin\{\hat{k}_{nb}b_s\cos(p_v\theta)\}d\theta \qquad \ldots (5.12)$$

where Q^c is the charge generated by a cosine modal sensor.

The term of $\sin[\hat{k}_{nb}b_s\cos(p_v\theta)]$ can be expressed in terms of Bessel functions as follows (Arfken [70])

$$\sin\{\hat{k}_{nb}b_s\cos(p_v\theta)\} = 2\sum_{m_v=1}^{\infty}(-1)^{m_v-1}J_{2m_v-1}(\hat{k}_{nb}b_s)\cos[(2m_v-1)p_v\theta]$$

Substituting it into equation (5.12), and using the property of orthogonality gives

$$Q^c = \sum_{n=1}^{\infty}\sum_{b=1}^{4}\frac{1}{\hat{k}_{nb}}4\pi\lambda_1 e^{j\hat{k}_{nb}s_c}A_{nb}\overline{\overline{W}}^{i}_{nb}\sum_{m_v=1}^{\infty}(-1)^{m_v-1}J_{2m_v-1}(\hat{k}_{nb}b_s)\delta_{nm_p} \qquad \ldots (5.13)$$

where $m_p = (2m_v - 1)p_v$.

$\delta_{nm_p} = 1$; for $n = m_p$ and

$= 0$; for $n \neq m_p$.

Equation (5.13) is a general expression for the total charge generated by the modal sensor for any modes with the form of the cosine function. It is clear that the sensor detects a series of mode displacements. In a specific case, in which p = 2, then the modal sensor will detect the displacements of modes of n = 2, 6, 10 and so on, which

correspond to the Bessel function of order 1, 3, 5 and so on, respectively. The result of which the modal sensor is sensitive to the higher modes is because of the non-constant axial and circumferential strains, over the width of the sensor.

Below the ring frequency, only the responses of the n = 2 and n = 6 modes are sensed by the n = 2 cosine modal sensor, which produces the total charge as given by

$$Q^c = 4\pi\lambda_1\left(\sum_{b=1}^{4}\frac{1}{\hat{k}_{2b}}A_{2b}\overline{\overline{W}}^{i}_{2b}J_1(\hat{k}_{2b}b_s)e^{j\hat{k}_{2b}s_c} - \sum_{b=1}^{4}\frac{1}{\hat{k}_{6b}}A_{6b}\overline{\overline{W}}^{i}_{6b}J_3(\hat{k}_{6b}b_s)e^{j\hat{k}_{6b}s_c}\right) \qquad ...(5.14)$$

Because the responses of the n = 2 and n = 6 modes depend upon b_s, the ratio of a half of width of the sensor to the radius of the pipe, it is of interest to evaluate the **cross sensitivity**, which is the ratio between the response of the n = 6 and the n = 2 mode, for various b_s. Using the pipe data and the PVDF properties given from appendix D, numerical assessments of the cross sensitivity in near and far fields are shown in figure 5.4. As expected, the cross sensitivity in the near field shown in figure 5.4 largely reduces at $\Omega = 0.05$ where the waves of the n = 2 mode cut on. This does not occur in the far field because there is no motion of the n = 6 mode before it cuts on. Figure 5.4.b clearly shows that the cross sensitivity increases with increasing b_s. Using a criteria of –20 dB cross sensitivity, it is illustrated in figure 5.3.c and 5.3.d that, with a value of b_s up to 0.4 in the near field of the vibration source and to 0.2 at the far field, the responses of the n = 6 modes are insignificant up to $\Omega = 0.66$. So, equation (5.14) can be reduced to the first term, which is the response of the n = 2 mode. Therefore, the expression of the generated charge becomes

$$Q^c = 4\pi\lambda_1\sum_{b=1}^{4}\frac{1}{\hat{k}_{2b}}A_{2b}\overline{\overline{W}}^{i}_{2b}J_1(\hat{k}_{2b}b_s)e^{j\hat{k}_{2b}s_c} \quad \text{for n = 2 and } b_s \le 0.2 \qquad ...(5.15)$$

The Bessel function can be expanded as (Arfken [70])

$$J_1(\hat{k}_{2b}b_s) = \frac{\hat{k}_{2b}b_s}{2} - \frac{(\hat{k}_{2b}b_s)^3}{2^3 2!} + \frac{(\hat{k}_{2b}b_s)^5}{2^5 2!3!} - \ldots$$

where ! is the factorial.

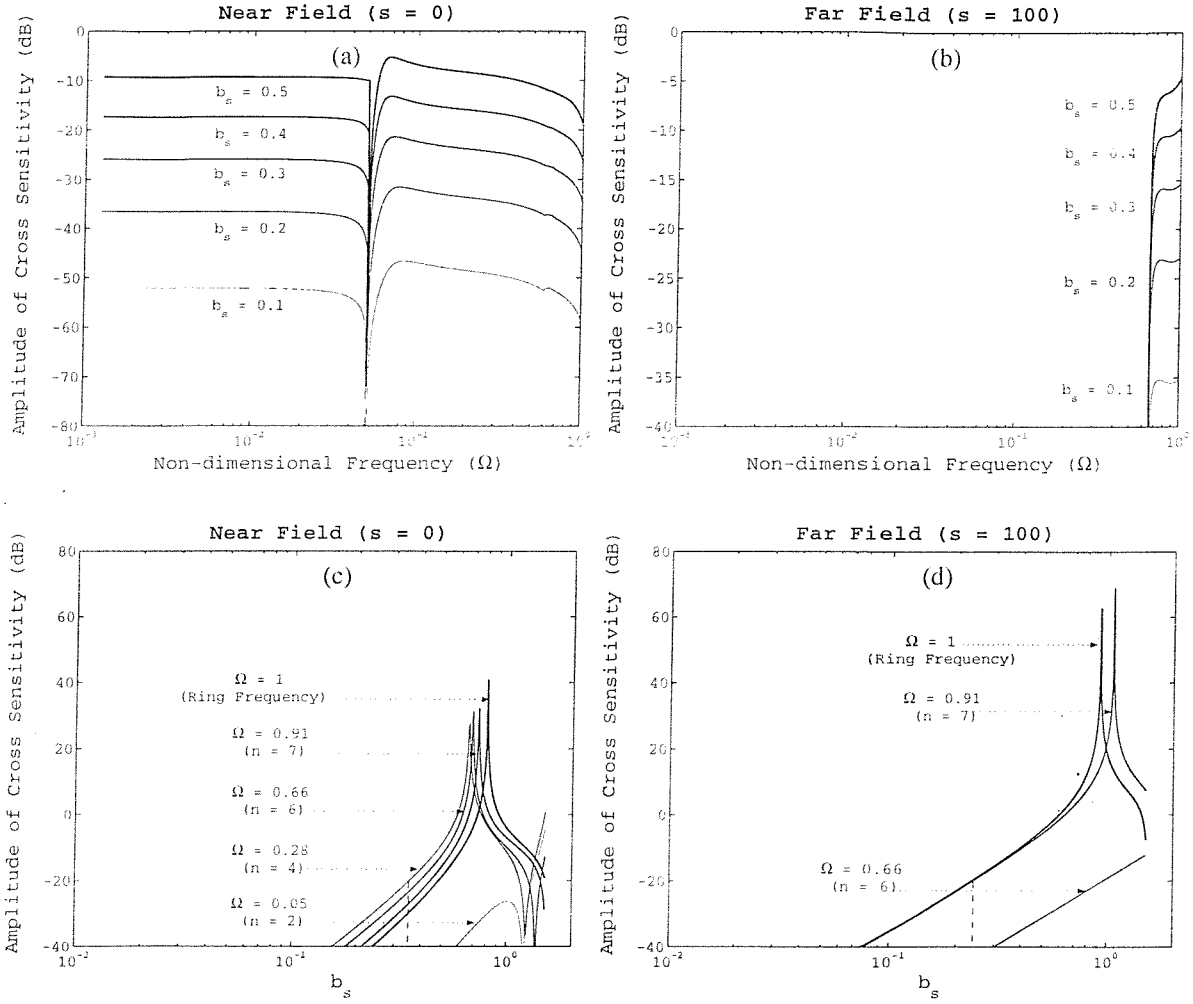

Figure 5.3: Cross sensitivities between the responses of the n = 6 and the n = 2 mode for various b_s.

If the product of $\hat{k}_{2b}b_s$ is less than unity, then higher orders can be ignored. Having the maximum wavenumber $\hat{k}_{2b}$ of the flexural propagating wave of the n = 2 mode at the ring frequency shown in figure 5.4 equal to approximately 6, b_s should be less than 0.16 to satisfy the above requirement that the cross sensitivity is less than –20 dB. Hence, the generated charge becomes

$$Q^c = 2\pi\lambda_1 b_s \sum_{b=1}^{4} A_{2b} \overline{\overline{W}}^{i}_{2b} e^{j\hat{k}_{2b}s_c}$$

$$= 2\pi\lambda_1 b_s z_o b_{31} \sum_{b=1}^{4} (n^2 + \frac{b_{32}}{b_{31}}\hat{k}_{2b}^2 - 1)\overline{\overline{W}}^{i}_{2b} e^{j\hat{k}_{2b}s_c} \text{ ; for } n = 2 \text{ and } b_s \leq 0.16 \qquad ...(5.16)$$

Since the maximum value of b_s above is less than that obtained from the numerical assessment shown in figure 5.3, it can be used as the criteria for determination of the ratio of a half of width of the sensor to the radius of the pipe and is

$$b_s < 1/\hat{k}_{2b} \text{ at the ring frequency.}$$

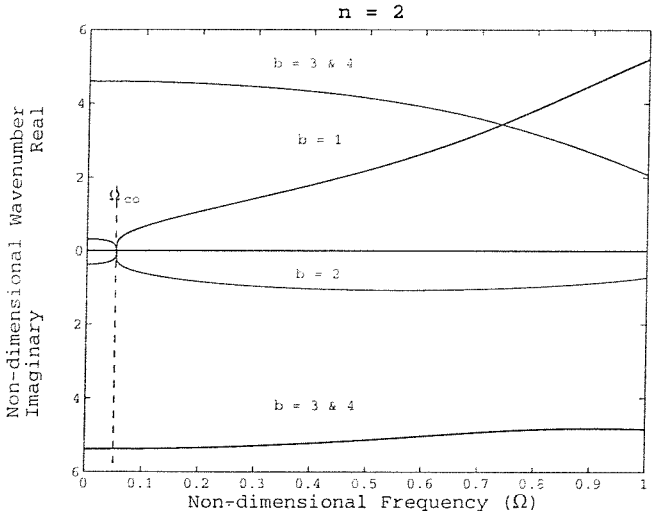

Figure 5.4: Dispersion curve of n = 2 mode calculated from equation (2.8) by using the pipe data given from Table 2.1.

Since $b_s = b_w/2a$, where b_w is the width of the modal sensor, and the non-dimensional wavenumber of the n = 2 mode at the ring frequency $\hat{k}_{2b} = 2\pi a/\lambda_{2r}$, where λ_{2r} ,is the wavelength of the n = 2 wave at the ring frequency, the criterion for determination of the width of the sensor is thus given by

$$b_w < \frac{\lambda_{2r}}{\pi} \approx \frac{1}{3}\lambda_{2r}$$

Since only the flexural wave can potentially propagate, it means that, if the width of the modal sensor is less than one third of the wavelength of the flexural wave at the ring frequency, it dominantly senses the response of the n = 2 mode.

For the modal sensor having the shape of a sine function, the same procedure to obtain the expression of the generated charge for the cosine function shape is applied. Since

$$\sin(\hat{k}_{nb} b_s \sin(p_v \theta)) = 2 \sum_{m_v=1}^{\infty} J_{2m_v-1}(\hat{k}_{nb} b_s) \sin[(2m_v - 1)p_v \theta]$$

the charge generated by a sensor shaped as a sine function is

$$Q^s = 2\pi\lambda_2 b_s z_o b_{31} \sum_{b=1}^{4} (n^2 + \frac{b_{32}}{b_{31}} \hat{k}_{2b}^2 - 1) \overline{\overline{W}}_{2b}^{i} e^{j\hat{k}_{2b} s_c} \text{ ; for } n = 2 \text{ and } b_s \leq 0.16 \qquad ...(5.17)$$

The total generated charge, Q_t, for a mode with arbitrary orientation can be obtained by a combination of both sine and cosine function shapes of the modal sensors in terms of the square root of the sum of the squares and it is

$$Q^t = \sqrt{(Q^c)^2 + (Q^s)^2}$$
$$= 2\pi b_s z_o b_{31} \sum_{b=1}^{4} (n^2 + \frac{b_{32}}{b_{31}} \hat{k}_{2b}^2 - 1) \overline{\overline{W}}_{2b}^{i} e^{j\hat{k}_{2b} s_c} \quad \text{for } n = 2 \text{ and } b_s \leq 0.16 \qquad ...(5.18)$$

The orientation angle can be determined as

$$\phi = \frac{1}{2} \tan^{-1}\left(\frac{\lambda_2}{\lambda_1}\right) = \frac{1}{2} \tan^{-1}\left(\frac{Q^s}{Q^c}\right) \qquad ...(5.19).$$

5.3 Experimental Work

5.3.1 Introduction

In this section, the experiments that were carried out to validate the modal sensor equation for the infinite pipe are described. The results are also compared with those obtained when using an accelerometer to evaluate the performance of the sensor for active vibration control purposes.

5.3.2 Experimental Setup and Procedure

Modal sensors for the n = 2 mode were fabricated by cutting 52 μm thick PVDF in the shape of a sine function with the width of 6 mm or b_s = 0.09 approximately (both sine and cosine function modal sensors are the same but there are placed at a 45^0 circumferential angle to each other on the pipe). This was done by generating the required shape of the PVDF on the computer and transferring it to the sensor material before cutting it out with the scissors to give four patches, whose poling is arranged as shown in figure 5.5 and figure D.1 (appendix D). The sections of the sensors were electrically connected with copper tape. Since the PVDF sheet manufactured from Measurement Specialties, Inc, has piezoelectric strain constants, $d_{31} = d_{32} = 23*10^{-12}$ m/V, with $E_{pv} = 2*10^9$ N/m^2 and $\nu_{pv} = 1/3$, then the piezoelectric stress constants are $b_{31} = b_{32} = 69*10^{-3}$ C/m^2. The schematic of the experimental setup is shown in figure 5.6. The 4.6 m plastic pipe, whose properties are given in Table D.1 (appendix D), was suspended by cords, and attached to wooden boxes being anechoic terminations at the both free ends in order to make the finite pipe behave as an infinite pipe. Both modal sensors shaped in sine and cosine functions were placed close together, 1200 mm and 1210 mm respectively from the excitation point. Driven by a random signal supplied by an HP 3566A Signal Analyzer, a shaker excited the pipe at the mid-point between the anechoic terminations. The arrangement of the modal sensors of n = 2 mode was such that individual elements were expected to detect the in-phase response of the n = 2

mode and out-of-phase response of other modes. Because the modal sensors were expected to detect only the motion of the n = 2 mode after they were electrically connected together, an experiment was conducted to verify this and the results were used to compare with those obtained from accelerometer measurements at the same position.

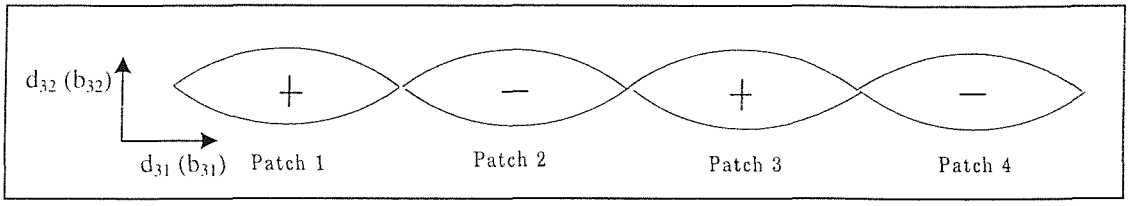

Figure 5.5: Arrangement of modal sensor.

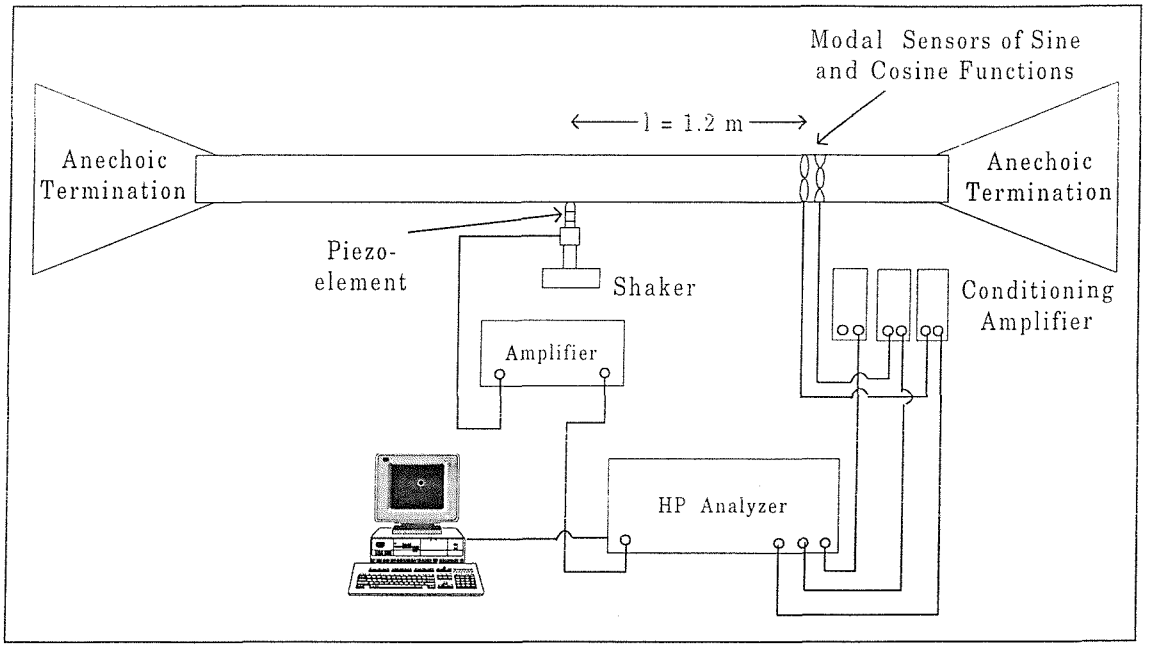

Figure 5.6: Experimental setup for evaluation of the modal sensor.

5.3.3 Experimental Results

In this section, experimental results are presented and compared with predictions in the form of the transfer function (Coulomb/ Newton) calculated using the theory described in the previous section. The results obtained from the modal sensors are also

compared with those obtained from the array of accelerometers described in the previous chapter.

The transfer functions of the n = 2 modal sensors are obtained by dividing equation (5.16) for the cosine modal sensor, and equation (5.17) for the sine modal sensor by the force amplitude, F_0, and are given as

$$T_q^c = \frac{Q^c}{F_0} = 2\pi\lambda_1 b_s z_o b_{31} \sum_{b=1}^{4} (n^2 + \frac{b_{32}}{b_{31}} \hat{k}_{2b}^2 - 1) \frac{\overline{\overline{W}}^i_{2b}}{F_0} e^{j\hat{k}_{2b}s_c}, \qquad \ldots(5.20\ a, b)$$

$$T_q^s = \frac{Q^s}{F_0} = 2\pi\lambda_2 b_s z_o b_{31} \sum_{b=1}^{4} (n^2 + \frac{b_{32}}{b_{31}} \hat{k}_{2b}^2 - 1) \frac{\overline{\overline{W}}^i_{2b}}{F_0} e^{j\hat{k}_{2b}s_c}, \text{ respectively.}$$

where $\overline{\overline{W}}^i_{2b} = -\frac{j\varepsilon_2 F_o}{2\pi\rho h a^2 \omega_r^2} Res_{2b}$ is the b^{th} amplitude of the n = 2 mode (equation 3.30)

$\ldots(5.20\ c)$

Hence, the total transfer function is

$$T_q^t = \frac{Q^t}{F_0} = -2\pi b_s z_o b_{31} \sum_{b=1}^{4} (n^2 + \frac{b_{32}}{b_{31}} \hat{k}_{2b}^2 - 1) \frac{\overline{\overline{W}}^i_{21}}{F_0} e^{j\hat{k}_{2b}s_c}. \qquad \ldots(5.21)$$

In order to compare the response of the modal sensors to that of the n = 2 mode decomposed by an array of accelerometers, the generated charge has to be converted into a mobility.

At $s = s_c$, which is assumed as the position in a far field region where the pipe has only a flexural wave propagating, the transfer function of the cosine modal actuator given in equation (5.20 a) becomes

$$T_q^c = \frac{Q^c}{F_0} = 2\pi\lambda_1 b_s z_o b_{31}(n^2 + \frac{b_{32}}{b_{31}}\hat{k}_{21}^2 - 1)\frac{\overline{\overline{W}}_{21}^i}{F_0} e^{j\hat{k}_{21}s_c}, \qquad ...(5.22)$$

Equation (5.22) can be rearranged to give the amplitude of the n = 2 propagating wave, $\overline{\overline{W}}_{21}^i$

$$\overline{\overline{W}}_{21}^i = \frac{F_0 T_q^c}{2\pi\lambda_1 b_s z_o b_{31}(n^2 + \frac{b_{32}}{b_{31}}\hat{k}_{2b}^2 - 1) e^{j\hat{k}_{21}s_c}} \qquad ...(5.23)$$

To transform the response sensed by the modal sensor to the mobility of the pipe, the expression for the mobility of the n = 2 mode for the cosine function, which is obtained from the decomposition method (described in appendix A), is repeated here for convenience.

$$(Y_2^i)_c = \lambda_1 A_2 \qquad ...(5.24)$$

where $A_2 = -\frac{\omega\varepsilon_2}{2\pi\rho h a^2 \omega_r^2}\sum_{b=1}^{4} Res_{2b} e^{j\hat{k}_{2b}s}$

With the modal amplitude, $\overline{\overline{W}}_{2b}^i$, given in equation (5.20 c), the cosine function mobility can be rewritten as

$$(Y_2^i)_c = -j\omega\frac{\lambda_1}{F_0}\sum_{b=1}^{4}\overline{\overline{W}}_{2b}^i e^{j\hat{k}_{21}s} \qquad ...(5.25)$$

At the position of s = s_c, which is in a far field, equation (5.25) becomes

$$(Y_2^i)_c = -j\omega\frac{\lambda_1}{F_0}\overline{\overline{W}}_{21}^i e^{j\hat{k}_{21}s_c} \qquad ...(5.26)$$

Substituting for $\overline{\overline{W}}_{21}^i$ from equation (5.23) into equation (5.26) gives

$$(Y_2^i)_c = -\frac{j\omega T_q^c}{2\pi b_s z_o b_{31}(n^2 + \frac{b_{32}}{b_{31}}\hat{k}_{2b}^2 - 1)} \quad \ldots(5.27)$$

Similar to the sine function modal sensor for the n = 2 mode, the mobility of the pipe detected by this sensor is given by

$$(Y_2^i)_s = -\frac{j\omega T_q^s}{2\pi b_s z_o b_{31}(n^2 + \frac{b_{32}}{b_{31}}\hat{k}_{2b}^2 - 1)} \quad \ldots(5.28)$$

Hence, the total mobility of the pipe sensed by the modal sensor is given by

$$Y_2^i = \sqrt{(Y_2^i)_c^2 + (Y_2^i)_s^2} = \frac{j\omega\sqrt{(T_q^c)^2 + (T_q^s)^2}}{2\pi b_s z_o b_{31}(n^2 + \frac{b_{32}}{b_{31}}\hat{k}_{2b}^2 - 1)} \quad \ldots(5.29)$$

The experimental results presented are as follows.

Figure 5.7 Total amplitude of modal sensor obtaining from the root sum square of the modals sensor shaped in sine and cosine function.

Figure 5.8 Orientation angle of pipe determined from modal sensor.

Figure 5.9 Comparison between the frequency response of the cosine function of the modal sensor and of the accelerometer array for n= 2 mode.

Figure 5.10 Comparison between the frequency response of the sine function of the modal sensor and of the accelerometer array for n= 2 mode.

Figure 5.11 Comparison between total response of the modal sensor and of the accelerometer array for n= 2 mode.

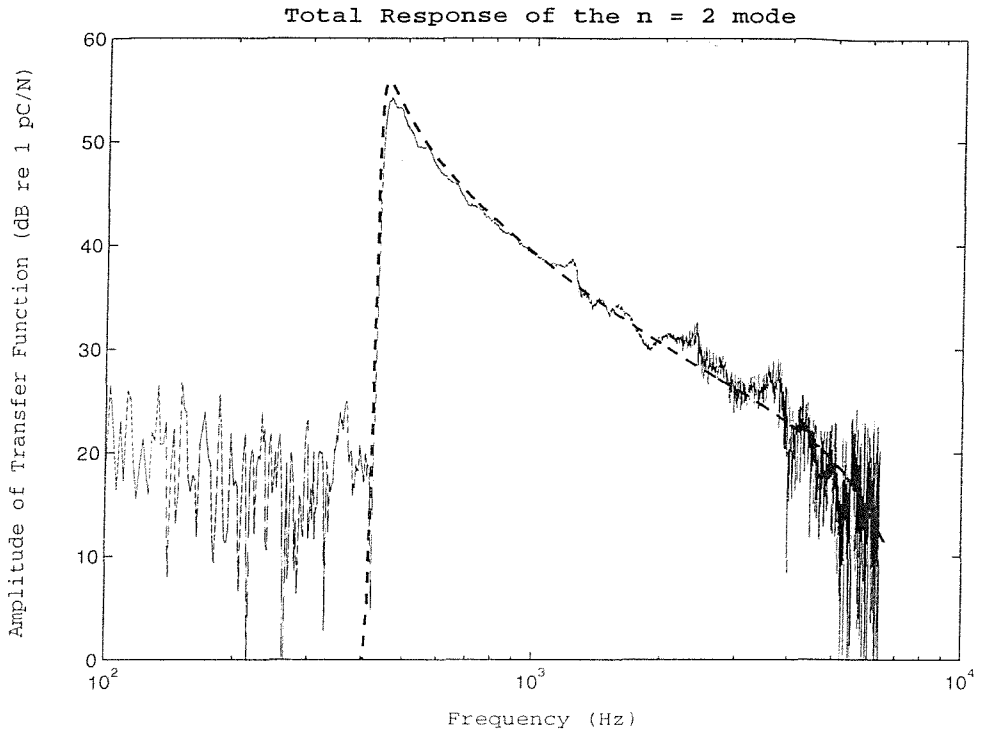

Figure 5.7: Amplitude of the total transfer function of the modal sensors obtained from the combination of the sine and cosine function shapes; __ Measured result; _ _ Equation (5.18)

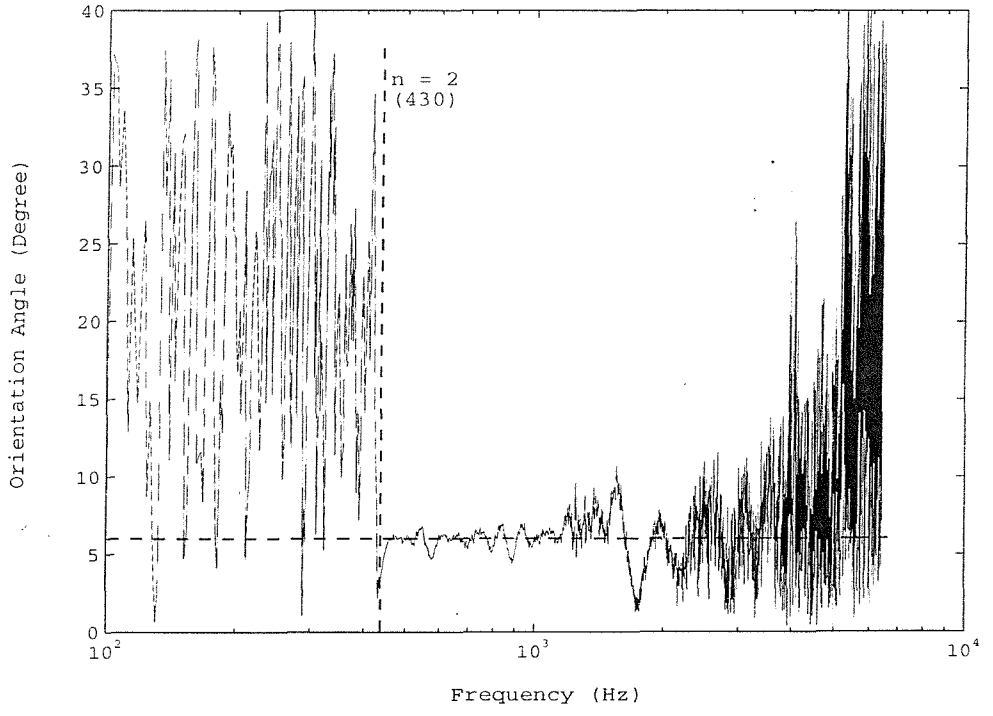

Figure 5.8: Orientation angle of the pipe with respect to the force position.

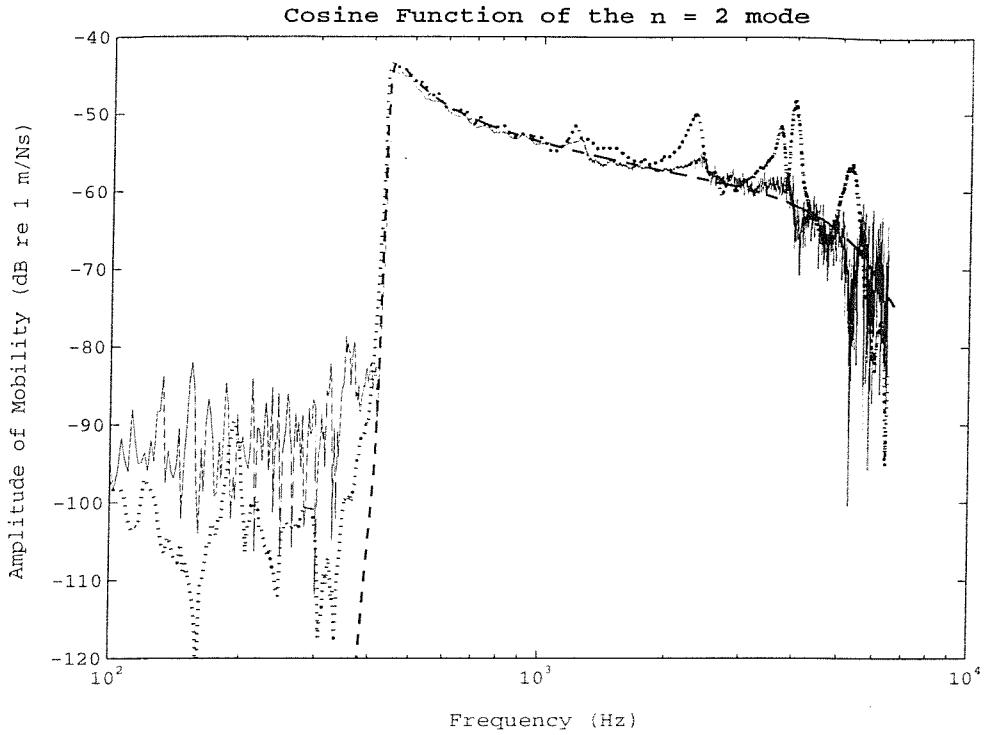

Figure 5.9: Comparison between the frequency response of the cosine function in terms of mobility for the n = 2 mode; __ Modal sensor output from equation (5.27) ; ...Output of array of accelerometers; _ _ Predicted mobility (equation 3.13) .

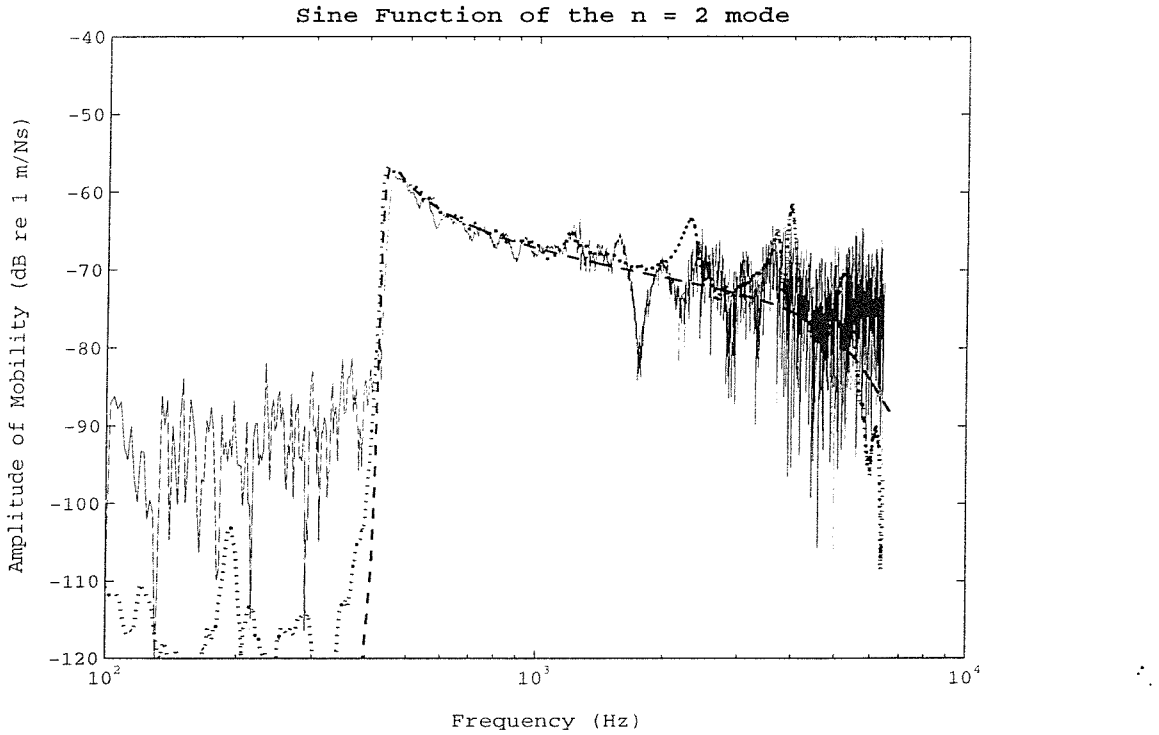

Figure 5.10: Comparison between the frequency response of the sine function in terms of mobility for the n = 2 mode; __ Modal sensor output from equation (5.28) ; ... Output of array of accelerometers; _ _ Predicted mobility (equation 3.13) .

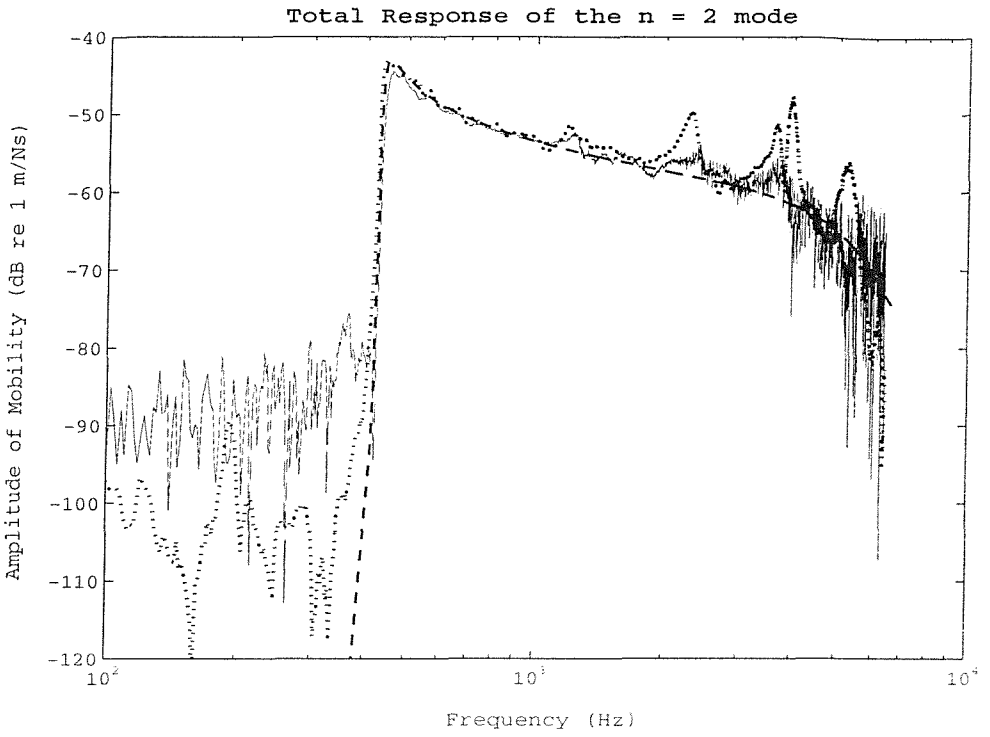

Figure 5.11: Comparison between the total response in terms of mobility for the n= 2 mode; __ Modal sensor output from equation (5.29) ; ...Output of array of accelerometers; _ _ Predicted mobility (equation 3.13) .

5.3.4 Discussion

Before the flexural wave of the n = 2 mode cuts on, all waves are evanescent. So the response of the pipe is very small resulting in a negligible generated charge from the modal sensor. However, due to the limit of the analyzer and instrumentation, there is a noise floor and this is evident in the experimental results presented. At high frequencies where the pipe motion is small, the noise floor also exists. Away from these frequencies, the total response of the n = 2 modal sensor, which was shown in figure 5.7, agrees reasonably well with the theory. Some small departure from the theory model occurs at the cut-on frequencies of other modes. This disagreement may be due to inaccuracy in the shapes of the modal sensors.

Before the waves cut on, the pipe has very small displacements, so the orientation angle of the pipe was determined after the wave cut on (430 Hz).

Good performance of the modal sensor was shown in figures 5.8-5.11 in which the response of the modal sensor and that of the accelerometer array are compared. It illustrates that the modal sensor has a better performance than the accelerometer due to a negligible mass effect even at high frequencies. Moreover, the inaccurate shape of the modal sensor has less of an effect than the inaccurate positioning of the array of accelerometers.

5.4 Conclusions

The work presented in this chapter has been an evaluation of the modal sensor for the n = 2 mode of the pipe. Based on Flugge's shell theory, the relationship between the charge generated from a PVDF sensor and the combination of the axial and circumferential bending strains has been established for the case of in-extensional deformation. By using the Bessel function to describe the pipe strains induced on the surface of a modal sensor, it is found that the modal sensor is sensitive to higher order modes as well as the n = 2 mode. This is because the circumferential strain is coupled with the axial strain via the Poisson's ratio of the pipe. If the strain over the width of the modal sensor is not constant, the higher order modes contribute to the output of the sensor. The cross-sensitivity is dependent upon the ratio of one half of the modal sensor width to the radius of the pipe (b_s). However, if b_s is small enough to keep the strain constant over its surface, the modal sensor will only be sensitive to the n = 2 mode. This means that the performance of the modal sensor in detecting only the n = 2 mode increases with the decrease of its sensitivity because of its surface area reduced. It is found that to keep the strain of n = 2 mode constant over the frequency range of interest, the width of the modal sensor has to be less than one third of the wavelength of the flexural wave at the ring frequency and hence it only senses the response of the n = 2 mode.

The analytical model for a modal sensor has been successfully validated by experimental results. It was also compared with an accelerometer array in terms of the mobility of the pipe. Clearly, the modal sensor provides a better performance than an accelerometer array since it does not change the mechanical properties of the structure as an accelerometer does. As described in the previous chapter, the motion of the pipe can be dramatically changed, especially at high frequencies, even if the mass of the accelerometer is small. Because the modal sensor is constructed from PVDF, it has very little mass and it does not affect the motion of the pipe. In addition, to measure the response of a particular mode by means of modal decomposition, an array of accelerometers has to be used and the outputs from these accelerometers has to be processed. Therefore in an active control system, a modal sensor, which only has two leads, is much more suitable than an accelerometer as a sensor for a particular mode.

CHAPTER 6

MODAL ACTUATOR FOR INFINITE PIPES

6.1 Introduction

In this chapter, the derivation of a model that couples a PZT modal actuator into the dynamic behaviour of an infinitely long pipe is described. However, some important expressions, which are the basis for the analysis, have to be determined first. They are for a static model of a composite PZT-pipe structure and for the transfer function of a pipe excited by a single PZT element.

Unlike a plate, strain over the thickness of a pipe is not linear. Nevertheless, for a thin pipe, in which the ratio of the thickness to the radius of the pipe is less than 0.1 (Leissa [2]), it can be assumed to be linear. With this assumption, the static model of a composite pipe can be treated like that of a composite plate. This is described in the next section

Based on the Flugge's shell theory [5], the motion of an infinite pipe excited by a single PZT element is derived and described in section 6.3. The derivation is conducted using the Residue method and the dynamic model of a composite pipe. Once the pipe motion is obtained, its transfer function can be determined in a straightforward manner.

Using the transfer function of a single PZT actuator and the radial vibration of the pipe, a modal actuator for the n = 2 mode can be analysed and is discussed in section 6.4. The

modal actuator is constructed from a set of PZT elements. By arranging them in the form of the n = 2 mode, the modal actuator can generate only the response of that mode.

Experiment work is carried out to validate the assumptions made and expressions for the transfer function of a single PZT actuator and of the modal actuator derived in this chapter.

6.2 Static Model of Composite Pipes

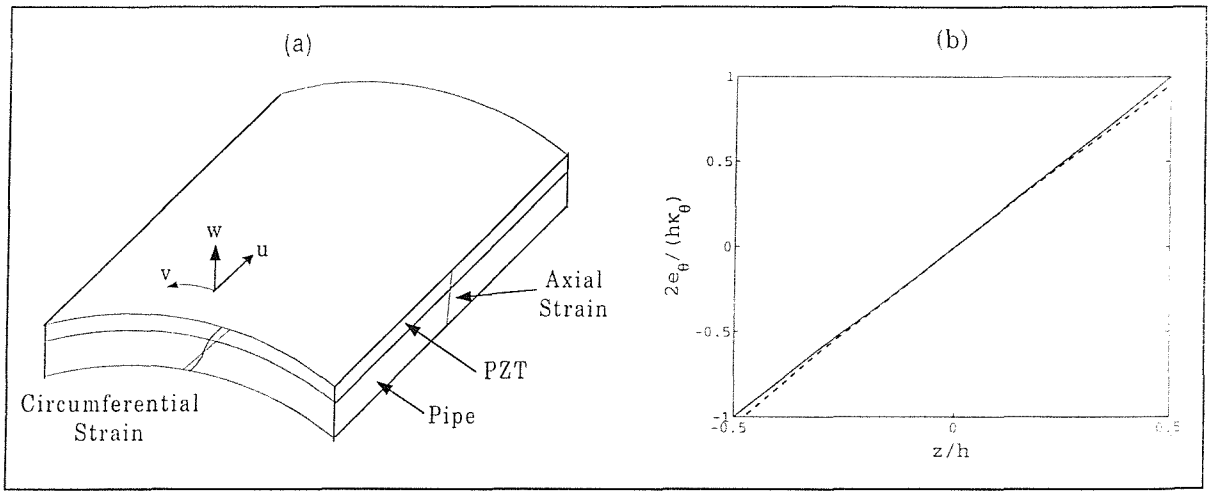

Figure 6.1: Strain model of a composite pipe: a) Schematic section of a pipe with axial and circumferential strain, b) Calculated ratio of circumferential strain, e_θ, to the product of circumferential curvature, κ_θ, and pipe thickness, h, at h/a = 0.1, ; __ using exact strain model (equation 6.3.a), _ _ using linear strain model (equation 6.3.b).

In this section, a composite section of a pipe as shown in figure 6.1.a, where a PZT actuator is bonded on the outer surface of the pipe, is examined. Due to the inverse piezoelectric effect (Morgan Matroc [27]), the PZT element is extended/contracted in proportion to the applied voltage. If the element is not bonded to the structure, the extension/contraction of the PZT is called the free strain, $\Lambda = \frac{Vd_{31}}{h_z}$ where V is the

applied voltage, d_{31} is the piezoelectric strain constant and h_z is the thickness of the PZT element. Coupled to the structure, the PZT induces stress/strain resulting in an effective moment and an effective in-plane force in the pipe.

Stresses in the pipe in the axial and circumferential direction at any position z from the mid-surface of the pipe, are given by (Leissa [2])

$$\sigma_\theta^p = \frac{E}{1-\nu^2}[e_\theta + \nu e_s]$$

$$\sigma_s^p = \frac{E}{1-\nu^2}[e_s + \nu e_\theta] \qquad \ldots(6.1\text{ a, b})$$

where $e_s = \varepsilon_s + z\kappa_s$ is the axial strain at radial position z, $\qquad \ldots(6.2\text{ a, b})$

$e_\theta = \frac{1}{1+z/a}(\varepsilon_\theta + z\kappa_\theta)$ is the circumferential strain at radial position z.

In the case of a thin pipe, its radius is much larger than its thickness and hence the thickness-radius ratio of the pipe, h/a, is very small. If this ratio can be ignored in comparison with unity, the strain of the pipe given in equation (6.2) can be treated as those of a plate, which are linear. So, it is worthwhile investigating the circumferential strain, e_θ, comparing with a linear strain. The circumferential strain given in equation (6.2) is a combination of an extensional strain, $\varepsilon_\theta/(1+z/a)$ and in-extensional strain, $z\kappa_\theta/(1+z/a)$ (Timoshenko [3] and Flugge [5]). For the n = 1 mode the pipe behaves like a rigid body (the cross-section remains undeformed), and for the $n \geq 2$ modes it changes shape. This means there is no extensional strain in the pipe for the $n \geq 1$ modes. Dividing equation (6.2.b) by $(h\kappa_\theta/2)$ gives

$$\frac{2e_\theta}{h\kappa_\theta} = \frac{2z/h}{1+\frac{z}{h}\frac{h}{a}} \qquad ; n \geq 1 \text{ modes.} \qquad \ldots(6.3\text{ a})$$

The non-dimensional parameter $(2e_\theta / h\kappa_\theta)$ in equation (6.3.a) is the ratio of the circumferential strain of the pipe at position z (e_θ) to the outer circumferential strain ($h\kappa_\theta / 2$) when it is modelled as a flat plate (z/a = 0). The reason for using this parameter is to compare with that of a plate, $(2e_{pt} / h\kappa_{pt})$, which is given by (Dimitriadis *et al* [38])

$$\frac{2e_{pt}}{h\kappa_{pt}} = 2z/h \qquad ; n \geq 1 \text{ modes.} \qquad \ldots(6.3\ b)$$

where h is the thickness of the pipe,

e_{pt} is the strain in the plate and

κ_{pt} is the change of curvature of the plate.

Since there is no significant difference between the exact and the linear strain as shown in figure 6.1.b, some authors such as Love (Leissa [2]) and Timoshenko [3], ignore the term z/a in comparison with unity. Hence, the strains induced in the pipe can be modelled as that induced in a plate and become

$$e_s = \varepsilon_s + z\kappa_s$$

$$e_\theta = \varepsilon_\theta + z\kappa_\theta \qquad \ldots(6.4\ a, b)$$

With the assumption of linear strain distribution across the thickness of the composite structure, pipe and PZT element, Dimitriadis *et al* [38] have shown that when the PZT element is activated, the change of curvature and the strains in both circumferential and axial directions over the entire pipe within a PZT element bonded are equal and are given by

$$\kappa_s = \kappa_\theta = \kappa$$

$$e_s = e_\theta = e \qquad \ldots(6.5\ a, b)$$

Substituting equation (6.5) into equation (6.4) gives

$$\varepsilon_s = \varepsilon_\theta = \varepsilon \qquad \ldots(6.6)$$

Equation (6.6) shows that the axial and the circumferential strains of the mid-surface of the pipe are equal. This is because the strains in the PZT element are similar in the axial and circumferetial directions when the voltage is applied resulting in the same extension in both directions.

Substituting for e_s, e_θ, κ_s, κ_θ from equation (6.5) and ε_s, ε_θ from equation (6.6) into equation (6.1) gives the normal stresses in a pipe, which are equal in both axial and circumferential directions, and are given by

$$\sigma^p = \sigma_s^p = \sigma_\theta^p = \frac{E}{1-\nu}(\varepsilon + z\kappa) \qquad \ldots(6.7\ a)$$

Due to the assumption of linear strain, the strain in a PZT element is given by (Kim and Jones [39])

$$\sigma^z = \sigma_s^z = \sigma_\theta^z = \frac{E_z}{1-\nu_z}(\varepsilon + z\kappa - \Lambda) \qquad \ldots(6.7\ b)$$

where E_z is the Young's modulus of the PZT element,

ν_z is the poisson's ratio of the PZT element,

For simplification, the assumption of no change to the mid-surface of the pipe (called the neutral axis for a beam and a plate) due to the attachment of a single PZT element is established (i.e. the neutral axis remains the same). Also perfect bonding and constant strain slope as shown in figure 6.2.a are assumed.

Unlike a pair of PZT elements bonded on both sides of the structure, a single PZT element gives a non-zero normal stress in the pipe as illustrated in Figure 6.2.b. With this result, the single PZT element induces both a moment and a normal force (perpendicular to the cross-section of the pipe). In order to determine them, the terms of ε and κ should first be found and can be obtained from the force and moment equilibrium about the mid surface of the pipe as given by

$$\int_{-h/2}^{h/2} \sigma^p dz + \int_{h/2}^{h/2+h_z} \sigma^z dz = 0$$

$$\int_{-h/2}^{h/2} \sigma^p z dz + \int_{h/2}^{h/2+h_z} \sigma^z z dz = 0 \qquad \ldots(6.8\ a, b)$$

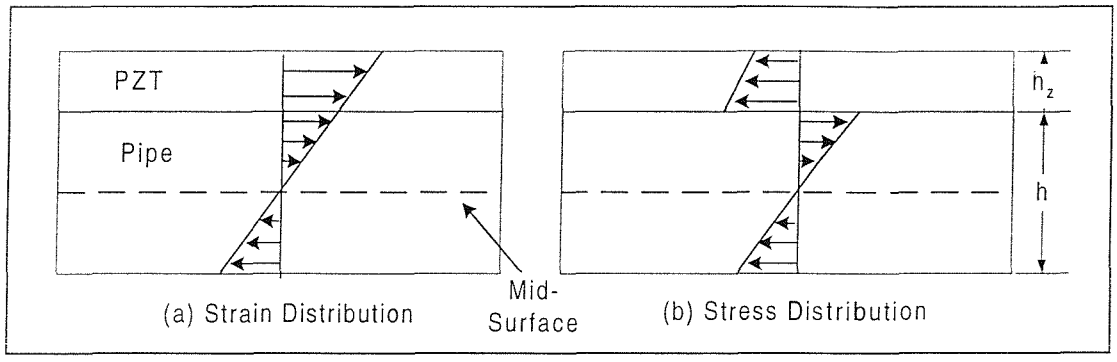

Figure 6.2: Distribution of Stress and Strain over the composite pipe (generally the term "Mid-surface" is used for a pipe, and the term "Neutral axis" is used for a beam and a plate).

Substituting equation (6.7) into equation (6.8) and evaluating the integrals gives

$$(1+\alpha\tau\mu)\varepsilon + \frac{1}{2}\alpha\tau\mu(1+\alpha)h\kappa = \alpha\tau\mu\Lambda$$

$$\alpha\tau\mu(1+\alpha)\varepsilon + \frac{1}{6}\left[1+\alpha\tau\mu\left(3+6\alpha+4\alpha^2\right)\right]h\kappa = \alpha\tau\mu(1+\alpha)\Lambda \qquad \ldots(6.9\ a, b)$$

where $\alpha = h_z/h$, $\psi = \frac{1-\nu^2}{1-\nu_z^2}\frac{E_z}{E}$, $\mu = \frac{1-\nu}{1-\nu_z}$, $\tau = \frac{E_z}{E}$ and $\gamma = \frac{E_z}{1-\nu_z}$.

Equation (6.9) can be rewritten in matrix form as

$$\begin{bmatrix} (1+\alpha\tau\mu) & \frac{1}{2}\alpha\tau\mu(1+\alpha)h \\ \alpha\tau\mu(1+\alpha) & \frac{1}{6}\left[1+\alpha\tau\mu\left(3+6\alpha+4\alpha^2\right)\right]h \end{bmatrix}\begin{bmatrix} \varepsilon \\ \kappa \end{bmatrix} = \alpha\tau\kappa\begin{bmatrix} 1 \\ (1+\alpha) \end{bmatrix}\Lambda \qquad \ldots(6.10)$$

Inverting the matrix gives

$$\begin{bmatrix} \varepsilon \\ \kappa \end{bmatrix} = \frac{\mu\tau\alpha}{1+\mu\tau\alpha\left(4+6\alpha+4\alpha^2+\mu\tau\alpha^3\right)}\begin{bmatrix} 1+\mu\tau\alpha^3 \\ \frac{6}{h}(1+\alpha) \end{bmatrix}\Lambda \qquad \ldots(6.11\text{ a, b})$$

The integral of the stress over the cross-sectional area ($L_p dz$ where L_p is the entire length of the plane perpendicular to the considered force, and dz is the infinitesimal thickness) gives the normal forces, and these forces (per unit length, i.e. axial and circumferential forces) induced on the pipe by the PZT element are given by

$$q_0 = q_{s0} = q_{\theta 0} = \int_{-h/2}^{h/2} \sigma^p dz$$

$$= \frac{Eh}{1-\nu}\varepsilon = \frac{\alpha\left(1+\mu\tau\alpha^3\right)}{1+\mu\tau\alpha(4+6\alpha+4\alpha^2+\mu\tau\alpha^3)}h\gamma\Lambda \qquad \ldots(6.12)$$

The moments per unit length induced on the pipe by the PZT element are determined as

$$m_0 = m_{s0} = m_{\theta 0} = \int_{-h/2}^{h/2} \sigma^p z dz = \frac{1}{12}\frac{Eh^3}{1-\nu}\kappa = \frac{\alpha(1+\alpha)}{2[1+\mu\tau\alpha(4+6\alpha+4\alpha^2+\mu\tau\alpha^3)]}h^2\gamma\Lambda \qquad \ldots(6.13)$$

Comparing equation (6.12) with (6.13), the relationship between both force and moment can be obtained in the simple form as

$$p_{mq} = \frac{m_0}{q_0} = \frac{1}{2}\frac{h(1+\alpha)}{1+\mu\tau\alpha^3} \qquad \ldots(6.14)$$

6.3 Transfer Function of Infinite Pipes Excited by a PZT Element

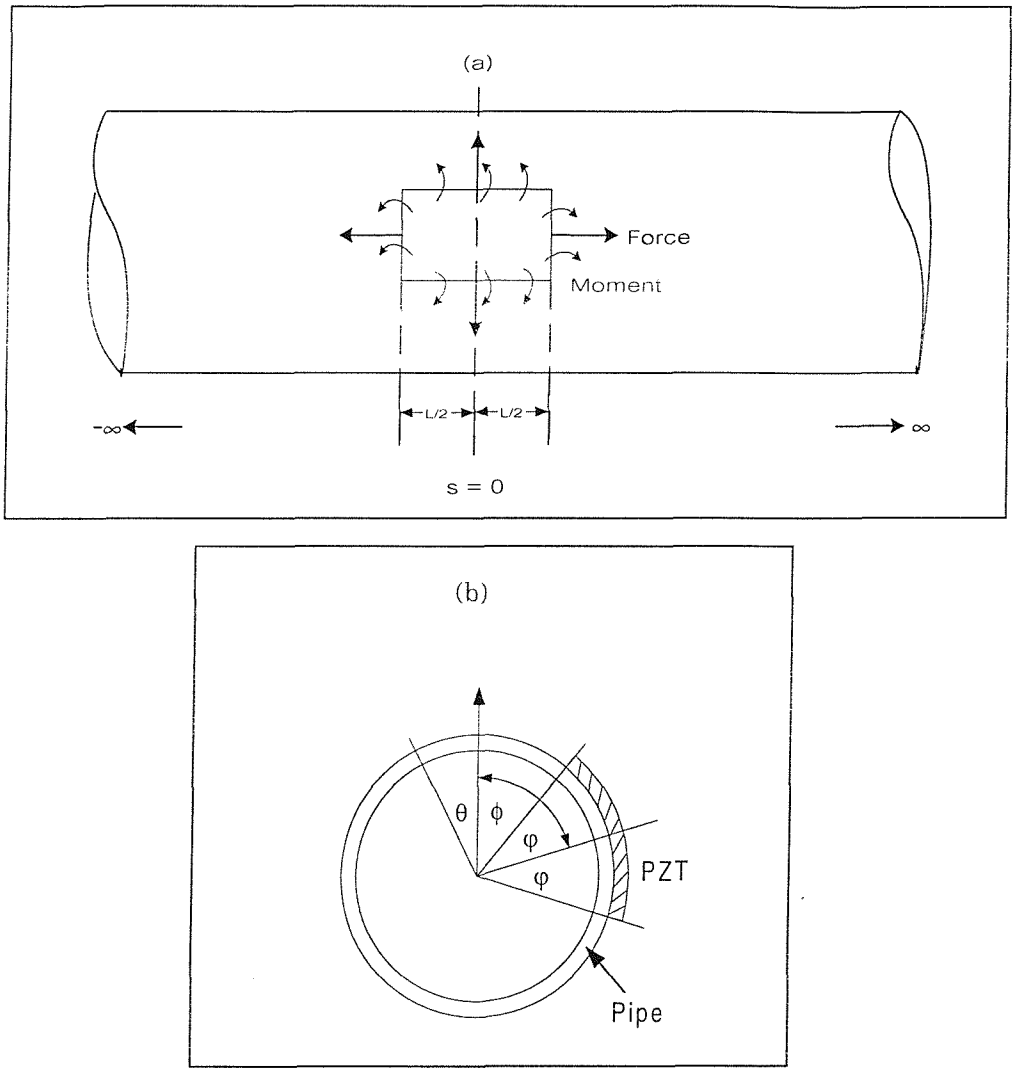

Figure 6.3: A PZT actuator bonded to an infinite pipe; a) Axial direction, b) Cross-section of the structure showing the co-ordinate.

In this section, the motion of a pipe excited by forces, q_{s0} and $q_{\theta 0}$, and moments, m_{s0} and $m_{\theta 0}$, generated by a PZT element bonded to the pipe as shown in figure 6.3 is formulated

before its transfer function is determined. This can be achieved by using the pair of Fourier and Inverse Fourier transforms and applying the Residue theory to obtain the pipe motion.

The equations of motion of the pipe excited by the PZT element can be formulated by considering the force and moment equilibrium of the pipe element as follows (Leissa [2])

$$\frac{\partial (N_s - q_s)}{\partial s} + \frac{\partial N_{\theta s}}{\partial \theta} - \rho a h \frac{\partial^2 u^{iz}}{\partial t^2} = 0$$
$$\frac{\partial (N_\theta - q_\theta)}{\partial \theta} + \frac{\partial N_{s\theta}}{\partial s} + Q_\theta - \rho a h \frac{\partial^2 v^{iz}}{\partial t^2} = 0 \qquad \ldots(6.15\ a, b, c, d, e)$$
$$(N_\theta - q_\theta) - \frac{\partial Q_s}{\partial s} - \frac{\partial Q_\theta}{\partial \theta} + \rho a h \frac{\partial^2 w^{iz}}{\partial t^2} = 0$$

$$\frac{\partial (M_s - m_s)}{\partial s} + \frac{\partial M_{\theta s}}{\partial \theta} - a Q_s = 0$$
$$\frac{\partial (M_\theta - m_\theta)}{\partial \theta} + \frac{\partial M_{s\theta}}{\partial s} - a Q_\theta = 0$$

where N_s, N_θ, $N_{\theta s}$, $N_{s\theta}$, Q_s, Q_θ,and M_s, M_θ, $M_{\theta s}$, $M_{s\theta}$ are internal forces and moments,

The superscript iz is used for the displacements excited by a PZT element.

Based on Flugge's shell theory (Flugge [5]), the equations of pipe motion can be written in matrix form as follows

$$\begin{bmatrix} A_{11} & A_{12} & A_{13} \\ A_{21} & A_{22} & A_{23} \\ A_{31} & A_{32} & A_{33} \end{bmatrix} \begin{bmatrix} u^{iz}(s,\theta,t) \\ v^{iz}(s,\theta,t) \\ w^{iz}(s,\theta,t) \end{bmatrix} = \frac{a}{K} \begin{bmatrix} \frac{\partial q_s}{\partial s} \\ \frac{\partial m_\theta}{a\,\partial \theta} + \frac{\partial q_\theta}{\partial \theta} \\ q_\theta - \frac{1}{a}\frac{\partial^2 m_s}{\partial s^2} - \frac{1}{a}\frac{\partial^2 m_\theta}{\partial \theta^2} \end{bmatrix} \qquad \ldots(6.16)$$

where the matrix **A** is given in equation (2.1).

Similar to the approach taken in section 3.2, the displacements in equation (6.16) can be derived using the Residue theory. To do this, these displacements, forces (q_s and q_θ), and moments (m_s and m_θ) have to be transformed from the spatial domain to the wavenumber domain. Using the Fourier transform, the displacements of a pipe due to a point force can be written as (equation 3.3)

$$u^{iz}(s,\theta,t) = \frac{1}{2\pi}\int_{-\infty}^{\infty}\sum_{n=0}^{\infty}\varepsilon_n \overline{U_n^{iz}(\hat{k}_n)}\cos(n\theta)\, e^{j(\hat{k}_n s-\pi/2-\omega t)}d\hat{k}_n$$

$$v^{iz}(s,\theta,t) = \frac{1}{2\pi}\int_{-\infty}^{\infty}\sum_{n=0}^{\infty}\varepsilon_n \overline{V_n^{iz}(\hat{k}_n)}\sin(n\theta) e^{j(\hat{k}_n s-\omega t)}d\hat{k}_n \qquad \ldots(6.17\text{ a, b, c})$$

$$w^{iz}(s,\theta,t) = \frac{1}{2\pi}\int_{-\infty}^{\infty}\sum_{n=0}^{\infty}\varepsilon_n \overline{W_n^{iz}(\hat{k}_n)}\cos(n\theta)\, e^{j(\hat{k}_n s-\omega t)}d\hat{k}_n$$

where $\varepsilon_n = 1$ for $n = 0$ and

$\varepsilon_n = 2$ for $n \geq 1$.

The dynamic model of the forces, q_s and q_θ, and moments, m_s and m_θ, are assumed to be uniform over the PZT surface (Dimitriadis *et al* [38]) and can be represented by the unit step function as follows (omitting terms of $e^{-j\omega t}$ for simplicity).

$$q_s = q_{s0}[H(s-L_a)-H(s+L_a)][H(\theta-\varphi)-H(\theta+\varphi)]$$

$$q_\theta = q_{\theta 0}[H(s-L_a)-H(s+L_a)][H(\theta-\varphi)-H(\theta+\varphi)]$$

$$m_s = m_{s0}[H(s-L_a)-H(s+L_a)][H(\theta-\varphi)-H(\theta+\varphi)] \qquad \ldots(6.18\text{ a, b, c, d})$$

$$m_\theta = m_{\theta 0}[H(s-L_a)-H(s+L_a)][H(\theta-\varphi)-H(\theta+\varphi)]$$

where $L_a = L/2a$ is the non-dimensional length of the PZT,

L is the length of the PZT and

H( ) is the unit step function.

As discussed in section 3.2, the spatial forces and moments can be transformed into the wavenumber domain using the Fourier transform of the delta function, δ(), which is related to the unit step function as given (Arfken [70])

$$H(s-s_0)=\int_{-\infty}^{s-s_0}\delta(s_i)ds_i\ . \qquad \ldots(6.19)$$

Following section 3.2, the delta functions of $\delta(s-L_a)$ and $\delta(\theta-\varphi)$ may be expressed as

$$\begin{aligned}\delta(s)&=\frac{1}{2\pi}\int_{-\infty}^{\infty}e^{j\hat{k}_n(s-L_a)}d\hat{k}_n\\ \delta(\theta-\varphi)&=\frac{1}{2\pi}\sum_{n=-\infty}^{\infty}e^{jn(\theta-\varphi)}\end{aligned} \qquad \ldots(6.20)$$

By substituting for the delta function from equation (6.20) into equation (6.19), the differences of unit step functions at the edges of the PZT in the axial and circumferential directions can be written as

$$H(\theta-\varphi)-H(\theta+\varphi)=-\frac{1}{\pi}\sum_{n=0}^{\infty}\frac{\varepsilon_n}{n}\sin(n\varphi)\cos(n\theta) \qquad \ldots(6.21\ a)$$

$$H(s-L_a)-H(s+L_a)=-\frac{1}{\pi}\int_{-\infty}^{\infty}\frac{1}{\hat{k}_n}\sin(\hat{k}_nL_a)e^{jk_as}d\hat{k}_n \qquad \ldots(6.21\ b)$$

Substituting for the displacements given in equation (6.17), and for the forces and moments given in equation (6.18) with the unit step function from equation (6.21) into equation (6.16) yields

$$\begin{bmatrix}L_{11}&L_{12}&L_{13}\\L_{21}&L_{22}&L_{23}\\L_{31}&L_{32}&L_{33}\end{bmatrix}\begin{bmatrix}\overline{U_n^{iz}(\hat{k}_n)}\\\overline{V_n^{iz}(\hat{k}_n)}\\\overline{W_n^{iz}(\hat{k}_n)}\end{bmatrix}=-\frac{a}{K}\sin(n\varphi)\sin(\hat{k}_nL_a)\begin{bmatrix}\frac{2}{n\pi}q_{s0}\\\frac{2}{\hat{k}_n\pi}\left(\frac{m_{\theta0}}{a}+q_{\theta0}\right)\\\frac{2}{a\pi}\left(\frac{a}{n\hat{k}_n}q_{\theta0}+\frac{\hat{k}_n}{n}m_{s0}+\frac{n}{\hat{k}_n}m_{\theta0}\right)\end{bmatrix} \qquad \ldots(6.22)$$

where the matrix **L** is given in equation (2.3).

Inverting the matrix **L**, the amplitudes of the displacements can be written as

$$\begin{bmatrix} \overline{U_n^{iz}(\hat{k}_n)} \\ \overline{V_n^{iz}(\hat{k}_n)} \\ \overline{W_n^{iz}(\hat{k}_n)} \end{bmatrix} = -2\frac{a}{\pi K}\sin(n\varphi)\sin(\hat{k}_n L_a)\begin{bmatrix} I_{11} & I_{12} & I_{13} \\ I_{21} & I_{22} & I_{23} \\ I_{31} & I_{32} & I_{33} \end{bmatrix}\begin{bmatrix} \frac{1}{n}q_{s0} \\ \frac{1}{\hat{k}_n}\left(\frac{m_{\theta 0}}{a}+q_{\theta 0}\right) \\ \frac{1}{a}\left(\frac{a}{n\hat{k}_n}q_{\theta 0}+\frac{\hat{k}_n}{n}m_{s0}+\frac{n}{\hat{k}_n}m_{\theta 0}\right) \end{bmatrix} \quad \ldots(6.23)$$

The radial displacement in the wavenumber domain is given by

$$\overline{W_n^{iz}(\hat{k}_n)} = -\frac{2a}{\pi K}\sin(n\varphi)\sin(\hat{k}_n L_a)\left[\left(\frac{q_{s0}}{n}I_{31}+\frac{q_{\theta 0}}{\hat{k}_n}I_{32}+\frac{q_{\theta 0}}{n\hat{k}_n}I_{33}\right)+\frac{1}{a\hat{k}_n}(I_{32}+nI_{33})m_{\theta 0}+\frac{\hat{k}_n}{an}I_{33}m_{s0}\right] \quad \ldots(6.24)$$

where $I_{31} = (L_{21}L_{32} - L_{22}L_{31})/|\mathbf{L}|$,

$I_{32} = (L_{12}L_{31} - L_{11}L_{32})/|\mathbf{L}|$ and $\quad \ldots(6.25\ a, b, c)$

$I_{33} = (L_{11}L_{22} - L_{12}L_{21})/|\mathbf{L}|$.

As described in the previous section, the relationship between induced force and induced moment in the pipe by the PZT are $q_{s0} = q_{\theta 0} = q_0$, $m_{s0} = m_{\theta 0} = m_0$, and $m_0 = p_{mq}q_0$ (equation 6.14). Substituting these relations into equation (6.24) gives

$$\overline{W_n^{iz}(\hat{k}_n)} = -\frac{2a}{\pi K}\frac{\sin(n\varphi)\sin(\hat{k}_n L_a)\,q_0}{n\hat{k}_n}\left[\left(\hat{k}_n I_{31}+nI_{32}+I_{33}\right)+\left(nI_{32}+(n^2+\hat{k}_n^2)I_{33}\right)\frac{p_{mq}}{a}\right] \quad \ldots(6.26)$$

Omitting terms of $e^{-j\omega t}$ for simplicity, the radial displacement for a particular mode in the frequency domain is obtained by substituting equation (6.26) into equation (6.17 c) as

$$W_n^{iz}(s,\theta) = -\frac{a\,\varepsilon_n}{\pi^2 K}\cos(n\theta)\int_{-\infty}^{\infty}\frac{\sin(n\varphi)\sin(\hat{k}_n L_a)\,q_0}{n\hat{k}_n}\left[\left(\hat{k}_n I_{31} + nI_{32} + I_{33}\right) + \left(n\,I_{32} + (n^2+\hat{k}_n^2)\,I_{33}\right)\frac{p_{mq}}{a}\right]d\hat{k}_n \qquad \ldots(6.27)$$

Because the sine function can be expanded as

$$\sin(A) = A - \frac{1}{3!}A^3 + \frac{1}{5!}A^5 + \ldots$$

by having the conditions $n\phi << 1$ and $\hat{k}_n L_a << 1$, then $\sin(n\phi) \cong n\phi$ and $\sin(\hat{k}_n L_a) \cong \hat{k}_n L_a$, respectively. Hence, the amplitude of the radial displacement becomes

$$W_n^{iz}(s,\theta) = -\frac{a\,\varepsilon_n \varphi L_a q_0}{\pi^2 K}\cos(n\theta)\int_{-\infty}^{\infty}\left[\left(\hat{k}_n I_{31} + nI_{32} + I_{33}\right) + \left(n\,I_{32} + (n^2+\hat{k}_n^2)\,I_{33}\right)\frac{p_{mq}}{a}\right]d\hat{k}_n \qquad \ldots(6.28)$$

In a similar way to that in section 3.2, the integral in equation (6.28) can be evaluated using residue theory. With this method, only the upper half plane of the complex plane of the wavenumbers is analysed by running above the negative real axis and running below the positive real axis so that only four poles are analysed (see the contour integral in figure 3.2). So, the solution of equation (6.28) can be expressed as (Arfken [70])

$$W_n^{iz}(s,\theta) = -j\frac{2a\,\varepsilon_n \varphi L_a q_0}{\pi K}\cos(n\theta)\sum_{b=0}^{4}\mathrm{Res}_{nb}^{z}\, e^{j\hat{k}_{nb}s} \qquad \ldots(6.29)$$

where $\mathrm{Res}_{nb}^{z} = \left[\left(\hat{k}_{nb} I_{31}^{r} + n\,I_{32}^{r} + I_{33}^{r}\right) + \left(n\,I_{32}^{r} + (n^2+\hat{k}_{nb}^2)\,I_{33}^{r}\right)\frac{p_{mq}}{a}\right]$

$$I_{31}^{r} = (L_{21}L_{32} - L_{22}L_{31})_{nb} / |\mathbf{L}|_{nb}'$$

$$I^{r}_{32} = (L_{12}L_{31} - L_{11}L_{32})_{nb} / |\mathbf{L}|'_{nb} \text{ and}$$

$$I^{r}_{33} = (L_{11}L_{22} - L_{12}L_{21})_{nb} / |\mathbf{L}|'_{nb}.$$

$$|\mathbf{L}|'_{nb} = \frac{\partial |\mathbf{L}|_{nb}}{\partial \hat{k}_{nb}}.$$

From the above equation, it should be noted that the analysis of the radial displacement has been taken with zero orientation for simplicity, and for the n^{th} mode with a small PZT element. The radial motion of the pipe in general form can be written by substituting for θ with $(\theta - \phi)$, where ϕ is the orientation of the pipe, and is given by

$$W^{iz}(s,\theta) = -j\frac{2a\varphi L_a q_0}{\pi K}\sum_{n=0}^{\infty}\sum_{b=1}^{4}\varepsilon_n \cos[n(\theta-\phi)]\ \mathrm{Res}^{z}_{nb}\ e^{j\hat{k}_{nb}s} \qquad \ldots(6.30)$$

Finally, the transfer function for the PZT element in terms of radial velocity can be easily determined using the static force, q_0, obtained from equation (6.12) to give:

$$T_z = -j\omega\frac{W^{iz}(s,\theta)}{V} = -\omega\frac{2a\varphi L_a}{\pi K}F_s\sum_{n=0}^{\infty}\varepsilon_n \cos[n(\theta-\phi)]\sum_{b=1}^{4}\mathrm{Res}^{z}_{nb}\ e^{j\hat{k}_{nb}s} \qquad \ldots(6.31)$$

where $F_s = \dfrac{\left(1+\mu\tau\alpha^3\right)}{1+\mu\tau\alpha(4+6\alpha+4\alpha^2+\mu\tau\alpha^3)}d_{31}\gamma$ is the static gain of the generated force, and

V is the voltage applied to the PZT element.

6.4 Modal Actuator for the n = 2 mode of Infinite Pipes

Generally, a PZT element generates radial motion of all modes as shown in equation (6.30). To generate only the radial displacement of the desired mode, a set of PZT elements is required. Arranged in the form of such a mode, it can force the pipe to vibrate only in the desired mode. With this arrangement, a set of PZT elements may be called **modal actuator**.

Excited by a single PZT element, the radial motion obtained from equation (6.31) is a function of three separate parameters, ϕ, θ and s. The radial motion, W^{iz}, activated by the PZT element located at the angle ϕ_p may be rewritten in a simple form as

$$W^{iz}(\phi=\phi_p)=V\sum_{n=0}^{\infty}A_n^z\cos[n(\theta-\phi_p)] \qquad ...(6.32)$$

where $A_n^z=-j\dfrac{2a\varphi L_a\varepsilon_n}{\pi K}F_s\sum_{b=1}^{4}Res_{nb}^z\,e^{j\hat{k}_{nb}s}$.

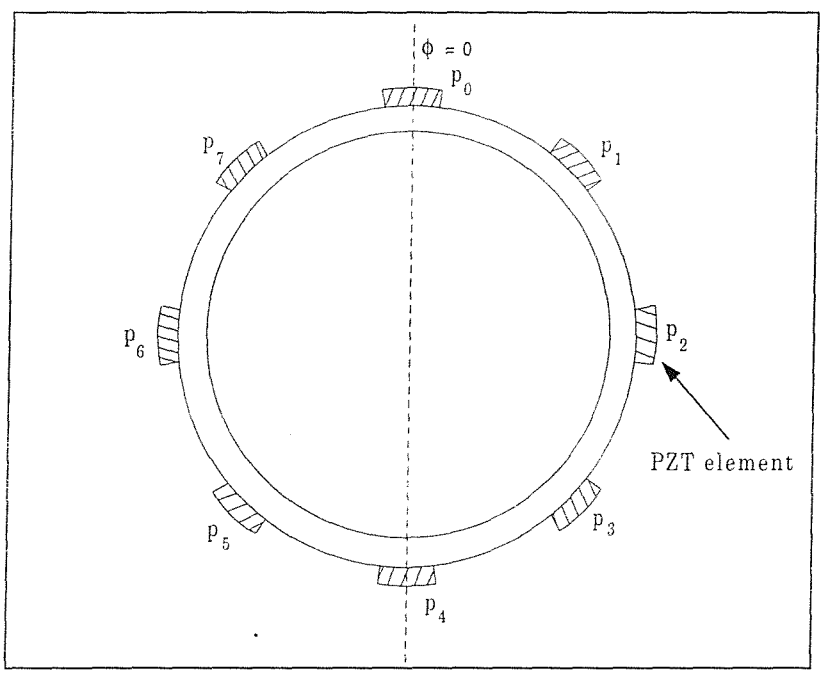

Figure 6.4: Cross-sectional schematic of a modal actuator

The sine and cosine functions have the property of orthogonality over a series of discrete, equally spaced points (Arfken [70]). By applying this property to the above expression, the radial motion of a particular mode can be derived. The schematic of a cosine function modal actuator, in which a set of PZT elements is arranged to satisfy the discrete orthogonality condition, is shown in figure 6.4. The PZT elements are positioned around the pipe with equal angle of

$$\phi = 0, \frac{2\pi}{N_e}, \frac{4\pi}{N_e}, ..., 2\pi$$

where N_e is the number of circumferential positions or the number of PZT elements.

The angle interval between the positions of the PZT elements is

$$\phi_p = 2\pi \frac{p_e}{N_e} \qquad ...(6.33)$$

where p_e is the circumferential position of the PZT element on the pipe.

Multiplying the radial motion, $W^{iz}(\phi = \phi_p)$ given in equation (6.32), by $\cos(2\pi m_z p_e/N_e)$ where m_z is the desired mode to be activated by a modal actuator yields the product of $W^{iz}(\phi = \phi_p)\cos(2\pi m_z \frac{p_e}{N_e})$. Substituting for the discrete angle, ϕ_p, into equation (6.32) and summing the product over all of the PZT elements give the radial response of the cosine modal actuator, W^c, for the m_z^{th} mode as

$$\begin{aligned} W^c &= \sum_{p_e=0}^{N_e-1} W^{iz}(\phi = \phi_p)\cos(2\pi m_z \frac{p_e}{N_e}) \\ &= V^c \sum_{p_e=0}^{N_e-1} \sum_{n=0}^{\infty} A_n^z \left[\cos(n\theta)\cos(2\pi n \frac{p_e}{N_e}) + \sin(n\theta)\sin(2\pi n \frac{p_e}{N_e})\right]\cos(2\pi m_z \frac{p_e}{N_e}) \end{aligned} \qquad ...(6.34)$$

With the assumption of N_e tending to infinity, applying the property of orthogonality gives

$$W^c = \sum_{p_e=0}^{N_e-1} V_r^c \sum_{n=0}^{\infty} A_n^z \cos\left[n(\theta - 2\pi n \frac{p_e}{N_e})\right] = \begin{cases} \frac{1}{2} N_e V^c A_{m_z}^z \cos(m_z\theta), & m_z \neq 0 \text{ or } m_z \neq \frac{N_e}{2} \\ N_e V^c A_{m_z}^z \cos(m_z\theta), & m_z = 0 \text{ or } m_z = \frac{N_e}{2} \end{cases} \qquad ...(6.35)$$

where $V_r^c = V^c \cos(2\pi m_z \frac{p_e}{N_e})$ is the required voltage for the cosine modal actuator.

However, when N_e is finite, there is spillover for the modes greater than $N_e/2$.

It can be clearly seen in equation (6.35) that the required voltage for the cosine modal actuator has to be varied as the cosine function of the position of the PZT elements and the desired mode.

For the sine function, the positions of the PZT elements around the pipe are given by

$$\phi = \frac{\pi}{N_e}, \frac{3\pi}{N_e}, ..., \frac{(2N_e - 1)}{N_e}\pi .$$

The angle of interval between the positions of the PZT for a sine modal actuator is

$$\phi_p = \frac{2\pi}{N_e}(p_e + \frac{1}{2}) \qquad ...(6.36)$$

Similar to the analysis of the cosine modal actuator, the radial response of the sine modal actuator for the m_z^{th} mode can be obtained by multiplying equation (6.32) with $\sin\left[\frac{2\pi m_z}{N_e}(p_e + \frac{1}{2})\right]$ and summing it over the discrete angles and is given by:

$$\begin{aligned} W^s &= \sum_{p_e=0}^{N_e-1} W^{iz}(\phi = \phi_p)\sin\left[\frac{2\pi m_z}{N_e}(p_e + \frac{1}{2})\right] \\ &= V^s \sum_{p_e=0}^{N_e-1}\sum_{n=0}^{\infty} A_n^z \left[\cos(n\theta)\cos(2\pi n\frac{p_e}{N_e}) + \sin(n\theta)\sin(2\pi n\frac{p_e}{N_e})\right]\sin\left[\frac{2\pi m_z}{N_e}(p_e + \frac{1}{2})\right] \end{aligned} \qquad ...(6.37)$$

Again, applying the property of orthogonality gives

$$W^s = \sum_{p_e=0}^{N_e-1} V_r^s \sum_{n=0}^{\infty} A_n^z \cos\left[n\left(\theta - 2\pi n \frac{p_e}{N_e}\right)\right] = \begin{cases} \frac{1}{2} N_e V^s A_{m_z}^z \sin(m_z\theta), & m_z \neq 0 \text{ or } m_z \neq \frac{N_e}{2} \\ N_e V^s A_{m_z}^z \sin(m_z\theta), & m_z = \frac{N_e}{2} \\ 0, & m_z = 0 \end{cases} \quad \ldots(6.38)$$

where $V_r^s = V^s \sin\left[\frac{2\pi m_z}{N_e}\left(p_e + \frac{1}{2}\right)\right]$ is the required voltage for the sine modal actuator.

Equations (6.35) and (6.38) imply that the minimum number of the PZT elements required to form the cosine or sine modal actuator as $N_e = 2m_z$. However, in practice, one has to be careful to avoid spillover due to an insufficient number of PZT elements used. To avoid this, the number of PZT elements should be at least twice the maximum mode number of the pipe. Since the mode number of interest in this work is below the ring frequency of the pipe, whose maximum mode number is 7, the number of PZT elements for any desired mode is at least 14.

Having $N_e > 2m_z$, where $m_z \geq 1$, the total radial response obtained from both sine and cosine modal actuator is given by

$$W^{tot} = \frac{1}{2} N A_{m_z}^z \left[V^s \sin(m_z\theta) + V^c \cos(m_z\theta)\right] \quad \ldots(6.39)$$

By letting

$$V^s = V^{tot} \sin(m_z\phi_{no}) \quad \text{and}$$
$$V^c = V^{tot} \cos(m_z\phi_{no}) \quad \ldots(6.40\ a, b, c, d)$$

where $V^{tot} = \sqrt{(V^s)^2 + (V^c)^2}$ is the total voltage supplied to the modal actuator, and

$\phi_{no} = \frac{1}{m_z} \tan^{-1}(V^s / V^c)$ is the orientation angle relative to the cosine modal actuator,

equation (6.39) becomes

$$W^{tot} = \frac{1}{2} N_e V^{tot} A^z_{m_z} \cos\left[m_z (\theta - \phi_{no})\right] \qquad \ldots(6.41)$$

For the $m_z = 2$ mode, the minimum number of the PZT elements required for either the cosine or the sine modal actuator is 4 ($N_e = 2m_z$). Substituting for N_e into equation (6.35) gives

$$W^c = V^c \sum_{p_e=0}^{N_e-1} \sum_{n=0}^{\infty} A^z_n \cos(n\theta) \cos\left(\pi p_e \frac{n}{m_z}\right) \left[\cos(\pi p_e)\right] \qquad \ldots(6.42)$$

Using the property of orthogonality, the above equation becomes

$$W^c = N_e V^c \left[A^z_{m_z} \cos(m_z\theta) + A^z_{3m_z} \cos(3m_z\theta) + A^z_{5m_z} \cos(5m_z\theta) + \ldots \right] \qquad \ldots(6.43)$$

This shows clearly that for the desired mode of m = 2 with eight PZT elements the cosine modal actuator excites the pipe modes n = 2, 6 and so on. The sine modal actuator for the m = 2 mode is also obtained by similar analysis and is given by:

$$W^s = N_e V^s \left[A^z_{m_z} \sin(m_z\theta) + A^z_{3m_z} \sin(3m_z\theta) + A^z_{5m_z} \sin(5m_z\theta) + \ldots \right] \qquad \ldots(6.44)$$

With the minimum number of PZT elements ($N_e = 2m_z$), the total radial response, which is the combination of equations (6.42) and (6.43), is determined by substituting V^c and V^s given in equation (6.40 a, b) yielding

$$W^{tot} = N_e V^{tot} \left\{ A^z_{m_z} \cos\left[m_z (\theta - \phi_{no})\right] + A^z_{3m_z} \cos\left[m_z (3\theta - \phi_{no})\right] + A^z_{5m_z} \cos\left[m_z (5\theta - \phi_{no})\right] + \ldots \right\} \quad \ldots(6.45)$$

6.5. Experimental Work

6.5.1 Introduction

In this section, several experiments are described that were set up in order to validate the expressions developed in the previous section. An experiment was carried out to validate the transfer function of a single PZT element and subsequent experiments were conducted to validate the theoretical model of the modal actuator.

In the present work, the objective is to develop the modal actuator for the n = 2 mode and the need is to use the smallest number of PZT elements as possible without causing significant spillover to the higher modes of the pipe. To satisfy this requirement, the minimum number of PZT elements for the modal actuator is used and its effectiveness is evaluated.

6.5.2 Experimental Set-up and Procedure

The schematic of the experimental setup for investigating the transfer function of a single PZT element is shown in figure 6.5.a. Since the 5.5 m long pipe, whose properties are given in Table D.1 (appendix D), was assumed to have infinite length (which means there are no reflected waves from the ends of the pipe), anechoic terminations were fixed at both ends of the pipe. The PZT elements were manufactured by Morgan Matroc Limited in the shape of a rectangular plate of 4x8x0.25 mm^3. Some important properties of the element are listed in Table D.3 (appendix D), and are used to predict the pipe response. The PZT element was bonded on the pipe at a position equidistant from both anechoic terminations. A random signal voltage from the HP 3566A Signal Analyzer

was supplied to the PZT element via a power amplifier. The resulting motion of the pipe was measured at the distance of 300 mm from the position of the PZT element by a set of the accelerometers located around the pipe. With the arrangement as shown in figure 6.5.a, the radial motion can be decomposed into each mode of the pipe by using the method of modal decomposition, which is described in appendix A. Hence, the expression for the transfer function of a single PZT element bonded to the pipe can easily be evaluated by comparing it with the experimental results for each mode.

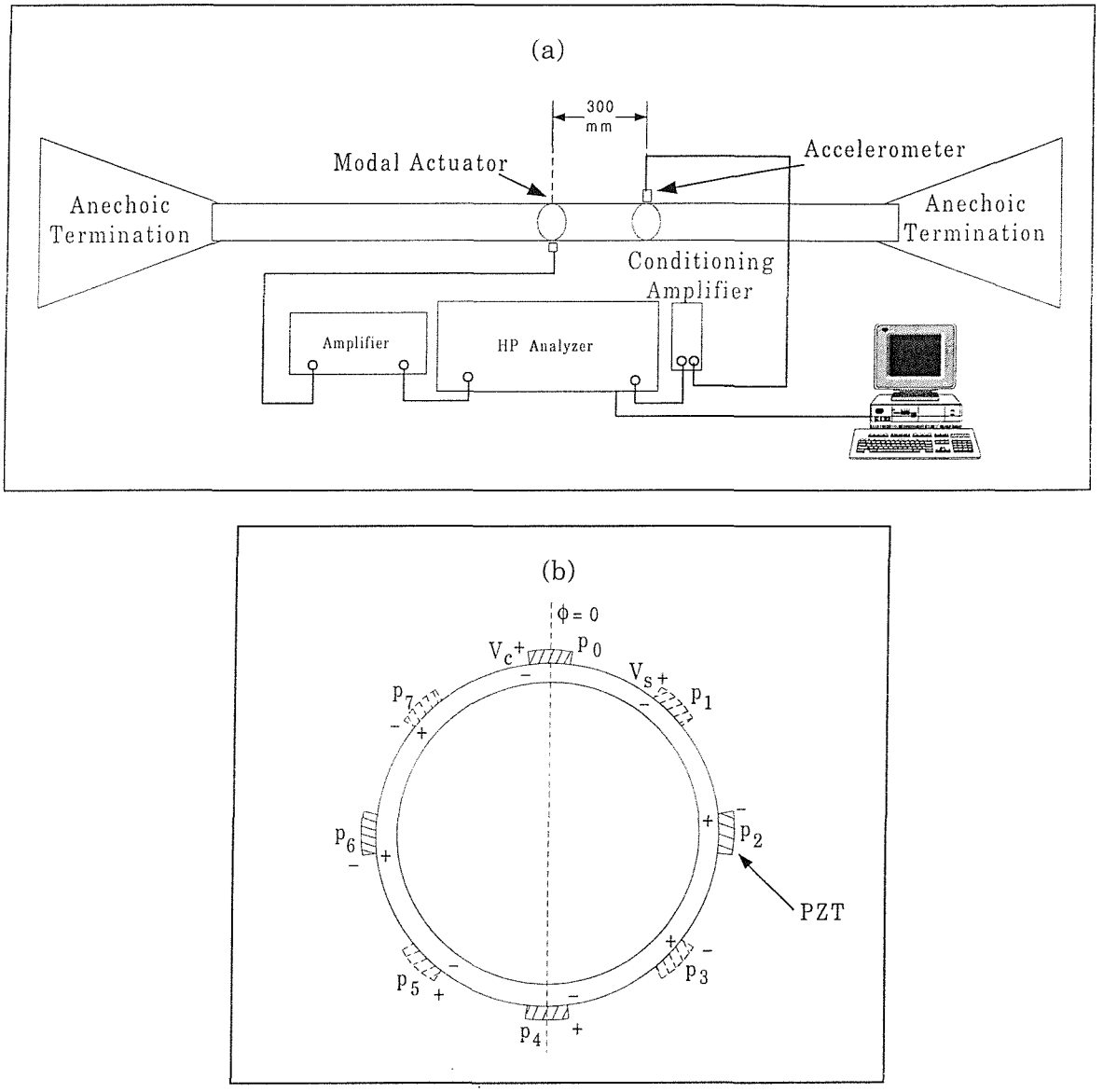

Figure 6.5: Experimental Setup for evaluation of the modal actuator for the n = 2 mode of the pipe; a) arrangement of the instruments, b) arrangement of the modal actuators where ___ cosine function, _ _ sine function.

The next experiment was carried out to validate the model for the n = 2 modal actuator. Eight PZT elements were bonded on the pipe as shown in figure 6.5.b and figure D.2 in appendix D (four elements for the sine modal actuator and other four elements for the cosine modal actuator). As described in the previous section, for the cosine modal actuator the voltage supplied to the PZT elements has to be varied as the cosine function of $V_{cp} = V_c \cos(2\pi n \frac{p}{N})$. Hence, only the PZT elements at the positions of p = 0, 2, 4 and 6 were activated with $+V_c$, $-V_c$, $+V_c$, $-V_c$, respectively, while those at the other positions had zero input voltage. Similar to the cosine modal actuator, the sine modal actuator required the voltage to be supplied to the elements at positions of p = 1, 3, 5 and 7 with $+V_s$, $-V_s$, $+V_s$, $-V_s$, respectively, while those at the other positions had zero input voltage. The radial motion of the pipe was excited by the cosine modal actuator and the measurement method was similar to that of the transfer function of the single PZT. Finally, both sine and cosine modal actuators were simultaneously actuated first with the same magnitude of input voltage and secondly with the input voltage of the sine modal actuator equal to half of that of the cosine modal actuator. This was to explore the change of the orientation angle.

6.5.3 Experimental Results

Several experimental results, i.e. the transfer function of the single PZT element, of the cosine modal actuator and total transfer function of the modal actuator for the n = 2 mode, are presented. Where applicable predictions obtained from the theory described in the previous section are overlaid. The results of the orientation angle arising from the use of both modal actuators are also presented.

As discussed in the previous section, the minimum number of PZT elements for a modal actuator to prevent spillover for any of the desired modes below the ring frequency is 14. With the four PZT elements for cosine and sine modal actuators, the problem of spillover as described in the previous section can not be avoided. So, they also produce the pipe motion of the n = 6 mode.

With the expressions of the radial displacement generated by the modal actuator for the n = 2 mode and described in equations (6.43) and (6.44), the transfer functions (velocity / supplied voltage) of the cosine, and the sine modal actuators are respectively given by

$$T_z^c = -j\frac{\omega W^c}{V^c} = -j\omega N_e \left[A_n^z \cos(n\theta) + A_{3n}^z \cos(3n\theta) + A_{5n}^z \cos(5n\theta) + \ldots \right] \quad \ldots(6.46)$$

$$T_z^s = -j\frac{\omega W^s}{V^s} = -j\omega N_e \left[A_n^z \sin(n\theta) + A_{3n}^z \sin(3n\theta) + A_{5n}^z \sin(5n\theta) + \ldots \right] \quad \ldots(6.47)$$

where $N_e = 2n$ and

$$A_n = -j\frac{2a\,\varphi L_a \varepsilon_n}{\pi K} F_s \sum_{b=1}^{4} Res_{nb}^z \, e^{j\hat{k}_{nb}s}$$

$$F_s = \frac{\left(1+\mu\tau\alpha^3\right)}{1+\mu\tau\alpha(4+6\alpha+4\alpha^2+\mu\tau\alpha^3)} d_{31}\gamma \text{ is the static gain of the actuator.}$$

In the case of both modal actuators simultaneously exciting the pipe, the transfer function is given by

$$T_z^{tot} = -j\frac{\omega W^{tot}}{V^{tot}} = -j\omega N_e \left\{ A_n^z \cos\left[n(\theta-\phi_{no})\right] + A_{3n}^z \cos\left[n(3\theta-\phi_{no})\right] + A_{5n}^z \cos\left[n(5\theta-\phi_{no})\right] + \ldots \right\} \quad \ldots(6.48)$$

where W^{tot} is obtained from equation (6.45).

The experimental results presented are as follows.

Transfer function of the pipe, which was excited by a single PZT actuator, and measured with the accelerometer array at 300 mm distance from the actuator.

Transfer function of the pipe, which was excited by the PZT modal actuators for the n = 2 mode, and measured at 300 mm distance from the actuator.

Orientation angle of the pipe, which was concurrently excited by both sine and cosine modal actuators for the n = 2 mode and measured at 300 mm distance from the actuator.

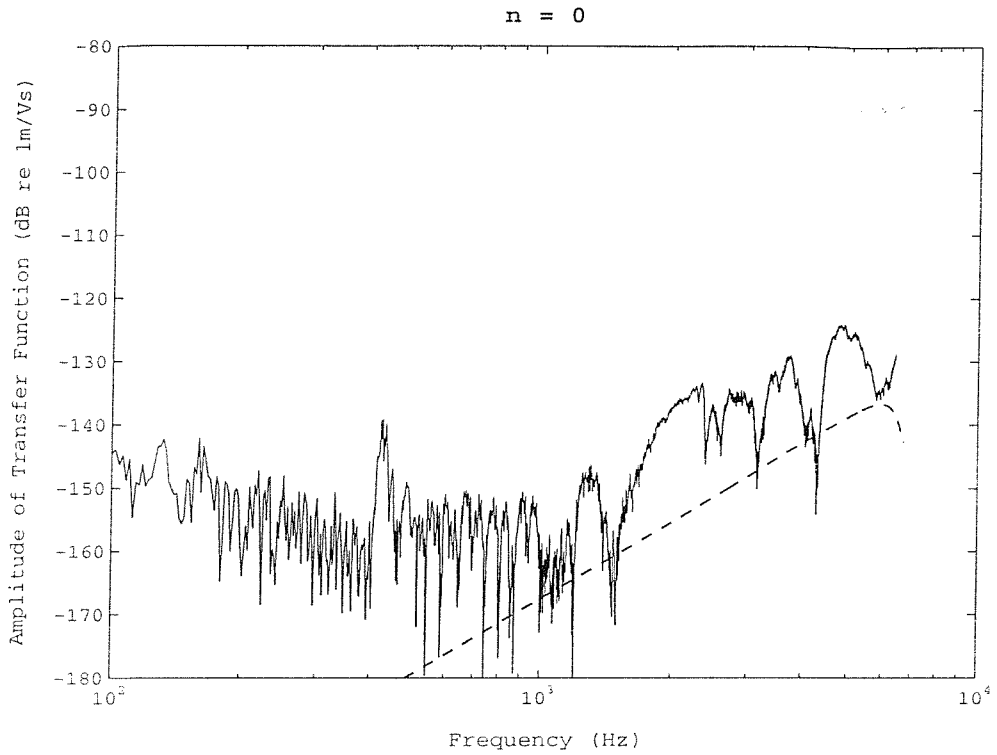

Figure 6.6: Amplitude of Transfer function of the n = 0 mode of the pipe, which is excited by a single actuator; --- prediction (equation 6.31),___ measurement.

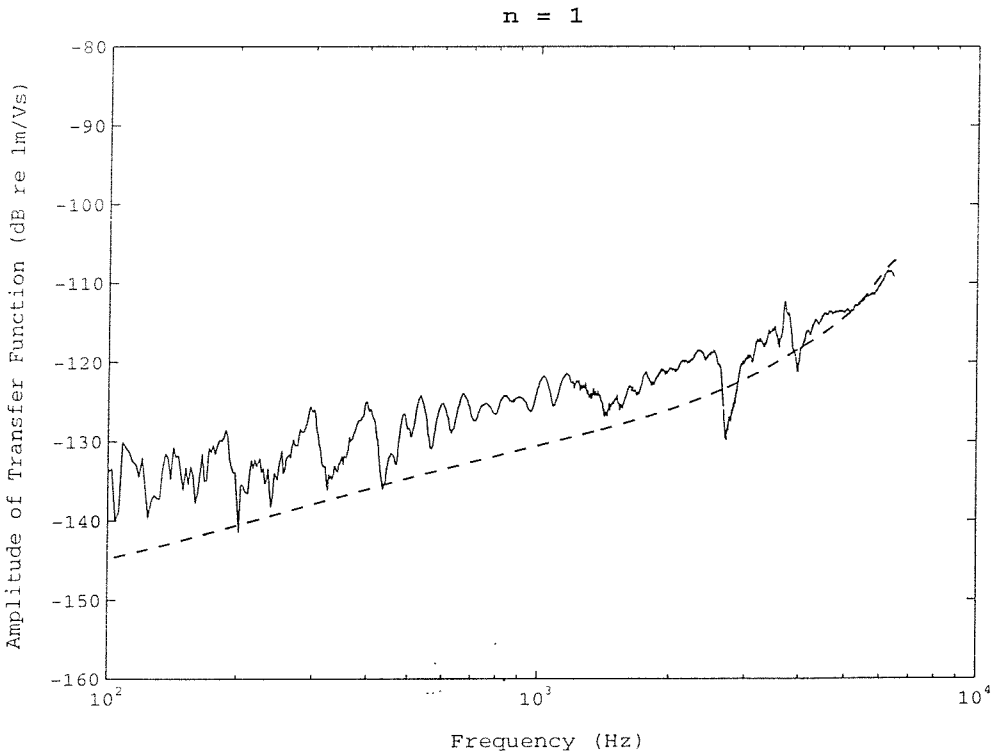

Figure 6.7: Amplitude of Transfer function of the n = 1 mode of the pipe, which is excited by a single actuator;--- prediction (equation 6.31), ___ measurement.

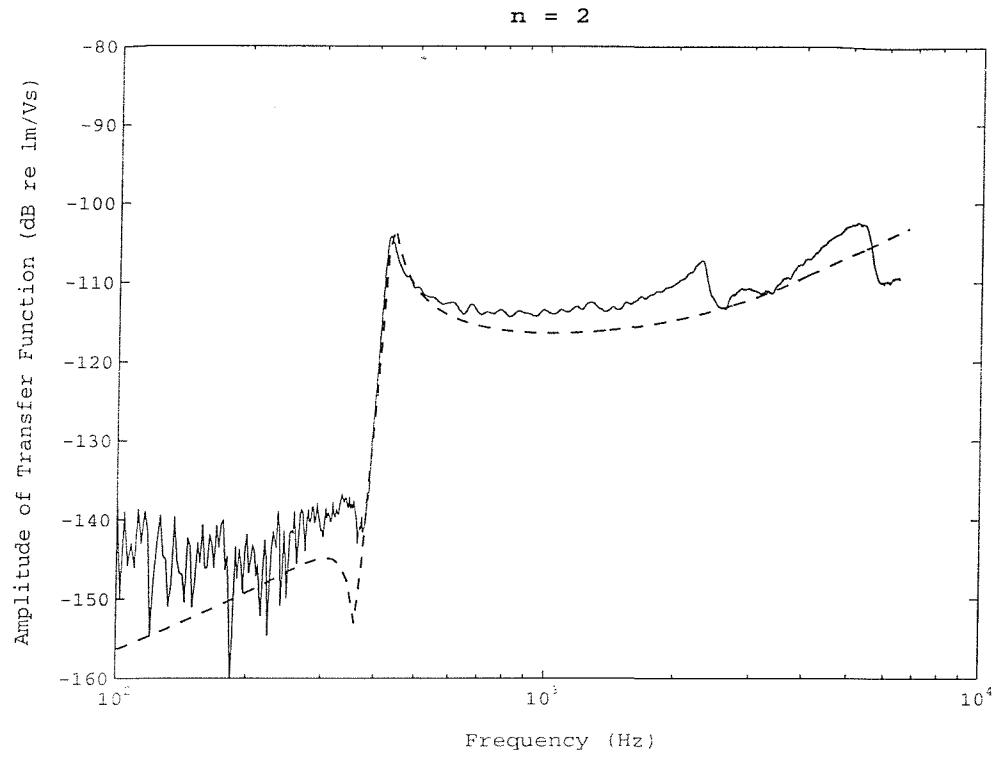

Figure 6.8: Amplitude of Transfer function of the n = 2 mode of the pipe, which is excited by a single actuator; --- prediction (equation 6.31), ___ measurement.

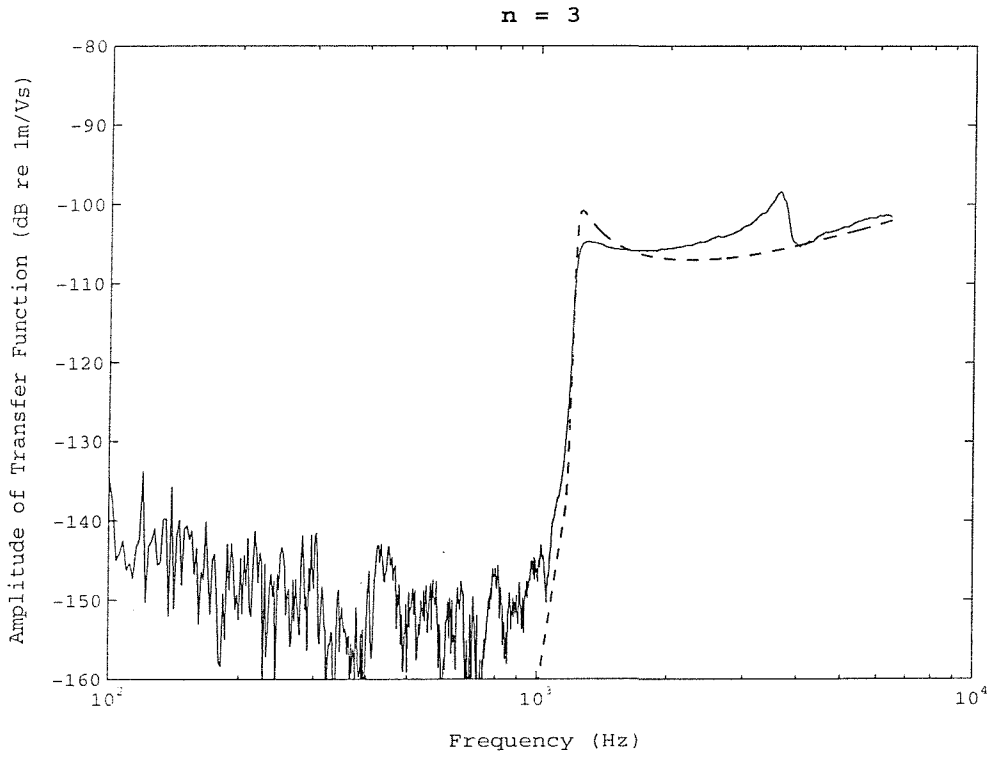

Figure 6.9: Amplitude of Transfer function of the n = 3 mode of the pipe, which is excited by a single actuator; --- prediction (equation 6.31), ___ measurement.

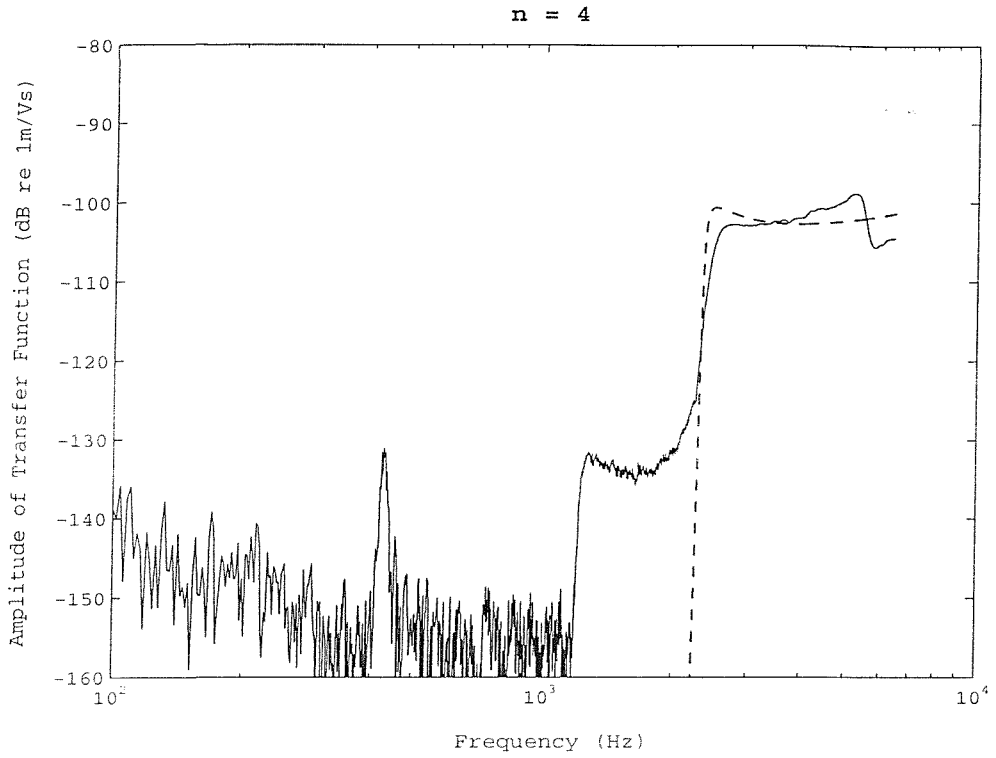

Figure 6.10: Amplitude of Transfer function of the n = 4 mode of the pipe, which is excited by a single actuator; --- prediction (equation 6.31), ___ measurement.

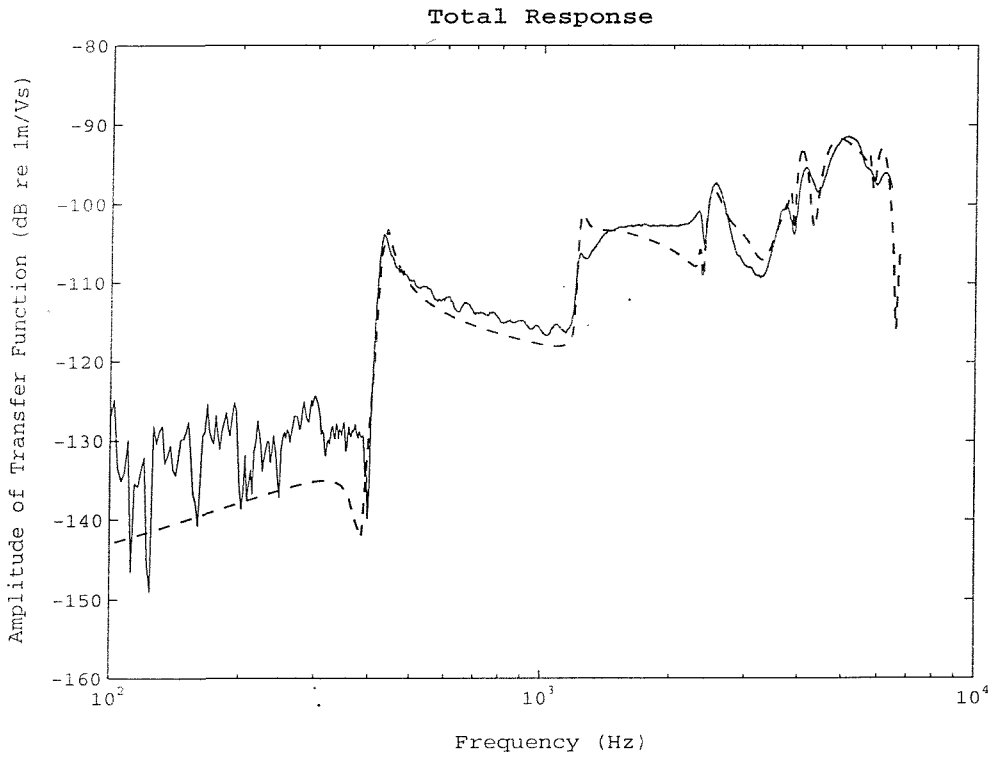

Figure 6.11: Amplitude of Transfer function of the pipe for all modes, which is excited by a single actuator; --- prediction (equation 6.31), ___ measurement.

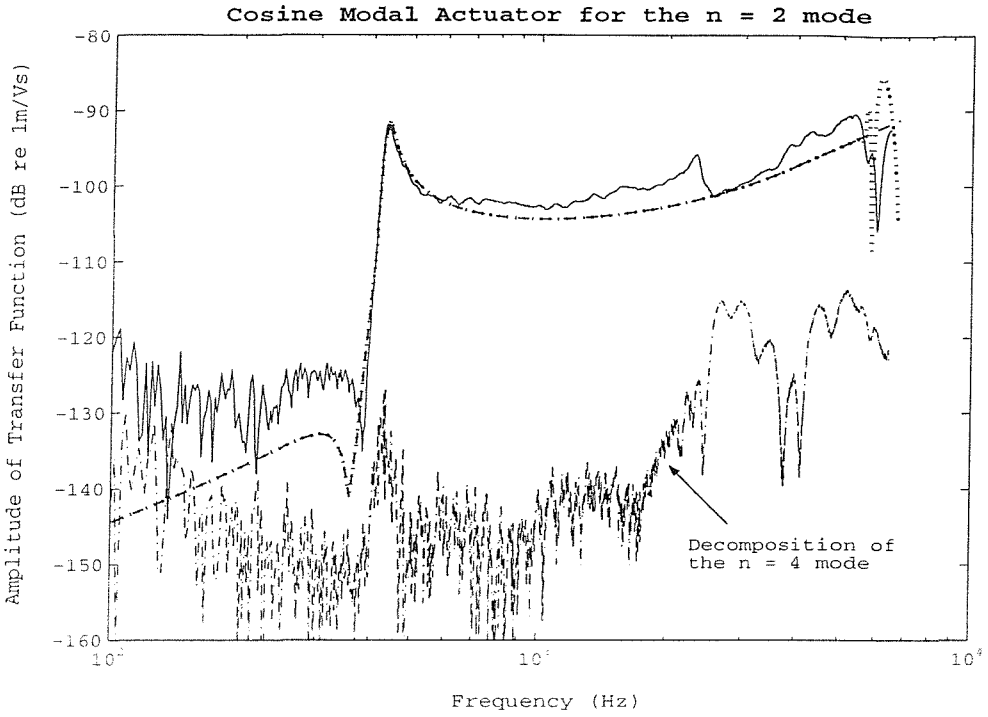

Figure 6.12: Amplitude of Transfer function of the pipe excited by the n = 2 cosine modal actuator; __ Measurement, _ _ Equation 6.46 considering only the n = 2 mode; ... Equation 6.46; _ . _ Response of decomposing the n = 4 mode

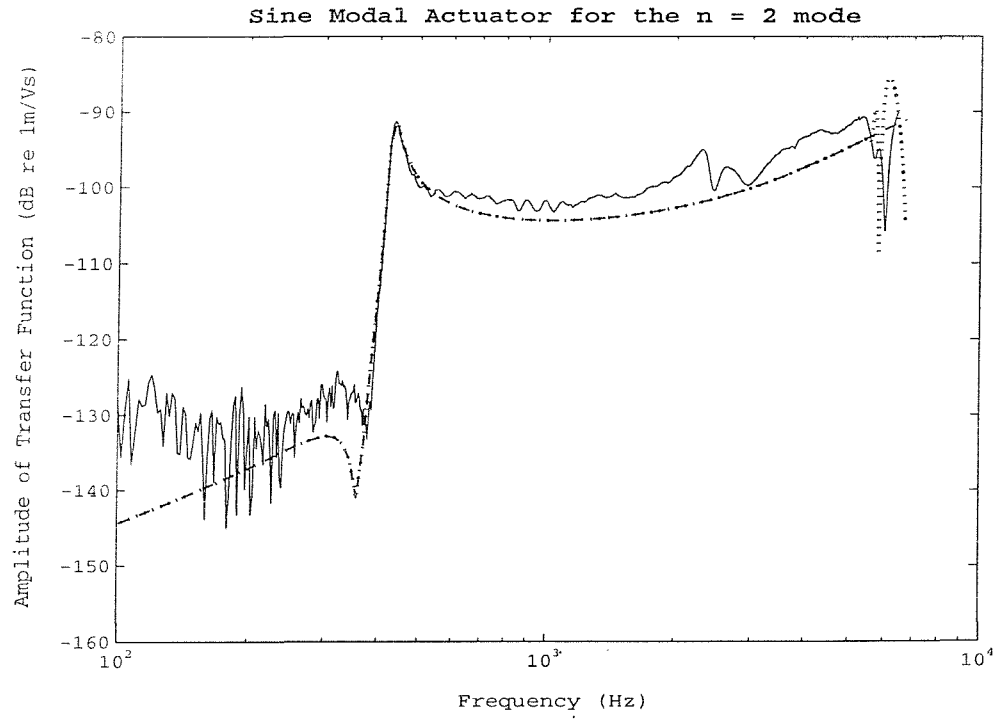

Figure 6.13: Amplitude of Transfer function of the pipe excited by the n = 2 sine modal actuator; __ Measurement, _ _ Equation 6.47) considering only the n = 2 mode; ... Equation 6.47.

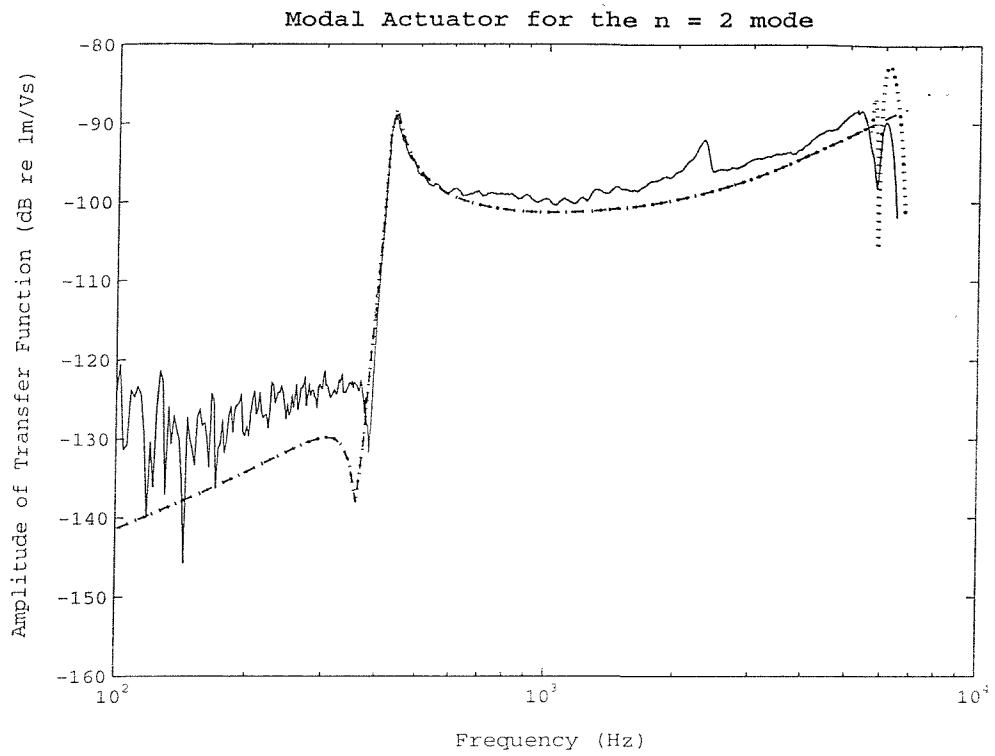

Figure 6.14: Amplitude of Transfer function of the pipe excited by both n = 2 modal actuators; ___ measurement, _ _ prediction (equation 6.48) considering only the n = 2 mode; ...prediction (equation 6.48).

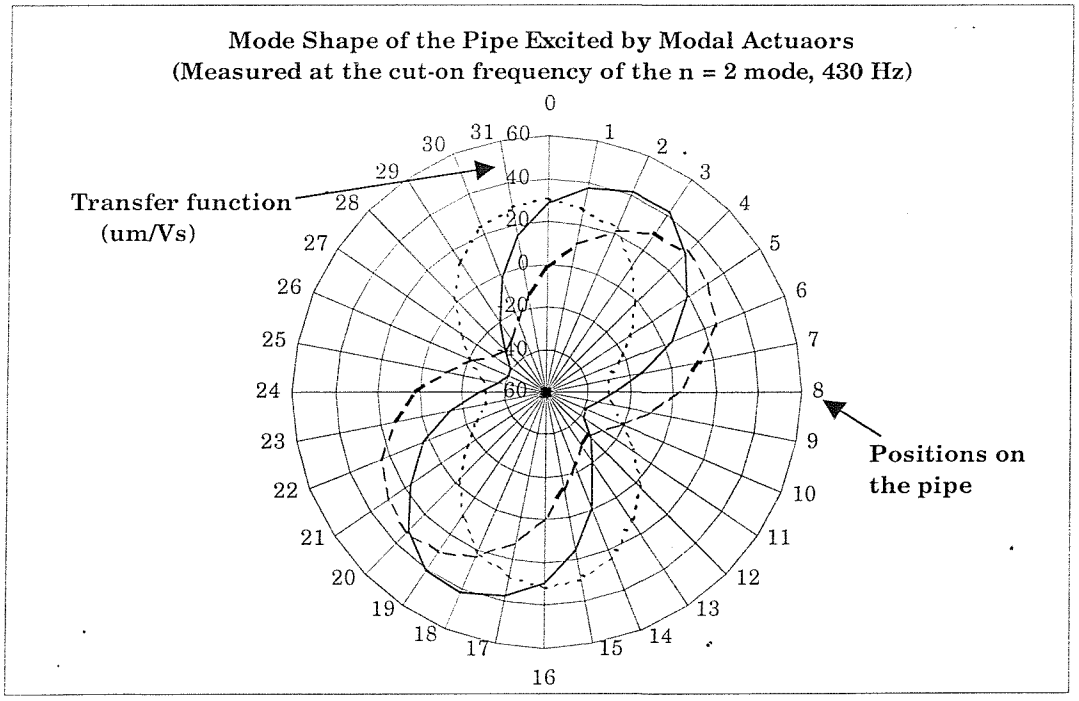

Figure 6.15: Orientation angle of the pipe arising from the excitation of both modal actuators with the same amplitude of the input voltage;...cosine, _ _ sine, __ both.

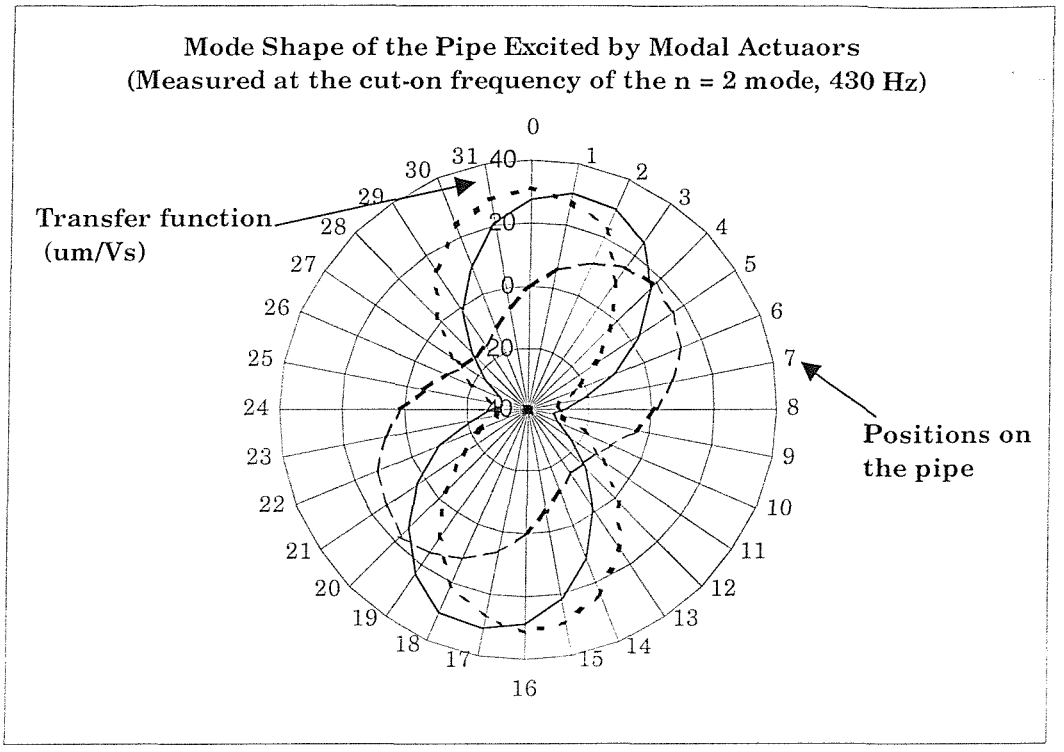

Figure 6.16: Orientation angle of the pipe arising from the excitation of both modal actuators with the input voltage of the sine modal actuator equal to half that of the cosine modal actuator; ...cosine, _ _ sine, __ both.

6.5.4 Discussion

Examination of figures 6.7-6.11 show that the predictions of the behaviour of the pipe excited from the single actuator are consistent with practice except at low frequencies, where the motion of the pipe is very small and difficult to effectively detect by the accelerometers. In addition, it is also limited by the ability of the analyzer.

As previously stated the elements of the cosine modal actuator require the input voltage as $+V_c$, $-V_c$, $+V_c$, $-V_c$, at an angle of 0, $\pi/2$, π, $3\pi/2$, respectively. With such input voltage, the response of the n = 2 mode of the pipe is strengthened and that of the other modes is cancelled when they work together in form of the modal actuator as shown in figures 6.12-6.14. The cancellation of the n = 4 mode can be seen clearly in figure 6.12 when the

response of the n = 4 mode is decomposed from the measurement. Excitation of the n = 6 mode, which is spillover due to there being insufficient elements in the modal actuator, was also expected to be excited, and appears in figures 6.12-6.14, but the response measured is less than that predicted. This is probably because of the effect of the mass loading from the accelerometers as previously discussed in chapters 3 and 4. Nevertheless, the effect of this spillover occurs at the relatively high frequency of 5532 Hz for the n = 6 mode, and so may be ignored. The graphs also show the good agreement between practice and theory.

Using both sine and cosine modal actuators, the changes of the orientation angle with respect to the cosine modal actuator are clearly demonstrated in figures 6.15 and 6.16. With the same voltage supplied to both modal actuators, the angle calculated from equation (6.40.d) is ϕ = 22.5 degree, while it is ϕ = 13.3 when the input voltage of the cosine modal actuator is twice of that of the sine modal actuator. Therefore, the orientation angle of the pipe can be readily controlled by both modal actuators.

6.6 Conclusions

Expressions for the radial motion of a pipe excited by a single PZT actuator and modal actuators for the n = 2 mode have been derived. They have also been successfully validated by experiment. This work clearly shows that a sine or cosine modal actuator for this can be created by using only four PZT elements, which is the minimum number for such an actuator. With this number of PZT elements, spillover of the n = 6 mode is introduced into the system. However, it has been shown that this may be neglected because it occurs at a high frequency.

When both modal actuators are used, the orientation angle of the response with respect to the cosine modal actuator can be controlled. By exploring the mode shape of the pipe generated by both actuators simultaneously, it can clearly be seen that the orientation angle of the pipe can be readily adjusted by controlling their input voltage.

CHAPTER 7

ACTIVE VIBRATION CONTROL OF PIPES

7.1 Introduction

In the problem of pipe vibration, the flexural wave of the n = 2 mode can cause large strain in the pipe wall after the wave cuts on, which may lead to the damage of the structure. From the fatigue aspect, an active control system is one way of suppressing this wave. Generally for single-channel control systems, the main problem is spillover (Balas [74]), which is the effect of the unobserved and uncontrolled modes. This effect will degrade the performance of the system. To avoid this problem, an n = 2 modal sensor described in chapter 5 and a reciprocal actuator described in chapter 6 are employed to selectively sense and actuate the vibration of this particular mode.

In this chapter, an active control system to minimise the n = 2 flexural wave is analysed. In practice, the orientation angle of the excitation load with respect to the actuator and the sensor is not known. However, the disturbance can be separated into sine and cosine components. Hence, a pair of sensors and actuators, which have the form of sine and cosine function, are used to suppress each component of the disturbance.

Once the theory of this control system has been developed, experimental work is carried out to validate it.

7.2 Model of Controlling n = 2 Flexural Wave of Pipes

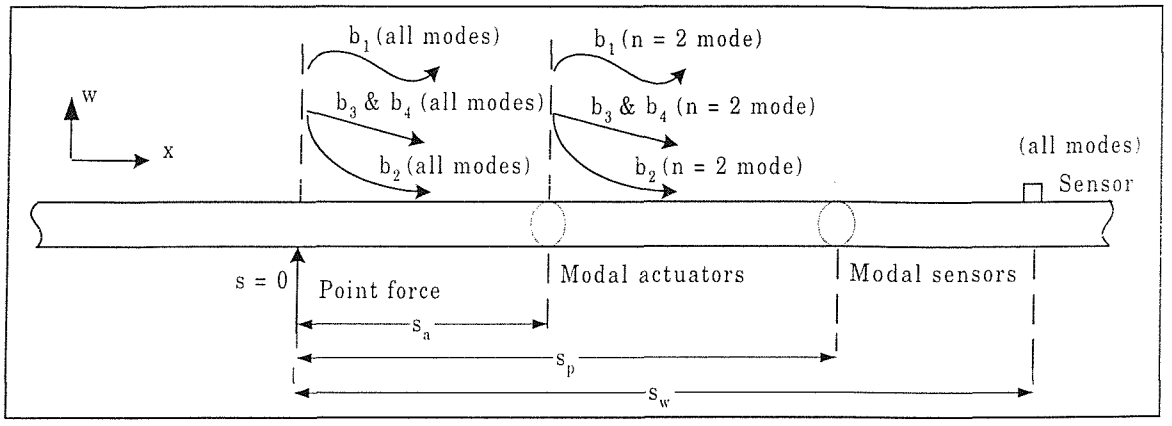

Figure 7.1: Diagram of the active control system for the flexural wave of the n = 2 mode with the modal actuator (showing only positive-going waves); b_1 = the flexural wave, b_2 = the near field wave, b_3 and b_4 = the standing near field waves.

A schematic diagram for control of the n = 2 mode of a pipe is shown in figure 7.1. The radial velocity at any position is the combination of the vibration excited by a point force and by PZT modal actuators for the n = 2 mode and is given by

$$\dot{W}(s,\theta) = F_0 Y^i(s,\theta) + V^c T_z^c(s,\theta) + V^s T_z^s(s,\theta) \qquad \ldots(7.1)$$

The first term in the right hand side of equation (7.1) is the radial velocity caused by the point force, where F_0 is the primary point force, and $Y^i(s,\theta)$ is the primary force mobility, which is given as (equation 3.13)

$$Y^i(s,\theta) = -\sum_{n=0}^{\infty} \frac{\varepsilon_n \omega \cos[n(\theta-\phi_c)]}{2\pi\rho\, h a^2 \omega_r^2} \sum_{b=1}^{4} \mathrm{Re}\, s_{nb} e^{j\hat{k}_{nb}s} \qquad \ldots(7.2)$$

where ϕ_c is the orientation angle related to the cosine modal actuator and

Res_{nb} is the residue term given in the chapter 3.

The second and the third terms on the right hand side of equation (7.1) are the radial velocity generated by the cosine and sine modal actuators, respectively, where V^c is the applied voltage to the cosine modal actuator, V^s is the applied voltage to the sine modal actuator, T_z^c and T_z^s are the transfer functions (velocity / applied voltage) of the pipe excited by the cosine and sine modal actuators for the n = 2 mode, respectively, which are given by (equations 6.46 and 6.47, respectively)

$$T_z^c(s,\theta) = -\frac{2\,\varepsilon_2\omega}{\pi K}\alpha_a \cos(2\theta)\sum_{b=1}^{4} Res_{2b}^z e^{j\hat{k}_{2b}(s-s_a)} \qquad ...(7.3\text{ a})$$

$$T_z^s(s,\theta) = -\frac{2\,\varepsilon_2\omega}{\pi K}\alpha_a \sin(2\theta)\sum_{b=1}^{4} Res_{2b}^z e^{j\hat{k}_{2b}(s-s_a)} \qquad ...(7.3\text{ b})$$

where $\alpha_a = a\varphi L_a F_s N$,

F_s is the static gain of the force generated by the PZT element (see equation 6.31.b),

Res_{2b}^z is the residue term obtained from the excitation by the PZT and given in the previous chapter.

At the position, s_p, where the n = 2 modal sensors are located, only the radial motion of the n = 2 mode is detected. For the cosine modal sensor used, the radial velocity from equation (7.1) becomes

$$\dot{W}_2(s=s_p,\theta) = F_0 Y_2^{ic}(s=s_p,\theta) + V^c T_z^c(s=s_p,\theta) \qquad ...(7.4)$$

where $Y_2^{ic} = -\frac{\varepsilon_2\omega\cos(2\theta)\cos(2\phi_c)}{2\pi\rho\, ha^2\omega_r^2}\sum_{b=1}^{4} Res_{2b}e^{j\hat{k}_{2b}s}$ is the cosine component of the mobility

for the n = 2 mode. ...(7.5)

It should be noted that the radial motion generated by the sine modal actuator and the sine component provided by the point force are not detected by the cosine modal sensor. From equation (7.4), it can be seen that the total radial motion generated by the primary force and the modal actuators can be minimised by driving the actuators until no radial motion is detected by the modal sensor (error sensor). To obtain zero radial motion at the sensor position, the voltage supplied to the cosine modal actuator has to be

$$V^c = -\frac{Y_2^{ic}(s = s_p, \theta)}{T_z^c(s = s_p, \theta)} F_0 \qquad \ldots(7.6)$$

Since $K = \rho h a^2 \omega_r^2$, substituting for $Y_2^i(s = s_p, \theta)$ from equation (7.5) and T_z^c from equation (7.3 a) gives

$$V^c = -\frac{\cos(2\phi_c)}{4\alpha_a}\left[\frac{\sum_{b=1}^{4} \mathrm{Res}_{2b} e^{j\hat{k}_{mb} s_p}}{\sum_{b=1}^{4} \mathrm{Res}^z_{2b} e^{j\hat{k}_{mb}(s_p - s_a)}}\right] F_0 \qquad \ldots(7.7)$$

With the optimal applied voltage, the mobility of the infinite pipe at a location, s_w (figure 7.1) given in equation (7.1), becomes

$$\frac{\dot{W}^c_{cont}(s = s_w, \theta)}{F_0} = -\frac{\omega}{2\pi K}\left\{\left[\sum_{n=0}^{\infty} \varepsilon_n \cos(n\phi_c)\cos(n\theta)\sum_{b=1}^{4} \mathrm{Res}_{nb} e^{j\hat{k}_{nb} s_w}\right]\right. \qquad \ldots(7.8)$$

$$\left. -\varepsilon_2 \cos(2\phi_c)\cos(2\theta)\left[\frac{\sum_{b=1}^{4} \mathrm{Res}_{2b} e^{j\hat{k}_{2b} s_p}}{\sum_{b=1}^{4} \mathrm{Res}^z_{2b} e^{j\hat{k}_{2b}(s_p - s_a)}}\right]\left[\sum_{b=1}^{4} \mathrm{Res}^z_{2b} e^{j\hat{k}_{2b}(s_w - s_a)}\right]\right\}$$

Instead of $\dot{W}$, $\dot{W}^{c}_{cont}$ is used in the above equation for the radial velocity that results from using the cosine modal actuator.

By considering the flexural propagating wave only, the optimal applied voltage obtained from equation (7.7) becomes

$$V^{c} = -\frac{\cos(2\phi_c)}{4\alpha_a}\frac{Res_{21}}{Res^{z}_{21}} e^{j\hat{k}_{m1}s_a} F_0 \qquad ...(7.9)$$

and the mobility given in equation (7.8) becomes

$$\frac{\dot{W}^{c}_{cont}(s=s_w,\theta)}{F_0} = -\frac{\omega}{2\pi K}\left[\sum_{n=0}^{\infty}\varepsilon_n \cos(n\phi_c)\cos(n\theta)\sum_{b=1}^{4} Res_{nb} e^{j\hat{k}_{nb}s_w}\right]_{n\neq 2} \qquad ...(7.10)$$

It can be seen from equation (7.10) that the cosine component of the n = 2 radial motion can completely be suppressed when the n = 2 cosine modal actuator is supplied by the optimal voltage (equation 7.9).

To suppress the sine component of the primary point force, the sine modal sensor/actuator is employed. Using this sensor, the radial velocity from equation (7.1) becomes

$$\dot{W}_2(s=s_p,\theta) = F_0 Y_2^{is}(s=s_p,\theta) + V^{s} T_z^{s}(s=s_p,\theta) \qquad ...(7.11)$$

where $Y_2^{is} = -\frac{\varepsilon_2 \omega \sin(2\theta)\sin(2\phi_c)}{2\pi\rho\, ha^2\omega_r^2}\sum_{b=1}^{4} Res_{2b} e^{j\hat{k}_{2b}s}$ is the sine component of the mobility for the n = 2 mode. ...(7.12)

By using the same analysis as the cosine component of the primary point force, the optimal voltage supplied to the sine modal actuator and the mobility at a location, s_w, are given by

$$V^s = -\frac{\sin(2\phi_c)}{4\alpha_a}\frac{Res_{21}}{Res_{21}^z}e^{j\hat{k}_{m1}s_a}F_0 \qquad ...(7.13)$$

$$\frac{\dot{W}^s_{cont}(s=s_w,\theta)}{F_0} = -\frac{\omega}{2\pi K}\left[\sum_{n=0}^{\infty}\varepsilon_n \sin(n\phi_c)\sin(n\theta)\sum_{b=1}^{4}Res_{nb}e^{j\hat{k}_{nb}s_w}\right]_{n\neq 2} \qquad ...(7.14)$$

where $\dot{W}^s_{cont}$, is the radial velocity resulting from using the sine modal actuator.

The total mobility of the pipe when controlled by both the sine and the cosine modal actuators is the combination of the mobility when the n = 2 wave is suppressed by each modal actuator and is given by:

$$\begin{aligned}\frac{\dot{W}_{cont}(s=s_w,\theta)}{F_0} &= \frac{1}{F_0}[\dot{W}^s_{cont}(s=s_w,\theta)+\dot{W}^c_{cont}(s=s_w,\theta)] \\ &= -\frac{\omega}{2\pi K}\left[\sum_{n=0}^{\infty}\varepsilon_n \cos[n(\theta-\phi_c)]\sum_{b=1}^{4}Res_{nb}e^{j\hat{k}_{nb}s_w}\right]_{n\neq 2}\end{aligned} \qquad ...(7.15)$$

7.3 Experimental Validation

7.3.1 Introduction

In this section, the experimental procedure is described. Experiments were conducted to verify the control model described in the previous section and to evaluate the effectiveness of the active control system of an infinite pipe.

Since the objective of this work is to suppress the flexural propagating wave of the n = 2 mode of an infinite pipe, PVDF modal sensors and PZT modal actuators for the n = 2 mode are used for this purpose. As described in chapter 3, the vibration of the pipe excited by a point force (primary force) has two components, which can be expressed in terms of sine and cosine functions. Hence, both the sensors and the actuators have to be constructed in the form of both configurations.

7.3.2 Experimental Setup and Procedure

A diagram showing the experimental set up is given in figure 7.2 and the picture of the active vibration control system of an infinite pipe is shown in figure D.3 (appendix D). The 5.5 m long pipe, whose properties are given in Table D.1 (appendix D), was suspended by cords, and had anechoic terminations fixed at both ends of the pipe. A shaker was used as the primary force, and was fixed on the pipe at a distance of 610 mm from the left hand side of the modal actuators located at the central position axially. A pair of sine and cosine modal actuators for the n = 2 mode described in the previous chapter was constructed from PZT elements manufactured by Morgan Matroc Limited [27] in the shape of a rectangular patch of 4x8x0.25 mm^3. Some properties of the element used for calculating the response of the pipe are listed in Table D.3 (appendix D). The n = 2 sine and cosine modal sensors, being the error sensors, were fixed close together at a position of 1210 mm from the shaker, while an accelerometer was located at a distance of 1610 mm from the shaker.

At discrete frequencies from 422 Hz (just before the n = 2 waves cut on) to 1466 Hz, the magnitude and phase of the modal actuators was manually adjusted accordingly to the primary force in order to suppress the flexural propagating waves excited by the primary force. Following equations (7.9) and (7.13), the optimal voltages supplied to the actuators are required, and are adjusted using the power amplifiers. From these equations, the phase shift ($e^{j\hat{k}_{m1}s_a}$) occurs due to different positions between the point force and the actuator. Hence, a phase control box was used to adjust the phase of the actuator. With control implemented using the actuators, the radial motion of the n = 2

mode was sensed by the modal sensor, which was monitored using the oscilloscope. The resultant downstream motion in the radial direction was measured using an accelerometer.

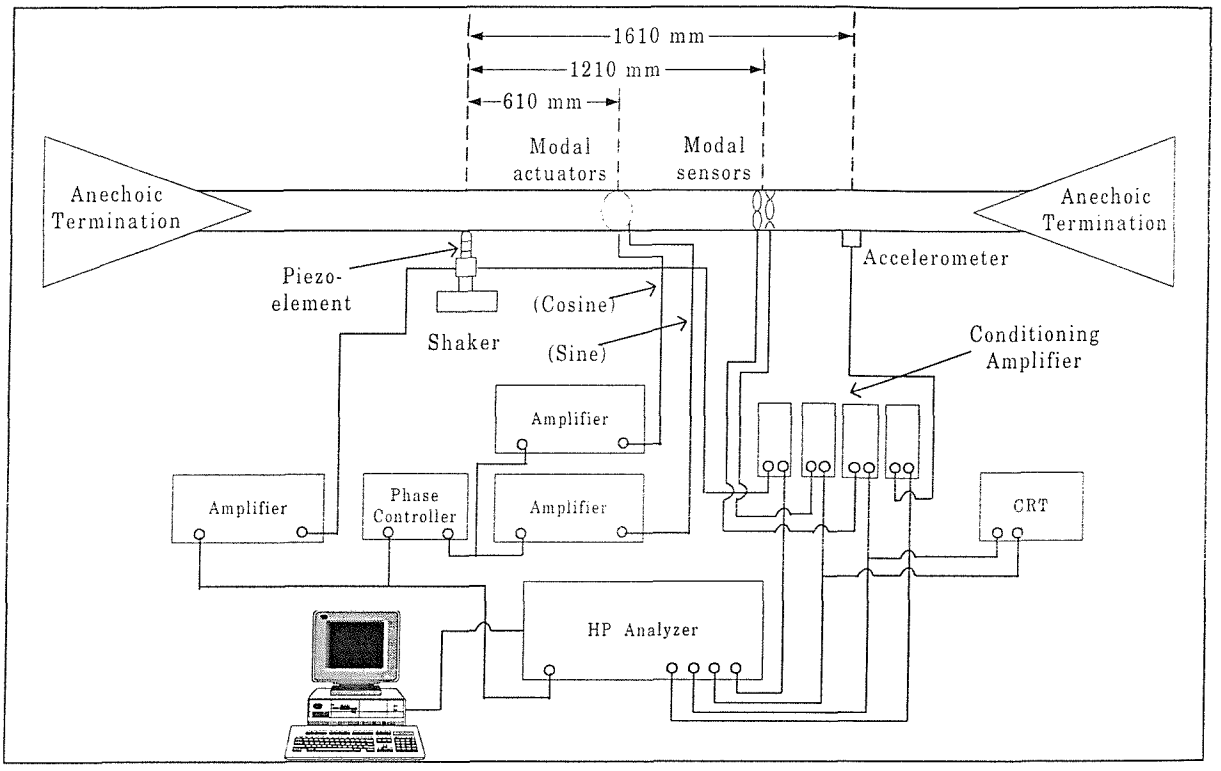

Figure 7.2: Diagram of experimental setup to control the n = 2 propagating flexural wave.

7.3.3 Experimental Results

In this section, the experimental results of the active control system for the infinite pipe using the modal sensors and actuators for the n = 2 mode are presented. The effectiveness was evaluated by comparing the downstream radial motion before and after control. A comparison is also made between the experiment and prediction from the theoretical model. However, before the motion can be predicted, the orientation angle, ϕ_c, with respect to the cosine modal sensor/actuator has to be determined. This angle can be calculated from the response of the sine and cosine modal sensors before control. For convenience, its expression is repeated here as given by (equation 5.19)

$$\phi_c = \frac{1}{2}\tan^{-1}\left(\frac{Q^s}{Q^c}\right) \qquad \ldots(7.16)$$

where Q^s is the generated charge of the sine modal sensor for the n = 2 mode and

Q^c is the generated charge of the cosine modal sensor for the n = 2 mode.

Even though the active control system in this experiment is for discrete frequencies, the measured mobility of the pipe with control can be constructed for the continuous frequencies. To do this, equations (7.6) and (7.13) are substituted into equation (1) to give the mobility with control at the accelerometer position as

$$\frac{\dot{W}(s=s_w,\theta)}{F_0} = Y^i(s=s_w,\theta) - \frac{Y_2^{ic}(s=s_p,\theta)}{T_z^c(s=s_p,\theta)}T_z^c(s=s_w,\theta) - \frac{Y_2^{is}(s=s_p,\theta)}{T_z^s(s=s_p,\theta)}T_z^s(s=s_w,\theta) \ldots(7.17)$$

As described in chapter 5, the relationship between the generated charge of the modal sensors and the pipe motion is linear. For only the flexural wave considered, the generated charges of the cosine and sine modal sensors are written as

$$Q^c = 2\pi\lambda_1 b_s z_o b_{31}\left(n^2 + \frac{b_{32}}{b_{31}}\hat{k}_{2b}^2 - 1\right)\overline{\overline{W}}^i_{2b} e^{j\hat{k}_{2b}s_c}, \qquad \ldots(7.18\text{ a, b})$$

$$Q^s = 2\pi\lambda_2 b_s z_o b_{31}\left(n^2 + \frac{b_{32}}{b_{31}}\hat{k}_{2b}^2 - 1\right)\overline{\overline{W}}^i_{2b} e^{j\hat{k}_{2b}s_c}, \text{ respectively.}$$

Where $\overline{\overline{W}}^i_{2b} = -\frac{\varepsilon_2 F_0}{2\pi\rho\, ha^2\omega_r^2}\mathrm{Res}_{2b}$

Using equation (7.18), equation (7.17) becomes

$$\frac{\dot{W}(s=s_w,\theta)}{F_0} = Y^i(s=s_w,\theta) - \frac{T_{qf}^c}{T_{qz}^c}T_z^c(s=s_w,\theta) - \frac{T_{qf}^s}{T_{qz}^s}T_z^s(s=s_w,\theta) \qquad \ldots(7.19)$$

where $T_{qf}^c = \frac{Q^c}{F_0}\Big|_{V^c=V^s=0}$ is the transfer function of the cosine modal sensor excited by the

primary force,

$T_{qf}^{s} = \left.\frac{Q^{s}}{F_0}\right|_{V^c=V^s=0}$ is the transfer function of the sine modal sensor excited by the primary force,

$T_{qz}^{c} = \left.\frac{Q^{c}}{V^{c}}\right|_{F_0=V^s=0}$ is the transfer function of the cosine modal sensor excited by the cosine modal actuator,

$T_{qz}^{s} = \left.\frac{Q^{s}}{V^{s}}\right|_{F_0=V^c=0}$ is the transfer function of the sine modal sensor excited by the sine modal actuator.

It can be seen from equation (7.19) that the measured mobility of the pipe with control for continuous frequencies can be constructed by measuring all parameters in that equation.

Experimental results presented are as follows:

Figure 7.3 Transfer function of the n = 2 PVDF modal sensors excited by the point force and measured at the distance of 1210 mm from the shaker before applying the active control.

Figure 7.4 Orientation angle, ϕ_c, extracted from the response of the n = 2 modal sensors.

Figure 7.5 Transfer function of the n = 2 PVDF modal sensor excited by the n = 2 modal actuator

Figure 7.6 Amplitude of mobility of the infinite pipe measured at a position of 1610 mm from the primary force.

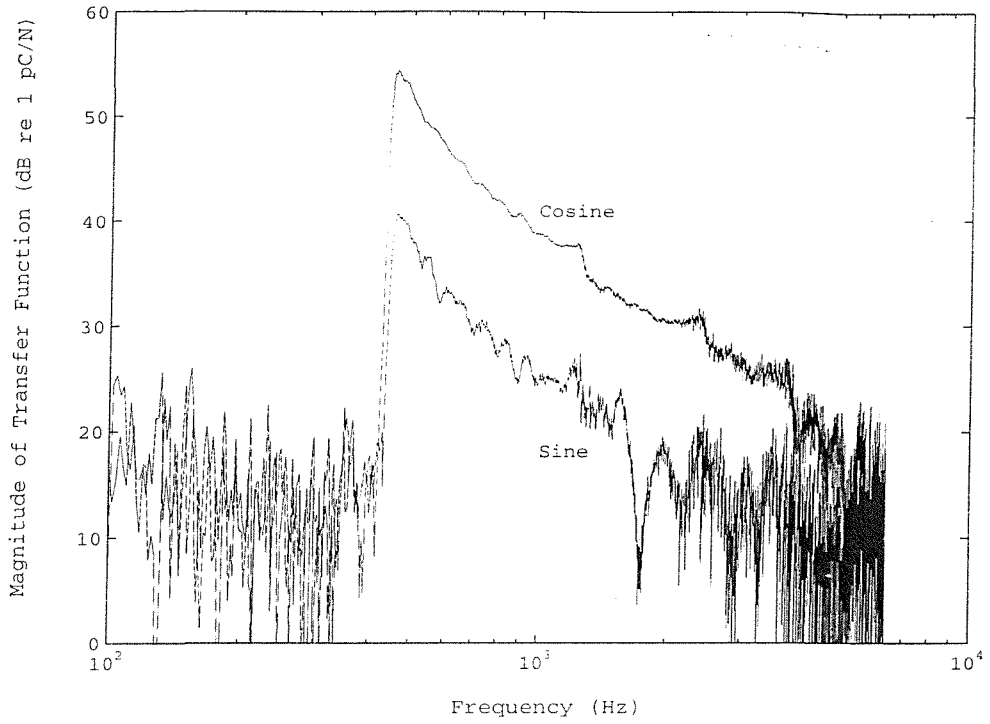

Figure 7.3: Transfer function (generated charge/primary force) of the n = 2 PVDF modal sensors without the active control; ___ the cosine modal sensor, _ _ the sine modal sensor.

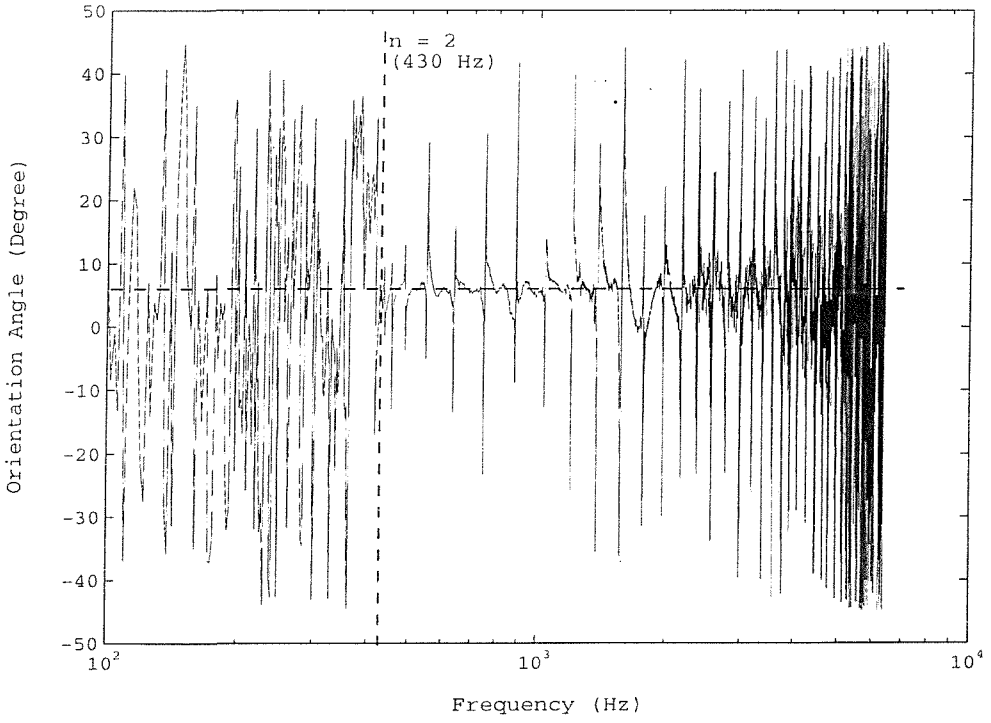

Figure 7.4: Orientation angle of the cosine modal actuator, ϕ_c, with respect to the primary force extracted from the sine and cosine modal sensors for the n = 2 mode.

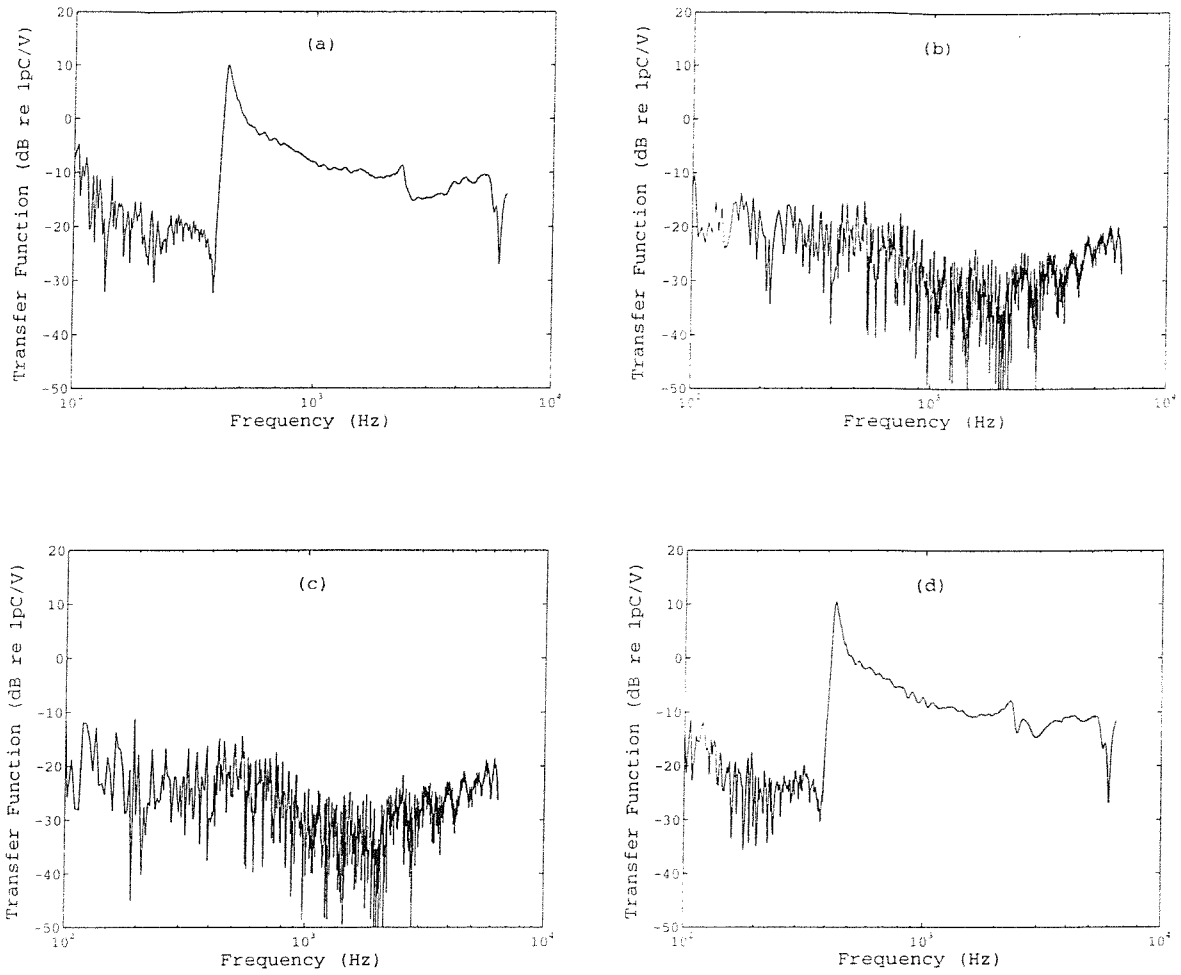

Figure 7.5: Transfer function of the n = 2 PVDF modal sensor (generated charge/voltage) excited by the n = 2 modal actuator;

a) Cosine modal sensor excited by the cosine modal actuator

b) Sine modal sensor excited by the cosine modal actuator

c) Cosine modal sensor excited by the sine modal actuator

d) Sine modal sensor excited by the sine modal actuator

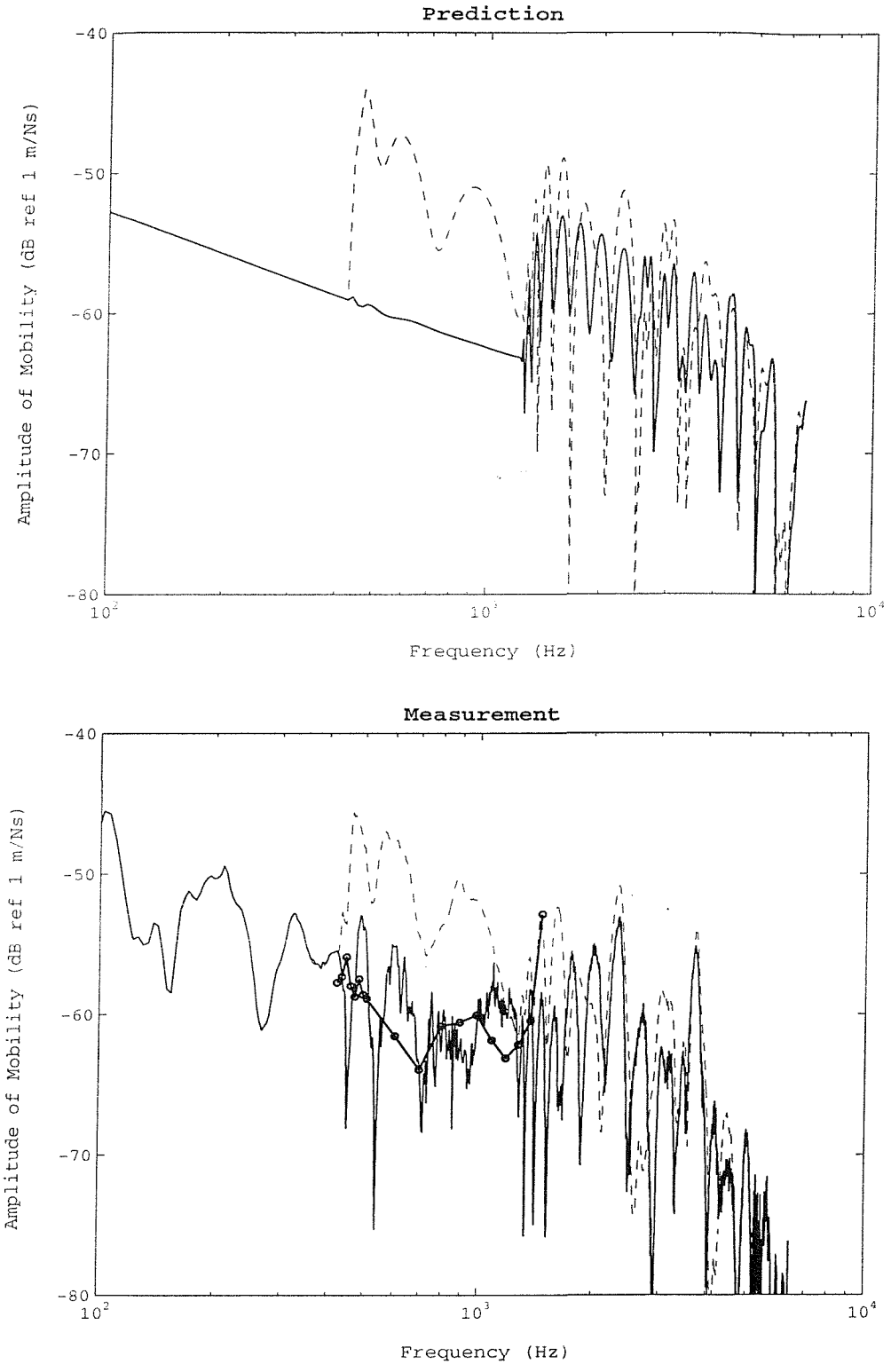

Figure 7.6: Amplitude of mobility of the infinite pipe measured at a position of 1610 mm from the primary force; a) Prediction, b) Measurement; _ _ without control, ___with control for continuous frequencies, o__o with control for discrete frequencies.

7.3.4 Discussion

In the experiment, ϕ_c, the orientation angle of the cosine modal actuator with respect to the primary force is required to predict the radial motion of the pipe at any position after control. It was found to be about 7 degrees as shown in figure 7.4. Because the angle is only 7 degrees, the dominant radial motion is the cosine component as shown in figure 7.3. Thus, the sine component was very small, and was difficult to monitor using the oscilloscope. Hence, only the cosine modal actuator was used to control the disturbance. To control the disturbance, good alignment between the cosine modal sensor and cosine modal actuator, and between the sine modal sensor and the sine modal actuator are required. This is evident in figure 7.5, in which the transfer functions of the sine modal sensor/cosine modal actuator and the cosine modal sensor/sine modal actuator are very small. The predicted and measured mobility of the pipe before and after control can be seen in figure 7.6. Comparing figures 7.6.a with 7.6.b, it can be seen that theory and practice are consistent. The discrepancies might be because of the inaccurate shape of the modal sensors so that the sensors still detect a response from other modes even if the radial motion of the n = 2 mode is completely suppressed.

7.4 Conclusions

Feedforward vibration control is the strategy that has been used in this work to suppress a flexural propagating wave of the n = 2 mode. The theoretical model for this type of control has used the n = 2 modal sensors/actuators described in chapters 5 and 6, respectively. Since the disturbance produced from the primary force can be separated into sine and cosine components, a pair of reciprocal sine and cosine modal sensors/actuators are applied in order to counteract each component of the disturbance. Within this framework, it is theoretically shown that the disturbance of the n = 2 mode of the infinite pipe can completely be suppressed. This principle has also been validated by experiment.

CHAPTER 8

PASSIVE AND ADAPTIVE-PASSIVE VIBRATION CONTROL OF INFINITE PIPES

8.1 Introduction

The pipe vibration control systems discussed in this chapter are passive and adaptive-passive. The performances of both control systems are investigated in order to compare their effectiveness with the active control system discussed in the previous chapter. In order to make a comparison with active control, the same pipe used in the previous chapter is also considered in this chapter. Some vibration control measures are applied such as damping material for passive vibration control and a PZT element shunted with an electrical circuit for adaptive-passive vibration control. This is restricted to a theoretical study.

Generally, passive control involves system modification such as changing the mass, stiffness and damping to reduce the response of a structure. These passive modifications can be done by adding elements to the system, such as masses, springs or damping materials. The addition of an unconstrained layer of damping material to a section of an infinite pipe is considered in this thesis. This can be considered as a discontinuous section of a composite pipe. As described by Mace [54], Brennan *et al* [72], Cremer and Heckl [17] and Fuller [57], a propagating wave incident on a discontinuity is reflected so that less vibration would be transmitted along the pipe. Since the discontinuous section is as a result of modifying the pipe, the attenuation gained from

the discontinuity is investigated with respect to its Young's modulus and the damping properties of the material attached to the pipe.

An advantage of the passive system is that it is simple and stable. However, its performance is limited because the properties of the passive elements are fixed. This is quite different to an active system, in which vibration control can occur in real-time. Adaptive-passive control, which is where the passive properties of a system can be changed as a function of time, combines the advantages of both passive and active systems. In this thesis, an adaptive-passive system is established from PZT elements shunted with a parallel L-R circuit, in which the inductance (L) and the resistance (R) can be adjusted. With the shunt, the properties of the PZT element such as stiffness and damping (loss factor) can be changed as reported by Hagood and von Flotow [13]. Large attenuation of vibration may be obtained by tuning the inductance and resistance of the parallel L-R circuit.

8.2 Passive Control of Infinite Pipes

8.2.1 Equation of Motion for Composite Pipes

By bonding unconstrained layer damping material to the pipe, a composite pipe section is formed. Since the composite section can be considered as a structural discontinuity, determination of the pipe motion with a composite section requires some boundary conditions at the discontinuity (described in detail later). In this section, the necessary parameters at the ends of the composite pipe such as forces, moments and displacements used to analyse the pipe motion are considered and are based on Flugge's shell theory.

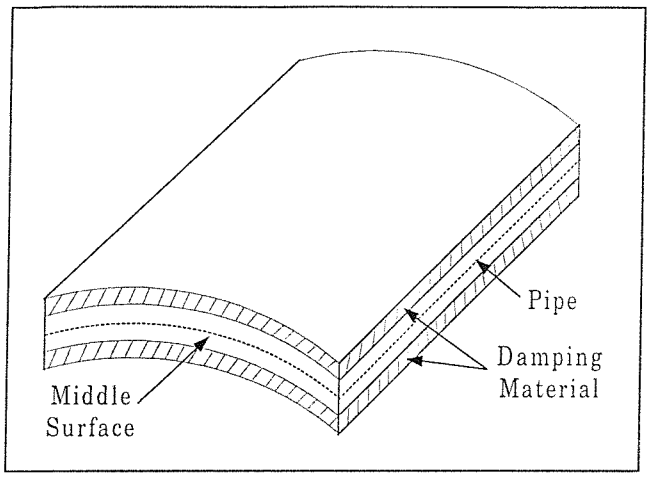

Figure 8.1: Diagram of a composite pipe with the damping material

For simplicity, the damping material is assumed to be bonded on both sides of a pipe as shown in figure 8.1. With this configuration, the composite pipe is symmetrical. Axial, circumferential and shear stresses in a pipe are respectively given by (Flugge [5])

$$\sigma_s^p = \frac{E}{1-\nu^2}[e_s + \nu e_\theta]$$

$$\sigma_\theta^p = \frac{E}{1-\nu^2}[e_\theta + \nu e_s] \qquad \ldots(8.2.1\ a, b, c, d)$$

$$\sigma_{s\theta}^p = \frac{E}{2(1+\nu)}\gamma_{s\theta}$$

$$\sigma_{\theta s}^P = \sigma_{s\theta}^P$$

and those in a damping material are

$$\sigma_s^z = \frac{E_d}{1-\nu_d^2}[e_s + \nu_d e_\theta]$$

$$\sigma_\theta^z = \frac{E_d}{1-\nu_d^2}[e_\theta + \nu_d e_s] \qquad \ldots(8.2.2\ a, b, c, d)$$

$$\sigma_{s\theta}^{z} = \frac{E_d}{2(1+\nu_d)}\gamma_{s\theta}$$

$$\sigma_{\theta s}^{z} = \sigma_{s\theta}^{z}$$

where $e_s = \varepsilon_s + z\kappa_s$ is the axial strain at radial position z,

$e_\theta = \frac{1}{1+z/a}(\varepsilon_\theta + z\kappa_\theta)$ is the circumferential strain at radial position z,

$\gamma_{s\theta} = \frac{1}{1+z/a}\left[\varepsilon_{s\theta} + z\left(1+\frac{z}{2a}\right)\kappa_{s\theta}\right]$ is the shear strain at radial position z,

$\varepsilon_s = \frac{1}{a}\frac{\partial u^c}{\partial s}$ is the axial strain at the mid-surface,

$\varepsilon_\theta = \frac{1}{a}\left(\frac{\partial v^c}{\partial \theta} + w^c\right)$ is the circumferential strain at the mid-surface,

$\varepsilon_{s\theta} = \frac{1}{a}\left(\frac{\partial u^c}{\partial \theta} + \frac{\partial v^c}{\partial s}\right)$ is the shear strain at the mid-surface,

$\kappa_s = -\frac{1}{a^2}\frac{\partial^2 w^c}{\partial s^2}$ is the axial change of curvature of the mid-surface,

$\kappa_\theta = \frac{1}{a^2}\left(\frac{\partial v^c}{\partial \theta} - \frac{\partial^2 w^c}{\partial \theta^2}\right)$ is the circumferential change of curvature of mid-surface

$\kappa_{s\theta} = \frac{2}{a^2}\left(\frac{\partial v^c}{\partial s} - \frac{\partial^2 w^c}{\partial s \partial \theta}\right)$ is the mid-surface twist,

E_d is the Young's modulus of the damping material,

ν_d is the Poisson's ratio of the damping material, and

the superscript c denotes the composite pipe section.

Forces and moments in the composite pipe can be determined by integrating the stresses over its thickness as given by

$$\begin{bmatrix} N_s^c \\ N_{s\theta}^c \end{bmatrix} = \int_{-h/2}^{h/2} \begin{bmatrix} \sigma_s^p \\ \sigma_{s\theta}^p \end{bmatrix} (1+z/a)\,dz + \int_{-(h_d+h/2)}^{-h/2} \begin{bmatrix} \sigma_s^z \\ \sigma_{s\theta}^z \end{bmatrix} (1+z/a)\,dz + \int_{h/2}^{h_d+h/2} \begin{bmatrix} \sigma_s^z \\ \sigma_{s\theta}^z \end{bmatrix} (1+z/a)\,dz$$

$$\begin{bmatrix} N_\theta^c \\ N_{\theta s}^c \end{bmatrix} = \int_{-h/2}^{h/2} \begin{bmatrix} \sigma_\theta^p \\ \sigma_{\theta s}^p \end{bmatrix} dz + \int_{-(h_d+h/2)}^{-h/2} \begin{bmatrix} \sigma_\theta^z \\ \sigma_{\theta s}^z \end{bmatrix} dz + \int_{h/2}^{h_d+h/2} \begin{bmatrix} \sigma_\theta^z \\ \sigma_{\theta s}^z \end{bmatrix} dz \qquad \ldots(8.2.3)$$

$$\begin{bmatrix} M_s^c \\ M_{s\theta}^c \end{bmatrix} = \int_{-h/2}^{h/2} \begin{bmatrix} \sigma_s^p \\ \sigma_{s\theta}^p \end{bmatrix} (1+z/a)\,zdz + \int_{-(h_d+h/2)}^{-h/2} \begin{bmatrix} \sigma_s^z \\ \sigma_{s\theta}^z \end{bmatrix} (1+z/a)\,zdz + \int_{h/2}^{h_d+h/2} \begin{bmatrix} \sigma_s^z \\ \sigma_{s\theta}^z \end{bmatrix} (1+z/a)\,zdz$$

$$\begin{bmatrix} M_\theta^c \\ M_{\theta s}^c \end{bmatrix} = \int_{-h/2}^{h/2} \begin{bmatrix} \sigma_\theta^p \\ \sigma_{\theta s}^p \end{bmatrix} zdz + \int_{-(h_d+h/2)}^{-h/2} \begin{bmatrix} \sigma_\theta^z \\ \sigma_{\theta s}^z \end{bmatrix} zdz + \int_{h/2}^{h_d+h/2} \begin{bmatrix} \sigma_\theta^z \\ \sigma_{\theta s}^z \end{bmatrix} zdz$$

where h_d is the thickness of the damping material.

Substituting for the stresses from equations (8.2.1) and (8.2.2) gives

$$N_s^c = K_c(\varepsilon_s + \nu_c\varepsilon_\theta) + \frac{D_c}{a}\kappa_s$$

$$N_\theta^c = K_c(\varepsilon_\theta + \nu_c\varepsilon_s) - \frac{D_c}{a}(\kappa_\theta - \frac{\varepsilon_\theta}{a})$$

$$N_{s\theta}^c = \frac{1}{2}K_c(1-\nu_c)\varepsilon_{s\theta} + \frac{1}{4a}D_c(1-\nu_{cd})\kappa_{s\theta}$$

$$N_{\theta s}^c = \frac{1}{2}K_c(1-\nu_c)\varepsilon_{s\theta} - \frac{1}{4a}D_c(1-\nu_{cd})(\kappa_{s\theta} - \frac{2\varepsilon_{s\theta}}{a}) \qquad \ldots(8.2.4)$$

$$M_s^c = D_c\left(\kappa_s + \nu_{cd}\kappa_\theta + \frac{\varepsilon_s}{a}\right)$$

$$M_\theta^c = D_c\left(\kappa_\theta + \nu_{cd}\kappa_s - \frac{\varepsilon_\theta}{a}\right)$$

$$M_{s\theta}^c = \frac{D_c}{2}(1-\nu_{cd})\kappa_{s\theta}$$

$$M_{\theta s}^c = \frac{D_c}{2}(1-\nu_{cd})(\kappa_{s\theta} - \frac{\varepsilon_{s\theta}}{a})$$

where $K_c = K(1+2\hat{K})$, $D_c = D(1+\hat{D})$, $\nu_c = \nu\left(\frac{1+2\hat{\nu}\hat{K}}{1+2\hat{K}}\right)$, $\nu_{cd} = \nu\left(\frac{1+\hat{\nu}\hat{D}}{1+2\hat{D}}\right)$

$$\hat{K} = \frac{K_d}{K}, \quad \hat{D} = \frac{D_d}{D}, \quad \hat{\nu} = \frac{\nu_d}{\nu}$$

$$K = \frac{Eh}{1-\nu^2}, \qquad D = \frac{Eh^3}{12(1-\nu^2)}$$

$$K_d = \frac{E_d h_d}{1-\nu_d^2}, \qquad D_d = \frac{E_z(h_t^3 - h^3)}{12(1-\nu_d^2)}$$

$$h_t = h + 2h_d .$$

Following the work done by Leissa [2], the equation of motion for the composite pipe is given by

$$\frac{\partial N_s^c}{\partial s} + \frac{\partial N_{\theta s}^c}{\partial \theta} - ah\rho_c \frac{\partial^2 u^c}{\partial t^2} = 0$$

$$\frac{\partial N_\theta^c}{\partial \theta} + \frac{\partial N_{s\theta}^c}{\partial s} + \frac{1}{a}\frac{\partial M_\theta^c}{\partial \theta} + \frac{1}{a}\frac{\partial M_{s\theta}^c}{\partial s} - ah\rho_c \frac{\partial^2 v^c}{\partial t^2} = 0 \qquad \ldots(8.2.5)$$

$$-N_\theta^c + \frac{1}{a}\frac{\partial^2 M_s^c}{\partial s^2} + \frac{1}{a}\frac{\partial^2 M_\theta^c}{\partial \theta^2} + \frac{1}{a}\frac{\partial^2 M_{\theta s}^c}{\partial s \partial \theta} + \frac{1}{a}\frac{\partial^2 M_{s\theta}^c}{\partial s \partial \theta} - ah\rho_c \frac{\partial^2 w^c}{\partial t^2} = 0$$

where $\rho_c = \rho(1+2\hat{\rho}\hat{h})$

$$\hat{\rho} = \frac{\rho_d}{\rho}$$

ρ_d is the density of the damping material, and

$$\hat{h} = h_d / h .$$

Substituting for the forces and moments from equation (8.2.4) into equation (8.2.5) and arranging them in matrix form gives

$$\begin{bmatrix} A_{11}^c & A_{12}^c & A_{13}^c \\ A_{21}^c & A_{22}^c & A_{23}^c \\ A_{31}^c & A_{32}^c & A_{33}^c \end{bmatrix} \begin{bmatrix} u^c(s,\theta,t) \\ v^c(s,\theta,t) \\ w^c(s,\theta,t) \end{bmatrix} = \mathbf{0} \qquad \ldots(8.2.6)$$

where $A_{11}^c = \left(\frac{\partial^2}{\partial s^2} + \frac{(1-\nu_c)}{2}\left(1+\hat{\nu}_0\beta_c^2\right)\frac{\partial^2}{\partial\theta^2} - \frac{1}{\omega_{rc}^2}\frac{\partial^2}{\partial t^2} \right)$,

$$A_{12}^c = \left(\frac{(1+\nu_c)}{2}\frac{\partial^2}{\partial s\partial\theta} \right),$$

$$A_{13}^c = \left(\nu_c\frac{\partial}{\partial s} - \beta_c^2\frac{\partial^3}{\partial s^3} + \beta_c^2\frac{(1-\nu_{cd})}{2}\frac{\partial^3}{\partial s\partial\theta^2} \right),$$

$$A_{21}^c = A_{12}^c,$$

$$A_{22}^c = \left(\frac{(1-\nu_c)}{2}(1+3\hat{\upsilon}_0\beta^2)\frac{\partial^2}{\partial s^2} + \frac{\partial^2}{\partial\theta^2} - \frac{1}{\omega_{rc}^2}\frac{\partial^2}{\partial t^2} \right),$$

$$A_{23}^c = \left(\frac{\partial}{\partial\theta} - \beta_c^2\frac{(3-\nu_{cd})}{2}\frac{\partial^3}{\partial s^2\partial\theta} \right),$$

$$A_{31}^c = A_{13}^c,$$

$$A_{32}^c = A_{23}^c,$$

$$A_{33}^c = \left(1+\beta_c^2 + 2\beta_c^2\frac{\partial^2}{\partial\theta^2} + \beta_c^2\nabla^4 + \frac{1}{\omega_{rc}^2}\frac{\partial^2}{\partial t^2} \right),$$

$\nabla^4 = \frac{\partial^4}{\partial s^4} + \frac{\partial^4}{\partial\theta^4} + \frac{\partial^4}{\partial s^2\partial\theta^2}$ and

$$\hat{\nu}_0 = \frac{1-\nu_{cd}}{1-\nu_c}$$

$$\beta_c^2 = \beta^2\left(\frac{1+\hat{D}}{1+2\hat{K}} \right),$$

$$\beta^2 = \frac{h^2}{12a^2},$$

$$\omega_{rc}^2 = \omega_r^2\left(\frac{1+2\hat{K}}{1+2\hat{\rho}\hat{h}} \right)$$

$\omega_r^2 = \frac{1}{a^2}\frac{E}{\rho(1-\nu^2)}$ is the ring frequency of the pipe.

The displacements can be written as (equation 2.2 in chapter 2)

$$u^c(s,\theta,t) = -j\sum_{n=0}^{\infty}\sum_{b=1}^{8}\overline{\overline{U}}^{c}_{nb}\cos[n(\theta-\phi)]e^{j(\hat{k}^c_{nb}s-\pi/2-\omega t)}$$
$$v^c(s,\theta,t) = \sum_{n=0}^{\infty}\sum_{b=1}^{8}\overline{\overline{V}}^{c}_{nb}\sin[n(\theta-\phi)]e^{j(\hat{k}^c_{nb}s-\omega t)} \qquad \ldots(8.2.7\text{ a, b, c})$$
$$w^c(s,\theta,t) = \sum_{n=0}^{\infty}\sum_{b=1}^{8}\overline{\overline{W}}^{c}_{nb}\cos[n(\theta-\phi)]e^{j(\hat{k}^c_{nb}s-\omega t)}$$

By substituting for the displacements from equation (8.2.7 a, b, c), equation (8.2.6) becomes

$$\begin{bmatrix} L^c_{11} & L^c_{12} & L^c_{13} \\ L^c_{21} & L^c_{22} & L^c_{23} \\ L^c_{31} & L^c_{32} & L^c_{33} \end{bmatrix}\begin{bmatrix} \overline{\overline{U}}^{c}_{nb} \\ \overline{\overline{V}}^{c}_{nb} \\ \overline{\overline{W}}^{c}_{nb} \end{bmatrix} = \boldsymbol{\theta} \qquad \ldots(8.2.8)$$

where $L^c_{11} = \left(\hat{k}^c_{nb}\right)^2 + \frac{(1-\nu_c)}{2}\left(1+\hat{\nu}_0\beta_c^2\right)n^2 - \Omega_c^2$

$$L^c_{12} = \frac{(1+\nu_c)}{2}n\hat{k}^c_{nb}$$

$$L^c_{13} = \left[\nu_c + \beta_c^2\left(\hat{k}^c_{nb}\right)^2 - \frac{(1-\nu_{cd})}{2}\beta_c^2 n^2\right]\hat{k}^c_{nb}$$

$$L^c_{21} = L^c_{12}$$

$$L^c_{22} = \frac{(1-\nu_c)}{2}(1+3\hat{\nu}_0\beta_c^2)\left(\hat{k}^c_{nb}\right)^2 + n^2 - \Omega_c^2$$

$$L^c_{23} = n + \frac{(3-\nu_{cd})}{2}\beta_c^2 n\left(\hat{k}^c_{nb}\right)^2$$

$$L^c_{31} = L^c_{13}$$

$$L^c_{32} = L^c_{23}$$

$$L^c_{33} = 1 + \beta_c^2 + \beta_c^2\left[\left(\hat{k}^c_{nb}\right)^2 + n^2\right]^2 - 2\beta_c^2 n^2 - \Omega_c^2 \text{ and}$$

$$\Omega_c = \omega / \omega_{rc}$$

Similar to a homogeneous pipe, the wavenumber solutions of the composite pipe can be found by setting

$$|\mathbf{L}^c| = 0 \qquad \ldots(8.2.9)$$

8.2.2 Modification of Pipe Motion by a Composite Pipe Section

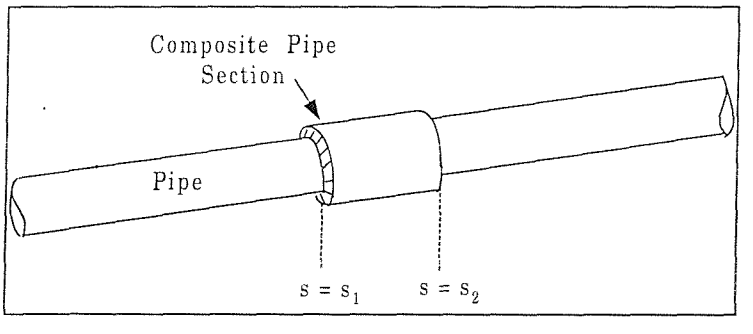

Figure 8.2: Diagram of a pipe with composite pipe section.

Considering the composite pipe section shown in figure 8.2, the motion of the pipe can be determined from boundary conditions at the interface between the composite section and the pipe. These involve the continuity of motion across the discontinuity and the equilibrium of forces and moments at the discontinuity. In this section, two methods, which are analytical and wave methods, are used to analyse the motion of the pipe. Two methods are used as a check on each other.

8.2.2.1 Analytical Method

The schematic of an infinite pipe having a discontinuous section is shown in figure 8.3. From the figure, the incident wave vector for any circumferential mode n $\mathbf{a}^+$, which is generated by a point force, produces the reflected wave vector $\mathbf{a}^-$, at $s = s_1$, and $\mathbf{b}^-$ at $s = s_2$, and the transmitted wave vector $\mathbf{b}^+$ at $s = s_1$, and $\mathbf{c}^+$ at $s = s_2$. From this model, the pipe motion for an axial position $s < s_1$ can be calculated by the superposition of the incident wave vector $\mathbf{a}^+$, and the reflected wave vector $\mathbf{a}^-$. It can be seen that at $s > s_2$ the displacement only depends on the transmitted wave vector $\mathbf{c}^+$. The motion of the pipe in the composite part of the pipe is the summation of the transmitted wave vector $\mathbf{b}^+$ and reflected wave vector $\mathbf{b}^-$. Hence, to determine the pipe motion, all of these waves have to be found and they can be obtained from the boundary conditions at the discontinuities at $s = s_1$ and $s = s_2$.

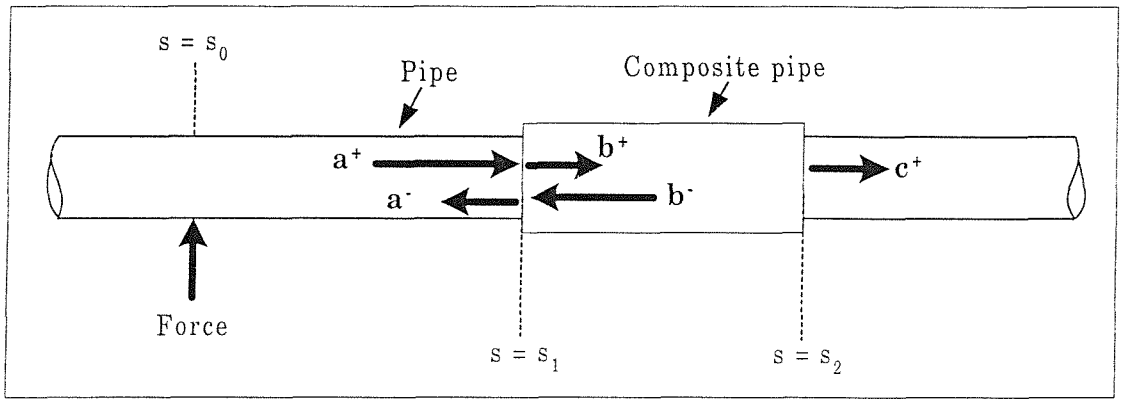

Figure 8.3: Model of the waves at the discontinuous pipe section.

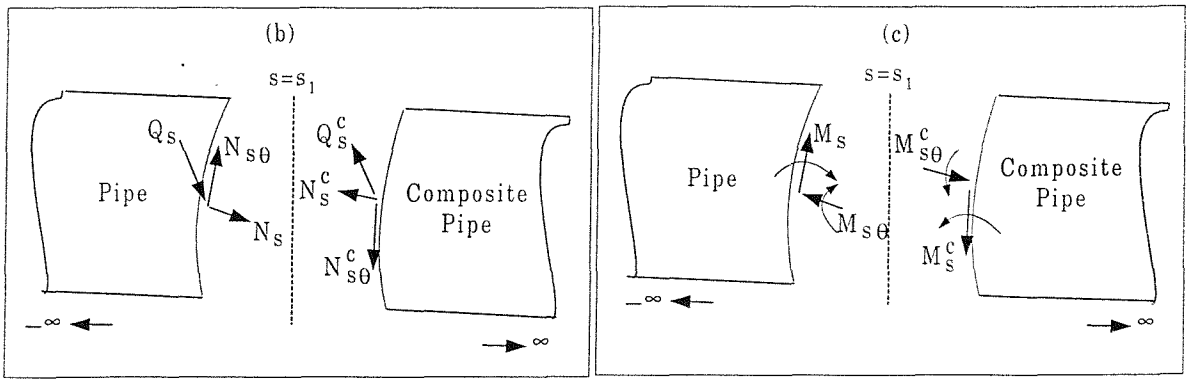

Figure 8.4: Notation and co-ordinate system at the discontinuity; a) Forces, b) Moment

At the discontinuity, the action of forces and moments is schematically shown in figure 8.4. The boundary conditions can be considered from motion continuity and, force and moment equilibrium as given by (Harari [56] and Fuller [57])

$$\begin{bmatrix} u(s_1,\theta,t) \\ v(s_1,\theta,t) \\ w(s_1,\theta,t) \\ \dfrac{\partial w(s_1,\theta,t)}{\partial s} \end{bmatrix} = \begin{bmatrix} u^c(s_1,\theta,t) \\ v^c(s_1,\theta,t) \\ w^c(s_1,\theta,t) \\ \dfrac{\partial w^c(s_1,\theta,t)}{\partial s} \end{bmatrix} \text{ and } \begin{bmatrix} N_s(s_1,\theta,t) \\ T_{s\theta}(s_1,\theta,t) \\ M_s(s_1,\theta,t) \\ V_s(s_1,\theta,t) \end{bmatrix} = \begin{bmatrix} N_s^c(s_1,\theta,t) \\ T_{s\theta}^c(s_1,\theta,t) \\ M_s^c(s_1,\theta,t) \\ V_s^c(s_1,\theta,t) \end{bmatrix} \quad \ldots(8.2.10)$$

where $V_s = \frac{1}{a}\left(\frac{\partial M_s}{\partial s} + \frac{\partial M_{\theta s}}{\partial \theta} + \frac{\partial M_{s\theta}}{\partial \theta}\right)$ is called the effective transverse shear force,

$T_{s\theta} = N_{s\theta} + \frac{1}{a} M_{s\theta}$ is called the effective in-plane shear.

The conditions given in the above equation all involve displacements. This makes the analysis complicated. However, they are related to each other as discussed in section 3.3. Both axial and circumferential displacements can be written in terms of the radial displacement as (equation 3.41)

$$\overline{\overline{U}}_{nb} = \alpha_{nb}\overline{\overline{W}}_{nb} \quad \text{and} \quad \ldots(8.2.11\text{ a, b})$$

$$\overline{\overline{V}}_{nb} = \psi_{nb}\overline{\overline{W}}_{nb}$$

Where $\alpha_{nb} = \left(\frac{L_{12}L_{23} - L_{22}L_{13}}{L_{11}L_{22} - L_{12}L_{21}}\right)_{nb}$ is the axial coefficient and $\ldots(8.2.11\text{ c})$

$\psi_{nb} = \left(\frac{L_{21}L_{13} - L_{11}L_{23}}{L_{11}L_{22} - L_{12}L_{21}}\right)_{nb}$ is the circumferential coefficient $\ldots(8.2.11\text{ d})$

These relationships for a composite pipe can be determined in the same manner given by

$$\overline{\overline{U}}^{c}_{nb} = \alpha^{c}_{nb}\overline{\overline{W}}^{c}_{nb} \quad \text{and} \qquad \text{...(8.2.12 a, b)}$$

$$\overline{\overline{V}}^{c}_{nb} = \psi^{c}_{nb}\overline{\overline{W}}^{c}_{nb}$$

Where $\alpha^{c}_{nb} = \left(\frac{L^{c}_{12}L^{c}_{23} - L^{c}_{22}L^{c}_{13}}{L^{c}_{11}L^{c}_{22} - L^{c}_{12}L^{c}_{21}}\right)_{nb}$ is the axial coefficient and ...(8.2.12 c)

$$\psi^{c}_{nb} = \left(\frac{L^{c}_{21}L^{c}_{13} - L^{c}_{11}L^{c}_{23}}{L^{c}_{11}L^{c}_{22} - L^{c}_{12}L^{c}_{21}}\right)_{nb} \quad \text{is the circumferential coefficient.} \qquad \text{...(8.2.12 d)}$$

Omitting the term of $e^{-j\omega t}$ for convenience, the displacements, forces and moments of the pipe can be written in the form of the radial displacement as (equation 3.43)

$$N_s(s,\theta) = \frac{K}{a}\sum_{b=1}^{4} Z_{N,nb}\overline{\overline{W}}_{nb}\cos[n(\theta-\phi)]e^{j\hat{k}_{nb}s}$$

$$T_{s\theta}(s,\theta) = j\frac{(1-\nu)K}{2a}\sum_{b=1}^{4} Z_{T,nb}\overline{\overline{W}}_{nb}\sin[n(\theta-\phi)]e^{j\hat{k}_{nb}s}$$

$$M_s(s,\theta) = \frac{D}{a^2}\sum_{b=1}^{4} Z_{M,nb}\overline{\overline{W}}_{nb}\cos[n(\theta-\phi)]e^{j\hat{k}_{nb}s}$$

$$V_s(s,\theta) = j\frac{D}{a^3}\sum_{b=1}^{4} Z_{V,nb}\overline{\overline{W}}_{nb}\cos[n(\theta-\phi)]e^{j\hat{k}_{nb}s} \qquad \text{...(8.2.13)}$$

$$U_n(s,\theta) = -j\sum_{b=1}^{4}\alpha_{nb}\overline{\overline{W}}_{nb}\cos[n(\theta-\phi)]e^{j\hat{k}_{nb}s}$$

$$V_n(s,\theta) = \sum_{b=1}^{4}\psi_{nb}\overline{\overline{W}}_{nb}\sin[n(\theta-\phi)]e^{j\hat{k}_{nb}s}$$

$$W_n(s,\theta) = \sum_{b=1}^{4}\overline{\overline{W}}_{nb}\cos[n(\theta-\phi)]e^{j\hat{k}_{nb}s}$$

$$\frac{\partial W_n(s,\theta)}{\partial s} = j\sum_{b=1}^{4}\hat{k}_{nb}\overline{\overline{W}}_{nb}\cos[n(\theta-\phi)]e^{j\hat{k}_{nb}s}$$

where $\overline{\overline{W}}_{nb}$ is the radial amplitude of the b^{th} wave of the n^{th} circumferential mode, U_n, V_n, W_n are the axial, circumferential and radial displacement in the frequency domain, respectively, and the Z's are given by:

$$Z_{N,nb} = \left[\hat{k}_{nb}\alpha_{nb} + \nu n\psi_{nb} + \beta^2\hat{k}_{nb}^2 + \nu\right]$$

$$Z_{T,nb} = \left[n\alpha_{nb} + \left(1+3\beta^2\right)\hat{k}_{nb}\psi_{nb} + 3\beta^2 n\hat{k}_{nb}\right]$$

$$Z_{M,nb} = \left[\hat{k}_{nb}\alpha_{nb} + \nu n\psi_{nb} + \hat{k}_{nb}^2 + \nu n^2\right] \qquad \ldots(8.2.14\text{ a, b, c, d})$$

$$Z_{V,nb} = \left[\left(\hat{k}_{nb}^2 - \left(\frac{1-\nu}{2}\right)n^2\right)\alpha_{nb} + \left(\frac{3-\nu}{2}\right)n\hat{k}_{nb}\psi_{nb} + \hat{k}_{nb}\left(\hat{k}_{nb}^2 + (2-\nu)n^2\right)\right]$$

With the forces and moments obtained from equation (8.2.13), a set of boundary conditions for the composite pipe section can also be written in terms of the radial displacement as given by

$$N_s^c(s,\theta) = \frac{K_c}{a}\sum_{b=1}^{4} Z_{N,nb}^c \overline{\overline{W}}_{nb}^c \cos[n(\theta-\phi)]e^{j\hat{k}_{nb}^c s}$$

$$T_{s\theta}^c(s,\theta) = j\frac{(1-\nu_c)K_c}{2a}\sum_{b=1}^{4} Z_{T,nb}^c \overline{\overline{W}}_{nb}^c \sin[n(\theta-\phi)]e^{j\hat{k}_{nb}^c s}$$

$$M_s^c(s,\theta) = \frac{D_c}{a^2}\sum_{b=1}^{4} Z_{M,nb}^c \overline{\overline{W}}_{nb}^c \cos[n(\theta-\phi)]e^{j\hat{k}_{nb}^c s}$$

$$V_s^c(s,\theta) = j\frac{D_c}{a^3}\sum_{b=1}^{4} Z_{V,nb}^c \overline{\overline{W}}_{nb}^c \cos[n(\theta-\phi)]e^{j\hat{k}_{nb}^c s} \qquad \ldots(8.2.15)$$

$$U_n^c(s,\theta) = -j\sum_{b=1}^{4} \alpha_{nb}^c \overline{\overline{W}}_{nb}^c \cos[n(\theta-\phi)]e^{j\hat{k}_{nb}^c s}$$

$$V_n^c(s,\theta) = \sum_{b=1}^{4} \psi_{nb}^c \overline{\overline{W}}_{nb}^c \sin[n(\theta-\phi)]e^{j\hat{k}_{nb}^c s}$$

$$W_n^c(s,\theta) = \sum_{b=1}^{4} \overline{\overline{W}}_{nb}^c \cos[n(\theta-\phi)]e^{j\hat{k}_{nb}^c s}$$

$$\frac{\partial W_n^c(s,\theta)}{\partial s} = j\sum_{b=1}^{4} \hat{k}_{nb}^c \overline{\overline{W}}_{nb}^c \cos[n(\theta-\phi)]e^{j\hat{k}_{nb}^c s}$$

where $T_{s\theta}^c = N_{s\theta}^c + \frac{1}{a}M_{s\theta}^c$,

$$V_s^c = \frac{1}{a}\left(\frac{\partial M_s^c}{\partial s} + \frac{\partial M_{\theta s}^c}{\partial \theta} + \frac{\partial M_{s\theta}^c}{\partial \theta}\right)$$

$\bar{\bar{W}}_{nb}^c$ is the radial amplitude of the composite pipe for the b^{th} wave of the n^{th} circumferential mode, U_n^c, V_n^c, W_n^c are the axial, circumferential and radial displacements of the composite pipe in the frequency domain, respectively, and the Z's are given by:

$$Z_{N,nb}^c = \left[\hat{k}_{nb}^c \alpha_{nb}^c + \nu_c n \psi_{nb}^c + \beta_c^2 \left(\hat{k}_{nb}^c\right)^2 + \nu_c\right]$$

$$Z_{T,nb}^c = \left[n\alpha_{nb}^c + \left(1 + 3\hat{\nu}_0 \beta_c^2\right)\hat{k}_{nb}^c \psi_{nb}^c + 3\hat{\nu}_0 \beta_c^2 n \hat{k}_{nb}^c\right]$$

$$Z_{M,nb}^c = \left[\hat{k}_{nb}^c \alpha_{nb}^c + \nu_{cd} n \psi_{nb}^c + \left(\hat{k}_{nb}^c\right)^2 + \nu_{cd} n^2\right] \qquad \ldots(8.2.16\ a, b, c, d)$$

$$Z_{V,nb}^c = \left[\left(\left(\hat{k}_{nb}^c\right)^2 - \left(\frac{1-\nu_{cd}}{2}\right)n^2\right)\alpha_{nb}^c + \left(\frac{3-\nu_{cd}}{2}\right)n\hat{k}_{nb}^c \psi_{nb}^c + \hat{k}_{nb}^c\left(\left(\hat{k}_{nb}^c\right)^2 + (2-\nu_{cd})n^2\right)\right]$$

Equating forces ($N_s = N_s^c$) and moments ($M_s = M_s^c$), and applying continuity of motion of v and w, gives the boundary conditions at $s = s_1$ as

$$\begin{bmatrix} N_s(s_1,\theta) \\ M_s(s_1,\theta) \\ V_n(s_1,\theta) \\ W_n(s_1,\theta) \end{bmatrix} = \begin{bmatrix} N_s^c(s_1,\theta) \\ M_s^c(s_1,\theta) \\ V_n^c(s_1,\theta) \\ W_n^c(s_1,\theta) \end{bmatrix} \qquad \ldots(8.2.17)$$

By setting $s_1 = 0$, the conditions from the above equation yield

$$\mathbf{D_{11}b^+ + D_{12}b^- = D_{13}a^+ + D_{14}a^-} \qquad \ldots(8.2.18)$$

where

$$\mathbf{D_{11}} = \begin{bmatrix} Z^c_{N,n1} & Z^c_{N,n2} & Z^c_{N,n3} & Z^c_{N,n4} \\ Z^c_{M,n1} & Z^c_{M,n2} & Z^c_{M,n3} & Z^c_{M,n4} \\ \psi^c_{n1} & \psi^c_{n2} & \psi^c_{n3} & \psi^c_{n4} \\ 1 & 1 & 1 & 1 \end{bmatrix}, \qquad \mathbf{D_{12}} = \begin{bmatrix} Z^c_{N,n5} & Z^c_{N,n6} & Z^c_{N,n7} & Z^c_{N,n8} \\ Z^c_{M,n5} & Z^c_{M,n6} & Z^c_{M,n7} & Z^c_{M,n8} \\ \psi^c_{n5} & \psi^c_{n6} & \psi^c_{n7} & \psi^c_{n8} \\ 1 & 1 & 1 & 1 \end{bmatrix}, \qquad \text{...(8.2.19 a, b)}$$

$\mathbf{D_{13}}$ and $\mathbf{D_{14}}$ are similar to $\mathbf{D_{11}}$, $\mathbf{D_{12}}$, respectively, except that the coefficients, Z's and ψ_{nb}, are used for the pipe.

The other boundary conditions, which are

$$\begin{bmatrix} T_{s\theta}(s_1,\theta) \\ V_s(s_1,\theta) \\ U_n(s_1,\theta) \\ \dfrac{\partial W_n(s_1,\theta)}{\partial s} \end{bmatrix} = \begin{bmatrix} T^c_{s\theta}(s_1,\theta) \\ V^c_s(s_1,\theta) \\ U^c_n(s_1,\theta) \\ \dfrac{\partial W^c_n(s_1,\theta)}{\partial s} \end{bmatrix} \qquad \text{...(8.2.20)}$$

produce another equation of motion

$$\mathbf{D_{21}b^+ + D_{22}b^- = D_{23}a^+ + D_{24}a^-} \qquad \text{...(8.2.21)}$$

where

$$\mathbf{D_{21}} = \begin{bmatrix} Z^c_{T,n1} & Z^c_{T,n2} & Z^c_{T,n3} & Z^c_{T,n4} \\ Z^c_{V,n1} & Z^c_{V,n2} & Z^c_{V,n3} & Z^c_{V,n4} \\ \alpha^c_{n1} & \alpha^c_{n2} & \alpha^c_{n3} & \alpha^c_{n4} \\ k^c_{n1} & k^c_{n2} & k^c_{n3} & k^c_{n4} \end{bmatrix}, \qquad \mathbf{D_{22}} = \begin{bmatrix} Z^c_{T,n5} & Z^c_{T,n6} & Z^c_{T,n7} & Z^c_{T,n8} \\ Z^c_{V,n5} & Z^c_{V,n6} & Z^c_{V,n7} & Z^c_{V,n8} \\ \alpha^c_{n5} & \alpha^c_{n6} & \alpha^c_{n7} & \alpha^c_{n8} \\ k^c_{n5} & k^c_{n6} & k^c_{n7} & k^c_{n8} \end{bmatrix} \qquad \text{...(8.2.22 c, d)}$$

The matrices $\mathbf{D_{23}}$, and $\mathbf{D_{24}}$ are similar to $\mathbf{D_{21}}$, and $\mathbf{D_{22}}$, respectively, except that the coefficients are for the pipe.

Because the wavenumbers of the pipe in the positive and the negative directions are related, i.e., $\hat{k}_{nb} = -\hat{k}_{n(b+4)}$ and $\hat{k}^c_{nb} = -\hat{k}^c_{n(b+4)}$ where b = 1, 2, 3 and 4, the relationships for the pipe are:

$\psi_{nb} = \psi_{n(b+4)}$, $\alpha_{nb} = -\alpha_{n(b+4)}$,

$Z_{N,nb} = Z_{N,n(b+4)}$, $Z_{T,nb} = -Z_{T,n(b+4)}$, $Z_{M,nb} = Z_{M,n(b+4)}$ and $Z_{V,nb} = -Z_{V,n(b+4)}$,

and for a composite pipe as

$\psi^c_{nb} = \psi^c_{n(b+4)}$, $\alpha^c_{nb} = -\alpha^c_{n(b+4)}$,

$Z^c_{N,nb} = Z^c_{N,n(b+4)}$, $Z^c_{T,nb} = -Z^c_{T,n(b+4)}$, $Z^c_{M,nb} = Z^c_{M,n(b+4)}$ and $Z^c_{V,nb} = -Z^c_{V,n(b+4)}$.

This leads to

$$\mathbf{D}_{11} = \mathbf{D}_{12}, \quad \mathbf{D}_{13} = \mathbf{D}_{14}, \quad \mathbf{D}_{21} = -\mathbf{D}_{22} \quad \text{and} \quad \mathbf{D}_{23} = -\mathbf{D}_{24} \qquad \ldots(8.2.23)$$

Substituting for the relationships given in equation (8.2.23) into equations (8.2.18) and (8.2.21), and arranging terms gives

$$\mathbf{b}^+ + \mathbf{b}^- = \mathbf{D}_{11}^{-1}\mathbf{D}_{13}\left(\mathbf{a}^+ + \mathbf{a}^-\right) \qquad \ldots(8.2.24\text{ a})$$

$$\mathbf{b}^+ - \mathbf{b}^- = \mathbf{D}_{21}^{-1}\mathbf{D}_{23}\left(\mathbf{a}^+ - \mathbf{a}^-\right) \qquad \ldots(8.2.24\text{ b})$$

The boundary conditions at s = s_2 are similar to that at s = s_1, and give

$$\mathbf{T}_f\mathbf{b}^+ + \mathbf{T}_f^{-1}\mathbf{b}^- = \mathbf{D}_{11}^{-1}\mathbf{D}_{13}\mathbf{c}^+ \qquad \ldots(8.2.25\text{ a})$$

$$\mathbf{T}_f\mathbf{b}^+ - \mathbf{T}_f^{-1}\mathbf{b}^- = \mathbf{D}_{21}^{-1}\mathbf{D}_{23}\mathbf{c}^+ \qquad \ldots(8.2.25\text{ b})$$

where $\mathbf{T}_f = \begin{bmatrix} e^{j\hat{k}_{n1}^c s_{cp}} & 0 & 0 & 0 \\ 0 & e^{j\hat{k}_{n2}^c s_{cp}} & 0 & 0 \\ 0 & 0 & e^{j\hat{k}_{n3}^c s_{cp}} & 0 \\ 0 & 0 & 0 & e^{j\hat{k}_{n4}^c s_{cp}} \end{bmatrix}$ is the transfer matrix , and $\qquad \ldots(8.2.25\text{ c})$

$s_{cp} = s_2 - s_1$ is the length of the composite section normalised to the radius of the pipe.

From equation (8.2.25), the relationships between the vectors $\mathbf{b}^+$ and $\mathbf{b}^-$ to the vector $\mathbf{c}^+$ are found to be

$$\mathbf{b}^+ = \frac{1}{2}\mathbf{T}_f^{-1}\mathbf{G}_+\mathbf{c}^+ \qquad \ldots(8.2.26\text{ a})$$

$$\mathbf{b}^+ = \frac{1}{2}\mathbf{T}_f\mathbf{G}_-\mathbf{c}^+ \qquad \ldots(8.2.26\text{ b})$$

where $\mathbf{G}_+ = \mathbf{D}_{11}^{-1}\mathbf{D}_{13} + \mathbf{D}_{21}^{-1}\mathbf{D}_{23}$ and

$$\mathbf{G}_- = \mathbf{D}_{11}^{-1}\mathbf{D}_{13} - \mathbf{D}_{21}^{-1}\mathbf{D}_{23} \qquad \ldots(8.2.26\text{ c, d})$$

By substituting the vectors $\mathbf{b}^+$ and $\mathbf{b}^-$ from equation (8.2.26) into equation (8.2.24), the vector $\mathbf{a}^-$ and $\mathbf{c}^+$ can be determined in terms of the incident vector $\mathbf{a}^+$ as given by

$$\mathbf{a}^- = \mathbf{G}_-^{-1}\left\{\mathbf{T}_f^{-1}\mathbf{G}_+[\mathbf{T}_f\mathbf{G}_- - \mathbf{G}_+\mathbf{G}_-^{-1}\mathbf{T}_f^{-1}\mathbf{G}_+]^{-1}[\mathbf{G}_- - \mathbf{G}_+\mathbf{G}_-^{-1}\mathbf{G}_+] - \mathbf{G}_+\right\}\mathbf{a}^+ \qquad \ldots(8.2.27\text{ a})$$

$$\mathbf{c}^+ = [\mathbf{T}\mathbf{G}_- - \mathbf{G}_+\mathbf{G}_-^{-1}\mathbf{T}^{-1}\mathbf{G}_+]^{-1}[\mathbf{G}_- - \mathbf{G}_+\mathbf{G}_-^{-1}\mathbf{G}_+]\mathbf{a}^+ \qquad \ldots(8.2.27\text{ b})$$

Once the all vectors are established, the pipe motion at any position can be obtained, and is given by:

$$\mathbf{w}_{s1-} = \mathbf{a}^{+} + \mathbf{a}^{-} \quad ; \qquad s < s_{1-}$$

$$\mathbf{w}_{s1+} = \mathbf{b}^{+} + \mathbf{b}^{-} \quad ; \qquad s_{1+} < s < s_{2-} \qquad \ldots(8.2.28\ a, b, c)$$

$$\mathbf{w}_{s2+} = \mathbf{c}^{+} \quad ; \qquad s < s_{2+}$$

8.2.2.2 Wave Method

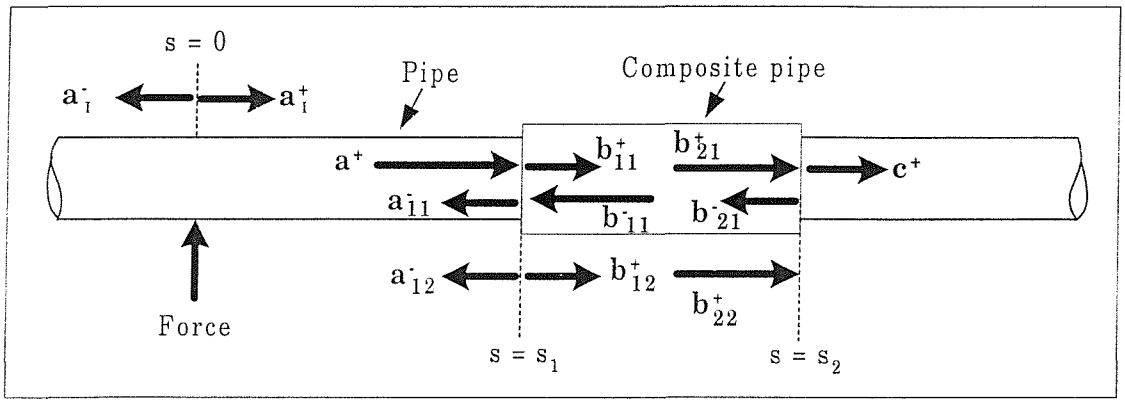

Figure 8.5: Diagram of the reflection and transmission of waves at the discontinuity for any circumferential mode n.

The analysis for the motion of an infinite pipe from the wave point of view is presented in this section. As discussed by Cremer and Heckl [17], and Mace [54], the reflected and transmitted waves for any circumferential mode n are in proportion to the incident wave at the discontinuity. These constants of proportionality are determined from the reflection and transmission matrices. The configuration shown in figure 8.5 represents the transmitted and reflected waves at the discontinuous section of composite pipe. The reflected wave $\mathbf{a}_{11}^{-}$ and the transmitted wave $\mathbf{b}_{11}^{+}$ arise at position $s = s_1$ from the

incident wave $\mathbf{a}^+$. The reflected wave $\mathbf{b}_{21}^-$ and transmitted wave $\mathbf{c}^+$ are the result of the wave $\mathbf{b}_{21}^+$ striking the boundary at s = s_2, while the wave $\mathbf{b}_{11}^-$ produces the reflected wave $\mathbf{b}_{12}^+$ and the transmitted wave $\mathbf{a}_{12}^-$ at the boundary s = s_1.

The relationships of the reflected and transmitted waves to the incident wave are given by:

$$\mathbf{a}_{11}^- = \mathbf{R}_1\mathbf{a}^+,\ \mathbf{b}_{11}^+ = \mathbf{T}_1\mathbf{a}^+,\ \mathbf{a}_{12}^- = \mathbf{T}_2\mathbf{b}_{11}^-,\ \mathbf{b}_{12}^+ = \mathbf{R}_2\mathbf{b}_{11}^-,\ \mathbf{c}^+ = \mathbf{T}_2(\mathbf{b}_{21}^+ + \mathbf{b}_{22}^+),$$

$$\mathbf{b}_{21}^- = \mathbf{R}_2(\mathbf{b}_{21}^+ + \mathbf{b}_{22}^+),\ \mathbf{b}_{21}^+ = \mathbf{T}_f\mathbf{b}_{11}^+,\ \mathbf{b}_{11}^- = \mathbf{T}_f\mathbf{b}_{21}^-, \mathbf{b}_{22}^+ = \mathbf{T}_f\mathbf{b}_{12}^+ \qquad \ldots(8.2.29)$$

where $\mathbf{R}_1$ and $\mathbf{R}_s$ are the reflection matrixes of waves in the pipe and in the composite pipe section at the discontinuity, respectively,

$\mathbf{T}_1$ is the transmission matrixes of waves in the pipe to the composite section

$\mathbf{T}_2$ is the transmission matrixes of waves in the composite section to the pipe,

$\mathbf{T}_f$ is the transfer matrix given in equation (8.2.25 c).

With a set of the boundary conditions obtained from equations (8.2.17) and (8.2.20), the equation of motion at s = s_2 can be established as

$$\mathbf{D}_{11}(\mathbf{b}_{21}^+ + \mathbf{b}_{22}^+) + \mathbf{D}_{12}\mathbf{b}_{21}^- = \mathbf{D}_{13}\mathbf{c}^+ \qquad \ldots(8.2.30\ a)$$

$$\mathbf{D}_{21}(\mathbf{b}_{21}^+ + \mathbf{b}_{22}^+) + \mathbf{D}_{22}\mathbf{b}_{21}^- = \mathbf{D}_{23}\mathbf{c}^+ \qquad \ldots(8.2.30\ b)$$

where the all matrices are given in equations (8.2.19) and (8.2.22).

Substituting for $\mathbf{b}_{21}^-$ and $\mathbf{c}^+$ from equation (8.2.29) into equation (8.2.30) yields

$$\mathbf{D}_{11}+\mathbf{D}_{11}\mathbf{R}_2=\mathbf{D}_{13}\mathbf{T}_2 \qquad \ldots(8.2.31\text{ a})$$

$$\mathbf{D}_{21}-\mathbf{D}_{21}\mathbf{R}_2=\mathbf{D}_{23}\mathbf{T}_2 \qquad \ldots(8.2.31\text{ b})$$

The transmission matrix, $\mathbf{T}_2$, is found by solving the above equation and the reflection matrix, $\mathbf{R}_2$, is obtained by substituting $\mathbf{T}_2$ back into equation (8.2.31 a). Doing this gives:

$$\mathbf{T}_2=2\left[\mathbf{D}_{11}^{-1}\mathbf{D}_{13}+\mathbf{D}_{21}^{-1}\mathbf{D}_{23}\right]^{-1} \qquad \ldots(8.2.32\text{ a})$$

$$\mathbf{R}_2=2\,\mathbf{D}_{11}^{-1}\mathbf{D}_{13}\left[\mathbf{D}_{11}^{-1}\mathbf{D}_{13}+\mathbf{D}_{21}^{-1}\mathbf{D}_{23}\right]^{-1}-\mathbf{I} \qquad \ldots(8.2.32\text{ b})$$

where $\mathbf{I}$ is the identity matrix.

At $s = s_1$, a set of the boundary conditions from equations (8.2.17) and (8.2.20) gives

$$\mathbf{D}_{11}(\mathbf{b}_{11}^{+}+\mathbf{b}_{12}^{+})+\mathbf{D}_{12}\mathbf{b}_{11}^{-}=\mathbf{D}_{13}\mathbf{a}^{+}+\mathbf{D}_{14}(\mathbf{a}_{11}^{-}+\mathbf{a}_{12}^{-}) \qquad \ldots(8.2.33\text{ a})$$

$$\mathbf{D}_{21}(\mathbf{b}_{11}^{+}+\mathbf{b}_{12}^{+})+\mathbf{D}_{22}\mathbf{b}_{11}^{-}=\mathbf{D}_{23}\mathbf{a}^{+}+\mathbf{D}_{24}(\mathbf{a}_{11}^{-}+\mathbf{a}_{12}^{-}) \qquad \ldots(8.2.33\text{ b})$$

Substituting for $\mathbf{a}_{11}^{-}$, $\mathbf{a}_{12}^{-}$, $\mathbf{b}_{11}^{-}$ and $\mathbf{b}_{12}^{-}$ from equation (8.2.29) into equation (8.2.33), and arranging the terms yields

$$\left[\mathbf{D}_{11}\mathbf{R}_2+\mathbf{D}_{12}-\mathbf{D}_{14}\mathbf{T}_2\right]\mathbf{b}_{11}^{-}=\left[-\mathbf{D}_{11}\mathbf{T}_1+\mathbf{D}_{13}+\mathbf{D}_{14}\mathbf{R}_1\right]\mathbf{a}^{+} \qquad \ldots(8.2.34\text{ a})$$

$$\left[\mathbf{D}_{21}\mathbf{R}_2+\mathbf{D}_{22}-\mathbf{D}_{24}\mathbf{T}_2\right]\mathbf{b}_{11}^{-}=\left[-\mathbf{D}_{21}\mathbf{T}_1+\mathbf{D}_{23}+\mathbf{D}_{24}\mathbf{R}_1\right]\mathbf{a}^{+} \qquad \ldots(8.2.34\text{ b})$$

In equation (8.2.23), it was shown that $\mathbf{D_{11}} = \mathbf{D_{12}}$, $\mathbf{D_{13}} = \mathbf{D_{14}}$, $\mathbf{D_{21}} = -\mathbf{D_{22}}$ and $\mathbf{D_{23}} = -\mathbf{D_{24}}$. Substituting these relationships into equation (8.2.34) and noting the relationship given in equation (8.2.31) shows that the left-hand sides of equations (8.2.34 a) and (8.2.34 b) are equal to zero. Thus:

$$-\mathbf{D}_{11}\mathbf{T}_1 + \mathbf{D}_{13} + \mathbf{D}_{13}\mathbf{R}_1 = 0 \qquad \text{...(8.2.35 a)}$$

$$-\mathbf{D}_{21}\mathbf{T}_1 + \mathbf{D}_{23} - \mathbf{D}_{23}\mathbf{R}_1 = 0 \qquad \text{...(8.2.35 b)}$$

Using a similar method as used to determine $\mathbf{T}_2$ and $\mathbf{R}_2$, $\mathbf{T}_1$ and $\mathbf{R}_1$ are found to be:

$$\mathbf{T}_1 = 2\left[\mathbf{D}_{13}^{-1}\mathbf{D}_{11} + \mathbf{D}_{23}^{-1}\mathbf{D}_{21}\right]^{-1} \qquad \text{...(8.2.36 a)}$$

$$\mathbf{R}_1 = 2\,\mathbf{D}_{13}^{-1}\mathbf{D}_{11}\left[\mathbf{D}_{13}^{-1}\mathbf{D}_{11} + \mathbf{D}_{23}^{-1}\mathbf{D}_{21}\right]^{-1} - \mathbf{I} \qquad \text{...(8.2.36 b)}$$

Once the reflection and transmission matrixes are determined, the wave vectors; i.e. $\mathbf{a}_{11}^{-}$, $\mathbf{a}_{12}^{-}$, $\mathbf{b}_{11}^{-}$, $\mathbf{b}_{11}^{+}$, $\mathbf{b}_{12}^{+}$ and $\mathbf{c}^{+}$ can be found as follows.

$$\begin{aligned}
\mathbf{b}_{11}^{-} &= \mathbf{T}_f\mathbf{b}_{21}^{-} \\
&= \mathbf{T}_f\mathbf{R}_2(\mathbf{b}_{21}^{+} + \mathbf{b}_{22}^{+}) \\
&= \mathbf{T}_f\mathbf{R}_2\mathbf{T}_f(\mathbf{b}_{11}^{+} + \mathbf{b}_{12}^{+}) \\
&= \mathbf{T}_f\mathbf{R}_2\mathbf{T}_f(\mathbf{T}_1\mathbf{a}^{+} + \mathbf{R}_2\mathbf{b}_{11}^{-}) \\
&= \left[\mathbf{I} - \mathbf{T}_f\mathbf{R}_2\mathbf{T}_f\mathbf{R}_2\right]^{-1}\mathbf{T}_f\mathbf{R}_2\mathbf{T}_f\mathbf{T}_1\mathbf{a}^{+}
\end{aligned} \qquad \text{...(8.2.37)}$$

The wave vector $\mathbf{c}^{+}$ is

$$\begin{aligned}
\mathbf{c}^{+} &= \mathbf{T}_2(\mathbf{b}_{21}^{+} + \mathbf{b}_{22}^{+}) \\
&= \mathbf{T}_2\mathbf{T}_f(\mathbf{b}_{11}^{+} + \mathbf{b}_{12}^{+}) \\
&= \mathbf{T}_2\mathbf{T}_f(\mathbf{T}_1\mathbf{a}^{+} + \mathbf{R}_2\mathbf{b}_{11}^{-})
\end{aligned} \qquad \text{...(8.2.38)}$$

Substituting $\mathbf{b}_{11}^{-}$ obtained from equation (8.2.37) into equation (8.2.38) and arranging the terms give

$$\mathbf{c}^{+} = \mathbf{T}_2\mathbf{T}_f\left\{\mathbf{I}+\mathbf{R}_2\left[\mathbf{I}-\mathbf{T}_f\mathbf{R}_2\mathbf{T}_f\mathbf{R}_2\right]^{-1}\mathbf{T}_f\mathbf{R}_2\mathbf{T}_f\right\}\mathbf{T}_1\mathbf{a}^{+} \qquad \ldots(8.2.39)$$

With all vectors obtained, the pipe motion at any position can be determined by the vectors of total wave motion given by

$$\begin{aligned}\mathbf{w}_{s1-} &= \mathbf{a}^{+} + \mathbf{a}_{11}^{-} + \mathbf{a}_{12}^{-} \\ &= \mathbf{a}^{+} + \mathbf{R}_1\mathbf{a}^{+} + \mathbf{T}_2\mathbf{b}_{11}^{-} \\ &= \left\{\mathbf{I}+\mathbf{R}_1+\mathbf{T}_2\left[\mathbf{I}-\mathbf{T}_f\mathbf{R}_2\mathbf{T}_f\mathbf{R}_2\right]^{-1}\mathbf{T}_f\mathbf{R}_2\mathbf{T}_f\mathbf{T}_1\right\}\mathbf{a}^{+}\end{aligned} \qquad \ldots(8.2.40\text{ a})$$

$$\begin{aligned}\mathbf{w}_{s1+} &= \mathbf{b}_{11}^{+} + \mathbf{b}_{12}^{+} + \mathbf{b}_{11}^{-} \\ &= \mathbf{T}_1\mathbf{a}^{+} + \mathbf{R}_2\mathbf{b}_{11}^{-} + \mathbf{b}_{11}^{-} \\ &= \left\{\mathbf{I}+\left[\mathbf{I}+\mathbf{R}_2\right]\left[\mathbf{I}-\mathbf{T}_f\mathbf{R}_2\mathbf{T}_f\mathbf{R}_2\right]^{-1}\mathbf{T}_f\mathbf{R}_2\mathbf{T}_f\right\}\mathbf{T}_1\mathbf{a}^{+}\end{aligned} \qquad \ldots(8.2.40\text{ b})$$

$$\mathbf{w}_{s2+} = \mathbf{c}^{+} \qquad \ldots(8.2.40\text{ c})$$

8.2.3 Numerical Validation for the Mobility of an Infinite Pipe Having a Composite Pipe Section

In the previous section, two methods have been used to analysis the motion of an infinite pipe, in which the composite pipe section is considered as a discontinuity. Both analysis and wave methods are used as a check on each other. Since their formulae are complex, it is difficult to compare them theoretically. Hence, in this section, the comparison is carried out numerically. The numerical predictions of both methods

calculated using the pipe data given in table D.1 (appendix D) and the Nitrile rubber data in table 8.1 for the composite pipe section. The reason for choosing the Nitrile rubber in the composite part of the pipe is because of its high young's modulus in comparison with other damping materials (Cremer and Heckl [17]). This means the composite section should have more effect on the incident wave and thus give distinction of the mobilities at both ends of the section. The mobilities are predicted at the positions of discontinuities, which are $s_1 = 50$ and $s_2 = 52$. The predicted mobilities obtained from both methods are compared for each circumferential mode and are shown in figure 8.6.

Table 8.1: Nitrile Rubber data

E_d (N/m^2)	ρ_d (kg/m^3)	ν_d	t (mm)	η_d
$3.3*10^9$	1100	0.4	0.25	0.8

The numerical results show clearly that both methods give the same results. However, the wave method seems to provide more physical information on the dynamic behaviour of an infinite pipe with a composite pipe section. This information such as the reflection of the incident wave and the wave motion in the composite part is expressed by the reflection matrixes, $\mathbf{R}_1$ and $\mathbf{R}_2$, and the transmission matrixes, $\mathbf{T}_1$ and $\mathbf{T}_2$. In the rest of this chapter, this method will be used for the simulation presented.

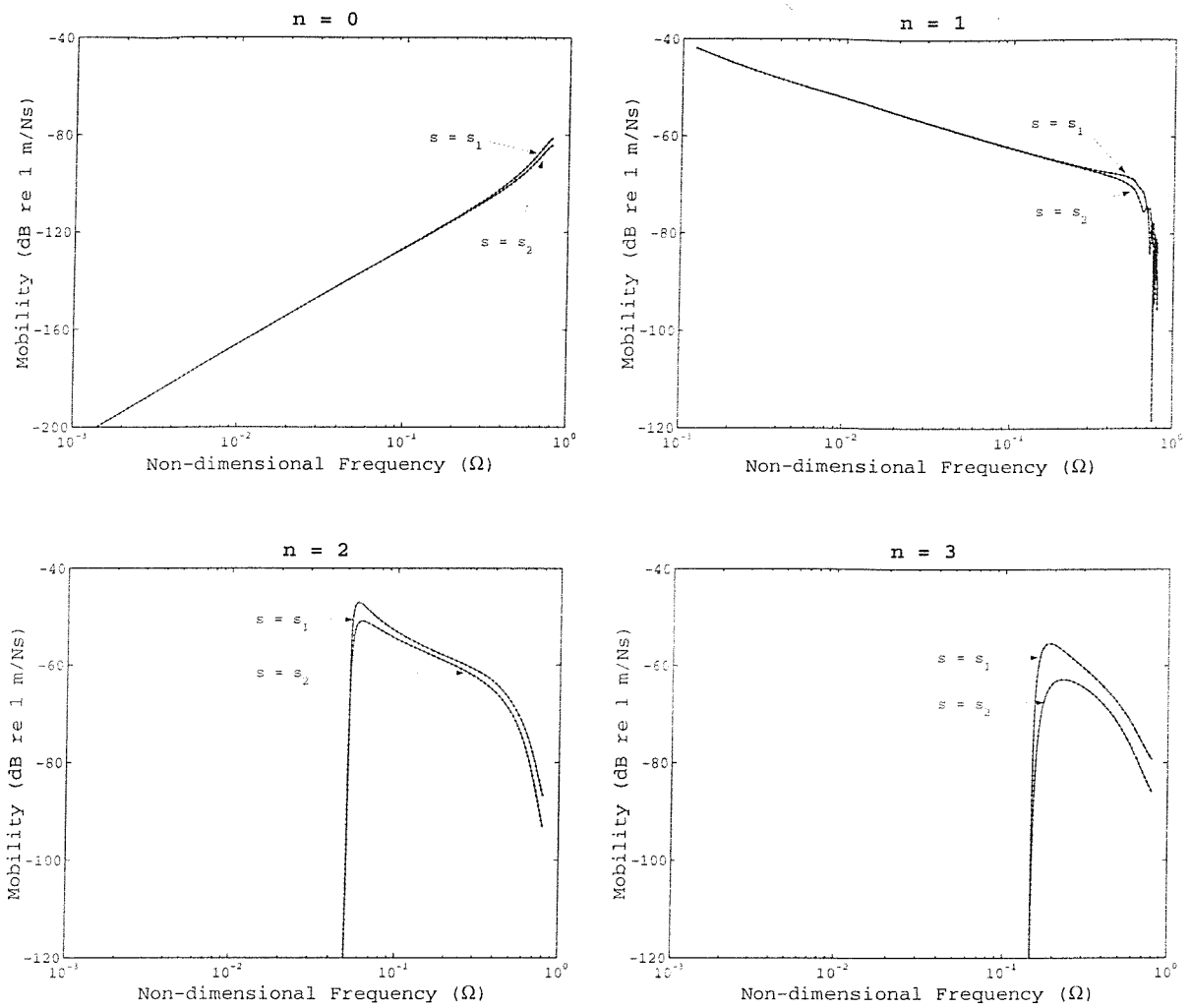

Figure 8.6: Amplitude of the mobility for the n = 0-3 modes of an infinite pipe having a composite pipe section, whose boundaries from the excitation are $s_1 = 50$ and $s_2 = 52$; ... Analytical method, __ Wave method.

8.2.4 Evaluation of Passive Control with a Damping Material

Damping can be used to reduce vibration by means of energy dissipation. A damping material can be used to increase the damping of the structure for this purpose. Apart from damping, the Young's modulus of a material is also an important property used to control vibration. In this section, the effects of stiffness and damping of an attached layer on vibration transmission along the pipe is investigated.

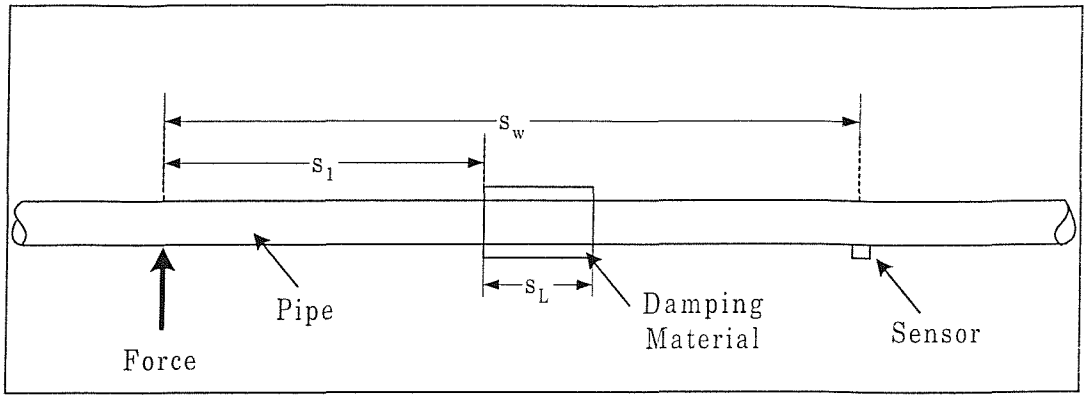

Figure 8.7: Diagram of an infinite pipe where the composite pipe section is formed by attaching a damping material.

An unconstrained-layer of damping material is attached to an infinite pipe to form a composite pipe section as shown in figure 8.7. With such a composite section, the analysis of the pipe motion is similar to that described in section 8.2 where the complex modulus of the damping material is given by $E_d^{'} = E_d(1 + j\eta_d)$ where η_d is the loss factor of the damping material.

From equation (8.2.40 c), the vector of waves downstream of the composite section at position s_w is given by

$$\mathbf{w}(s = s_w, \theta) = \begin{bmatrix} e^{j\hat{k}_{n1}(s_w - s_1 - s_L)} & 0 & 0 & 0 \\ 0 & e^{j\hat{k}_{n2}(s_w - s_1 - s_L)} & 0 & 0 \\ 0 & 0 & e^{j\hat{k}_{n3}(s_w - s_1 - s_L)} & 0 \\ 0 & 0 & 0 & e^{j\hat{k}_{n4}(s_w - s_1 - s_L)} \end{bmatrix} \mathbf{c}^+ \qquad \ldots(8.2.41)$$

where vector $\mathbf{c}^+$ is obtained from equation (8.2.39).

Since the transmission of propagating flexural waves is of concern in this thesis, the composite section and sensor position are set so that $s_1 = 50$, $s_w = 100$ and s_L is varied. This means that they are in the far field of the excitation force, where there are no standing near field and near field waves. The effects of the Young's modulus and the

loss factor of the attached material (Nitrile rubber) to the pipe motion are examined and shown for the n = 0-2 modes in figure 8.8-8.10 and 8.11-8.13, respectively. The investigation is also carried out for the several lengths (s_L) of the damping material (Nitrile rubber), the results of which are presented in figures 8.14-8.16.

Figures 8.8, 8.9, 8.11 and 8.12 show that the changes of the Young's modulus and the loss factor of the attached material have a negligible effect on the pipe motion for the n = 0 and n = 1 modes, especially at low frequencies. This is because at low frequencies the longitudinal wave for the n = 0 mode (extensional mode), and flexural wave for the n = 1 modes (bending mode) have long wavelengths compared with the composite section. At high frequencies where the wavelengths are shorter, an axial mode can be formed in the composite section due to the interference of the transmitted and reflected waves at the boundary of this section so that the attenuation of the incident wave for both modes can be obtained (although not shown in this thesis).

Unlike the n = 0 and n = 1 mode, the Young's modulus and the loss factor of the attached material have a greater affect on the pipe motion for the n = 2 mode. Figures 8.10 and 8.13 show that the attenuation increases with increasing Young's modulus and loss factor. The higher stiffness gives greater attenuation because the high stiffness of the composite section resists the changing shape of the pipe in the circumferential direction.

As discussed above, it clearly shows that for effective passive control using an unconstrained-layer material bonded to the pipe a high Young's modulus or high damping of such material is required. Even though the damping materials such as Polyvinylchloride, Polystyrene and Nitrile rubber normally have a low Young's modulus about $0.3*10^9$ - $3.3*10^9$ Nm^{-2}, they have a high loss factor about 0.8-2 (Cremer and Heckl [17]). Since the loss factor of the damping material is added to the system, the effective loss factor of the system can be increased by increasing the length of such materials giving a larger attenuation as shown in figures 8.14-8.16 when the Nitrile rumber is used as the damping material.

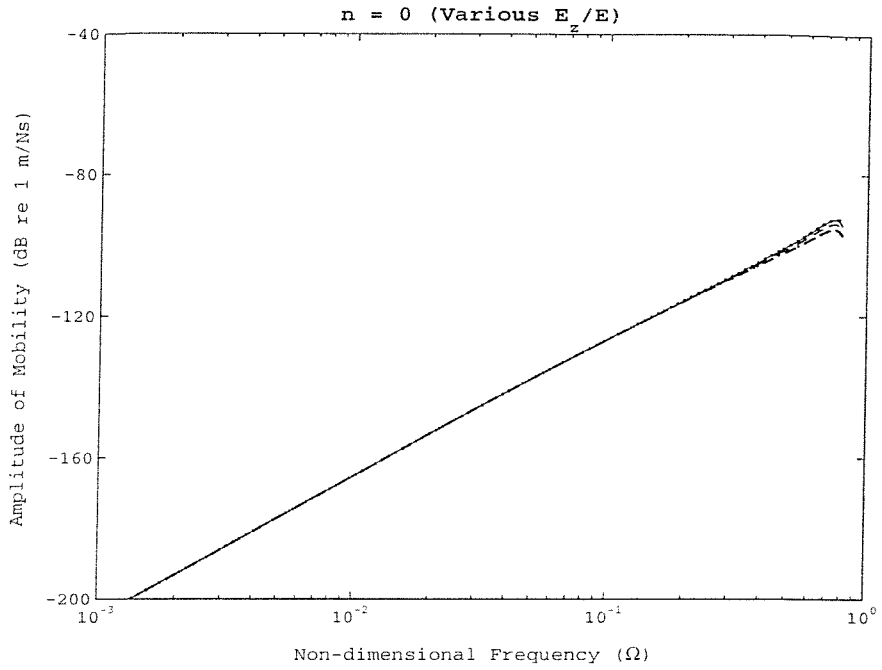

Figure 8.8: Amplitude of the mobility of the n = 0 mode of an infinite pipe with the attached material having s_L = 2, η_d = 0.8; __ E_d/E= 0.01, _ _ E_d/E= 1, _.._ E_d/E= 100, ...without the attached material.

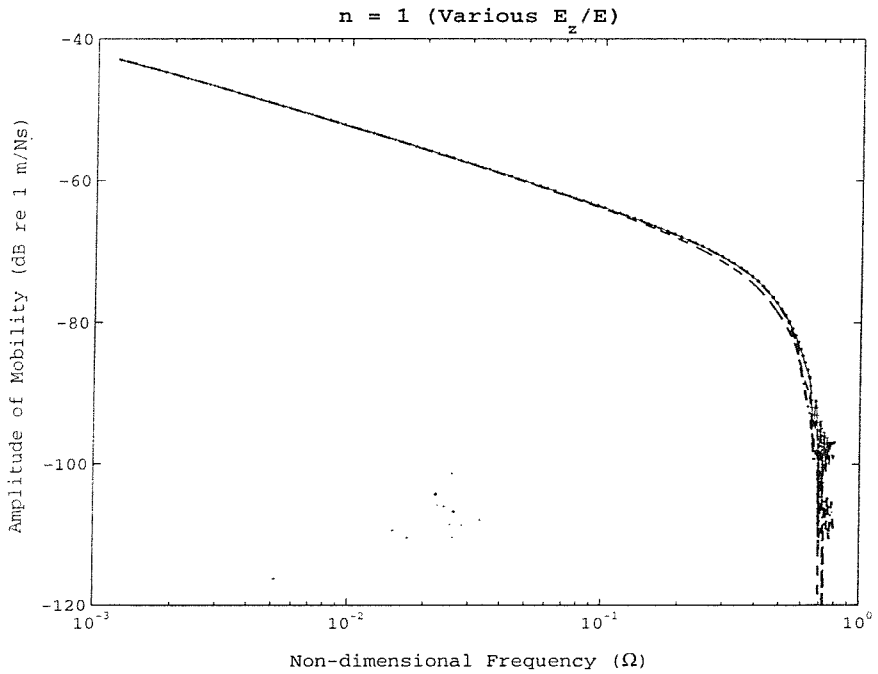

Figure 8.9: Amplitude of the mobility of the n = 1 mode of an infinite pipe with the attached material having s_L = 2, η_d = 0.8; __ E_d/E= 0.01, _ _ E_d/E= 1, _ . _E_d/E= 100, ...without the attached material.

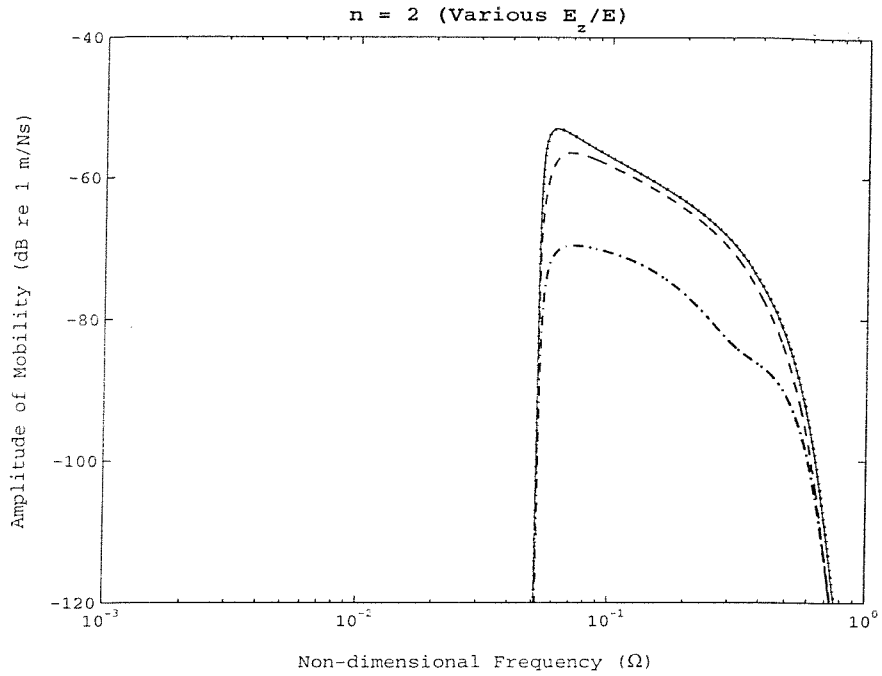

Figure 8.10: Amplitude of the mobility of the n = 2 mode of an infinite pipe with the attached material having s_L = 2, η_d = 0.8; __ E_d/E= 0.01, _ _ E_d/E= 1, _ . _E_d/E= 100, ...without the attached material.

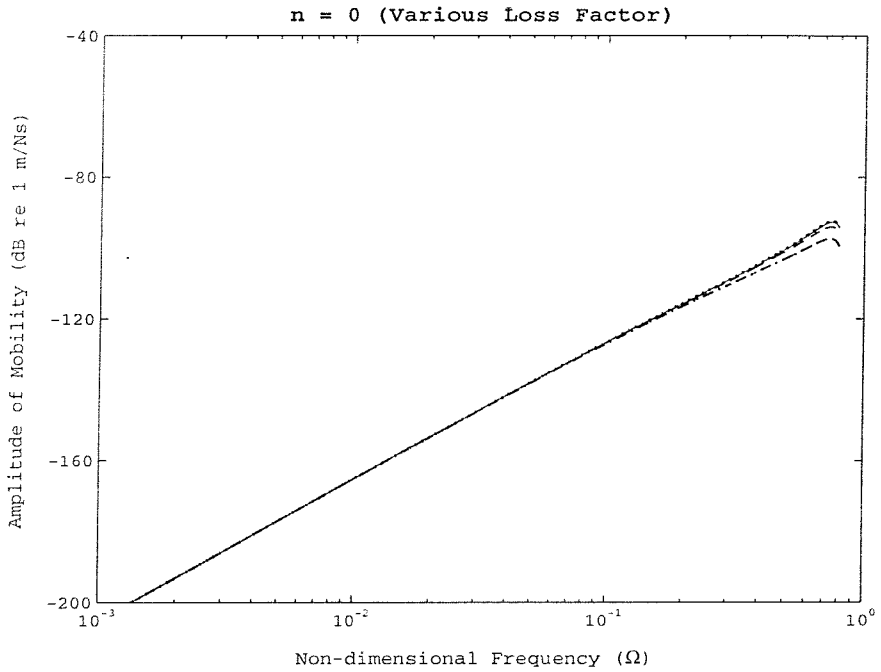

Figure 8.11: Amplitude of the mobility of the n = 0 mode of an infinite pipe with the attached material having s_L = 2, E_d/E = 0.83; __η_d = 0.1, _ _η_d = 1, _ .. _η_d = 10, ...without the attached material.

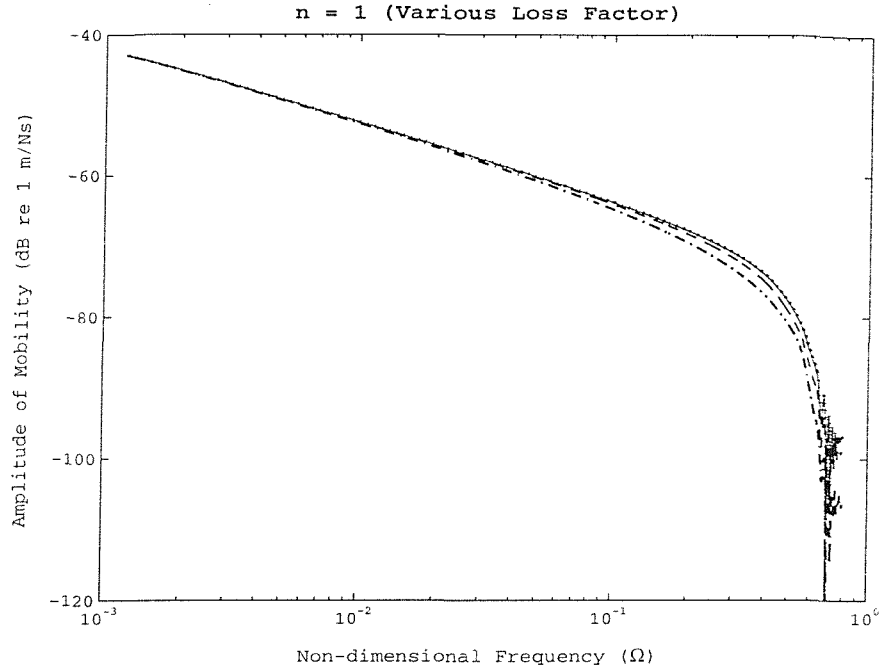

Figure 8.12: Amplitude of the mobility of the n = 1 mode of an infinite pipe with the attached material having s_L = 2, E_d/E = 0.83; __ η_d = 0.1, _ _ η_d = 1, _ .. _ η_d = 10, ...without the attached material.

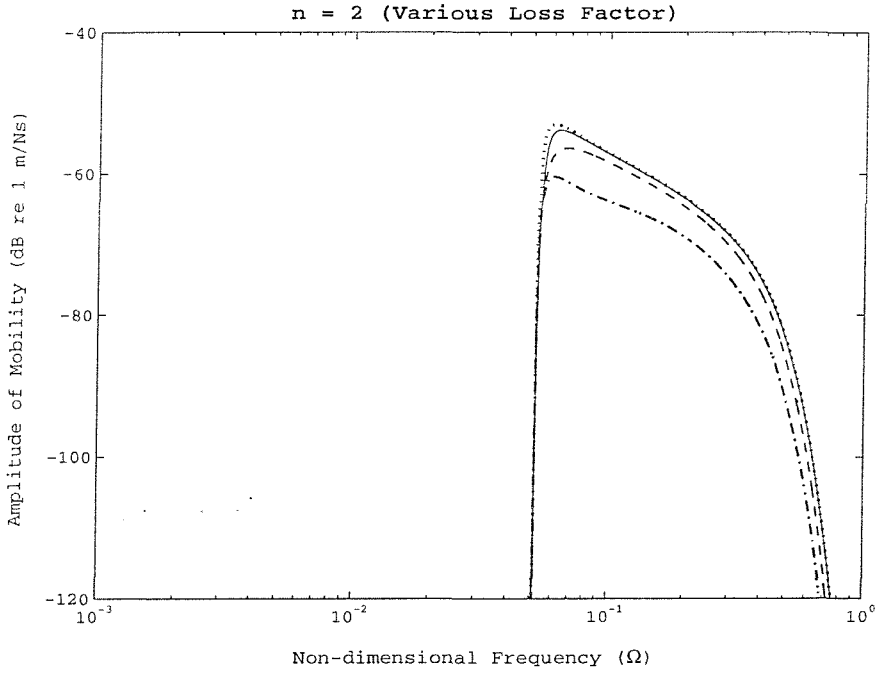

Figure 8.13: Amplitude of the mobility of the n = 2 mode of an infinite pipe with the attached material having s_L = 2, E_d/E = 0.83; __ η_d = 0.1, _ _ η_d = 1, _ .. _ η_d = 10, ...without the attached material.

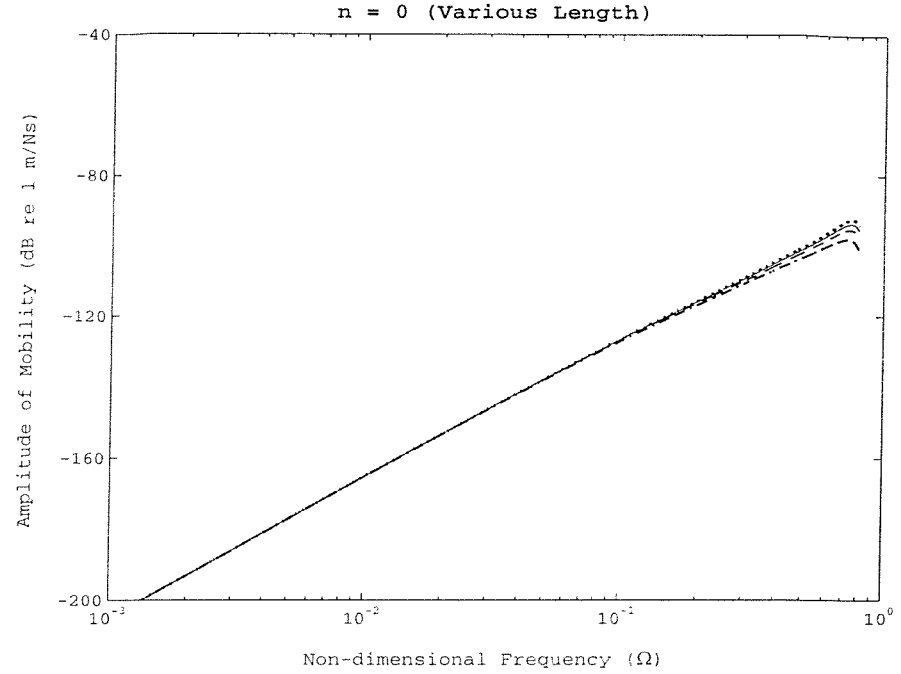

Figure 8.14: Amplitude of the mobility of the n = 0 mode of an infinite pipe with the damping material having E_d/E = 0.83 and η_d = 0.8; __ s_L = 2, _ _ s_L = 5, _ .. _ s_L = 20, ...without the damping material.

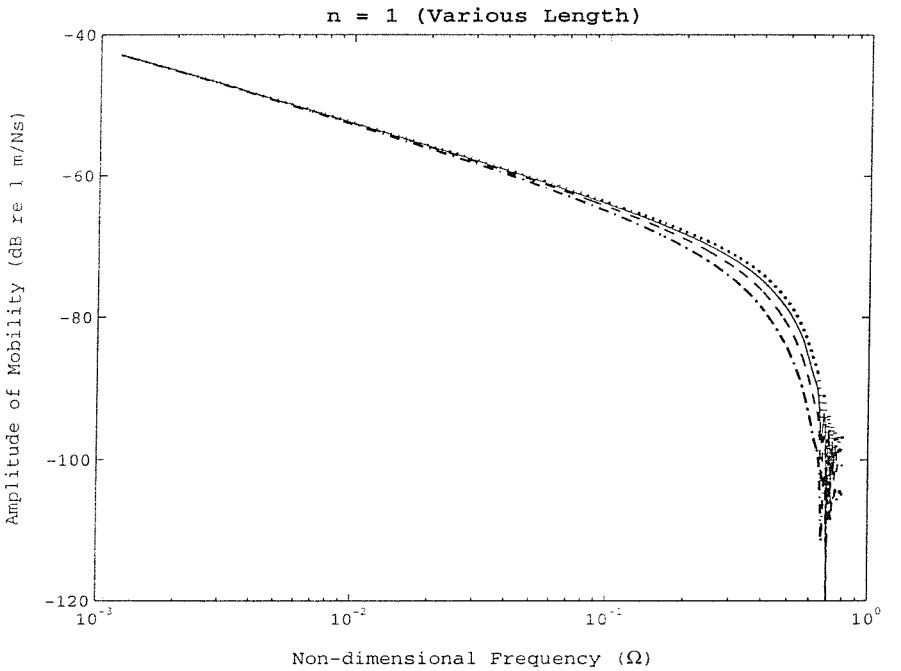

Figure 8.15: Amplitude of the mobility of the n = 1 mode of an infinite pipe with the damping material having E_d/E = 0.83 and η_d = 0.8; __ s_L = 2, _ _ s_L = 5, _ .. _ s_L = 20, ...without the damping material.

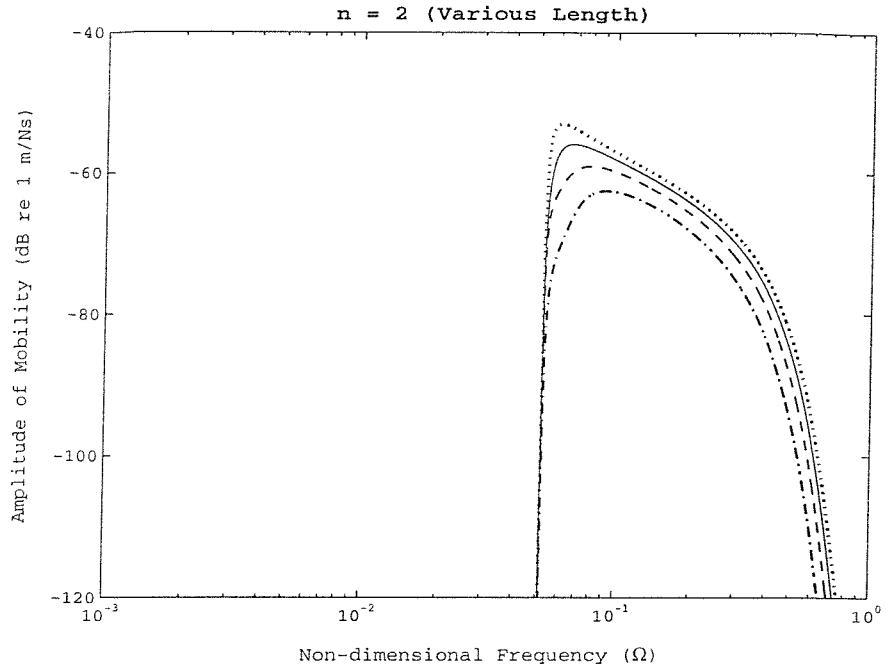

Figure 8.16: Amplitude of the mobility of the n = 2 mode of an infinite pipe with the damping material having $E_d/E = 0.83$ and $\eta_d = 0.8$; __ $s_L = 2$, _ _ $s_L = 5$, _ .. _ $s_L = 20$, ...without the damping material.

8.3 Adaptive-passive Control for Infinite Pipes by Tuning Piezoelectric Shunt

8.3.1 Static Model of a Shunted PZT Element

The configuration of a composite pipe section with a PZT element shunted by an external circuit is shown in figure 8.17.a. It is well known that a piezoelectric material has the ability of converting a mechanical strain to an electrical charge called the direct piezoelectric effect (Morgan Matroc [27]). From the electrical point of view, this material is equivalent as the current source shown in figure 8.17.b or the voltage source in figure 8.17.c where q_z is the electrical charge generated by the PZT element, V_z is the open circuit voltage generated by the PZT element, and C_z is the capacitance of the PZT element .

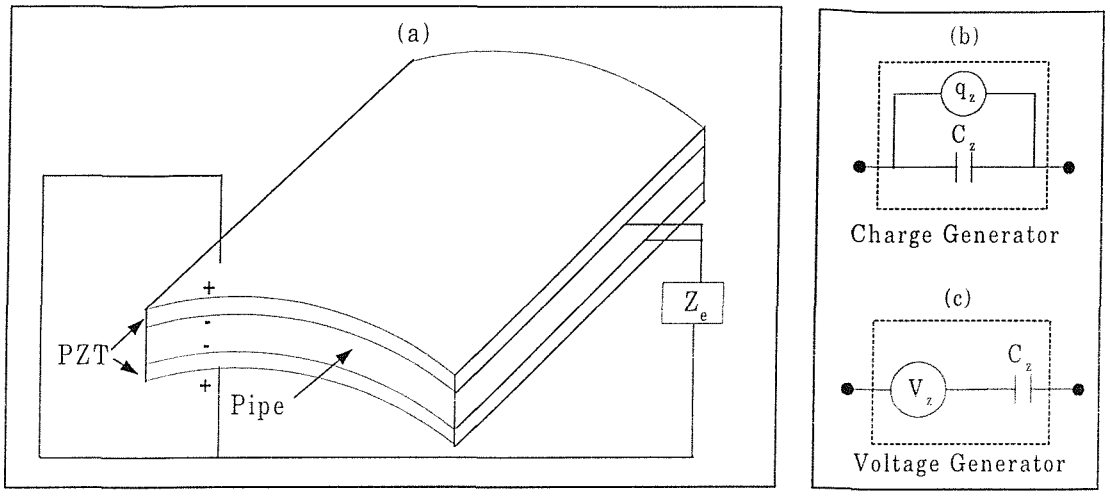

Figure 8.17: Diagram of the composite pipe with a PZT element connected to a shunt circuit; a) the PZT element shunted with the electrical impedance Z_e, b) An electrical equivalent of the PZT element as the current source, c) An electrical equivalent of the PZT element as the voltage source.

The electro-mechanical equation for piezoelectric plates or pipes can be given by (Lee [29])

$$\begin{bmatrix} \sigma_s^z \\ \sigma_\theta^z \\ \sigma_{s\theta}^z \end{bmatrix} = [C]\left(\begin{bmatrix} e_s \\ e_\theta \\ e_{s\theta} \end{bmatrix} - E_3 d_{31}\begin{bmatrix} 1 \\ 1 \\ 0 \end{bmatrix}\right) \qquad \ldots(8.3.1)$$

$$\text{where } [C]=\begin{bmatrix} \frac{E_z}{1-\nu_z^2} & \frac{\nu_z E_z}{1-\nu_z^2} & 0 \\ \frac{\nu_z E_z}{1-\nu_z^2} & \frac{\nu_z E_z}{1-\nu_z^2} & 0 \\ 0 & 0 & \frac{2E_z}{1+\nu_z} \end{bmatrix} \qquad \ldots(8.3.2)$$

E_3 is the electric field, and

E_z is the Young's modulus of the short-circuit PZT.

The electrical displacement on the surface of the PZT element is given by

$$D_3 = \varepsilon_{33} E_3 + d_{31}(\sigma_s^z + \sigma_\theta^z) \qquad \ldots(8.3.3)$$

Substituting for the stresses from equation (8.3.1) gives

$$D_3 = \varepsilon_{33} E_3 + b_{31}(e_s + e_\theta) \qquad \ldots(8.3.4)$$

where $b_{31} = \dfrac{d_{31} E_z}{1 - \nu_z}$

From Maxwell's equation, the electric field, E_3, is related to the electric potential by

$$V_z = -\int_0^{h_z} E_3 dz = \frac{A_z}{C_z}[b_{31}(e_s + e_\theta) - D_3] \qquad \ldots(8.3.5)$$

where h_z is the thickness of the PZT element,

A_z is the surface area of the PZT element, and

$C_z = \dfrac{A\varepsilon_{33}}{h_z}$ is the capacitance of the PZT element.

For the open circuit condition, when $D_3 = 0$, the generated voltage from the PZT element is

$$V_z = j\omega A_z Z_o b_{31}(e_s + e_\theta) \qquad \ldots(8.3.6)$$

where $Z_o = \dfrac{1}{j\omega C_z}$ is the open-circuit electrical impedance of the PZT element.

Shunted with the external electrical circuit of impedance Z_s, the PZT element produces the voltage, which is given as

$$V_z = j\omega A_z Z_e b_{31}(e_s + e_\theta) \qquad \ldots(8.3.7)$$

where $Z_e = Z_s + Z_o$ is the net impedance of the PZT element shunted.

Because the electric field across the PZT element, E_3, is equal to V_z/t, by substituting for V_z from equation (8.3.7) into equation (8.3.1), the stresses in the PZT shunted with the external circuit is given by

$$\begin{bmatrix} \sigma_s^z \\ \sigma_\theta^z \\ \sigma_{s\theta}^z \end{bmatrix} = [C] \begin{bmatrix} e_s + j\omega A_z Z_e b_{31} d_{31} (e_s + e_\theta) \\ e_\theta + j\omega A_z Z_e b_{31} d_{31} (e_s + e_\theta) \\ e_{s\theta} \end{bmatrix} \qquad \ldots(8.3.8)$$

Substitution for $k_{31}^2 = \dfrac{E_z d_{31}^2}{\varepsilon_{33}}$, which is the electro-mechnical coupling factor (Morgan Matroc [27]), gives

$$\begin{bmatrix} \sigma_s^z \\ \sigma_\theta^z \\ \sigma_{s\theta}^z \end{bmatrix} = [C] \begin{bmatrix} e_s + k_{31}^2 \hat{Z}_e (e_s + e_\theta)/(1 - \nu_z) \\ e_\theta + k_{31}^2 \hat{Z}_e (e_s + e_\theta)/(1 - \nu_z) \\ e_{s\theta} \end{bmatrix} \qquad \ldots(8.3.9)$$

where $\hat{Z}_e = \dfrac{Z_e}{Z_o}$

Since $\sigma_{s\theta}^z$ is not changed by the shunted circuit, this term is omitted in the following analysis. By substituting for the matrix **C** obtained from equation (8.3.2) into equation (8.3.9) and arranging the terms, the stresses in the shunted PZT can be rewritten as

$$\begin{bmatrix} \sigma_s^z \\ \sigma_\theta^z \end{bmatrix} = \frac{E_{zn}}{1 - \nu_{zn}^2} \begin{bmatrix} e_s + \nu_{zn} e_\theta \\ \nu_{zn} e_s + e_\theta \end{bmatrix} \qquad \ldots(8.3.10)$$

$$\text{where } E_{zn} = \left(\frac{p_z^2 - q_z^2}{p_z + \nu_z q_z} \right) E_z, \qquad \ldots(8.3.11\text{ a})$$

$$\nu_{zn} = \frac{q_z + \nu_z p_z}{p_z + \nu_z q_z}, \qquad \ldots(8.3.11\ b)$$

$$p_z = 1 + \frac{k_{31}^2 \hat{Z}_e}{1-\nu_z} \text{ and}$$

$$q_z = \frac{k_{31}^2 \hat{Z}_e}{1-\nu_z}.$$

Equation (8.3.11) shows clearly that the Young's modulus and the Poisson's ratio of the PZT material can be changed with the change of the impedance of the external circuit.

8.3.2 Adaptive-passive Control with a PZT Element Shunted with a Parallel L-R Circuit

It was pointed out by Wu [62], Wu and Bicos [63] that the inherent resistance of the inductor should be considered when a series L-R circuit (L is the inductance and R is the resistance) is used for shunting a PZT element. This can make the tuning of the electrical resonant frequency complex. In this section, however, a parallel L-R circuit is used for a shunt where the resistance of the inductor is neglected for simplicity, and the properties of a PZT element modified by this circuit are investigated.

As discussed in section 8.2.6, the requirement for the large attenuation of a propagating wave is a high stiffness or high damping of a PZT element attached to an infinite pipe. This can be done by tuning inductance and resistance in a parallel L-R circuit (external circuit) shunting to the PZT element as shown in figure 8.17.

With the parallel L-R circuit and with the piezoelectric's capacitance, the non-dimensional electrical impedance is given by

$$\hat{Z}_e = -\frac{\omega^2 L_z C_z R_z}{R_z - \omega^2 L_z C_z R_z + j\,\omega L_z} \qquad \ldots(8.3.12)$$

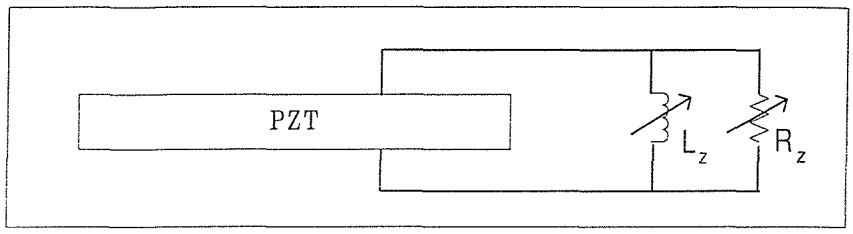

Figure 8.18: A PZT element shunted with the parallel L-R circuit.

By setting non-dimensional parameters, equation (8.3.12) becomes

$$\hat{Z}_e = -\frac{\alpha_e^2 \tau_e}{\delta_e^2 \tau_e - \alpha_e^2 \tau_e + j\alpha_e} \qquad \ldots(8.3.13)$$

where $\tau_e = R_z C_z \omega_n$,

$$\alpha_e = \frac{\omega}{\omega_n}, \qquad \ldots(8.3.14\ a, b, c, d)$$

$$\delta_e = \frac{\omega_e}{\omega_n},$$

$\omega_e = \dfrac{1}{\sqrt{L_z C_z}}$ is the electrical resonant frequency and

ω_n is the cut-on frequency of the n = 2 mode of the pipe.

Substituting for $\hat{Z}_e$ from equation (8.3.13) into equation (8.3.11) and arranging the terms gives

$$E_{zn} = E_z\left(1 + Z_r^p + j\,Z_i^p\right) \qquad \ldots(8.3.15\ a)$$

$$\nu_{zn} = \nu_z\left[1+\left(\frac{1+\nu_z}{\nu_z}\right)Z_r^p + j\left(\frac{1+\nu_z}{\nu_z}\right)Z_i^p\right] \qquad \ldots(8.3.15\ b)$$

where $Z_r^p = k_{31}^2 \dfrac{\left[\left(1+\dfrac{1+\nu_z}{1-\nu_z}k_{31}^2\right)\alpha_e^2-\delta_e^2\right]\alpha_e^2\tau_e^2}{\alpha_e^2+\left[\left(1+\dfrac{1+\nu_z}{1-\nu_z}k_{31}^2\right)\alpha_e^2-\delta_e^2\right]^2\tau_e^2}$ and

$$Z_i^p = k_{31}^2 \frac{\alpha_e^3\tau_e}{\alpha_e^2+\left[\left(1+\dfrac{1+\nu_z}{1-\nu_z}k_{31}^2\right)\alpha_e^2-\delta_e^2\right]^2\tau_e^2}$$

Equation (8.3.15 a) yields the complex elastic modulus of the PZT element. By comparing this with the mathematical notation as $E_{zn} = E_n(1+j\eta_z)$, the Young's modulus, E_n, and the loss factor, η_z, of the parallel L-R shunted PZT are found as

$$E_n = E_z\left(1+Z_r^p\right) \qquad \ldots(8.3.16\ a)$$

$$\eta_z = \frac{Z_i^p}{1+Z_r^p} \qquad \ldots(8.3.16\ b)$$

The properties of the PZT element, E_n, η_z, and ν_{zn}, can be changed at any frequency via the inductance L resulting in a change of the electrical resonant frequency. Their values can also be adjusted by changing the resistance.

8.3.3 Evaluation of Adaptive-passive Control with a PZT Shunt

In this section, the effectiveness of adaptive-passive control for suppressing the motion of an infinite pipe is investigated. As described in the previous section, a high Young's modulus and a high damping are required. So, before the control strategy is evaluated, a change of the mechanical properties of the PZT material by tuning the shunt

inductance (L_z) and resistance (R_z) is first investigated. Using the data for the PZT element in table D.3 (appendix D) and a length of $s_L = 5$, its properties shunted with the parallel L-R circuit are calculated and are shown in figure 8.19. With the shunt, its properties are frequency dependent and sharply change around the resonance frequency of the electrical system. Figure 8.19.a shows the high loss factor and the high Young's modulus do not occur at the same frequency, and is not at the electrical resonance frequency (tuned frequency). As expressed in equation (8.3.15), the Young's modulus and the loss factor depend on the inductance and resistance of the shunt circuit so that their value changes with increasing resistance. Figure 8.19.b illustrates the change of the Poisson's ratio with the phase shift, $\mathrm{Im}(\nu_{zn})/\mathrm{Re}(\nu_{zn})$. This phase shift arises because the delay of the lateral contraction due to the inertia of the PZT material. Generally, Poisson's ratio has a positive value giving the phenomenon of Poisson contraction. However, it shows an inverse phenomenon at some frequencies where it has a negative value. This means that the lateral sides are expanded rather than contracted.

Under the tuning of L_z (set so that the electrical resonance frequency is equal to the cut-on frequency of the n = 2 mode) and R_z, the mobility of the pipe for the n = 0-2 modes is shown in figure 8.20-8.22. As expected, it is difficult to obtain attenuation for the n = 0 mode at the tuning frequency due to the long wavelength of the longitudinal wave. Only a small attenuation of the n = 1 mode is obtained at the tuning frequency. The increase in Young's modulus of the shunted PZT also means there is some attenuation of this mode at the tuning frequency. At high frequencies where the wavelength of the longitudinal and bending waves are shorter, both modes are attenuated slightly due to the increased Young's modulus of the PZT element. As discussed in the previous section, an increase in Young's modulus and the loss factor of the material bonded to the pipe have a greater affect on the n = 2 mode, and this is demonstrated in figure 8.22. In this figure, the mobility of the infinite pipe with the PZT element attached and shunted with $R_z = 500$ reduces by about 8 dB compared with that of the open circuit. This figure also shows the response of the n = 2 wave in the composite section cutting on at higher frequency because of its higher stiffness. It can be seen more clearly in the dispersion curve shown in figure 8.23.

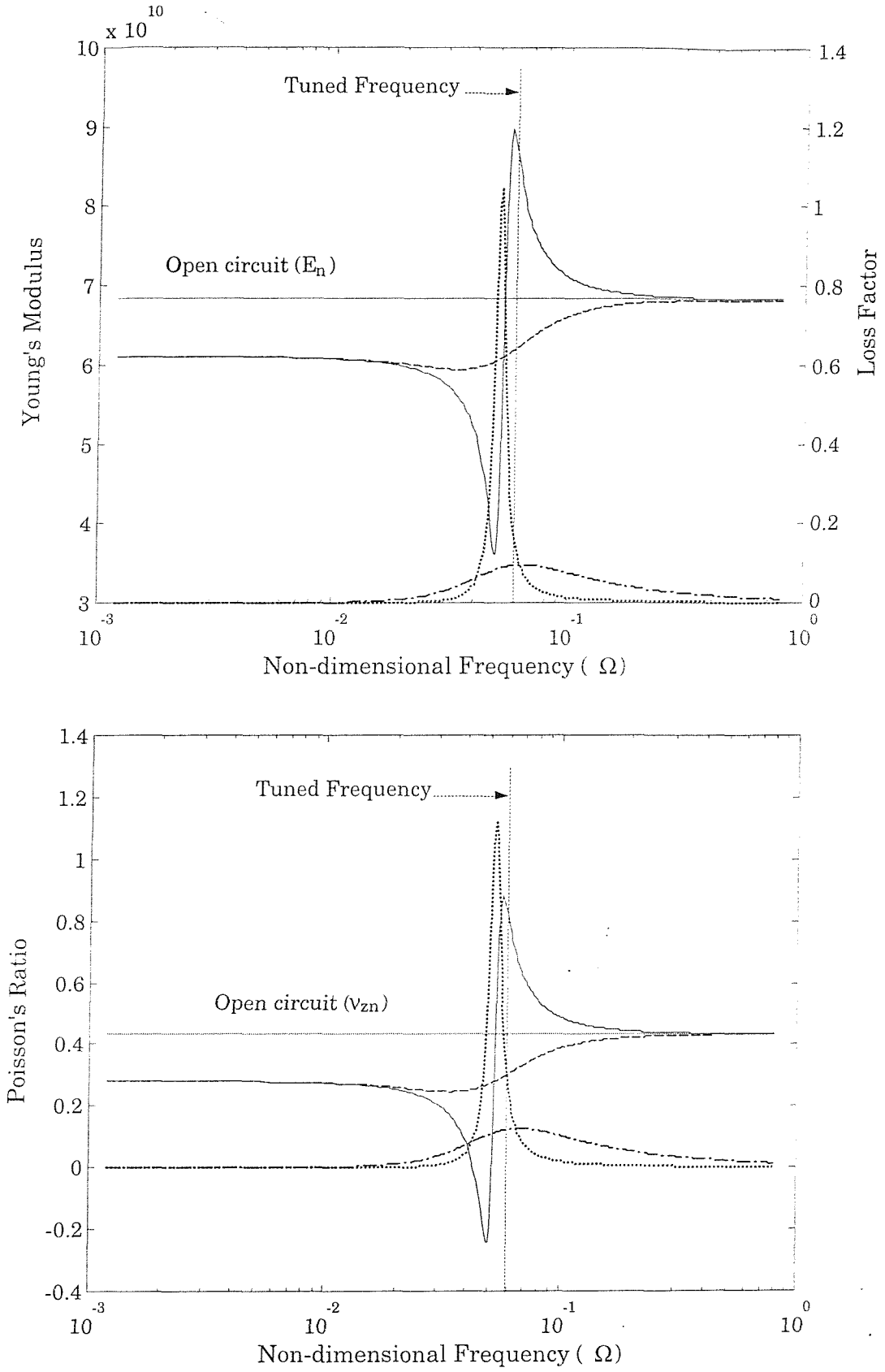

Figure 8.19: PZT properties shunted with a parallel L-R circuit; a) for E_n: _ _ R_z = 50, __ R_z = 500; for η_z: _ . _ R_z = 50, ... R_z = 500, b) for Re(ν_{zn}): _ _ R_z = 50, __ R_z = 500; for Im(ν_{zn}): _ . _ R_z = 50, ... R_z = 500.

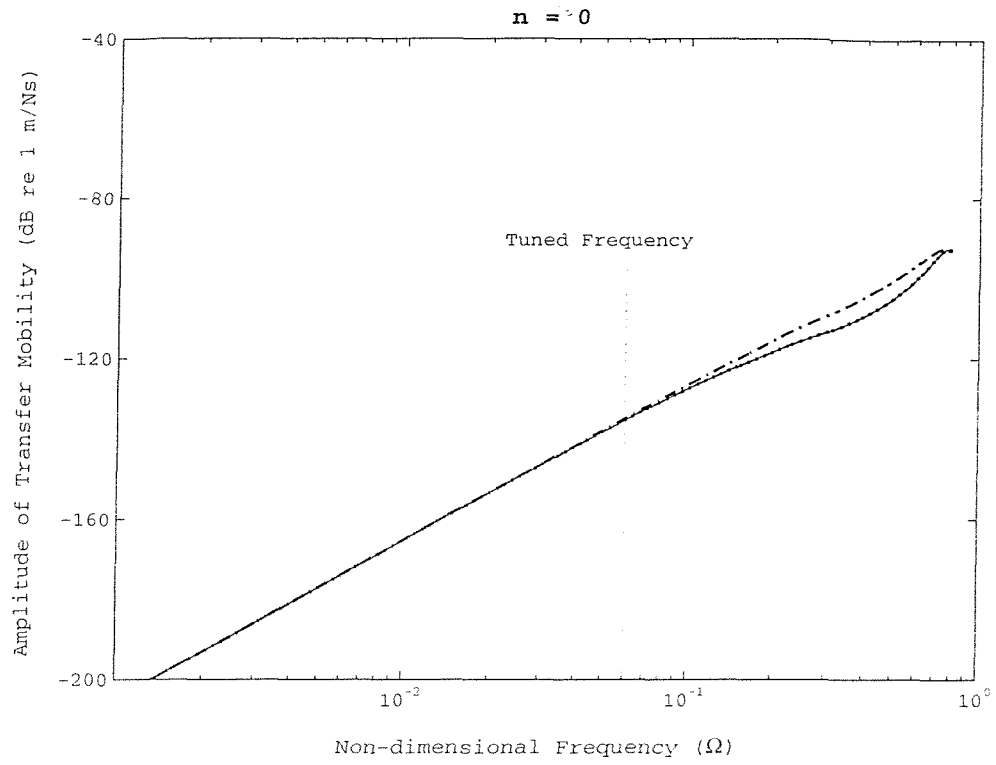

Figure 8.20: Transfer Mobility of the n = 0 mode of the infinite pipe with PZT shunt; _ _ $R_z = 50$, __ $R_z = 500$, ...Open circuit, _ .._Without PZT.

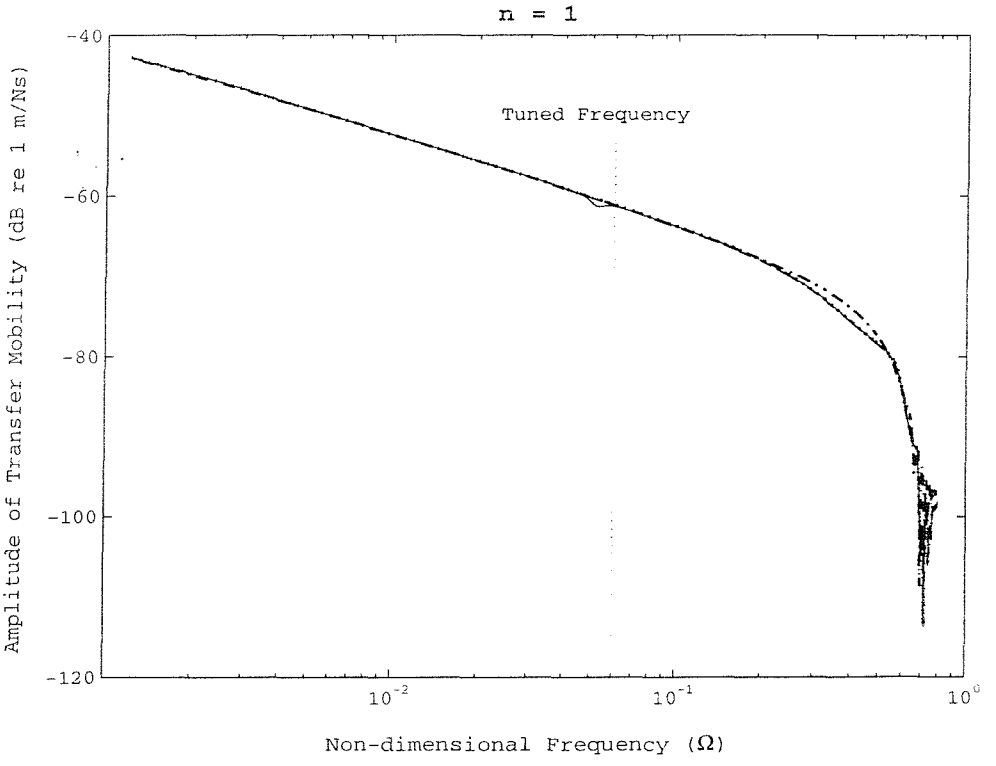

Figure 8.21: Transfer Mobility of the n = 1 mode of the infinite pipe with PZT shunt; _ _ $R_z = 50$, __ $R_z = 500$, ...Open circuit, _ .._Without PZT.

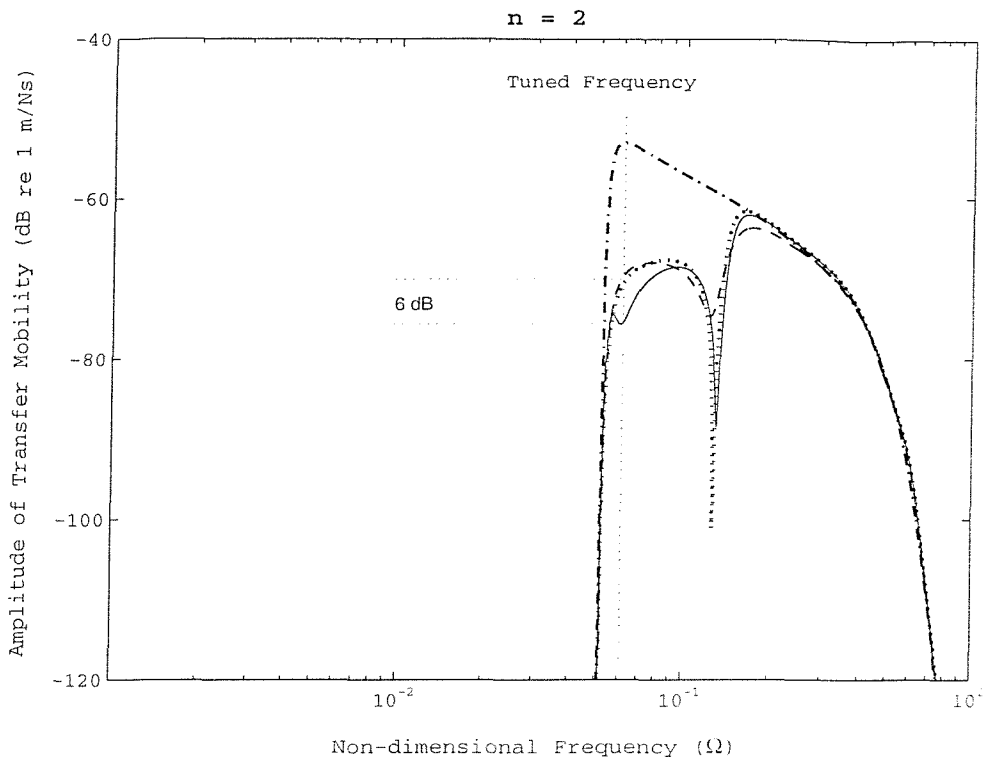

Figure 8.22: Transfer Mobility of the n = 2 mode of the infinite pipe with PZT shunt; _ _ R_z = 50, __ R_z = 500, ...Open circuit, _ .._Without PZT.

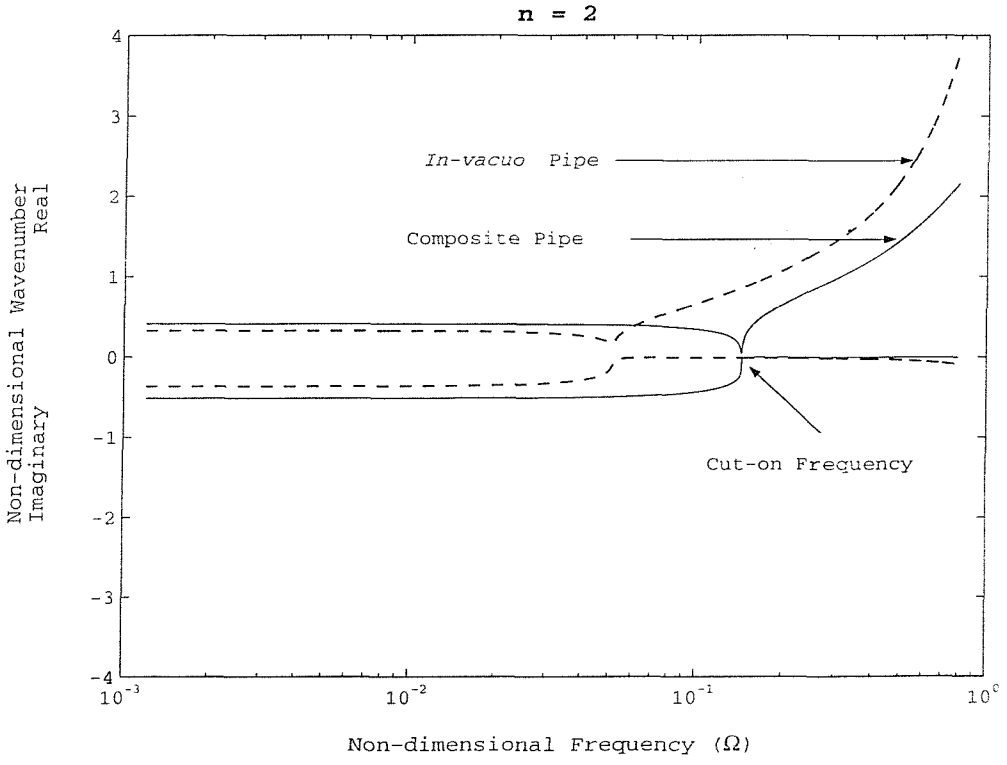

Figure 8.23: Non-dimensional wavenumber of the n = 2 mode of a composite infinite pipe with PZT material attached; _ _ *In-vacuo* pipe (t/h = 0), __ Composite pipe (t/h = 0.11).

8.4 Discussion

8.4.1 Passive Control

The effectiveness of one type of passive vibration control treatment has been numerically evaluated by comparing the motion of an infinite pipe before and after applying a damping material over a section of the pipe. With the simulations in section 8.2.4, it has been found that for control of the pipe motion, a high stiffness and a highly damped material bonded on the pipe is required to reduce an incident wave downstream. The incident wave is reflected at the composite section by the stiffness of the attached material resulting in less transmitted waves, while its energy is dissipated by the damping of the attached material. A small attenuation is obtained at high frequencies for the n = 0 and n = 1 modes, where the longitudinal waves of the n = 0 mode and the flexural wave of the n = 1 mode have a small wavelength compared with the length of the attached material. For the circumferential mode ($n \geq 2$), both the high stiffness and the high damping of the attached material can give a large attenuation.

Passive control of the n = 2 mode by using a very high stiffness such as steel is possible for a PVC pipe, whose stiffness is relatively small. However, in the case of a pipe with high stiffness such as steel or aluminium, it is difficult to reduce vibration. For passive vibration control by increasing the damping of the system, a material with high loss factor is required. Nevertheless, commercial damping materials have loss factor about 0.8-2 (Cremer and Heckl [17]), which is not effective for attenuating vibration of the pipe.

Compared with the active vibration control system discussed in chapter 7, it can be seen that the passive vibration control strategy investigated is much less effective.

8.4.2 Adaptive-passive Control

According to the investigation for passive control, a high loss factor and a high Young's modulus of the PZT material is required for reducing the transmission of the n = 2 incident flexural wave. These can be obtained by tuning an inductance and a resistance of the shunt circuit. However, appreciable attenuation for the n = 0 and n = 1 modes cannot be achieved at the tuning frequency, as described in the passive case, which is due to the long axial wavelengths of these modes. This is not the case for the n = 2 mode so that greater attenuation can be achieved for this mode.

Even though, adaptive-passive vibration control has the ability to attenuate vibration of the n = 2 mode, its performance is limited to about 6 dB at the cut-on frequency (figure 8.22). Thus it is less effective than the active control system.

8.5 Conclusions

Based on the analysis of the composite pipe, an expression for the pipe motion has been established using two methods, an analytical and a wave method. With this expression, the performance of passive and adaptive-passive control system is investigated.

For passive control, a material with high stiffness and high damping is required to reduce vibration of the pipe. It is found that the attachment of this material to a pipe can give greater attenuation a disturbance of the n = 2 mode than the modes n = 0 and n = 1. However, with damping materials available, it is difficult to make this control strategy effective.

Properties of a PZT element such as Young's modulus, Poisson's ratio, and loss factor, can be changed with a shunt of a parallel L-R circuit and they are frequency dependent. Based on the analysis for the passive control, the motion of an infinite pipe having a

shunted PZT material bonded to it can be predicted. As mentioned in the passive case, even though the high damping and high stiffness of the PZT element is obtained by adjusting the values of inductance and resistance, the adaptive-passive control system is only effective in attenuating vibration of the n = 2 mode. However, this attenuation is not much greater than simply adding the PZT element without a shunt circuit.

Compared with active vibration control of the n = 2 flexural propagating wave described in chapter 7, the performance of passive and adaptive-passive vibration control seems to be less effective.

CHAPTER 9

CONCLUSIONS

9.1 General Conclusions

This chapter contains general conclusions of the whole thesis. The detailed conclusions have been given at the end of each chapter. Even though this work contains three control strategies, which are the passive, adaptive-passive and active control for an *in-vacuo* pipe, the main objective in this thesis has been to use active control to suppress the vibration of the n = 2 flexural propagating wave. Hence, most details in the thesis are dedicated to the development of an active vibration control system for this particular wave. The other control systems, passive and adaptive-passive control, have only been investigated for comparison with the active control system.

The development of the active control system for the n = 2 flexural wave involved three elements; (a) the analysis of the behaviour of the pipe to be controlled, (b) the analysis of the n = 2 modal sensor and the n = 2 modal actuator coupling with the pipe and, (c) the analysis of the behaviour of the system when the active control is implemented. The dynamic behaviour of the pipe was analysed and presented into two ways. The first involved an investigation of the waves propagating in the pipe wall and was characterised by the wavenumber, and the other involved the forced vibration of the pipe characterised by the mobility.

In chapter 2, the wave characteristics of an *in-vacuo* pipe were discussed. The dynamic behaviour of the pipe is complex due to its curvature, but Flugge's shell theory is used to make the interpretation of the wavenumbers easier. This simplification was based on the following assumptions; the thickness of the pipe wall is much smaller than the radius of the pipe, the frequency range of interest is below the ring frequency, and the product of the wavenumber and the radius of the pipe (except for the longitudinal and the torsional waves) is much larger than the non-dimensional frequency. With these assumptions, it was shown that the pipe behaves like a membrane for the n = 0 mode and like a beam for the n = 1 mode. Moreover, at very low frequencies it behaves like an Euler-Bernoulli beam for the n = 1 mode. A simplified expression for the cut-on frequency of the $n \geq 2$ modes was also obtained using the assumptions.

The mobility of an infinite pipe was discussed in chapter 3, and was derived using the residue and analytical methods. Even though both methods are different, the resultant mobility was found to be the same. The advantage of the analytical method is that it provides additional, physical information; i.e. no slope, no twist and no axial displacement at the point force excitation position. Once the mobility of the infinite pipe had been established, it was simplified. This was done for very low frequencies on the basis of the assumptions used for simplifying the wavenumber in chapter 2. With the approximate mobility expression, it was shown that the pipe behaves like a membrane for the n = 0 mode and like an Euler-Bernoulli beam for the n = 1 mode.

In a similar manner to the infinite pipe, the mobility of a semi-infinite pipe described in chapter 4 was derived using two methods, which are the analytical and the wave methods. Even though there was no theoretical comparison for wave amplitudes due to the complexity of the pipe, the simulations showed that both methods gave the same result. The mobility expression in this case was simplified for very low frequencies by applying the assumptions used for simplifying the wavenumbers in chapter 2. The simplified mobility of the semi-infinite pipe was found to be similar to that of the membrane and the Euler-Bernoulli beam for the n = 0 and n = 1 mode, respectively.

Chapter 5 involved an analysis of sine and cosine modal sensors for the n = 2 mode of a pipe. Based on Flugge's shell theory, the relationship between the charge generated from a PVDF sensor and the combination of the axial and circumferential bending strains has been established for the case of an in-extensional deformation. From the analysis, it was found that the higher order modes can be detected by the sensor, because the axial strain over the surface of the modal sensor is not constant. In order to minimise the cross-sensitivity, which is the ratio of the response of the higher mode to that of the n = 2 mode, the width of the sensor should be small. For a cross-sensitivity of –20 dB between modes n = 6 and n = 2, the width of the sensor should be about one third of the wavelength of the n = 2 flexural wave at the ring frequency. By using both sine and cosine modal sensors, the orientation of the wave in the pipe can be detected.

The design of the sine and cosine modal actuators for the n = 2 mode were described in chapter 6. Each type of modal actuator was created using four PZT elements, which are the minimum number to form such an actuator. Using the minimum elements, spillover into the n = 6 mode occurs. However, it may be neglected because it occurs at a high frequency. From the analysis and experiment, it was found that the orientation of the wave can be changed to any angle when both sine and cosine modal actuators are simultaneously used. The orientation angle depends on the voltages supplying to the actuators. Thus the modal actuator can be used for suppressing disturbances, which have any orientation.

For an infinite pipe, only flexural waves can propagate along the pipe, while other waves, near field and standing near field waves, have negligible amplitude at some distance from the point of excitation. Hence, the control system was focused on suppressing this wave. The control strategy used in this thesis was an active control system. The others, which are passive and adaptive-passive control, were also investigated in order to compare the performance of the active control system.

Having established the dynamic behaviour of the pipe in terms of the mobility, the active control system to suppress the flexural wave of the n = 2 circumferential mode was modelled. A PVDF modal sensor and a PZT modal actuator for the n = 2 mode were

developed to sense and actuate this wave. Since the disturbance caused by the excitation load consisted of sine and cosine components, the modal sensor/actuator was also designed in the form of a pair of sine and cosine functions to counteract each component. It was shown that the disturbance of the n = 2 flexural wave can in principle be completely suppressed. Generally, this wave is dominant in the pipe response after it cuts on and before the higher order modes cut on. Hence, the performance of the active control system is over a limited frequency range. However, spillover into the n = 6 mode occurs with this control strategy because the modal sensor/actuator also detect and actuate the pipe response of this mode. It occurs because the strains are not constant over the width of the modal sensor and for the actuator because the minimum number of PZT elements to form the modal actuator was used. The effect of this spillover can be reduced by decreasing the width of the sensor and increasing the number of PZT elements for the actuator. Nevertheless, this effect can be regarded as being insignificant since it occurs at high frequencies compared to the cut-on frequency of the n = 2 mode.

For the passive control system, an expression for the pipe motion with an unconstrained material bonded to it has been established. This was done by considering a composite pipe section. With the boundary conditions at the ends of the composite section, the motion of the infinite pipe was determined. In this control strategy, the loss factor plays a role on dissipating energy, while the stiffness plays a role in resisting the change in circumferential shape of the pipe. Both are effective for the circumferential n = 2 mode but not for the n = 0 and n = 1 modes. In order to achieve high vibration attenuation with this strategy, high stiffness and high loss factor of the material attached to the pipe in the composite section are required. However, damping material normally has a high loss factor but low stiffness so that it is difficult to achieve good performance with this control strategy.

For adaptive-passive control, an expression of the pipe motion was found to be similar to that for passive control except that the properties of the PZT element (attached material) can be changed with a shunt of a parallel L-R circuit (an external circuit). These properties are Young's modulus, Poisson's ratio, and loss factor, which can be increased by tuning the inductance (L) and the resistance (R). Like passive control, the

increase of the stiffness and loss factor of the PZT element can significantly attenuate vibration of the n = 2 mode, but not that of the modes n = 0 and n = 1.

Even though both strategies, passive and adaptive-passive control, can reduce vibration of the n = 2 mode, they are less effective than fully active control. With the length of a composite section s_L = 5, the attenuation obtained from the passive approach using the Nitrile rubber (damping material) attached to the pipe is approximately 6 dB at the cut-on frequency, while the attenuation obtained from the adaptive-passive system using a PZT shunt is about 6 dB greater than that using a simple PZT element without shunting. Unlike both approaches, the active vibration control system can in-principle completely suppress the vibration of the n = 2 mode (with a 15 dB reduction in the overall vibration at the cut-on frequency measured in practice) with the PZT modal actuator having the length of s_L = 0.24.

9.2 Recommendations for Further Work

The analysis of modal sensors/actuators described in chapters 5 and 6, respectively, is general for the n ≥ 2 modes of an infinite pipe before concentrating on the n = 2 mode. However, further experimental work on the higher modes could be carried out.

In chapter 7, the work concentrates on the active control of the n = 2 flexural wave of an infinite pipe. It could be extended to suppress the n = 2 near field wave by using two sets of sine and cosine modal actuators.

The work in chapter 8 is an investigation in some aspects of passive and adaptive-passive vibration control of an infinite pipe. For passive control, further investigation could be continued on the effective ratio of the length of damping materials to the flexural wavelength of circumferential mode of an infinite pipe. This could be useful for evaluating the attenuation of an incident wave. For adaptive-passive control, an

investigation into the optimum tuning frequency and the stability of the control system could be conducted.

REFERENCES

1. Fahy F. J., 1985, "Sound and structural vibration: radiation, transmission and response", Academic Press.

2. Leissa A. W., 1973, "Vibrations of shells", NASA SP-288, Washington DC: U.S. Gov Printing Office.

3. Timoshenko S. and Woinowsky-Krieger S., 1956, "Theory of plates and shells", 2nd Edn., McGraw-Hill Book Company, INC.

4. Kennard E. H., 1953, "The new approach to shell theory: circular cylinders", J. Appl Mech., Vol. 20, No. 1, pp. 33-40.

5. Flugge W., 1962, "Stresses in shells", 2nd Edn., Springer-Verlag, Berlin, Heidelberg, New York..

6. Pavic G., 1992, "Vibroacoustical energy flow through straight pipes", J. of Sound and Vibration, Vol. 154, No. 3, pp. 411-429.

7. Pinnington R. J. and Briscoe A. R., 1994, "Externally applied sensor for axisymmetric waves in a fluid filled pipe", J. of Sound and Vibration, Vol. 173, No. 4, pp. 503-516.

8. Brennan M. J., Elliott S. J. and Pinnington R. J., 1996, "A non-intrusive fluid-wave actuator and sensor pair for the active control of fluid-borne vibrations in a pipe", Smart Mater. Struct., No. 5. Pp. 281-296.

9. Fuller C.F.,1983, "The input mobility of an infinite circular cylindrical elastic shell filled with fluid", J. of Sound and Vibration, Vol. 87, No. 3, pp. 409-427.

10. Mace B. R., 1987, "Active control of flexural vibration", J. of Sound and Vibration, Vol. 114, No. 2, pp. 253-270.

11. Brennan M. J., Elliott S. J. and Pinnington R. J., 1995, "Strategies for the active control of flexural vibration on a beam", J. of Sound and Vibration, Vol. 186, No. 4, pp. 657-688.

12. Mead D. J., 1988, "Passive vibration control", John Wiley & Sons Ltd.

13. Hagood N. W. and von Flotow A., 1991, "Damping of structural vibrations with piezoelectric materials and passive electrical networks", J. of Sound and Vibration, Vol. 146, No. 2, pp. 243-268.

14. Fuller C. R. and Brevart B. J., July 1995, "Active control of coupled wave propagation and associated power in fluid-filled elastic long pipes", Active 95, pp. 3-14.

15. Zhang X. M., Liu G. R. and Lam K. Y., 2001, "Vibration analysis of thin cylindrical shells using wave propagation approach", J. of Sound and Vibration, Vol. 239, No. 3. Pp. 397-403.

16. Lin T. C. and Morgan G. W., 1956, "Wave propagation through fluid contained in a cylindrical, elastic shell", J. of the Acoustical Society of America, Vol. 28, No. 6, pp. 1165-1176.

17. Cremer L., Heckl M. and Ungar E. E., 1988, "Struture-borne sound", 2nd Edn., Springer-Verlag, Berlin, Heidelberg, New York..

18. Fuller C. R. and Fahy F. J., 1982, "Characteristics of wave propagation and energy distributions in cylindrical elastic shells filled with fluid", J. of Sound and Vibration, Vol. 81, No. 4, pp. 501-518.

19. Brennan M. J., Elliott S. J. and Pinnington R. J., Dec 1993, "Waves in fluid filled pipes", RNEC-RR-93035, Royal Naval Engineering College, Mechanics Group Research Report.

20. Finnveden S., 1997, "Simplified equations of motion for the radial-axial vibrations of fluid filled pipes", J. of Sound and Vibration, Vol. 208, No. 5, pp. 685-703.

21. Franken P. A., 1960, "Input impedances of simple cylindrical structures", J. of the Acoustical Society of America, Vol. 32, No. 4, pp. 473-477.

22. Heckl M., 1962, "Vibrations of point-driven cylindrical shells", The Journal of the Acoustical Society of America, Vol. 34, No. 10, pp. 1553-1557.

23. Brevart B. J. and Fuller C. R., 1993, "Active control of coupled wave propagation in fluid-filled elastic cylindrical shells", J. Acoust. Soc.Am., Vol. 94, No. 3, pp. 1467-1475.

24. Vinson J. R., 1974, "Structural mechanics : the behavior of plate and shells", John Wiley & Sons, Inc.

25. Young A. J., 1995, "Active control of vibration in stiffened structures", Ph.D. Thesis, University of Adelaide, South Australia.

26. Pan X. and Hansen C. H., 1997, "Active control of vibration transmission in a cylindrical shell", J. of Sound and Vibration, Vol. 203, No. 3, pp. 409-434.

27. Morgan Matroc Limited, " Piezoelectric ceramics: Data book for designers", Transducer products division, Morgan Matroc Limited, Bewdley Road, Stourport-on-Severn, Worcestershire, DY13 8QR.

28. Burke S. E. and Hubbard, Jr J. E., 1991, "Distributed transducer vibration control of thin plates", J. Acoust. Soc. Am., Vol. 90, No. 2, pp. 937-944.

29. Lee C. K., 1990, "Theory of laminated piezoelectric plates for the design of distributed sensors/actuators. Part I: Governing equations and reciprocal relationships", J. Acoust. Soc. Am., Vol. 87, No. 3, pp. 1144-1158.

30. Lee C. K. and Moon F. C., 1990, "Modal sensors/actuators", J. of Applied Mechanics, ASME, Vol. 57, pp. 434-441.

31. Tzou H. S., 1992, "A new distributed sensor and actuator theory for intelligent shells", J. of Sound and Vibration, Vol. 153, No. 2, pp. 335-349.

32. Sung C. K., Chen T. F. and Chen S. G., 1996, "Piezoelectric modal sensor/actuator design for monitoring/generating flexural and torsional vibrations of cylindrical shells", J. of Vibration and Acoustics, ASME, Vol. 118, pp. 48-55.

33. Brennan M. J. and Day M. J., "Distributed piezoelectric actuators and sensors", Royal Naval Engineering Research Report, RNEC-RR-93034.

34. Tani J., Qiu J. and Miura H., 1995, "Vibration control of a cylindrical shell using piezoelectric actuators", J. of Intelligent Material Systems and Structures, Vol. 6, pp. 380-388.

35. Qiu J. and Tani J., 1995, "Vibration control of a cylindrical shell using distributed piezoelectric sensors and actuators", J. of Intelligent Material Systems and Structures, Vol. 6, pp. 380-388.

36. Crawley E. F. and de Luis J., 1987, "Use of piezoelectric actuators as elements of intelligent structures", AIAA Journal, Vol. 25, No. 10, pp. 1373-1385.

37. Crawley E. F., and Lazarus K. B., 1991, "Induced strain actuation of isotropic and anisotropic plates", AIAA Journal, Vol. 29, No. 6, pp. 944-951.

38. Dimitriadis E. K., Fuller C. R. and Rogers C. A., 1991, "Piezoelectric actuators for distributed vibration excitation of thin plates", J. of Vibration and Acoustics, ASME, Vol. 113, pp.100-107.

39. Kim S. J. and Jones J. D., 1991, "Optimal design of piezoactuators for active noise and vibration control", AIAA Journal, Vol. 29, No. 12, pp. 2047-2053.

40. Lester H. C. and Lefebvre S., 1991, "Piezoelectric actuator models for active sound and vibration control of cylinders", Proceedings, Recent Advances in Active Control of Sound and Vibration, Blacksburg, VA, pp. 3-26.

41. Lalande F., Chaudhry Z. and Rogers C. A., 1995, "Impedance-based modeling of actuators bonded to shell structures", SPIE Conference on Smart Structures and Materials, San Diego, CA 2443, pp. 396-408.

42. Gu Y., Clark R. L. and Fuller C. R., 1994, "Experiments on active control of plate using piezoelectric actuators and polyvinylidene fluoride (PVDF) modal sensors", ASME J. of Vibration and Acoustics, Vol. 116, pp. 303-308.

43. Tzou H. S. and Bao Y., 1996, "Parametric study of segmented transducers laminated on cylindrical shells, Part 1 : Sensor patches", J. of Sound and Vibration, Vol. 197, No. 2, pp. 207-224.

44. Callahan J. and Baruh H., 1999, "Modal sensing of circular cylindrical shells using segmented piezoelectric elements", Smart Materials and Structures, No. 8, pp. 125-135.

45. Guicking D., 1990, "On the invention of active noise control by Paul Lueg", J. of the Acoustical Society of America, Vol. 24, pp. 2251-2255.

46. Nelson P. A. and Elliott S. J., 1992, "Active control of sound", Academic Press.

47. Bailey T. and Hubbard J. E., 1985, "Distributed piezoelectric-polymer active vibration control of a cantilever beam", J. of Guidance, Control, and Dynamics, Vol. 8, No. 5, pp. 62-80.

48. Scheuren J., 1985, "Active control of bending waves in beams", Proc. Inter-Noise 85, pp. 591-595.

49. Scheuren J., 1988, "Non-reflecting termination for bending waves in beams by active means", Proc. Inter-Noise 88, pp. 1065-1068.

50. Pan J. and Hansen C. H., 1991, "Active control of total vibratory power flow in a beam. I: Physical system analysis", J. of the Acoustical Society of America, Vol. 89, No. 1, pp. 200-209.

51. Fuller C. R. and Jones J. D., 1987, "Experiments on reduction of propeller induced interior noise by active control of cylinder vibration", J. of Sound and Vibration, Vol. 112, pp. 389-395.

52. Harper M. and Leung R., 1993, "Active vibration control in pipes", Proceedings of Inter-Noise 93, pp. 871-874.

53. Hansen C. H. and Young A. J., 1995, "Control of flexural vibration in a ring-stiffened cylinder using piezoceramic stack actuators", Active 95, pp. 221-232.

54. Mace B. R., 1984, "Wave reflection and transmission in beams", J. of Sound and Vibration, Vol. 97, No. 2, pp. 237-246.

55. Brennan M. J., 1998, "Control of flexural waves on a beam using a tunable vibration neutraliser", J. of Sound and Vibration, Vol. 222, No. 3, pp. 389-407.

56. Harari A., 1977, "Wave propagation in cylindrical shells with finite regions of structural discontinuity", J. of the Acoustical Society of America, Vol. 62, No. 5, pp. 1196-1205.

57. Fuller C. R., 1981, "The effects of wall discontinuities on the propagation of flexural waves in cylindrical shells", J. of Sound and Vibration, Vol. 75, No. 2, pp. 207-228.

58. Munjal M. L. and Thawani P. T., "Prediction of the vibro-acoustic transmission loss of planar hose-pipe systems", J. of the Acoustical Society of America, Vol. 101, No. 5, pp. 2524-2535.

59. Patten W. N., Sack R. L. and Yu W. K., 1996, "A controlled semiactive hydraulic vibration absorber for bridges, J. of Struct. Engrg., ASCE, Vol. 122, No. 2, pp. 187-192.

60. Choi S. B., Choi J. H., Nam M. H, Cheong C. C. and Lee H. G., 1998, "A semi-active suspension using ER fluids for a commercial vehicle seat", Proceedings of the 4th European and 2nd MIMR Conference, Smart Materials and Structures, pp. 217-224.

61. Hagood N. W. and Crawley E. F., 1991, "Experimental investigation of passive enhancement of damping for space structures", J. of Guidance, Control, and Dynamics, Vol. 14, No. 6, pp. 1100-1109.

62. Wu S., 1996, "Piezoelectric shunts with a parallel R-L circuit for structural damping and vibration control", Proceedings of SPIE, Smart Structures and Materials, Vol.2720, pp. 259-269.

63. Wu S. and Bicos A. S., 1997, "Structural vibration damping experiments using improved piezoelectric shunts", Proceedings of SPIE, Smart Structures and Materials, Vol. 3045, pp. 40-50.

64. Hollkamp J. J. and Starchville Jr. T. F., 1994, "A self tuning piezoelectric vibration absorber", J. of Intelligent Material Systems and Structures, Vol. 5, pp. 559-566.

65. Davis C. L. and Lesieutre G. A., 2000, "An actively tuned solid-state vibration absorber using capacitive shunting of piezoelectric stiffness", J. of Sound and Vibration, Vol. 232, No. 3, pp. 601-607.

66. Tang J., Liu Y. and Wang K. W., 2000, "Semiactive and active-passive hybrid structural damping treatments via piezoelectric materials", The Shock and Vibration Digest, Vol. 32, No. 3, pp. 189-200.

67. Lesieutre G. A., 1998, "Vibration damping and control using shunted piezoelectric materials", The Shock and Vibration Digest, Vol. 30, No. 3, pp. 187-195.

68. Variyart W. and Brannan M. J., "Measurement of flexural propagating waves in pipes using shaped PVDF modal sensors", ISVR Technical Memorandum, 1999, No. 847.

69. Soedel W., 1993, "Vibrations of shells and plate", 2nd Edn., MARCEL DEKKER, INC.

70. Arfken G.,1985, "Mathematical methods for physicists", 3rd Edn., Academic Press, INC.

71. Harris C. M., 1995, "Shock and vibration handbook", 4th Edn., McGraw-Hill.

72. Brennan M. J., Elliott S. J. and Pinnington R. J., 1997, "The dynamic coupling between piezoceramic actuators and a beam", J. Acoust. Soc.Am., Vol. 102, No. 4, pp. 1931-1942.

73. Brennan M. J., 1994, "Active control of waves on one-dimensional structures", Ph.D. Thesis, ISVR, University of Southampton.

74. Balas M., 1978, "Feedback control of flexible systems", IEEE Transactions on Automatic Control, AC-23, No.4, pp.673-679.

APPENDIX A

MODAL DECOMPOSITION

To investigate the reduction of each circumferential structural mode amplitude that is achieved by applying active vibration control, modal decomposition of the measured response should be carried out so that a comparison of the response before and after control applied to each mode can easily be undertaken. Moreover, the modal decomposition technique may be used to measure the effectiveness of a distributed PVDF modal sensor. This technique is based on the principle of discrete orthogonality (Arfken [20]). To illustrate this technique, equation (3.13) is considered. By expanding the term $\cos[n(\theta - \phi)]$ into sine and consine functions, this equation is written as

$$Y_n^i = -\frac{\varepsilon_n \omega[\lambda_1 \cos(n\theta) + \lambda_2 \sin(n\theta)]}{2\pi\rho h a^2 \omega_r^2} \sum_{b=1}^{4} Res_b e^{jk_{nb}s} \qquad \ldots(A.1)$$

where $\lambda_1 = \cos(n\phi)$,

$\lambda_2 = \sin(n\phi)$ and

ϕ is the orientation angle.

Since the term on the right hand side of this equation consists of two separate parameters, θ and s , the total mobility may be written as

$$Y^i = \sum_{n=0}^{\infty} A_n [\lambda_1 \cos(n\theta) + \lambda_2 \sin(n\theta)] \qquad \ldots(A.2)$$

where $A_n = -\frac{\varepsilon_n \omega}{2\pi \rho h a^2 \omega_r^2} \sum_{b=1}^{4} Res_b e^{j k_{nb} s}$

Assuming the measurement is made using a point sensor (i.e. accelerometer) at N points around a pipe with equal angle. Then,

$$\theta = \frac{2\pi}{N} p_\theta$$

where p is the position of the measurement.

To decompose pipe modes in terms of the cosine function, both sides of equation (A.2) are multiplied by $\frac{1}{\varepsilon_n N} \cos(\frac{2\pi p_\theta}{N} m)$ and all responses measured around the pipe are summed to give

$$\frac{1}{\varepsilon_m N} \sum_{p=0}^{N-1} Y_n^i \cos(\frac{2\pi p_\theta}{N} m) = \frac{1}{\varepsilon_m N} \sum_{p=0}^{N-1} \sum_{n=0}^{\infty} A_n \left(\lambda_1 \cos(\frac{2\pi p_\theta}{N} n) + \lambda_2 \sin(\frac{2\pi p_\theta}{N} n) \right) \cos(\frac{2\pi p_\theta}{N} m) \qquad \ldots(A.3)$$

where m is the desired mode to be decomposed.

By assuming N is equal to infinity, the response of the desired mode for the cosine function can be determined using the property of orthogonality and is

$$\frac{1}{N} \sum_{p=0}^{N-1} Y_n^i \cos(\frac{2\pi p_\theta}{N} m) = \left(Y_n^i\right)_c = \lambda_1 A_m \qquad \ldots(A.4)$$

In practice, N is finite and hence an alising error arises. To avoid this for any particular mode, N has to be at least twice of the mode number ($N \geq 2^*m$).

To decompose pipe modes in terms of the sine function, the same procedure is applied except that both sides are multiplied by $\frac{1}{N}\sin(\frac{2\pi p_\theta}{N}m)$ instead of $\frac{1}{N}\cos(\frac{2\pi p_\theta}{N}m)$. Hence, the response of the desired mode for the sine function is

$$\frac{1}{N}\sum_{p=0}^{N-1} Y_n^i \sin(\frac{2\pi p_\theta}{N}m) = \left(Y_n^i\right)_s = \lambda_2 A_m \qquad \ldots(A.5)$$

The total response, A_m, of the desire mode can be obtained by combining equation (A.4) and (A.5) as follows to give

$$A_m = \sqrt{\left(Y_n^i\right)_c^2 + \left(Y_n^i\right)_s^2} \qquad \ldots(A.6)$$

and the orientation angle is obtained from

$$\phi = \frac{1}{m}\tan^{-1}\left(\frac{\lambda_2}{\lambda_1}\right) = \frac{1}{m}\tan^{-1}\frac{\left(Y_n^i\right)_s}{\left(Y_n^i\right)_c} \qquad \ldots(A.7)$$

APPENDIX B

WAVE DECOMPOSITION FOR INFINITE PIPES

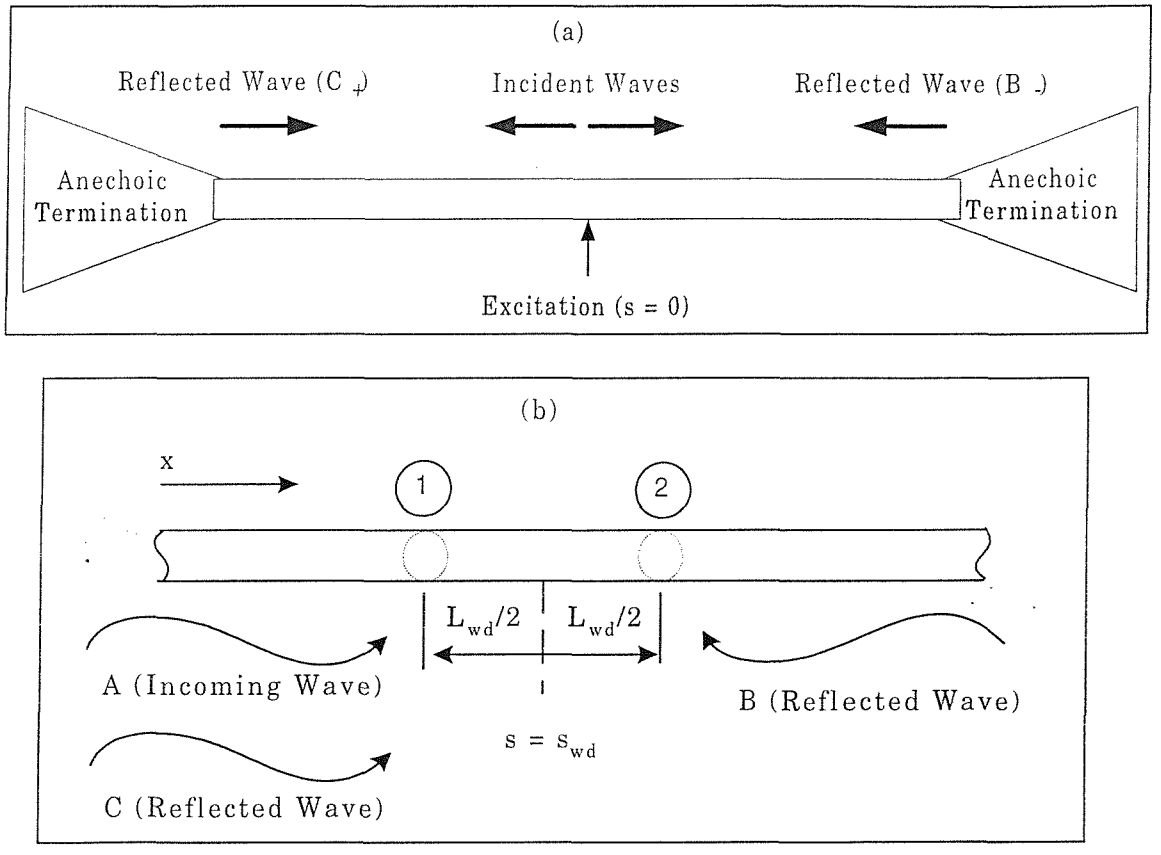

Figure B.1: Decomposition of incoming and reflected waves.

Brennan et al [29] proposed a method to decompose flexural propagating waves of a beam by using an array of two sensors, and method of wave decomposition was extended for a semi-infinite pipe by Variyart and Brennan [68]. In this section, the wave decomposition method is applied for an infinite pipe. In this method shown in

figure B.1, two sets of measurements around the pipe are taken in the far field where there are no evanescent waves. Before the method is applied, the modal decomposition technique described in the next section is used to separate the measurement results into each mode, which may be expressed in the form of separated waves as

$$W_n(s) = \sum_{b=1}^{b=4} A_0 e^{j\hat{k}_{nb}s} + \sum_{b=1}^{b=4} C_+ e^{j\hat{k}_{nb}(L_0+s)} + \sum_{b=5}^{b=8} B_- e^{-j\hat{k}_{nb}(L_0-s)} \qquad \ldots(B.1)$$

where A_0 is the amplitude of the incoming wave and

B_- is the amplitude of the reflected wave arose at the right termination

C_+ is the amplitude of the reflected wave arose at the left termination.

L_0 is the half length of the pipe normalised to the radius of the pipe.

In this method, two sets of measurements around the pipe are taken at the far field where there are no evanescent waves. Prior to decomposition of the waves, the modal decomposition technique is applied to separate the measurement results into each mode. Since $\hat{k}_{nb} = -\hat{k}_{n(b+4)}$ the expression of radial motion in which only the propagating wave is present, may be expressed as

$$W_n(s) = (A_0 + C_0) e^{j\hat{k}_{nb}s} + B_0 e^{-j\hat{k}_{nb}s} \qquad \ldots(B.2)$$

where $C_0 = C_+ e^{j\hat{k}_{nb}L_0}$ and $B_0 = B_- e^{j\hat{k}_{nb}L_0}$.

Then the displacement at points 1 and 2 are

$$W_n^1 = (A_0 + C_0) e^{j\hat{k}_{nb}(s_{wd} - L_{wd}/2)} + B_0 e^{-j\hat{k}_{nb}(s_{wd} - L_{wd}/2)},$$

$$W_n^2 = (A_0 + C_0) e^{j\hat{k}_{nb}(s_{wd} + L_{wd}/2)} + B_0 e^{-j\hat{k}_{nb}(s_{wd} + L_{wd}/2)}. \qquad \ldots(B.3)$$

where x_{wd} is the centre location between the point 1 and point 2,

$s_{wd} = x_{wd}/a$ and

L_{wd} is the non-dimensional distance between the point 1 and point 2, which is normalised to the radius of the pipe.

Equation (B.3) may be written in the form of a matrix as

$$\begin{bmatrix} e^{-j\hat{k}_{nb}L_{wd}/2} & e^{j\hat{k}_{nb}L_{wd}/2} \\ e^{j\hat{k}_{nb}L_{wd}/2} & e^{-j\hat{k}_{nb}L_{wd}/2} \end{bmatrix} \begin{bmatrix} D_{sc} \\ B_{sc} \end{bmatrix} = \begin{bmatrix} W_n^1 \\ W_n^2 \end{bmatrix} \qquad \ldots(B.4)$$

where $D_{sc} = (A_0 + C_0)e^{j\hat{k}_{nb}s_{wd}}$ and $B_{sc} = B_0 e^{-j\hat{k}_{nb}s_{wd}}$.

Therefore, the amplitudes of D_{sc} and B_{sc} are

$$\begin{bmatrix} D_{sc} \\ B_{sc} \end{bmatrix} = \frac{j}{2\sin\hat{k}_{nb}l} \begin{bmatrix} e^{-j\hat{k}_{nb}L_{wd}/2} & -e^{j\hat{k}_{nb}L_{wd}/2} \\ -e^{j\hat{k}_{nb}L_{wd}/2} & e^{-j\hat{k}_{nb}L_{wd}/2} \end{bmatrix} \begin{bmatrix} W_n^1 \\ W_n^2 \end{bmatrix} \qquad \ldots(B.5)$$

It was pointed out by Brennan et al [29] that equation (B.5) tends to ill-conditioning at frequencies where integer numbers of half wavelengths are equal to the distance between the two sensors. It also is ill-conditioning at cut-on frequencies.

In order to separate the positive-going incident wave and reflected positive-going waves, the same radial amplitude of the reflected waves from both sides of anechoic terminations is assumed and is given as $B_- = C_+$. Hence, replacing this assumption into equation (B.5) gives the incident wave and reflected positive-going wave at the $s = s_c$ as given by

$$A_{sc} = A_0 e^{j\hat{k}_{nb}s_{wd}} = D_{sc} - B_{sc}e^{2j\hat{k}_{nb}s_{wd}}$$

$$C_{sc} = C_0 e^{j\hat{k}_{nb}s_{wd}} = B_{sc}e^{2j\hat{k}_{nb}s_{wd}} \qquad \ldots(B.6\ a, b)$$

APPENDIX C

EFFECT OF MASS LOADING ON PIPES

With accelerometers attached, a motion of a pipe itself is changed. In this appendix, the effect of two accelerometer masses is analysed in order to obtain the actual motion of a pipe.

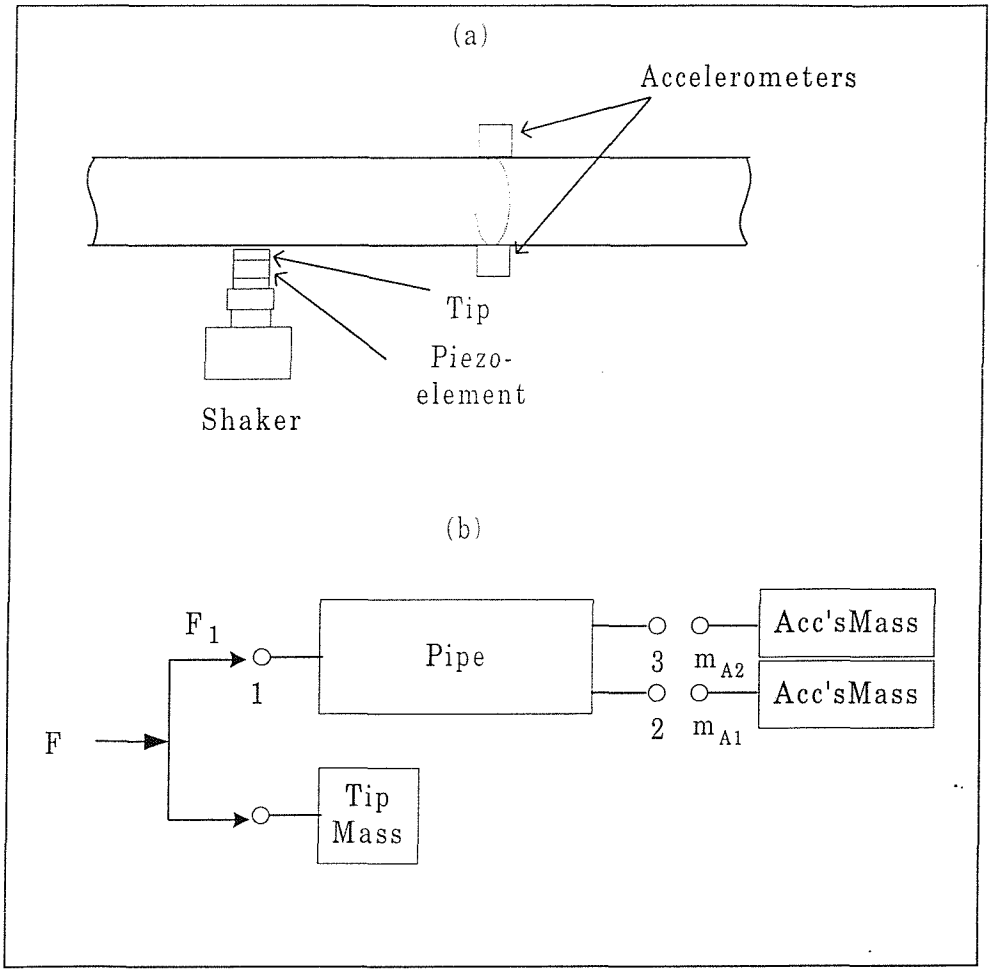

Figure C.1: General framework of the connection between pipe and mass

Attached masses such as accelerometers change the dynamic behaviour of the pipe structure. To predict the motion of the pipe with masses attached, the effect of mass loading has to be considered. The mobility method is applied for analysis of this effect and it is schematically shown in figure C.1 in which a force, F_1, excites a pipe at the location (1) and a response of the pipe is measured by two accelerometers (Masses) at the locations (2) and (3).

$$F_1 = \frac{1}{1+\frac{Y_{11}}{Y_T}} F \qquad \ldots(C.1)$$

Where Y_{11} is the point mobility of pipe for which the force and velocity are taken at the position 1

Y_T is the mobility of tip mass.

Following the work done by Mead [24], the velocities at the interface between the accelerometers and the pipe at the locations (2) and (3) in figure C.1 are respectively as follows.

$$v_2 = Y_{21}F_1 + Y_{22}F_2 + Y_{23}F_3$$

$$v_3 = Y_{31}F_1 + Y_{32}F_2 + Y_{33}F_3 \qquad \ldots(C.2\ a, b)$$

where Y_{ij} is the mobility of pipe for which the force is taken at the position j and velocity is measured at the position i.

The continuity of motion and force equilibrium at the connection of the accelerometers give $v_2 = v_{A2}$, $v_3 = v_{A3}$, $F_2 = -F_{A2}$, and $F_3 = -F_{A3}$. This leads to

$$v_2 = -Y_{A1}F_2 \quad \text{and} \quad v_3 = -Y_{A2}F_3 \qquad \ldots(C.3\ a, b)$$

where Y_{A1} and Y_{A2} are the mobilitis of the accelerometers' mass.

Solving equations (C.1), (C.2) and (C.3) gives

$$\frac{v_2}{F} = \frac{\left[Y_{21}(1+Y_{33}/Y_{A2}) - Y_{23}Y_{31}/Y_{A2}\right]}{\left(1+\frac{Y_{11}}{Y_T}\right)\left[\left(1+\frac{Y_{22}}{Y_{A1}}\right)\left(1+\frac{Y_{33}}{Y_{A2}}\right) - \frac{Y_{23}Y_{32}}{Y_{A1}Y_{A2}}\right]}$$

$$\frac{v_3}{F} = \frac{\left[Y_{31}(1+Y_{22}/Y_{A1}) - Y_{21}Y_{32}/Y_{A1}\right]}{\left(1+\frac{Y_{11}}{Y_T}\right)\left[\left(1+\frac{Y_{22}}{Y_{A1}}\right)\left(1+\frac{Y_{33}}{Y_{A2}}\right) - \frac{Y_{23}Y_{32}}{Y_{A1}Y_{A2}}\right]} \qquad \text{...(C.4 a, b)}$$

Since $Y_T = -1/j\omega m_T$, $Y_{A1} = -1/j\omega m_{A1}$ and $Y_{A2} = -1/j\omega m_{A2}$, the transfer mobility with taking account of mass loading becomes

$$\frac{v_2}{F} = \frac{\left[Y_{21}(1-j\omega m_{A2}Y_{33}) + j\omega m_{A2}Y_{23}Y_{31}\right]}{(1-j\omega m_T Y_{11})\left[(1-j\omega m_{A1}Y_{22})(1-j\omega m_{A2}Y_{33}) + \omega^2 m_{A1}m_{A2}Y_{23}Y_{32}\right]}$$

$$\frac{v_3}{F} = \frac{\left[Y_{31}(1-j\omega m_{A1}Y_{22}) + j\omega m_{A1}Y_{21}Y_{32}\right]}{(1-j\omega m_T Y_{11})\left[(1-j\omega m_{A1}Y_{22})(1-j\omega m_{A2}Y_{33}) + \omega^2 m_{A1}m_{A2}Y_{23}Y_{32}\right]} \qquad \text{...(C.5 a, b)}$$

For the application of an infinite pipe, the transfer mobility taking mass loading is more easy to solve because $Y_{11} = Y_{22} = Y_{33}$ and $Y_{23} = Y_{32}$. It is more complicated on a semi-infinite pipe because the forces for Y_{22} and Y_{33} are considered to excited at the position of accelerometers, not at the edge of the pipe. However, the point mobility Y_{22} and Y_{33} can be determined from the radial amplitude, as described in section 2.4.

APPENDIX D

EXPERIMENTAL APPARATUS

Details of the experimental equipment and materials used in the thesis are described in this appendix.

D.1 Experimental Equipment and Properties of Materials

Table D.1: Properties of a PVC pipe

E (N/m^2)	ρ (kg/m^3)	ν	a (mm)	h (mm)	η
$3.974*10^9$	1460	0.33	33.2	2.2	0.035

Table D.2: Properties of a PVDF sheet (Measurement Specialist) used for modal sensors

E_{pv} (N/m^2)	ρ_{pv} (kg/m^3)	ν_{pv}	d_{31} (m/V)	k_{31}	h_{pv} (mm)
$2*10^9$	1780	0.33	$23*10^{-12}$	0.12	0.052

Table D.3: Properties of a PZT element (Morgan Matroc) used for modal actuators

E_z (N/m^2)	ρ_z (kg/m^3)	ν_z	d_{31} (m/V)	k_{31}	t (mm)
$61*10^9$	7450	0.31	$274*10^{-12}$	-0.39	0.25

Note: The magnitude of d_{32} is equal to d_{31} for the PVDF sheet and the PZT element.

Table D.4: Experimental equipment

	Supplier	Type	Serial No	Sensitivity
Accelerometers	Bruel&Kjael	4374	1265993	0.094 pC/ms^{-2}
		4374	1341877	0.105 pC/ms^{-2}
Force transducer (PZT)				341.7 pC/N
Conditioning Amplifiers	Bruel&Kjael	2635	1278233	
		2635	1318160	
		2635	1827830	
		2635	777627	
		2635	814962	
Power amplifiers	H‖H Electronic	TPA100-D	15397	
	Ariston	AX-910	747-AX910-0700-0259	
	Ariston	AX-910	777-AX910-1197-0223	
Shaker	Ling Dynamic Systems	V101	55586-33	
Oscilloscope	Hameg	HM203-7	60574	
Phaser				
Analyzer	Hewlett-Packard	3566A	2911A00263	
Personal computer	Hi-Grade	PV2	007341701003	

Note: 1) a PZT element is used as a force transducer, whose sensitivity is calibrated with a known mass of 4.357 kg, and 2) a phaser (phase controller) has been developed by Day [77].

D.2 Measurement of Properties of the Pipe

In order to determine the Young's modulus, the cut-on frequencies of a slice of pipe of 60 mm long were measured. Since the slice of pipe is short in length compared to a wavelength, it can be considered as a ring, whose cut-on frequencies are given by (Soedel [69])

$$f_n^r = \frac{\beta n(n^2-1)}{2\pi a}\sqrt{\frac{E}{\rho(n^2+1)}} \qquad \ldots(D.1)$$

By taking a least mean square fit to the natural frequencies of modes n = 2, 3 and 4, its young's modulus could be determined. The loss factor of the pipe was easily determined using the half power point method (Harris [71]). The same method of obtaining the Young's modulus was utilised to define the Poisson's ratio except that the cut-on frequencies of the pipe, f_n^p, are measured at a distance of 300 mm from the excitation force and are given by (equation 2.9)

$$f_n^p = \frac{\beta n(n^2-1)}{2\pi a}\sqrt{\frac{E}{\rho(n^2+1)(1-\nu^2)}} \qquad \ldots(D.2)$$

The difference between the cut-on frequencies of a pipe (equation D.2) and of a ring (equation D.1) is due to Poisson's ratio because, for the ring, waves are only propagating in the circumferential direction, while they are also propagating in the axial direction for the pipe resulting in coupled strains in both directions via the Poisson's ratio.

With the method described above, the pipe properties were obtained and are given in Table D.1.

D.3 Experimental Configuration of the Active Control System for the n = 2 Flexural Wave

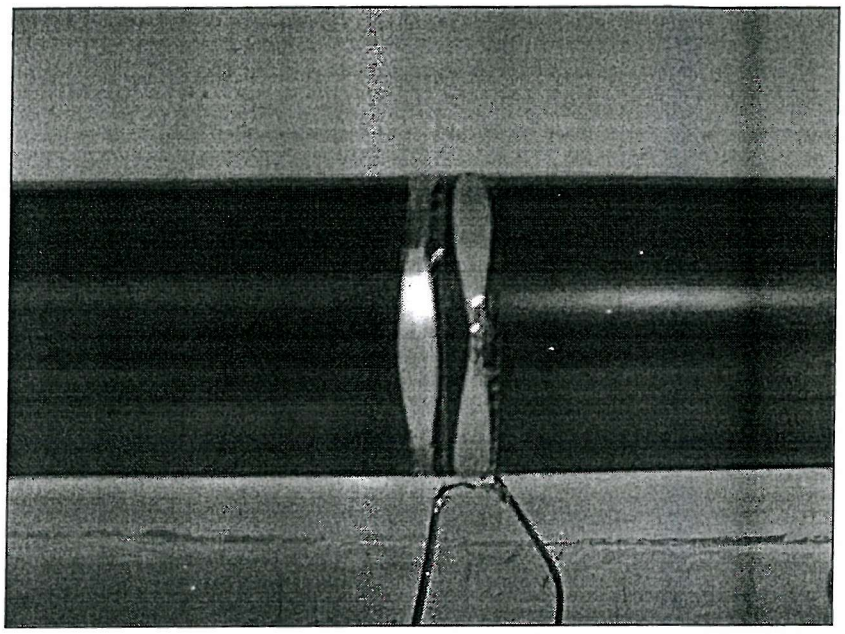

Figure D.1: Picture of the n = 2 PVDF modal sensor for a pipe.

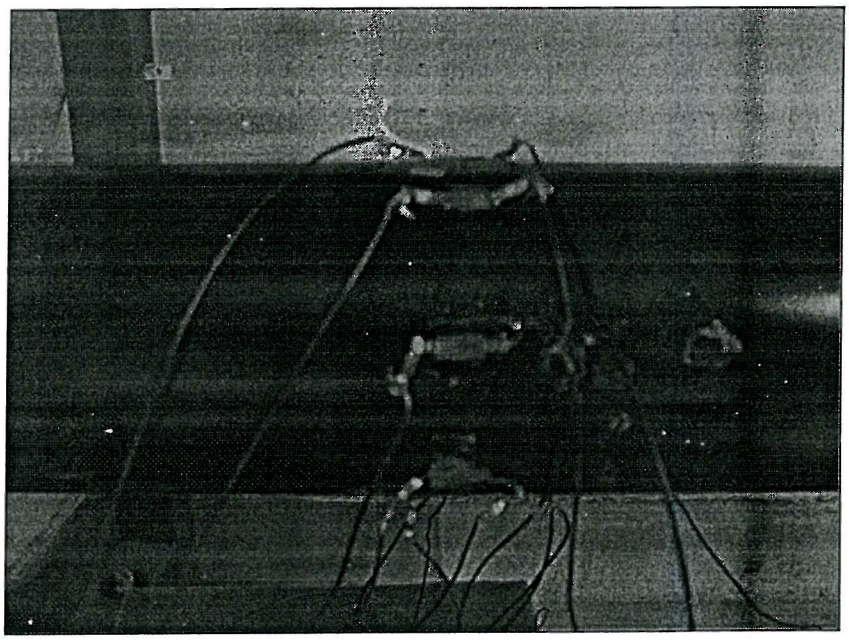

Figure D.2: Picture of the n = 2 PZT modal actuator for a pipe.

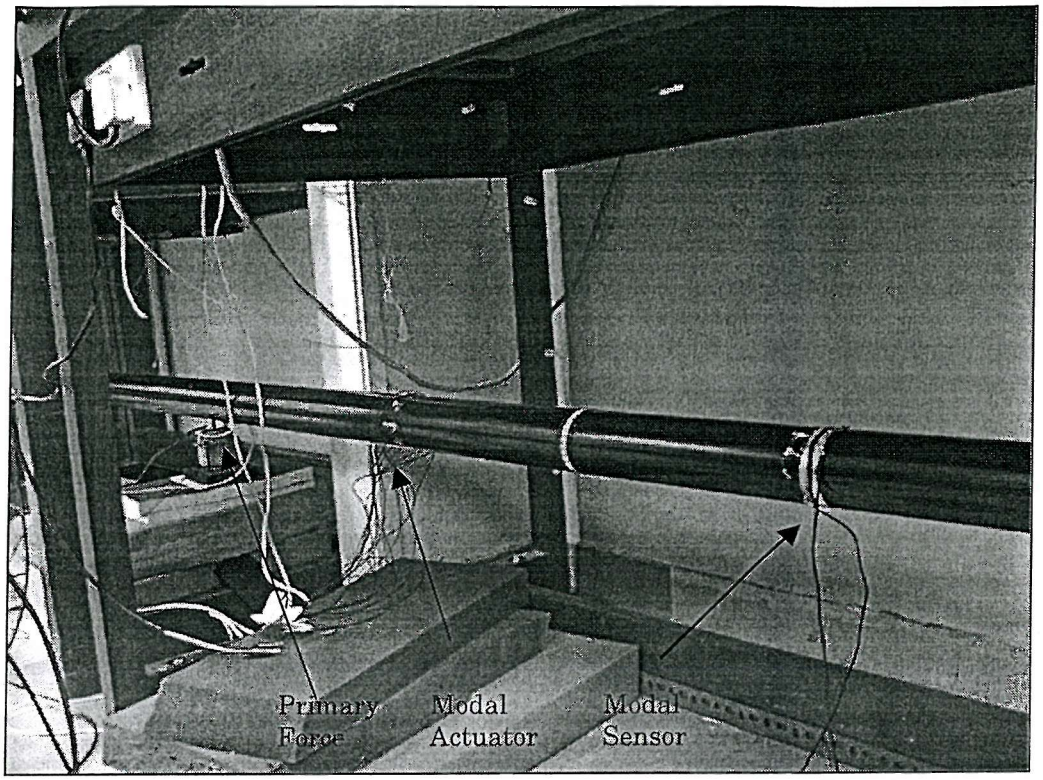

Figure D.3: Picture of the active control system for the n = 2 flexural wave.